DEVELOPING NEW TREATMENTS FOR BRAIN ARTERIOVENOUS MALFORMATIONS: MOLECULAR RESPONSES TO RADIATION IN *IN VITRO* AND *IN VIVO* MODELS

Newsha Raoufi-Rad, B. Biotechnology (Honours)

A thesis submitted in fulfilment of the requirements for the degree of Doctor of Philosophy at the Faculty of Medicine and Health Sciences, Macquarie University

November 2015

MACQUARIE
University
SYDNEY·AUSTRALIA

I would like to dedicate this thesis to my beloved
parents, Zahra Bazargan and Majid Raoufi-Rad,
who contributed more to this work than they could
ever imagine.

Declaration of originality

I acknowledge that the work presented in this thesis is my original research work. I declare that the content of this thesis has not been presented to any other institution for any award. To the best of my knowledge no material from this thesis has been previously published or written by another person, except where due acknowledgements are made.

The work was carried out with ethical approval from the Macquarie University Animal Ethics Committee (protocol 2011/011 – 15).

Newsha Raoufi-Rad

November 2015

Acknowledgements

I would like to express my thanks and appreciation to my supervisor, Prof. Marcus Stoodley, who provided this opportunity for me to work on this challenging and rewarding project. His endless patience, encouragement and advice will always be appreciated. I have been extremely lucky to have a supervisor who cared so much about my work and supported me during this amazing journey.

My sincere gratitude goes to my co-supervisor Prof. Jacqueline Phillips for her help and kindness during my candidature. Her encouragement and guidance will always be remembered.

I would like to thank everyone in Neurosurgery research team, particularly those working on the AVM project. My special thanks goes to Dr. Lucinda McRobb who kindly helped me with the final stages of my work in the lab and carefully reviewed my document. She always provided me with very helpful and encouraging feedback with lots of moral support. Thanks also goes to Dr. Sarah Hemley for her motivation, help and kindness during my candidature. I would also like to thank Dr. Jun Zhao for his patience, invaluable guidance and kindness. Thanks also goes to Vivienne Lee for patiently teaching me experimental techniques and helped me throughout my candidature. I would also like to thank Dr. Nirav Patel and Dr. David Bervini, for creating the AVM animal model. Thanks to Dr. Elmira Najafi and Jude Amal Raj for their moral support, kindness and help.

I would like to express my gratitude to the Genesis Care team at Macquarie University Hospital, (Jaysree Ukath, Vivek Gupta, Yunfei Hu and Michael Grace), who helped me with all my irradiation procedures with LINAC and Gamma Knife. They put in many hours of overtime to enable us to irradiate the rats.

I would also like to thank Joshua McHattan at Bruker Molecular Imaging who taught me the molecular *in vivo* imaging technique and opened my eyes toward an amazing research field. Also many thanks to Dr. Matthew Leevy at University of Notre Dame; Dr. Todd Sasser at Bruker Molecular Imaging; and Dr. Prof. David Stout at Crump Institute for Molecular Imaging in United States who provided a great opportunity for me to visit their labs and learn more about molecular *in vivo* imaging.

Thank you to Macquarie University for providing me with the Macquarie University Research Excellence Scholarship throughout my candidature. Also thank you to Faculty of Medicine and Health Sciences and Skipper-Jacobs Trust for providing the funding to attend conferences and meet so many interesting people.

I would like to thank everyone at the Faculty of Medicine and Health Sciences, especially Prof. Mark Connor who introduced me to this first class research institute where I could meet fantastic people who made this journey possible for me. Many thanks goes to my friends here at the Faculty, especially Dr. Rozhin Asghari, Nurul Jufri and Dr. Varun Sreenivasan, who not only being wonderful friends, but also taught me many experimental techniques. Thank you also to my other great friends, Dr. Anita Turner, Marina Santiago, Dr. Azadeh Farnoush,

Publications and presentations

Publications arising from this thesis

1. **Raoufi-Rad N.,** McRobb L., Ukath J., Sreenivasan V., Hu Y., Marcus Stoodley, "Molecular responses to radiation in bEnd.3 cells" (In preparation).

2. **Raoufi-Rad N.,** Patel N., Mchattan J., Zhao J., Lee V., Bervini D., Grace M., Amal Raj J., Kashba S., McRobb L., Hong Duong TT., Marcus Stoodley, "Phosphatidylserine translocation in responses to radiation in an animal model of arteriovenous malformations" (In preparation).

Publications related to work not presented in this thesis

1. Saleh R Kashba, Nirav J Patel, Michael Grace, Vivienne S Lee, **Newsha Raoufi-Rad,** Jude V Amal Raj, Thi Thuy Hong Duong, Marcus Stoodley, "Angiographic, hemodynamic, and histological changes in an animal model of brain arteriovenous malformations treated with Gamma Knife Radiosurgery", Journal of Neurosurgery, 123(4):954-60, 2015 Oct.

2. B. Chen, Z. Zhao, **N. Raoufi-Rad**, V. Lee, M. Grace, R. Reddy, M. Stoodley, "Radiation-induced expression of platelet endothelial cell adhesion molecule-1 in cerebral endothelial cells" (In preparation).

Conference presentations and posters

1. **Raoufi-Rad N.,** Hong Duong TT, Stoodley M., "Irradiation induces gene expression changes in cultured murine brain endothelial cells", International Stroke Conference, 6-8, February 2013, Hawaii, USA (Oral presentation).

2. **Raoufi-Rad N.,** Asghari R., Lee V., Hong Duong TT., Stoodley M., "Effects of reduced radiation dose on gene expression changes in cultured murine brain endothelial cells", Australian Neuroscience Society, 2-6 February 2013, Melbourne, Australia (Poster presentation).

3. **Raoufi-Rad N.,** Zhao J., Hong Duong TT, Grace M., Patel N, Lee V., Kashba S., Amal Raj J., Stoodley M., "Gamma radiation induced phosphatidylserine externalization on endothelial cells in a rat arteriovenous malformation model", The Australian Vascular Biology Society 2013 Scientific Meeting, 5-8 September 2013, Adelaide, Australia (Poster presentation).

4. **Raoufi-Rad N.,** Patel N., McHattan J., Zhao J., Lee V., Grace M., Kashba S., Hong Duong TT, Stoodley M., "Irradiation induces molecular changes in endothelial cells of AVM rat model", World Molecular Imaging Congress (WMIC), 17-22 September 2013, Savannah, USA (Poster presentation).

5. **Raoufi-Rad N.,** Ukath J., Stoodley M., "Effects of radiation dose on gene expression in cultured murine brain endothelial cells", International Stroke Conference, 12-14, February 2014, San Diego, USA (Oral presentation).

6. **Raoufi-Rad N.,** Gupta KK., Stoodley M., "Effects of high and low radiation dose on gene expression changes in cultured murine brain endothelial cells", Australian Neuroscience Society, 28-31 January 2014, Adelaide, Australia (Poster presentation).

7. Chen B., **Raoufi-Rad N.,** Reddy R., Zhao J., Lee V., Grace M., Ukath J., Stoodley M., "Radiation induced expression of platelet endothelial cell adhesion molecular-1 in arteriovenous malformations and cerebral endothelial cells", Australian Neuroscience Society, 28-31 January 2014, Adelaide, Australia (Poster presentation).

Abstract

Brain arteriovenous malformations are a leading cause of stroke in children and young adults. They account for 4% of haemorrhagic strokes. Arteriovenous malformations (AVMs) are complex vascular lesions, characterised by abnormal connections between arteries and veins that lack a capillary network. The treatment options for AVMs include surgery, radiosurgery and embolisation. However, over one third of AVM patients with large and deep AVMs cannot be safely and effectively treated with current methods. Therefore, a new treatment method is required for these patients with life-threatening AVMs. A biological technique that can be harnessed to enhance the rate of occlusion or thrombosis inside the AVM blood vessels is highly attractive. A proposed method to achieve this goal is vascular targeting. This approach has been applied in cancer therapy where unique molecular markers expressed on the surface of tumour vessels are targeted by conjugated antibodies and pro-thrombotic factors to induce thrombosis inside the tumour vessels. If such a technique can be used for AVM treatment, it will open a new window toward treatment of life-threatening AVMs. In order to follow this path, specific markers on the surface of the AVM endothelium need to be identified for selective targeting. However, previous studies have shown that AVM endothelial cells are not dramatically different to normal endothelial cells. Therefore, a priming mechanism is required. It is hypothesised that radiosurgery induces molecular changes on the surface of endothelial cells that can be used to discriminate irradiated vessels from normal vessels. Previous studies have shown radiation can induce endothelial membrane changes, such as phosphatidylserine (PS) translocation and up-regulation of various cell adhesion molecules (CAMs), including intercellular adhesion molecule 1 (ICAM-1), vascular cell adhesion molecule 1 (VCAM-1), P-selectin and E-selectin, both *in vitro* and *in vivo*. Therefore, the aims of this study were as follows: 1) to examine which of the CAMs elicits the greatest response to radiation in endothelial cells *in vitro* and may provide the best candidate for a vascular targeting approach; 2) to determine the lowest radiation dose (5, 15 or 25 Gy) able to elicit a significant response in these molecules *in vitro*, as lower doses reduce the risk of off-target radiation damage to normal cells; 3) to determine the most discriminating CAMs in an AVM animal model; and 4) to examine the *in vivo* externalisation of PS in response to radiosurgery in the AVM animal model. While all four CAMs were up-regulated by irradiation *in vitro,* among the candidate molecules, ICAM-1 and VCAM-1 demonstrated the highest level of expression, followed by P-selectin. A dose of 15 Gy was as effective as 25 Gy at inducing expression while minimal response was evident at a dose of 5 Gy. The results of

these studies led to the selection of candidate molecules for *in vivo* imaging, (ICAM-1 and VCAM-1), with 15 Gy as the treatment dose. In the AVM animal model, ICAM-1 and VCAM-1 were expressed at the luminal endothelial surface in the AVM region only. Expression of the two molecules was high in the AVM prior to radiosurgery. No significant increases in ICAM-1 and VCAM-1 were found in response to the 15 Gy radiation dose. The inability to detect differences *in vivo* suggested that the dose was not sufficient to further induce surface expression above the high background level, at least in this model. However, *in vivo* imaging of phosphatidylserine externalisation in the rat AVM model demonstrated that radiation could significantly increase PS exposure at the luminal surface. This was despite rat AVMs also displaying significantly elevated PS externalisation relative to the normal vasculature. This molecule may provide the most promising candidate to move toward vascular targeting of AVMs.

Abbreviations

AEC	Animal Ethics Committee
ANG-2	Angiopoietin 2
ANOVA	Two-way analysis of variance
ARC	Animal Resources Centre
AVF	Arterio-venous fistula
AVM	Arteriovenous malformation
BBB	Blood brain barrier
BCA	Bicinchoninic acid
bEnd.3	Mouse brain microvascular endothelial cell
BLI	Bioluminescence imaging
BSA	Bovine serum albumin
CAM	Cell adhesion molecule
CCA	Common carotid artery
Cd	Cadmium
CNT	Carbon nanotube
CRP	Complement regulatory proteins
CSF	Cerebrospinal fluid
Ct	Cycle threshold
CT	Computed tomography
DAPI	4',6-diamidino-2-phenylindole
DCN	Downconversion molecule 1
DMEM	Dulbecco's Modified Eagle's Medium
DMSO	Dimethyl sulfoxide
DMXAA	5,6-dimethylxanthenone-4-acetic acid
ECL	Enhanced chemiluminescence
EDTA	Ethylenediaminetetraacetic acid
EGF	Epidermal growth factor
EJV	External jugular vein
ELAM-1	Endothelial leukocyte adhesion molecule 1
ELISA	Enzyme-linked immunosorbent assay
ER	Endoplasmic reticulum

FAA	Flavonoid
FDA	Food and Drug Administration
FGF-2	Fibroblast growth factor-2
GAPDH	Glyceraldehyde-3-phosphate dehydrogenase
GI	Gastrointestinal
GIa	Gamma-carboxyglutamic acid
GMP-140	Granule membrane protein 140
Gy	Gray
h	Hour
HCl	Hydrochloric acid
HDMEC	Human dermal microvascular endothelial cell
HIV	Human immunodeficiency virus
H_2O_2	Hydrogen peroxide
HPRT	Hypoxanthine guanine phosphoribosyltransferase
HRP	Horseradish peroxidase
HRP-streptavidine	Horseradish peroxidase-conjugated streptavidin
HUVEC	Human umbilical vein endothelial cell
IAEA	International atomic energy agency
ICAM-1	Intercellular adhesion molecule 1
ICC	Immunocytochemistry
ICG	Indocyanin green
ICH	Intracerebral haemorrhage
IF	Immunofluorescence
IL-1	Interleukin-1
IL-1 β	Interleukin-1 β
IL-4	Interleukin-4
IP	Intraperitoneal
IV	Intravenous
LFA-1	Lymphocyte function-associated antigen-1
LINAC	Linear accelerator
LPS	Lipopolysaccharide
Mac-1	Macrophage-1-antigen
MAM	Mitochondria-associated membrane

MFI	Mean fluorescence intensity
Min	Minute
MRI	Magnetic resonance imaging
MU	Monitor units
MUH	Macquarie University Hospital
NFκB	Nuclear factor kappa B
NIR	Near-infrared
NIRF	Near-infrared fluorophores
NOS	Nitric oxide synthase
NOS3	Nitric oxide synthase 3
OI	Optical imaging
PADGEM	Platelet activation-dependent granule external membrane protein
PBS	Phosphate-buffered saline
PBST	Phosphate-buffered saline with tween 20
PC	Phosphatidylcholine
PCNA	Proliferating cell nuclear antigen
PE	Phosphatidylethanolamine
PET	Positron emission tomography
PS	Phosphatidylserine
PSGL-1	P-selectin glycoprotein ligand-1
PSR	Phosphatidylserine receptor
PSS1	Phosphatidylserine synthase 1
PSS2	Phosphatidylserine synthase 2
PVDF	Polyvinylidene difluoride
QD	Quantum dot
qRT-PCR	Quantitative real-time polymerase chain reaction
Raf-1	Rapidly accelerated fibrosarcoma-1
RIPA	Radioimmunoprecipitation assay
ROI	Region of interest
ROS	Reactive oxygen species
RPM	Revolutions per minute
RT	Room temperature
RT-PCR	Reverse transcription polymerase chain reaction

SCR	Short consensus repeats
SEM	Standard error of the mean
SI	International System of Units
sLe$^{x.}$	Sialyl Lewis x
SPECT	Single photon emission computed tomography
SRS	Stereotactic radiosurgery
SSD	Source to surface distance
TBE	Tris-borate-EDTA
TBST	Tris-buffered saline with tween 20
TGF-β	Transforming growth factor-β
Tie-2	Endothelial angiopoietin receptor
TMB	3, 3', 5, 5'- tetramethylbenzidine
TNF-α	Tumour necrosis factor alpha
TNR	Tumour-to-normal tissue ratio
UCN	Upconversion
US	Ultrasound
UV	Ultraviolet
VCAM-1	Vascular cell adhesion molecule 1
VEGF	Vascular endothelial growth factor
VEGFR-1	Vascular endothelial growth factor receptor 1
VTA	Vascular targeting agent
vWF	Von Willebrand factor
Zn^{2+}-DPA	zinc (II)-dipicolylamine
γ -IFN	γ-interferon
β_2GP1	β_2-glycoprotein 1

Table of Contents

List of Figures

List of Tables

Chapter 1. Introduction

1.1 Arteriovenous malformations

Many types of vascular disorders occur in the central nervous system. Among these, arteriovenous malformations (AVMs) are a significant cause of stroke in children and young adults (Achrol et al., 2009). Over one third of patients with AVMs are not treatable using existing techniques (Han et al., 2003). New treatment methods are needed for these patients.

1.2 Pathology

Arteriovenous malformations (AVMs) consist of direct connections between arteries and veins, without the normal interconnecting capillary network (Mohr, 1999). The lack of a capillary network results in high pressure arterial blood flowing directly into the veins and leads to dilation and branching growth of abnormal vessels. This tangled collection of abnormal vessels is called a nidus (Figure 1.1) (McCormick & Schochet, 1976; Mohr et al., 1998). Arteriovenous shunting of blood occurs in a central nidus or in a single fistula between one feeding artery and one draining vein (Al-Shahi et al., 2002). The risk of rupture is due to the high pressure of arterial blood flowing directly into fragile veins (Park et al., 2009). AVMs are found in the brain, spinal cord, gastrointestinal (GI) tract, liver, lung and spleen (Park et al., 2009). Most brain AVMs are located in superficial areas of the brain, however about 15% of lesions are present in deep areas (e.g., corpus callosum, brainstem, basal ganglia) (Khaw et al., 2004).

Brain AVMs are dynamic lesions that can change, with development of a feeding artery aneurysm, venous stenosis, or venous varices. The dynamic characteristics of an AVM may change the risk of haemorrhage and the actual rate of AVM haemorrhage may not be readily predicted (Abdulrauf et al., 1999). Factors that can increase the risk of spontaneous haemorrhage are high intranidal blood pressure (Duong et al., 1998; Stapf et al., 2000; Todaka et al., 2003), exclusive deep venous drainage (Khaw et al., 2004; Mansmann et al., 2000; Pollock et al., 1996), venous ectasias and stenosis, a small number of draining veins, AVM-related aneurysms (Gross & Du, 2013), previous haemorrhage (Halim et al., 2004; Henning et al., 1997), periventricular location, and large nidus size (Inoue & Ohye, 2002; Jayaraman et

al., 2007; Richling et al., 2006). Most commonly, AVMs are present as single lesions, but there are also cases of multiple AVMs (Schlachter et al., 1980; Willinsky et al., 1990).

Eighteen percent of AVM patients also have aneurysms, half of which are in feeding arteries (Gross & Du, 2013). Brown *et al.* reported an annual risk of haemorrhage of 8.3% for patients with associated aneurysms and 2.4% for patients without aneurysms (Brown et al., 1990). In a similar study by da Costa *et al.*, the annual risk of haemorrhage was demonstrated to be 7% and 4% for patients with and without aneurysms respectively (Da Costa et al., 2009).
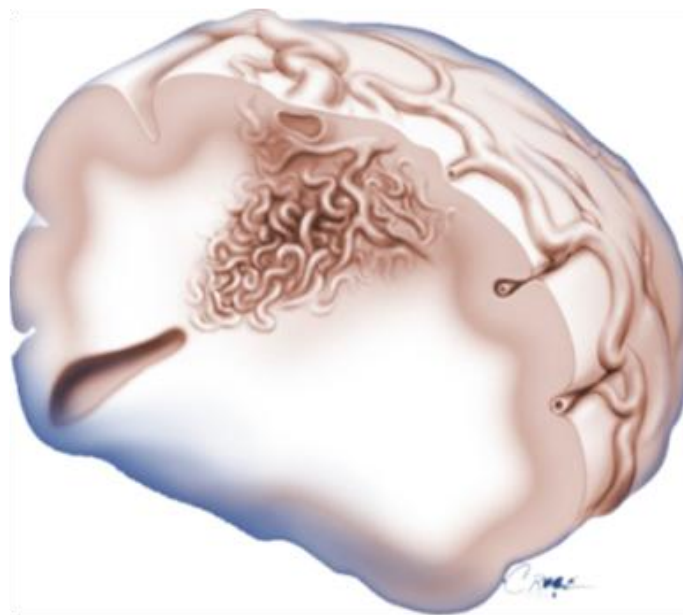
Figure 1.1. Diagram representing an AVM. The nidus is typically based on the cortical surface with a cone shape directed towards the ventricle. Figure courtesy of Professor Marcus Stoodley.

1.3 Epidemiology

According to a population-based study of 10 million people, the AVM detection rate is 1.21/100,000 persons per year (95% confidence interval [CI] 1.02 to 1.42) (Stapf et al., 2001). AVMs can present at any age with equal distribution in the sexes (Al-Shahi et al., 2003; ApSimon et al., 2002; Halim et al., 2004; Stapf et al., 2003). The peak incidence is in the second to fourth decades of life, and presentation between 40 to 50 years of age is more likely than between birth and 10 years (Jeffree & Stoodley, 2009). The mean age of presentation tends to be in the third decade of life (Choi & Mohr, 2005).

The annual rate of intracerebral haemorrhage (ICH) in AVM patients ranges from 2 to 4% (Ondra et al., 1990). The annual risk of initial haemorrhage in patients with low-risk AVMs, that is, AVMs with a compact nidus and multiple draining veins and no other risk factors, is 1%. In patients with high risk AVMs with at least one other risk factor, the annual risk is 2% (Pollock et al., 1996). The rate of mortality associated with ICH is 29% and there is a long-term disability rate of about 23% (Brown et al., 1988). AVMs are the leading cause of ICH in children and young adults (Achrol et al., 2009; Al-Shahi & Warlow, 2001), accounting for 14 to 57% of paediatric cerebral haemorrhages (Al-Jarallah et al., 2000; Jordan & Hillis, 2007). AVMs rupture predominantly in children and young adults with a mortality rate of 15 – 20% and a neurological complication rate of 35 – 45% (Hartmann et al., 1998; Mast et al., 1997; Mohr, 1999).

The annual risk of recurrent ICH in patients with low risk AVMs is 3.7% and in patients with high risk AVMs (one draining vein or diffuse morphology) is 8.95% (Pollock et al., 1996). Patients who present with ICH suffer a higher rate of subsequent ICH than those who present without ICH (Mast et al., 1997). The rate of recurrent ICH is higher in the first year or so and afterwards seems to decrease to the baseline. It seems that the lesion becomes unstable and vulnerable to more bleeding after the first ICH (Choi & Mohr, 2005; Crawford et al., 1986; Mast et al., 1997). The morbidity rate after a first rupture is as high as 53 to 81% (Graf et al., 1983; Perret & Nishioka, 1969), whereas mortality rate is 10 to 17.6% (Brown et al., 1996; Graf et al., 1983; Wilkins, 1985).

1.4 Aetiology

The aetiology and genetic patterns of AVMs remain incompletely elucidated (Achrol et al., 2007; Achrol et al., 2006). There are two main hypotheses postulated for AVM presence: congenital (Andaluz et al., 2004; Mullan et al., 1996; Parkinson & Bachers, 1980) or post-natal in nature. There are cases of AVMs present since birth but also rare cases of *de novo* development (Hashimoto et al., 2001; Houtteville, 1997). Growth after initial AVM diagnosis, and regrowth after successful treatment have also been reported (Fournier et al., 1990; Gonzalez et al., 2005; Hladky et al., 1994).

Recent studies suggest a role for genetic factors in the pathogenesis of sporadic AVMs (Achrol et al., 2009). This is further supported by reports of familial occurrence of AVMs and

the association of brain AVMs with known systemic genetic disorders, such as Olser-Weber-Rendu disease, Von Hippel Lindau disease, Sturge-Weber disease, and Wyburn-Mason syndrome (Herzig et al., 2000; Kadoya et al., 1994; Putman et al., 1996). Apart from familial occurrence of AVM with hereditary diseases, familial AVMs have only been reported in 20 families (44 cases) (Herzig et al., 2000).

Studies have suggested that there is a likelihood that AVMs arise from an embryonic disturbance at the stage of vessel formation (Padget, 1956). Cerebral AVMs are often found in the border-zone region shared by the distal anterior, middle, and/or posterior cerebral arteries (Stapf et al., 2000). This phenomenon suggests that early lesions may be formed during late foetal or immediate postpartum life, at the time that the border zones are arising (Nelson et al., 1991). Studies propose that AVM formation can also be due to germ line, congenital and even somatic mutations, that influence angiogenic pathways (Stapf et al., 2001).

AVMs may also represent aberrant adult vasculogenesis (not just persistent neonatal angiogenesis) or could represent benign slow growing vascular tumours (not just static congenital lesions) (Stapf et al., 2001). Moreover, the trigger for growth during childhood or early adulthood could be increasing haemodynamic stress in the abnormal vessels that stimulates growth factor expression in the endothelial cells lining the AVM vessels, resulting in secondary vascular changes that all finally lead to maturation of the AVM (Lasjaunias, 1996). The fact that there is initially a simple direct arteriovenous fistula that gradually leads to the mature AVMs lends weight to this argument (Potter, 1955; Yasargil, 1987).

In contrast to the proposed congenital origin of AVMs, there is considerable evidence in favour of post-natal development. In 1987, Yasargil postulated that AVMs are formed from the 'proliferative capillarophy'. That is, capillaries in the AVM area proliferate and form metamorphic dysplastic vessels. In other words, AVMs might not be created by the dilation of the existing vessels but rather by *de novo* growth of vessels that did not exist before (Yasargil, 1987).

In 1996, Mullan and colleagues showed that it is generally impossible to detect AVMs in *utero* or with pre-natal ultrasound. This suggests either they are too small for detection or they form after birth (Mullan et al., 1996).

1.5 Diagnosis

Diagnostic tools for brain AVMs include: computed tomography (CT) (Figure 1.2); magnetic resonance imaging (MRI) (Stapf et al., 2001); and catheter angiography (Meder et al., 1998; Turjman et al., 1994).

Computed tomography was introduced at the beginning of the 1970s and MRI in the 1980s (Choi & Mohr, 2005). These modalities are the major diagnostic tools for patients who present with headache, seizure, focal neurological deficits or haemorrhage (Ogilvy et al., 2001). MRI is suitable for identification of the size and location of an AVM as well as its relation to surrounding intracranial structures (Figure 1.3) (Choi & Mohr, 2005).

Angiography, first introduced in 1927, remains essential for detection of small AVMs. Angiography is important for assessment of angioarchitectural characteristics of all AVMs (Choi & Mohr, 2005). Complete obliteration always needs to be checked with angiography, as MRI is only 80% reliable in predicting complete occlusion. Angiography and MRI complement each other in defining the nidus (Flickinger et al., 1992).
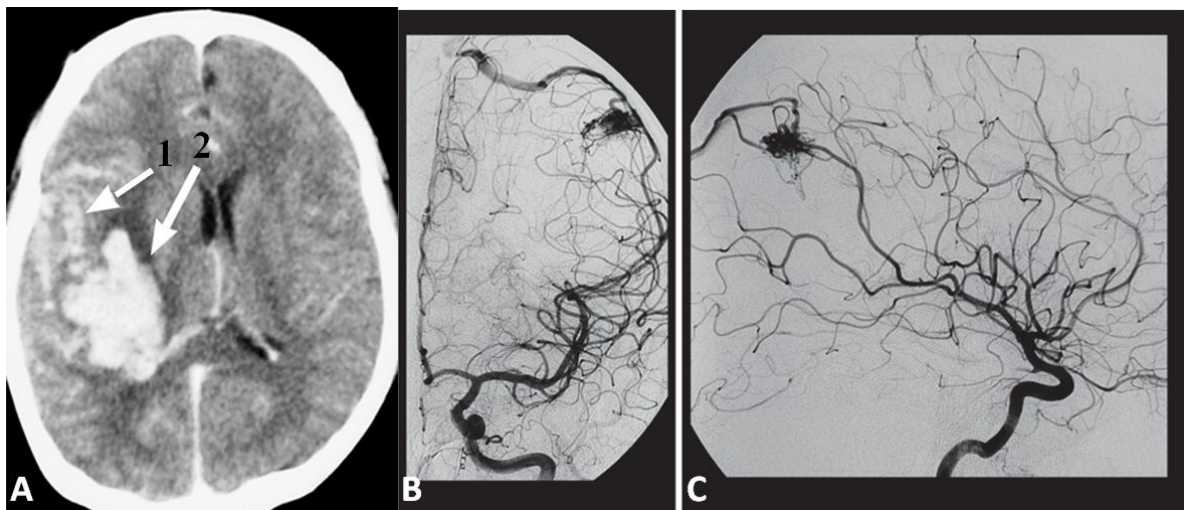
Figure 1.2. (A) CT image of ruptured brain AVM, (arrow 1) AVM vessels and (arrow 2) haemorrhage detected with contrast. (B) and (C) Left internal carotid angiography in two different patients demonstrates a superficial left parietal AVM. Figure courtesy of Professor Marcus Stoodley.
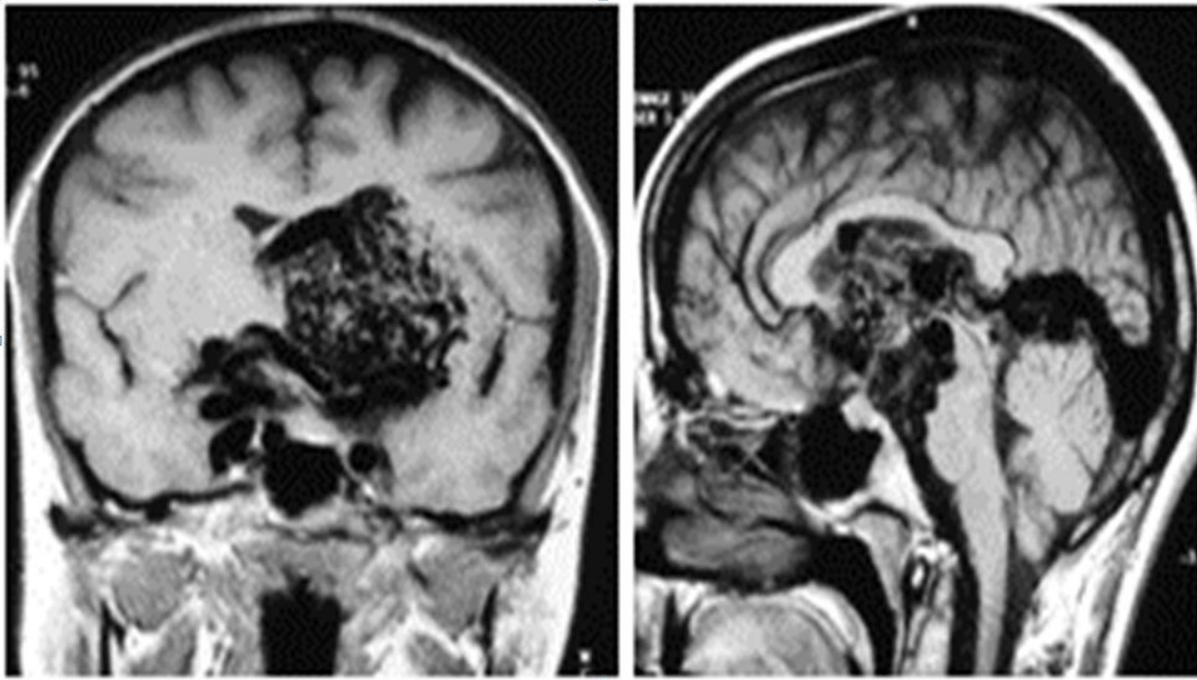
Figure 1.3. MRI image of a young male patient with a grade VI AVM. The AVM is located in the midbrain and thalamus. This is an example of an untreatable AVM. Figure courtesy of Professor Marcus Stoodley.

1.6 Clinical features

The clinical presentations of AVM include ICH, progressive neurological deficits, epileptic seizures, headaches, and congestive heart failure in newborns (Fleetwood & Steinberg, 2002; Laakso & Hernesniemi, 2012; Stapf et al., 2001). AVMs may also be detected incidentally (Sun et al., 2011).

1.7 AVM treatment

The primary aim of AVM treatment is to prevent haemorrhage by removal or complete obliteration of AVM vessels while maintaining the patients' neurological function (Skjøth-Rasmussen et al., 2010; Yen & Steiner, 2011). Treatment options include microsurgical resection, endovascular embolisation and stereotactic radiosurgery (SRS) (Choi & Mohr, 2005; Jabbour et al., 2009). Treatment methods depend on the patient's age, presenting symptoms, medical history, AVM size, location, vascular supply to the nidus and bleeding history (Lunsford et al., 2008). Successful treatment is defined by the complete disappearance of the AVM nidus, absence or normalisation of veins draining the AVM, disappearance of visible arteriovenous shunts and appearance of normal circulatory kinetics. An incompletely

treated AVM can increase in size and in density of vessels (Andaluz et al., 2004; Parkinson & Bachers, 1980; Yasargil, 1987).

1.7.1 Microsurgical resection

Microsurgical resection physically removes the nidus and eliminates the risk of ICH (Spetzler & Martin, 1986). Surgery is normally the first option for treating superficial lesions that are not located in the eloquent cortex (Choi & Mohr, 2005). The efficacy of microsurgery has been established by many investigators at 94 – 100% for small lesions ($\leq$ 3 cm) (Heros et al., 1990; Schaller et al., 1998; Sisti et al., 1993). The decision to recommend surgery is crucial; it depends on offering lower rates of morbidity and mortality than the natural history of the untreated AVM (Spetzler & Martin, 1986).

The difficulty of the surgery can be defined by important factors including AVM size, amount of flow through the lesion, location, surgical accessibility, eloquence of adjacent brain, number of feeding arteries, degree of steal from surrounding normal brain, and venous drainage pattern (Spetzler & Martin, 1986). The risk of morbidity and mortality related to surgery is predicted by an objective grading system. The Spetzler-Martin grading system defines for each AVM the risk involved in removing the malformation. The six point system considers three features of AVMs – the maximum diameter of the AVM, the pattern of venous drainage, and neurological eloquence of the brain regions adjacent to the AVM (Spetzler & Martin, 1986).

The size of the lesion, determined by angiographic measurement of the diameter of the nidus, is divided into three groups: small (< 3 cm), medium (3 to 6 cm), or large (> 6 cm), and the AVM is scored accordingly (Table 1.1). The size of the AVM influences the number of feeding arteries, the amount of flow, and the degree of steal (Spetzler & Martin, 1986).

Eloquent brain regions regulate senses, movement and speech. These brain areas are vital for human function and if injured, the results can be disastrous to the quality of life of the individual. The regions that are considered eloquent are: the sensorimotor, language, and visual cortex; the hypothalamus and thalamus; the internal capsule; the brain stem; the cerebellar peduncles; and the deep cerebellar nuclei. The areas where damage does not cause a major disabling deficit (such as the anterior portion of the frontal or temporal lobes, or the cerebral cortex) are considered non-eloquent (Spetzler & Martin, 1986). Eloquent regions of the brain are identified by techniques such as intraoperative electrophysiological cortical

mapping, functional magnetic resonance imaging, and the use of neurosurgical navigation systems (Burchiel et al., 1989; Latchaw et al., 1995). Around 71% of AVMs occur in eloquent areas of the brain (Spetzler & Martin, 1986). Dissection of an AVM in an eloquent area carries a much greater risk of disabling neurological morbidity compared to a non-eloquent area due to the AVM resection itself as well as post-operative haemorrhage or oedema (Spetzler & Martin, 1986).

The pattern of venous drainage is an essential factor in determining the surgical accessibility of an AVM as deep venous drainage further complicates surgery (Spetzler & Martin, 1986). The pattern of venous drainage is assessed by angiogram. There are two types of draining veins: superficial and deep. The venous drainage is considered superficial if all the drainage from the AVM is through the cortical venous system. The drainage is considered deep if any or all of the drainage is through deep veins (such as internal cerebral veins, basal veins, or precentral cerebellar vein). Exclusively deep venous drainage is present in 55% of AVMs (Spetzler & Martin, 1986).

In order to objectively determine the grade of an AVM, a numerical value is assigned for each of the categories described above (Table 1.1). The points assigned for each feature are added together to derive the final grade (Spetzler & Martin, 1986).

Table 1.1. Determination of AVM grade*

Graded Feature	Points Assigned
Size of AVM	
small (< 3 cm)	1
medium (3 – 6 cm)	2
large (> 6 cm)	3
Eloquence of adjacent brain	
non-eloquent	0
eloquent	1
Pattern of venous drainage	
superficial only	0
deep	1

*Grade = [size] + [eloquence] + [venous drainage] (Spetzler & Martin, 1986)

The lowest grade possible is grade I if the AVM is smaller than 3 cm (1 point), located in a non-eloquent area (0 points) and has superficial drainage (0 points). The highest grade (V)

represents an AVM that is larger than 6 cm in diameter, located within or close to an eloquent region, with deep venous drainage (Spetzler & Martin, 1986). Complete removal of an AVM with a Spetzler-Martin score of 1, 2 or 3 would present relatively minor technical difficulties during surgery and also result in lower risks of persistent neurological deficits after surgery than those with scores of 4 or 5 (Hamilton & Spetzler, 1994). There is a group of AVM lesions which fall into a category called Grade VI or, more simply, "inoperable" where their excision would lead to totally disabling deficit or death. They are extremely large AVMs that are located in eloquent regions of the brain and have deep venous drainage. There is a correlation between the AVM grading system and the difficulty of removing the lesion (Spetzler & Martin, 1986).

Microsurgical resection is the best option among the three modalities for treating small and superficial AVMs. Resection does, however, have disadvantages and risks including infection, brain oedema, perioperative haemorrhage, stroke, death, and long term clinical complications post-surgery (Choi & Mohr, 2005).

1.7.2 Endovascular embolisation

The aim of endovascular embolisation is to obliterate the feeding arteries and the vessels at the site of the nidus or to reduce the amount of blood flow through the AVM nidus so that the surrounding brain has near-normal filling (Choi & Mohr, 2005). During vascular embolisation a catheter is used to transfer a variety of occlusive agents, sclerosing drugs, permanent balloons, thrombosing coils or quick-acting glues to the nidus (Mohr, 1999). There is a short period of time needed for the embolising agent to set which is facilitated by reducing the systemic arterial pressure by general anaesthetics, vasoactive agents or even by brief adenosine-induced cardiac pause (Pile-Spellman et al., 1999).

Embolisation treatment can either be carried out alone or used before surgery or radiosurgery to reduce the blood flow or AVM size (Choi & Mohr, 2005; Friedlander, 2007). Endovascular treatment is effective in 2 to 16% of patients, but it can have a higher efficacy if it accompanies either surgery or radiosurgery (Chang et al., 2007; Dawson et al., 1990; Deruty et al., 1993). Reduction in flow within an AVM does not provide any advantage to SRS treatment (Lunsford et al., 2008). Pre-radiosurgical embolisation may be helpful for large AVMs if the nidus volume can be reduced to 10 to 12 mL that may facilitate target coverage with a therapeutically effective radiation dose (Alexander & Tolbert, 2006; Bollet et al., 2004;

Haw et al., 2006). From 5 to 83% of the patients treated by radiosurgery had pre-radiosurgery embolisation (Friedman et al., 2003; Inoue, 2006; Izawa et al., 2009). In reported studies, the combination of embolisation and SRS led to 47 to 55% nidus obliteration, 5 to 12% permanent neurological deficits, and 1.5 to 2.7% mortality (Gobin et al., 1996; Henkes et al., 1998).

In some cases, pre-radiosurgery embolisations have led to higher morbidity, lower obliteration rate, and poorer outcomes compared to radiosurgery alone (Andrade-Souza et al., 2007; Pan et al., 2005; Pollock et al., 1998). In a study performed by Andrade-Souza *et al.*, 47 patients treated with embolisation and SRS were compared with 47 matching patients treated with SRS alone. The results showed an obliteration rate of 47% and 70% for the embolisation and SRS group and the SRS alone group, respectively. The groups were comparable in marginal radiation dose, AVM volume, and location (Andrade-Souza et al., 2007).

Several factors could be responsible for the poorer results of pre-radiosurgery embolisations such as patient selection bias, as large AVMs are always chosen for combined treatment and because of the angioarchitecture, they may take longer to obliterate (Izawa et al., 2009; Miyawaki et al., 1999; Veznedaroglu et al., 2008). Secondly, embolisation is potentially beneficial prior to radiosurgery if a particular anatomical compartment of the lesion, located on its periphery, is occluded (Alexander & Tolbert, 2006; Inoue & Ohye, 2002). Moreover, partial embolisation of the nidus may lead to dissociation of the nidus into irregular clusters, that can make conformal radiosurgery difficult (Guo et al., 1993; Zabel-du Bois et al., 2007). Irregular clusters of AVMs can cause delivery of higher irradiation doses to the surrounding brain, which leads to greater risk of long-term complications (Alexander & Tolbert, 2006). Thirdly, recanalisation can occur after embolisation in 2 to 19% of the AVM cases, especially if polyvinyl alcohol particles are used (Gobin et al., 1996; Henkes et al., 1998; Mathis et al., 1995). Proximal obliteration of the main feeding vessels without occlusion of the nidus itself can lead to an increase in the haemodynamic stress in the adjacent small vessels and also higher blood pressure into the unobliterated area of the AVM resulting in stimulation of vessel growth (Deruty et al., 1993; Miyachi et al., 2000).

Embolisation morbidity and mortality rates can vary from 6 to 28% and 1 to 8% respectively (Haw et al., 2006; Ledezma et al., 2006; Raymond et al., 2005). In retrospective studies, complications from embolisation have been reported in 6 to 14% of the cases, although most

of the problems are minor complications related to catheterisation. Major ICH and death have been reported however (Hartmann et al., 2002; Taylor et al., 2004; Weber et al., 2007).

1.7.3 Stereotactic radiosurgery

Stereotactic radiosurgery (SRS) has been used for more than three decades to treat patients with AVMs (Colombo et al., 1994; Friedman et al., 1995; Kjellberg et al., 2010). The principal of radiosurgery is the delivery of a highly focused radiation dose to the AVM nidus while the surrounding normal brain tissue receives a minimal dose (Barr & Ogilvy, 2012). The ionising radiation dose in International System of Units (SI) is Gray (Gy). Gray is defined as one joule of radiation energy that is absorbed by one kilogram of matter (Khan, 1994).

SRS is a good therapeutic option for AVMs smaller than 3 cm in diameter and located in an eloquent area where it cannot be removed by surgery without risk of neurologic deficit (Friedlander, 2007). This technique is suited for lesions located in central structures, such as the brain stem, thalamus, and basal ganglia. In comparison to surgery, SRS is less invasive and is more tolerable for children, although it should be considered that the neurological tissues are still developing in children and there is a risk of long-term side effects from ionising radiation (Yen & Steiner, 2011).

AVMs smaller than 15 mL in volume are considered for single-stage radiosurgery treatment and those with 15 mL or more volume are considered for volume-staged radiosurgery (also called fractionated radiosurgery). With volume-staged radiosurgery the volume is divided into 7 − 15 mL portions for two or three treatment sessions five to six months apart (Lunsford et al., 2008). Fractionated radiosurgery (2 − 4 Gy per fraction with a total dose of up to 50 Gy) leads to slow obliteration and significant side effects (Karlsson et al., 2005).

The dose that is considered for treatment of an AVM depends on many aspects such as the AVM volume, location, pre-existing neurological conditions, bleeding history and estimated adverse radiation risks. In a single session, the dose that is allocated for the margin of the AVM typically ranges from 16 to 25 Gy. It is important that the normal tissue surrounding the nidus have no radiation damage (Lunsford et al., 2008). There is an inverse relationship between the safe marginal radiation dose and AVM volume (Sun et al., 2011).

There are factors positively affecting the post-radiosurgery AVM obliteration rate including smaller AVM volume (odds ratio = 1.25; 95% CI, 1.03 − 1.52), larger marginal dose (odds

ratio = 0.29; 95% CI, 0.1 − 0.82), pre-treatment haemorrhage (p = 0.042) (Choi & Mohr, 2005; Sun et al., 2011), smaller radiosurgery-based grading score and larger embolised nidus volume (Flickinger et al., 1997). It has been shown that both haemorrhage (Carmichael et al., 2008) and high dose gamma radiation (Major et al., 2002) lead to activation of transforming growth factor-β (TGF-β) signalling that causes myoblast proliferation and fibroblast transformation. Therefore the inflammatory response as a result of both radiation and haemorrhage can potentially have an effect on occlusion of the abnormal lesion (Sun et al., 2011). In contrast, retrospective studies have shown that embolisation and large AVMs are negative predictors of AVM obliteration. According to Flickinger *et al.* (Flickinger et al., 2002), embolisation can result in target missing for radiosurgery as it may lead to difficulties in visualising the AVM nidus on MRI. Moreover, larger AVMs inherently are harder to treat (Sun et al., 2011). Factors such as the patient's age, sex, time interval between embolisation and radiosurgery, manifestation of the disease and the marginal prescription isodose have no association with AVM obliteration (Izawa et al., 2009).

Several studies reported the occlusion rate for small AVMs to be 90% or better and for large AVMs to be 30% during the latency period of 1 − 3 years (Friedman et al., 2003; Karlsson et al., 1997). The obliteration rate at 5 years for hypo-fractionated stereotactic radiosurgery is 61% and for stereotactic radiosurgery is 81% (Chang et al., 2004). The reported rate of obliteration in children post-radiosurgery ranged from 45 to 86% (Brown et al., 1996; Iwama et al., 2002; Stapf et al., 2003).

Radiosurgery is not without limitations. Larger AVMs are not amenable to this treatment, as they require higher doses of radiation, which can have serious off-target effects. Moreover, after radiosurgery it takes up to 2 − 4 years for complete occlusion of an AVM and during this latency period, the risk of haemorrhage remains constant (Pollock et al., 2003; Söderman et al., 2003). Outcomes after SRS are dependent on the patient's age, nidus volume and location (Pollock & Flickinger, 2002). Adverse effects of radiosurgery include short-term complications such as nausea as a result of pain medication and headache from the frame, also the possibility of a small increased risk of seizure in patients with cortical lobar AVMs, which is most pronounced in patients with a history of episodic seizures (Flickinger et al., 2000; Flickinger et al.,1998; Pollock et al., 1996). After complete obliteration of AVMs, delayed complications due to radiosurgery can occur such as risk of temporary or permanent radiation injury to the brain; cyst formation (Hara et al., 1998; Kihlstrom et al., 1997; Pollock & Brown,

2001); radiation necrosis; persistent oedema; radiation-induced tumours (Kaido et al., 2001; Labatts et al., 2001; Pollock et al., 2003; Sanno et al., 2004); and haemorrhage (Lunsford et al., 2008). Factors that can have an effect on haemorrhage rate post-radiation are intranidal or paranidal aneurysms, minimum dose and complete coverage (Choi & Mohr, 2005). Factors that can increase the risk of haemorrhage in patients after radiosurgery are large AVM size and higher age (Karlsson et al., 2001). In a study involving 312 patients who underwent radiosurgery, Pollock *et al.* noted the annual actuarial haemorrhage rate in the first 2 years was 4.8% (95% confidence interval, 2.4 – 7%) and in the third to fifth years was 5% (95% confidence interval, 2.3 – 7.3%) (Pollock et al., 1996). In a retrospective study of 500 AVM patients with radiosurgery treatment, Maruyama *et al.* noted that the risk of ICH decreased by 54% during the latency period and by 88% after obliteration (Maruyama et al., 2005). In another study shown by Sun *et al.*, annual risk of haemorrhage post radiosurgery was 2.2% and the mortality rate was 0.6 – 1.3 % (Sun et al., 2011).

A grading system for radiosurgery was developed at the Gamma Knife treatment centre (the Mayo clinic) based on patient's age, AVM size and location to predict the outcome after GKS treatment for large patient populations (Flickinger et al., 2000). The grading system predicts a decreasing probability for excellent SRS outcomes (unchanged neurological function and nidus obliteration) with increasing AVM score. With a score of 1, the probability of excellent outcome is 90%, with a score of 1.5 and 2, the probability is 70% and 50%, respectively (Flickinger et al., 1999).

Stereotactic radiosurgery – definition and types

In general, there are three different modalities for SRS: Gamma Knife; linear accelerator (LINAC; e.g., CyberKnife, Synergy S, and Trilogy); and proton-beam (Fleetwood & Steinberg, 2002). All the modalities use stereotactic apparatuses such as a head ring or real-time imaging of landmarks. Cerebral angiography, stereotactic MRI or CT are used to localise an AVM nidus for treatment planning. Specialised software is applied for dose planning (Yen & Steiner, 2011). Stereotactic radiosurgery allows precise radiation delivery to the target tissue with an accuracy of around 1 mm (Figure 1.4) (Maciunas, 1996; Pollock et al., 2000).
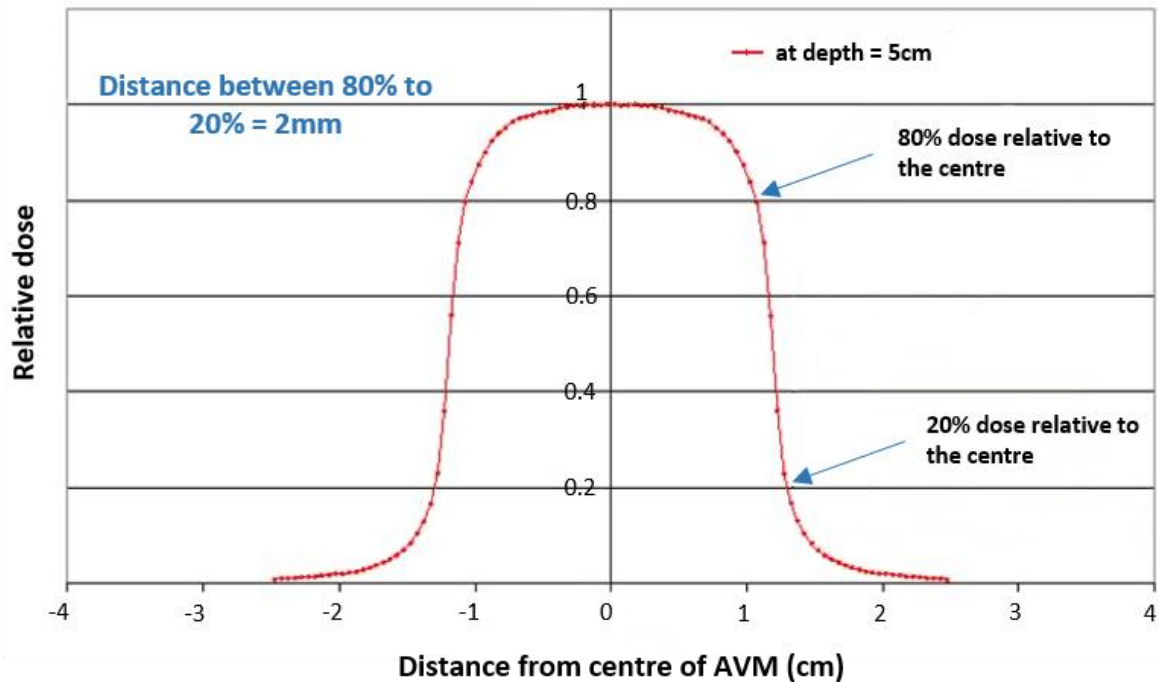
Figure 1.4. Radiation dose distribution with radiosurgery, showing a high dose at the AVM area with an accuracy of < 1 mm and a sharp drop-off of dose to the surrounding tissues. A normal dose range for AVM treatment is 20 to 25 Gy. Figure courtesy of Professor Marcus Stoodley.

1.7.3.1 Gamma Knife

The Gamma Knife was invented by Lars Leksell in 1967 and treatment using this machine is referred to as Gamma Knife surgery (GKS) (Leksell, 1951). GKS uses radioactive cobalt (^{60}Co) sources for the administration of gamma rays through an array of ports that focus the beams at a single target volume (Figure 1.5). Gamma rays are collimated at two locations with two sets of collimators: one close to the cobalt sources and the other one on a stereotactic frame that fixes to the patient's head (Phillips et al., 1994). The collimators' size on the stereotactic frame can be altered, which leads to different dose distributions. The dose is controlled based on the duration of target exposure to the cobalt source (Phillips et al., 1994). The first AVM patient was treated in 1970 in Stockholm (Steiner et al., 1972).
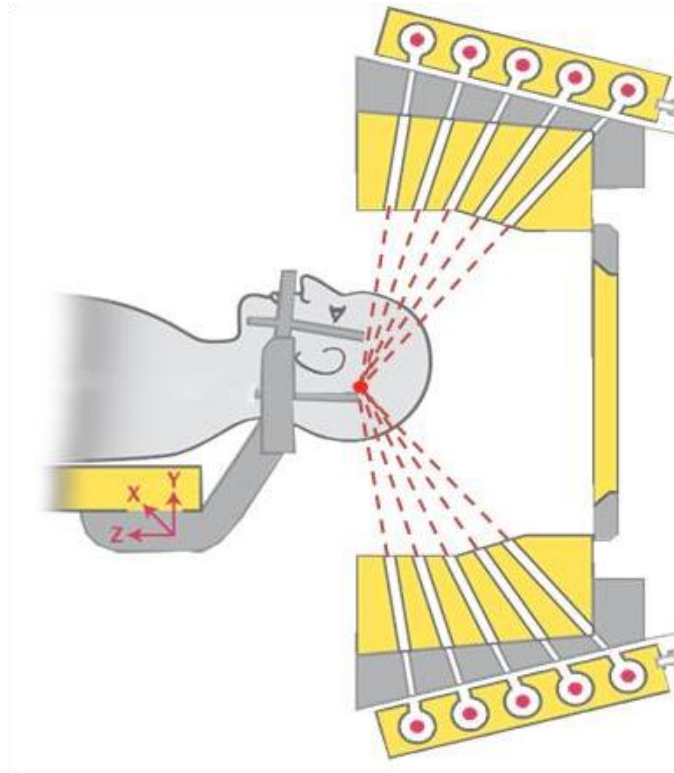
Figure 1.5. Gamma Knife surgery treatment. Gamma rays focus on the AVM from multiple directions. Figure courtesy of Professor Marcus Stoodley.

1.7.3.2 Linear accelerator

The first AVM patient was treated with a Linear accelerator (LINAC) in 1985 (Ogilvy, 1990). A LINAC uses the acceleration of electrons to produce X-ray beams directed at the target area (Blamek et al., 2011; See et al., 2012). A stereotactic LINAC machine delivers convergent arcs focused on the isocentre (Lutz et al., 1988; Podgorsak et al., 1989). The target receives the highest dose at the isocentre which drops off in the adjacent normal tissue (Phillips et al., 1994).

1.7.3.3 Proton-beam

Proton-beam therapy was used for AVM treatment first at Lawrence Berkeley and Harvard Cyclotron Laboratories (Ogilvy, 1990). Proton-beam therapy administers accelerated heavy charged particles to the target area by synchrotron (See et al., 2012). Proton energy follows the law of exponential decay. As a result, its energy is passed to the target without changing, before or after reaching the target (Barr & Ogilvy, 2012). The dose received by the tissue is roughly constant with depth until near end of the particle range at which the dose reaches its highest and immediately drops off to zero. The near end of the particle range is referred to as

the Bragg Peak. The Bragg peak for protons and helium ions is around 16 cm depth in water. The location of the Bragg peak in the brain is used to precisely shape the dose distribution. Normally around three to five different charged particles are used to achieve a uniform dose distribution for an irregular target volume (Khan, 1994).

1.8 Possible new biological therapies for AVMs

Large and deep AVMs are challenging for treatment with any of the current methods. They can sometimes be approached by combination therapies, but a population of patients remains untreatable (Lunsford et al., 2008). Patients with high grade AVMs (IV-V) account for one third of AVM patients and over 90% of them are untreatable (Han et al., 2003). Of the 25% of grade III AVM patients, many are not treatable without high risk.

All current treatment modalities for AVMs have limitations. Surgery is not applicable for large lesions located in critical areas of the brain or involving deep perforating arteries (Ferch & Morgan, 2002). Moreover, it carries a risk of perioperative death or disability (Spetzler & Martin, 1986). Radiosurgery treatment requires $1 - 3$ years for complete obliteration to occur, but during this latency period the risk of haemorrhage remains (Friedman et al., 2003). Additionally, only lesions less than 10 mL in size (2.6 cm in diameter) can be effectively and safely treated without conveying damage to the surrounding cells (Friedman et al., 2003). Endovascular embolisation is usually not able to achieve complete occlusion unless it is carried out with either radiosurgery or surgery (Han et al., 2003).

Therefore, there is an urgent need for new treatment methods for these patients with life-threatening AVMs that cannot be either safely or effectively treated with the existing treatment methods.

It is unlikely that advances in surgical technique can open new paths for removing AVMs in eloquent regions of the brain, or lesions involving perforating arteries. Endovascular embolisation does not seem promising for large AVMs with hundreds of feeding arteries that also supply normal areas of the brain, even with the introduction of new occluding substances. Advances in radiosurgery technique, in spatial delivery of the radiation beam to the AVM target area, may slightly improve the treatable size of AVMs.

A theoretically attractive method for treating large and deep AVMs in functional areas of the brain is new biological and molecular therapies. One of these therapies is gene therapy that

could address the inherent phenotypic abnormalities of the AVM vessels, although by this approach it is unlikely to eliminate the AVM fistula. A biological technique that can be harnessed to increase the rate of occlusion or thrombosis inside the AVM blood vessels is highly attractive. A proposed new therapy that can fulfil this goal is vascular targeting. Vascular targeting has been used in the field of cancer therapy to induce thrombosis inside tumour vessels (Neri & Bicknell, 2005). By the use of this technique, occlusion occurs inside the tumour vessels which causes tumour cell death as a result of ischemia and extensive necrosis (Thorpe, 2004).

1.8.1. Vascular targeting

A promising approach to cancer treatment is to cut off the tumour's nutrient and oxygen supply from the blood (Hu et al., 2003). A therapy that can fulfil this goal is vascular targeting: the selective targeting of tumour vessels. Damage and destruction of endothelial cells of solid tumours induces local thrombosis in tumour vessels leading to tumour cell death from ischaemia and extensive haemorrhagic necrosis (Gerber et al., 2009; Thorpe, 2004).

Vascular targeting therapy relies on inherent physical and molecular differences between tumour endothelial cells and normal endothelial cells. A successful vascular targeting therapy can be achieved by identifying pathophysiological differences between the tumour and normal tissue (Gerber et al., 2009). The difference between tumour and normal tissue includes: increased proliferation rate of tumour cells; increased tumour vascular permeability; lack of associated pericyte cells; and tumour reliance on tubulin cytoskeleton for cell shape maintenance and functional integrity (Darland & D'Amore, 1999; Denekamp, 1982; Denekamp, 1990; Jain, 2003; Jain, 2005; Neri & Bicknell, 2005). There are also a number of molecules that are expressed in higher amounts in tumour vessels compared to normal vessels. These include: molecules involved in vascular remodelling and angiogenesis; molecules associated with prothrombotic changes; and cell adhesion molecules induced by inflammatory mediators, such as tumour necrosis factor-α (Thorpe, 2004).

For vascular targeting therapy, a vascular targeting agent (VTA) is required. This was first introduced by Juliana Denekamp in the early 1980s (Denekamp, 1982; Denekamp, 1993). The VTAs are divided into two main groups: small molecule VTAs and ligand-directed VTAs (Thorpe et al., 2003; Thorpe, 2004).

Small molecule VTAs are low molecular weight compounds that exploit the inherent biological and molecular differences between tumour endothelial cells and normal endothelial cells to result in selective targeting of tumours (Thorpe et al., 2003; Thorpe, 2004). Small molecule VTAs are either microtubule destabilising agents or cytokine inducers. As microtubule destabilising agents, VTAs prevent the proliferation of the tumour endothelial cells as they rely on the tubulin cytoskeleton for maintaining their cell shape. Tubulin-binding agents have anti-vascular and anti-mitotic effects that cause reduced tumour blood flow and disruption of spindle formation (mitotic arrest), respectively (Nihei et al., 1999). Examples of microtubule destabilising agents are Combretastatin A-4 disodium phosphate and the phosphate pro-drug of *N*-acetylcolchinol (Thorpe, 2004). Examples of cytokine-inducing VTAs include flavonoid (FAA) and the flavonoid analogue (5,6-dimethylxanthenone-4-acetic acid; DMXAA) (Jameson et al., 2003; Kerr et al., 1986).

Ligand-directed VTAs use a targeting ligand to achieve selective targeting of tumour endothelial cells (Gerber et al., 2009). This type of VTA requires a targeting moiety and an effector moiety. The targeting moiety is an antibody, peptide or growth factor that selectively binds to tumour endothelial cells and the effector moiety induces thrombosis inside the tumour vessels. The effector moieties include cytokines, cytotoxic agents, coagulation-inducing proteins, immunotoxins (e.g., monoclonal antibodies to endoglin conjugated to ricin A), fusion proteins (e.g., vascular endothelial growth factor linked to the plant toxin gelonin), and liposomally encapsulated effectors (Neri & Bicknell, 2005). The effector moieties can either directly or indirectly cause thrombosis inside the tumour vessels. They indirectly cause thrombosis by killing endothelial cells or changing the shape of endothelial cells leading to physical blockage of the tumour vessels. Targeting and effector moieties are linked together via chemical cross linkers or peptic bonds. An advantage of ligand-based VTAs is that they cause little or no systemic toxicity (Thorpe, 2004).

The potential of vascular targeting therapy has been confirmed as a cancer therapy in experimental studies. Preclinical studies have shown that VTAs can enhance the effect of other cancer therapies, including radioimmunotherapy, anti-angiogenic agents, hyperthermia, conventional chemotherapeutic agents and radiation. Studies have shown that VTAs can induce necrosis in 95% of tumours (Thorpe, 2004). VTAs lead to reduction in tumour blood flow and eventually necrosis of the tumour cells in experimental tumours. They resulted in more successful outcomes in larger tumours than in small tumours (Thorpe, 2004).

Applying this technique for AVM treatment requires the presence of highly specific molecular markers on the surface of the AVM endothelial cells that can be targeted with antibodies carrying pro-thrombotic agents that can cause thrombosis inside the AVM vessels. To pursue this, a deep understanding of AVM morphology and molecular biology is required.

1.9 Normal and arteriovenous malformation vessel morphology

1.9.1 Morphology of the blood vessel wall

The normal blood vessel wall is composed of three layers or tunics. From outside to inside they are called: tunica adventitia; tunica media; and tunica intima (Ross et al., 1995). The tunica adventitia consists of connective tissue and collagen fibres. The tunica media is comprised of elastic fibres and circularly arranged smooth muscle cells (Ross et al., 1995). The tunica intima is made up of a specialised squamous cell layer, often called the endothelium. Endothelial cells line all the blood vessels as well as the endocardium of the heart. The endothelial layer is supported by a subendothelial layer comprised of connective tissue (mainly collagens IV, V, and laminin), called the basement membrane (Fajardo, 1989; Weibel & Palade, 1964).

1.9.1.1   Structure and Function of Arteries, Capillaries, and Veins

The arteries need to be stronger and more elastic than veins and capillaries, as they withstand the force of the heart's pumping action in its entirety. They are therefore exposed to higher blood pressure than veins and capillaries and they have the thickest tunica media. The smooth muscle cells in the tunica media help the arteries to constrict and dilate while the elastin helps them to stretch and recoil (Figure 1.6 A) (Ross et al., 1995).

Capillaries are the smaller vessels that link arteries and veins with a responsibility of nutrient and waste exchange between the blood and the interstitial fluid. As a result their wall is comprised of only one layer of squamous endothelial cells that are supported by the basement membrane (Allt & Lawrenson, 2001).

When the blood reaches the veins, after transit through a capillary bed, it has lower blood pressure than arteries. As a result, veins have thinner walls and a larger lumen than arteries. Therefore in veins the heaviest wall layer is the tunica adventitia which is generally thicker than the tunica media (Ross et al., 1995).

1.9.1.2 Endothelial cells

Endothelial cells lining all the blood vessels play a key role in blood vessel integrity and normal function (Fajardo, 1989). Endothelial cells are the interface between the blood and parenchyma, playing an important role in homeostasis (Guo et al., 2008). Also, endothelial cells have special functions in coagulation, permeability, inflammation and immune responses, vascular tone regulation, synthesis of stromal components and angiogenesis (Fajardo, 1989). Any damage to endothelial cells that can be triggered by inflammation or other chemical or physical insults, can lead to endothelial cell death (Fisher, 2008). Clinical studies and animal experiments have shown that injury or death of brain microvasculature contributes to inflammatory, ischaemic, and degenerative disorders of the central nervous system (del Zoppo, 2006; Hamel et al., 2008; Hawkins & Davis, 2005).

Brain endothelial cells in comparison to endothelial cells from vessels of peripheral organs have unique morphological and functional properties (Aird, 2007). Cerebral endothelial cells have tight junctions between the cells with no fenestrations (Kniesel & Wolburg, 2000). Cerebral endothelial cells have an electrical resistance of $1000 - 2000$ Ωcm^2 which is 100 times more than peripheral endothelial cells (Crone & Olesen, 1982). Brain endothelial cells possess a low number of pinocytotic vesicles and an increased number of mitochondria which limit transcytosis and endocytosis (Oldendorf et al., 1977; Sedlakova et al., 1999). These properties of cerebral endothelial cells allow them to transfer oxygen, glucose, and other nutrients faster to the brain. Brain endothelial cells also contribute to the formation of the blood brain barrier (BBB) with the help of perivascular microglia, pericytes, and astrocytes. The blood brain barrier protects the brain from toxic, infectious, environmental, and metabolic insults. It also supplies nutrients and participates in the creation of a parenchymal microenvironment conducive for neuronal activity and function (Hawkins & Davis, 2005). Brian endothelial cells play an important role in neurogenesis at a time of brain development and also in the post-natal period (Carmeliet & Tessier-Lavigne, 2005; Shen et al., 2004). Brain endothelial cells have essential roles in haemostasis, brain development, maturation, and disease processes (Rizzo & Leaver, 2010).

More detail on brain endothelial cells is out of the scope of this thesis although a number of important endothelial molecules that are relevant to this thesis and are involved in inflammation and apoptosis are covered in more detail in subsequent sections.

1.9.2 Arteriovenous malformation vessel components

1.9.2.1 Arteriovenous malformation vessel morphology

In AVMs, the abnormal conglomerations of dilated veins and arteries, loss of normal vascular organisation at the sub-arteriolar level and lack of a capillary bed, lead to abnormal arteriovenous shunting (Friedlander, 2007). Arteriovenous shunting results in medial hypertrophy at the nidus site, which makes differentiation of arteries and veins difficult (Choi & Mohr, 2005) and also leads to abnormal vessel walls (Mandybur & Nazek, 1990). The feeding arteries are often thickened but the walls generally have a normal ultrastructure (Wong et al., 2000). The small arteries in AVMs can be deficient in the smooth muscle layer (Mandybur & Nazek, 1990).
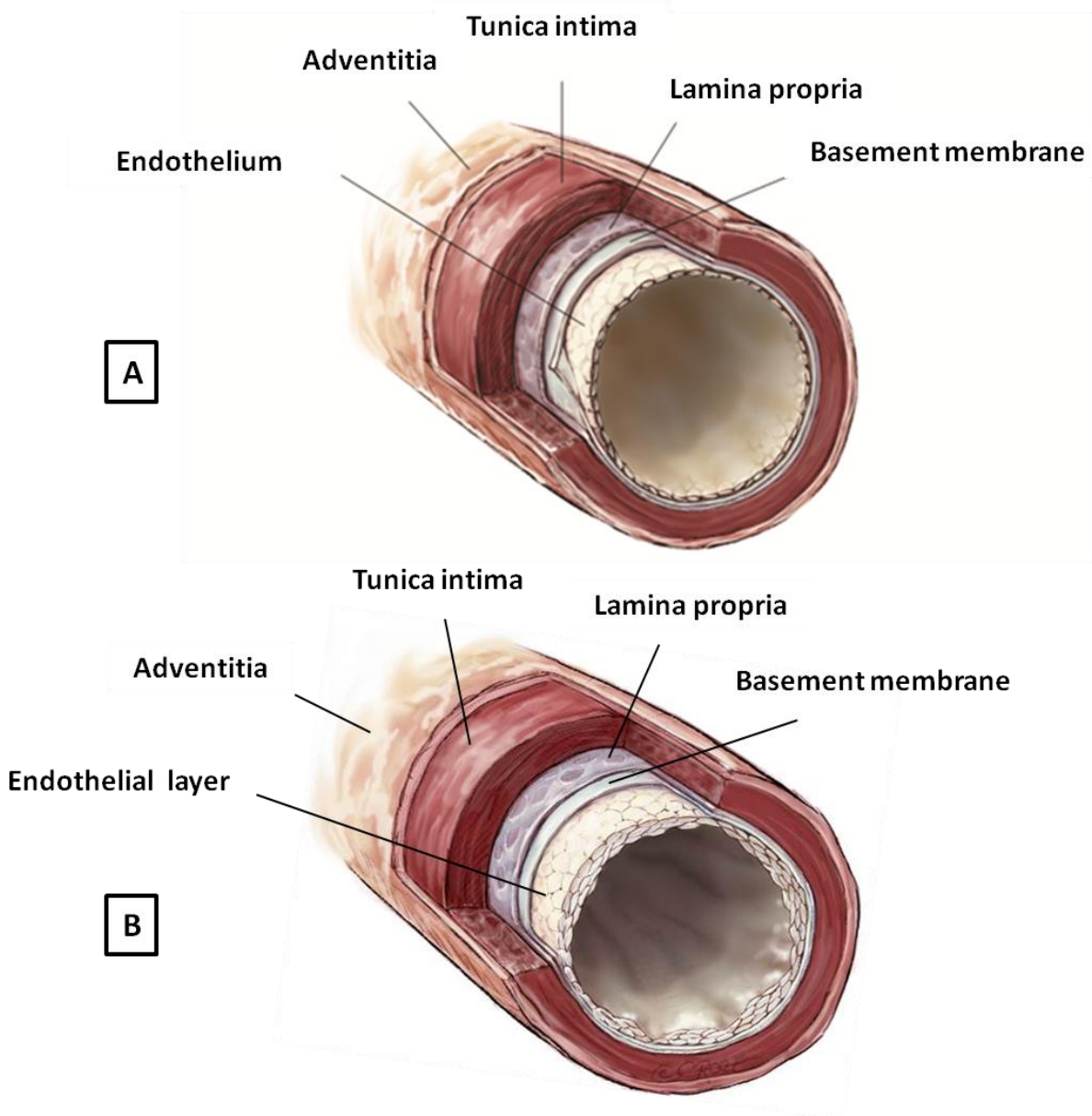
Figure 1.6. Morphology of (A) normal artery with one endothelial layer and (B) an AVM artery with several endothelial layers. Figure courtesy of Professor Marcus Stoodley.

Nidus vessels have alternating thick and thin wall segments (Tu et al., 2006). The direct connection between arteries and veins results in high pressure blood in the veins which leads to fibromuscular thickening and deficient elastic lamina (Friedlander, 2007). The mass of vessels in the nidus is usually embedded in gliotic parenchyma with a diffuse astrocyte proliferation (Karunanyaka et al., 2008). The veins in the nidus present some artery-like characteristics, with a fibro-hyalinised internal elastic lamina and varying thickness of tunica media (Karunanyaka et al., 2008).

1.9.2.2 Arteriovenous malformation endothelial cells

In addition to the morphological changes that exist between normal blood vessels and AVM blood vessels, there are also differences at the molecular and cellular level (Karunanyaka et al., 2008). Endothelial cells in AVMs can form multiple layers (Figure 1.6 B) (Tu et al., 2010). They also show immature features, including many filopodia on the luminal surface, lysosomes, fenestrated processes, cytoplasmic vesicles and vacuoles on the discontinuous endothelial lining (Tu et al., 2010).

There are up to 900 genes that are reported to have altered expression associated with AVMs (Lim et al., 2006). These genes encode cell adhesion and extracellular matrix factors, inflammatory factors, growth factors, endocrine hormones, and matrix metalloproteinases (Moftakhar et al., 2009).

The level of proliferative markers, namely Ki-67, nestin, and proliferating cell nuclear antigen (PCNA), are greater in AVM endothelial cells compared to normal brain endothelial cells (Hashimoto et al., 2001; Shimizu et al., 2006). Expression of vascular endothelial growth factor (VEGF), a growth factor responsible for vasculogenesis and angiogenesis, is elevated in AVM endothelial cells (Hatva et al., 1996; Kiliç et al., 2000; Rothbart et al., 1996; Sonstein et al., 1996). The expression of a specific receptor of VEGF called vascular endothelial growth factor receptor 1 (VEGFR-1), is increased in the endothelium of AVMs (Koizumi et al., 2002). This receptor is normally only expressed on the vascular endothelium of the developing fetal brain (Sure et al., 2001). Expression of angiopoietin 2 (ANG-2), a deconstructive signal that promotes vascular remodelling or destabilisation, is also up-regulated in brain AVMs (Hashimoto et al., 2001).

There are two main theories regarding the molecular differences between normal endothelial cells and AVM endothelial cells. The first is that AVM endothelial cells have an inherent phenotypic difference to normal endothelial cells. The second theory is that all the observed molecular differences are secondary to the shear stress caused by the high blood flow through the fistula (Jeffree & Stoodley, 2009).

To enable the success of vascular targeting therapy for AVM treatment, there is a requirement for the expression of highly discriminating molecules on the AVM endothelium for targeting. To date however, studies have not identified proteins on the surface of AVM endothelial cells that are significantly different from normal endothelial cells to be targeted with antibodies

carrying pro-thrombotic agents. Therefore, a priming technique is required to introduce molecular changes on the surface of the AVM endothelial cells to qualify them for vascular targeting. A proposed technique is stereotactic radiosurgery (SRS). The precise nature of SRS allows induction of proteins in the specified zone and hence precise localisation of induced targets (Figure 1.7). To have a better understanding of the effect of radiosurgery on endothelial cells, radiation effects on normal vessels and AVM endothelial cells are examined in more detail.
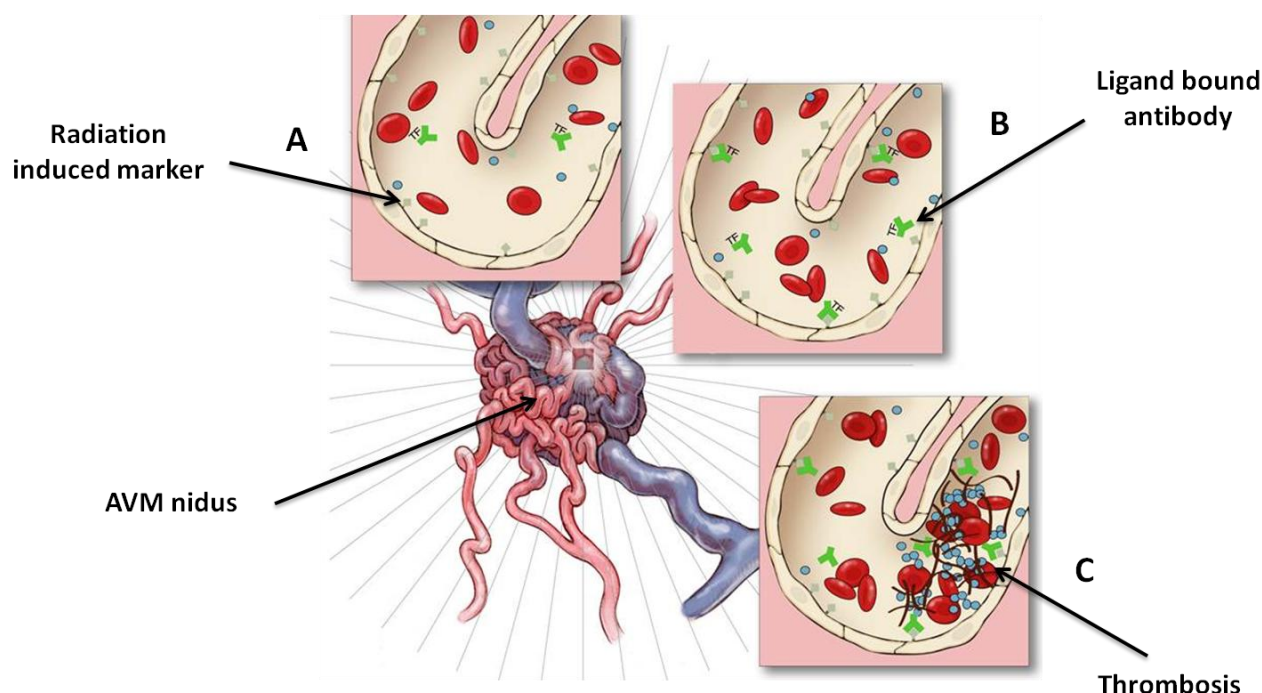
Figure 1.7. Schematic representation of vascular targeting of AVM. (A) Induction of molecular markers on the surface of the endothelial cells after irradiation with Gamma Knife. (B) Ligand binding using an antibody specific for each induced molecular marker, conjugated to a pro-thrombotic molecule. (C) Thrombus formation as a result of locally concentrated pro-thrombotic agent. Figure courtesy of Professor Marcus Stoodley.

1.10 The effect of radiation on normal and AVM vessels

1.10.1 Radiation effects on normal cells

The primary effect of irradiation on cells is DNA damage. DNA injury can either cause irreversible damage that leads to cell senescence or death. Alternatively, a cell may be fully repaired, or in some situations result in cells with mutations (Elkind & Whitmore, 1967). There is a proportional effect at the DNA level on the cell response to radiation (Hall & Giaccia, 2006). Radiation in general exhibits varied effects on different cell types, according

to their heterogeneity, such as the level of hypoxia, radiosensitivity and proliferation rate (Butterworth et al., 2010). Recent studies have also shown one of the major factors affecting cell response to radiation is cell-to-cell communication post-irradiation when neighbouring cells are irradiated (Prise & O'Sullivan, 2009). Moreover, *in vitro* studies have found that similar doses delivered over a protracted period result in less cell death (Bewes et al., 2008; Ogino et al., 2005; Shibamoto et al., 2004).

In normal tissues, blood vessels are important targets of radiation. Many early and late radiation effects are mediated by vascular injury (Fajardo & Berthrong, 1988; Reinhold & Hopewell, 1980). In blood vessels, the most radiosensitive elements are endothelial cells (Johnson et al., 1982; Prabhakarpandian et al., 2001). Radiation can have acute and late effects on endothelial cells, which can initiate, progress or maintain an injury (Gaugler, 2005).

As a result of acute radiation, endothelial cells may undergo mitotic death or apoptosis (Haimovitz-Friedman & Fuks, 1998). Several studies have shown that radiation higher than 10 Gy can cause endothelial cell apoptosis which has been shown to lead to central nervous system (Pena et al., 2000) and small intestine toxicities (Paris, 2001). Surviving cells can develop altered morphology, including detachment of endothelial cells from the basement membrane and hypertrophy of endothelial cells due to the re-organisation of F-actin filaments (Johnson et al., 1982). In pulmonary microvascular endothelial cells, doses between 6 Gy and 30 Gy led to cytoskeletal disorganisation with changes to actin filaments (Friedman et al., 1986; Onoda et al., 1999). In dermal endothelial cells, a rapid increase in stress fibre formation occurred due to the exposure of these cells to $15 - 20$ Gy doses of radiation (Gabryś et al., 2007; Rousseau et al., 2011). Various studies have demonstrated an increase in endothelial cell permeability for various molecules after irradiation (Graham & Peterson, 1998; Milliat et al., 2008; Ward et al., 1998), however serotonin transport was shown to be decreased (Kwock et al., 1998). In addition, there is increased chemo-attraction for leukocytes and enhanced expression of endothelial cell adhesion molecules (Murray, 1998). Radiation has also been shown to induce hyper-coagulation and platelet aggregation occurring as a result of higher release of von Willebrand factor (vWF), which leads to high tendency for thrombosis (Fajardo, 1998). Radiation also induces secondary effects, thickening of basement membrane, collapse of the microvessel, and prolonged activation of an endothelial phenotype that promotes coagulation, and eventually leads to senescence (Oh et al., 2001). As a result of radiation effects, the environment surrounding the irradiated area becomes a hypoxic, pro-

inflammatory environment. This environmental change can lead to damage in normal cells by inducing necrosis, ischemia, and fibrosis (Corre et al., 2013). Radiation can cause dysfunction of the endothelium by producing oxidants and also accumulation of oxidant-forming neutrophils (Kukielka et al., 1993). Radiation exposure can cause inhibition of angiogenesis, which is more effective if occurring before the angiogenic stimulus rather than following it (Hopewell, 1983; Prionas et al., 1990).

1.10.2 Effect of radiation on the AVM endothelium

The effect of radiation on AVMs has been studied to elucidate the histopathological changes post-irradiation. The effect of radiation on AVMs includes: proliferation of smooth-muscle cells (Tu et al., 2006a) and intimal fibroblasts, vessel wall hyalinisation, accumulation of foam cells, cellular degeneration (Schneider et al., 1997), thrombosis (Steiner, 1986), narrowing of the vessel lumen and eventually obliteration of the blood vessel (O'Connor & Mayberg, 2000; Schneider et al., 1997). Post-radiosurgery, AVM endothelial cells in general go through hypertrophy (Schneider et al., 1997), a high rate of early death, and proliferation of the surviving cells (Steiner & Lindquist, 1987). The effect on AVM endothelial cells is similar to the effect that high doses of radiation have on normal endothelial cells, both in animals and humans (Brant-Zawadzki et al., 1980; Fajardo & Berthrong, 1988).

It has been shown that a significant cause of these changes is due to the induction of inflammation, which possibly involves leukocyte entrapment and infiltration into the irradiated area (Prabhakarpandian et al., 2001). The first step in many inflammatory processes is the leukocyte-endothelial adhesion that is mediated by endothelial cell adhesion molecules (CAMs) (Kukielka et al., 1993).

1.11 Effect of radiation on expression of endothelial cell adhesion molecules

1.11.1 Endothelial cell adhesion molecule (CAM) expression

Endothelial cell adhesion molecules (CAMs) are expressed on the surface of activated endothelial cells and are responsible for leukocyte adhesion through a four-step process. The first step is rolling of leukocytes on the surface of the endothelium, followed by leukocyte activation, firm adhesion to the endothelium, and finally transmigration of leukocytes into the

tissue (Ernst et al., 1987; Lawrence, 1991). For rolling and adhesion of leukocytes on the surface of the endothelium a threshold level of fluid shear stress is required (Lawrence et al., 1997).

Endothelial CAMs include E-selectin, P-selectin, intercellular adhesion molecule 1 (ICAM-1), and vascular cell adhesion molecule 1 (VCAM-1) (Kalogeris et al., 1999). E-selectin and P-selectin mediate the initial tethering of the leukocytes to the endothelium, whereas ICAM-1 and VCAM-1 are involved in firm and irreversible adhesion of leukocytes to the endothelium (Springer, 1990). Inflammatory stimuli (e.g. cytokines, reactive oxidant metabolites, oxidised lipoproteins, endotoxin), sheer stress, hypoxia, and ionising radiation can induce transcription, translation, and cell surface mobilisation of endothelial CAMs (Cybulsky & Gimbrone, 1991; Khan et al., 1995; Prabhakarpandian et al., 2001; Read et al., 1995; Storer et al., 2008).

1.11.1.1 E-selectin

E-selectin (CD62E or endothelial leukocyte adhesion molecule 1 (ELAM-1)) is a member of the selectin family (E-, P-, and L-selectin), a family of cell surface glycoproteins that is expressed exclusively on the surface of endothelial cells (Bevilacqua et al., 1991; Carlos & Harlan, 1994; Hallahan et al., 1995; Ley, 2001). E-selectin is a C-type lectin (McEver, 1997; Phillips et al., 1990; Stoolman, 1989) of 115 kDa (Pober et al., 1986; Wellicome et al., 1990) that is expressed in response to pro-inflammatory cytokines such as interleukin-1 beta (IL-1β) or tumour necrosis factor-α (TNF-α) (Bevilacqua et al., 1987; Bevilacqua et al., 1989; Montgomery et al., 1991; Nelson & Bevilacqua, 1993; Pober et al., 1986; Wellicome et al., 1990), thrombin, bacterial lipopolysaccharide (LPS) (Bevilacqua et al., 1987; Shankar et al., 1994; Vestweber & Blanks, 1999), reactive oxygen species (ROS) (Kokura et al., 2000), or radiation (Hallahan & Virudachalam, 1997; Hallahan et al., 1996).

E-selectin mediates recruitment and adhesion of a subpopulation of T lymphocytes, monocytes, polymorphonuclear leukocytes, neutrophils (Bevilacqua et al., 1989; Carlos et al., 2014; Graber et al., 1990) eosinophils and basophils to the site of inflammation or injury (Bochner et al., 1991). E-selectin binds to its ligand, a tetrasaccharide sialyl Lewis x (sLe[x.1]; Neu5Acα2,3Galβ1,4 (Fucα l,3)-GlcNAc-) structure that is expressed on the surface of leukocytes (Nelson et al., 1995). SLe[x] binds to the lectin domain at the N terminus of E-selectin in the presence of calcium (Goelz et al., 1990; Martens et al., 1995; Phillips et al., 1990).

The transient interaction between E-selectin and sLe^x causes tethering and subsequent rolling of leukocytes on the surface of vascular endothelium (Lasky, 1992; Springer, 1994). The neutrophil-endothelial interaction is the first step of a complex multistep process in many inflammatory-mediated diseases including ischaemia-reperfusion (Granger & Kubes, 1994), sepsis (Xu et al., 1994), and atherosclerosis (Steinberg, 1987).

Expression of E-selectin *in vitro* requires *de novo* synthesis of both RNA and protein (Nelson & Bevilacqua, 1993). Induction of E-selectin expression in response to cytokine stimulation occurs relatively rapidly *in vitro*. The peak expression of E-selectin in human umbilical vein endothelial cells (HUVEC) *in vitro* was shown to occur within 4 – 6 h of activation and returning to basal levels after 16 – 24 h (Nelson & Bevilacqua, 1993). In another *in vitro* study of human endothelial cells, the maximum level of expression of E-selectin was reached at 4 to 6 h after activation which then decreased to basal levels by 24 – 48 h (Bevilacqua, 1993). In the human body it takes 2 – 8 h for E-selectin production after cytokine induction (Bevilacqua et al., 1987). Various stresses within a blood vessel can however alter E-selectin expression. In a study showing that E-selectin expression in endothelial cells was activated by TNF-α, the application of laminar shear stress blocked the expression (Chiu et al., 2004). The E-selectin promoter lacks a shear stress response element, therefore laminar shear stress leads to no expression of E-selectin (Nagel et al., 1994). In contrast, oscillatory shear stress causes E-selectin up-regulation (Chappell et al., 1998).

Radiation can induce E-selectin expression within a similar time frame to cytokine stimulation. Hallahan's group reported up-regulation of E-selectin on HUVEC at 4 h post-irradiation (Hallahan et al., 1997; Hallahan et al., 1996). According to Heckman and colleagues, E-selectin mRNA levels at 6 h and 24 h post-irradiation with either 5 or 10 Gy were increased in human dermal microvascular endothelial cells (HDMEC) (Heckmann, 1998). Another group also showed up-regulation of E-selectin on HDMEC at 5 h and 24 h post-irradiation (Prabhakarpandian et al., 2001). A human brain endothelial cell line showed E-selectin expression post-irradiation with 50 Gy with a peak expression level at 72 h (Sharp et al., 2003).

In vivo, irradiation has also been shown to stimulate E-selectin expression. Irradiation of mice resulted in up-regulation of E-selectin in pulmonary endothelial cells of large vessels within 6 h which decreased to baseline levels within 72 h (Hallahan & Virudachalam, 1997). Immunohistochemical studies showed that expression of E-selectin after radiosurgery in a rat

model of AVM was shown to peak at 24 h and sustained for another 24 h, before gradually reducing to baseline at 84 days (Storer et al., 2010).

1.11.1.2 P-selectin

P-selectin (CD62P), a cell surface glycoprotein of approximately 140 kDa, is also a member of the selectin family (Lasky, 1991; Springer, 1990). P-selectin was previously known as granule membrane protein 140 (GMP-140) or platelet activation-dependent granule to external membrane protein (PADGEM) (Bevilacqua et al., 1991).

P-selectin is produced and typically stored intracellularly in the α-granules of platelets and Weibel-Palade bodies in the vascular endothelium. P-selectin is expressed on the cell surface during cell activation (Pinsky et al., 1996; Vestweber & Blanks, 1999). The cells can be activated by mediators of haemostasis such as thrombin and histamine, but also by inflammation and oxidants such as hydrogen peroxide (H_2O_2) (Hattori et al., 1989; Patel et al., 1991; Smith & Anderson, 1991). Radiation (Hallahan et al., 1999; Hallahan & Virudachalam, 1999; Mollà et al., 1999), viral infection (Etingin et al., 1991), hypoxia (Suzuki et al., 1998; Zhang et al., 1999), hypercholesterolaemia (Scalia et al., 1998), and mechanical injury (Hayashi et al., 2000; Kennedy et al., 2000) can also cause P-selectin surface expression. These mediators cause the transient expression of P-selectin on the endothelial surface (Yao et al., 1999) and lead to binding of leukocytes at the site of tissue injury (Geng et al., 1990; Larsen et al., 1989). P-selectin glycoprotein ligand-1 (PSGL-1), a transmembrane o-glycosylated protein, is a P-selectin ligand present on the surface of leukocytes and lymphoid cells (Asa et al., 1995).

Besides making a contribution to the inflammatory process, P-selectin also has important roles in thrombosis and coagulation (Frenette et al., 1995). P-selectin mediates the rolling of platelets on the surface of the endothelium during inflammation (Frenette et al., 1995). P-selectin is responsible for adhesion of platelets to neutrophils and monocytes (Klinger, 1997; Shebuski & Kilgore, 2002) which helps in the communication between thrombotic and inflammatory processes. P-selectin participates in coagulation by binding to tissue factor and leading to acceleration of fibrin formation and deposition (Shebuski & Kilgore, 2002).

There is evidence in the literature for increased surface expression of P-selectin in the vasculature in response to radiation. In one study, thoracic irradiation of mice with doses

between $2 - 20$ Gy led to rapid P-selectin expression in the vascular lumen with subsequent accumulation in endothelial cells of larger vessels in the pulmonary vascular system (Hallahan & Virudachalam, 1997). Another study of mice receiving total body irradiation with $9 - 10$ Gy showed a 3-fold increase in the expression of P-selectin in lung between $10 - 18$ days post-irradiation (Van der Meeren et al., 2003). Increased P-selectin expression was also reported in rat mesenteric vessels post-irradiation (Molla et al., 1999; Molla et al., 2001).

1.11.1.3 Intercellular adhesion molecule 1

Intercellular adhesion molecule 1 (ICAM-1, CD54) is a member of the immunoglobulin superfamily of membrane proteins. Members of this superfamily share the immunoglobulin domain which is comprised of $90 - 100$ amino acids (Alzari et al., 1988; Williams & Barclay, 1988). ICAM-1 is a 90 kDa glycoprotein that is normally expressed at low levels on the surface of unstimulated endothelial cells (Dustin et al., 1986; Pober et al., 1986). Expression can be increased however in the presence of inflammatory stimuli (Pohlman et al., 1986) including tumour necrosis factor alpha (TNF-α), interleukin-1 (IL-1), γ-interferon (γ-IFN), and lipopolysaccharide (LPS) (Dustin & Springer, 1988; Dustin et al., 1988; Springer et al., 1987), that result in firm attachment of leukocytes to the surface of endothelial cells (Farhood et al., 1995; Kukielka et al., 1993; Lawrence & Springer, 1991). The expression of ICAM-1 is also up-regulated in response to radiation (Hallahan & Virudachalam, 1997; Hallahan et al., 1996; Handschel et al., 1999), ultraviolet light (Van de Stolpe & Van der Saag, 1996), lasers (Shen et al., 1998), hypercholesterolemia (Scalia et al., 1998), and shear stress (Nagel et al., 1994; Nomura et al., 2001). The induction of ICAM-1 expression is regulated at the transcriptional level (Roebuck & Finnegan, 1999) and depends on mRNA and protein synthesis (Dustin et al., 1986).

ICAM-1 is also expressed on activated B lymphocytes and follicular dendritic cells (Dustin et al., 1986), epithelial cells, fibroblast-like cells, and macrophages (Roebuck & Finnegan, 1999; Van de Stolpe & Van der Saag, 1996). ICAM-1 binds to two members of the β_2 integrin subfamily that are expressed on leukocytes (Diamond & Springer, 1993; Hogg et al., 2002) namely; macrophage-1-antigen (Mac-1, $\alpha_M\beta_2$; CD11b/CD18) and lymphocyte function-associated antigen-1 (LFA-1, $\alpha_L\beta_2$; CD11a/CD18) (Gahmberg et al., 1999; Hogg et al., 2002; Van de Stolpe & Van der Saag, 1996). ICAM-1 also binds to extracellular matrix components hyaluronan (McCourt et al., 1994) and soluble fibrinogen (Clark et al., 2003; Languino et al., 1995). There is also a soluble form of ICAM-1 present in the plasma, that is elevated in

54

disorders of vascular (Blann et al., 1999; Kerner et al., 2001), inflammatory (Van de Stolpe & Van der Saag, 1996), or malignant origin (Alexiou et al., 2003). Besides participation in the inflammatory process, ICAM-1 also contributes to thrombosis and haemostasis (Bombeli et al., 1998; Etienne et al., 1998; Thompson et al., 2002).

Radiation is well known to induce ICAM-1 expression in various cells and tissue types. Up-regulation of ICAM-1 mRNA levels was caused by ionising radiation of HDMECs at 24 h (Heckmann, 1998). However, there was disagreement in regards to the time course of up-regulation of ICAM-1 on endothelial cells post-irradiation in studies, at 24 h (Hallahan et al., 1996) and 48 h (Gaugler et al., 1997; Haubner et al., 2013; Quarmby et al., 1999). In HUVEC 24 h post-irradiation there was an up-regulation of ICAM-1 (Hallahan et al., 1996) which continued up until at least 10 days post-irradiation (Gaugler et al., 1997). Twenty four hours after a human brain endothelial cell line received a 50 Gy dose of radiation, ICAM-1 expression was up-regulated over four-fold which returned to baseline by 72 h (Sharp et al., 2003). ICAM-1 expression was up-regulated in a human bone marrow endothelial cell line after irradiation with 2 Gy (Gaugler et al., 1998).

More studies provide evidence for ICAM-1 contribution in radiation-induced inflammation *in vivo*. In mice pulmonary microvascular endothelium, ICAM-1 expression was increased 24 h after receiving radiation as low as 2 Gy that was sustained for several days. Post-irradiation, inflammatory cells then migrated into the lung. Larger vessels showed minimal ICAM-1 expression (Hallahan & Virudachalam, 1997). In mice treated with anti-ICAM-1 antibody there was a significant decrease in the inflammatory response of lung post-irradiation (Hallahan & Virudachalam, 1997). In another study of the effect of radiation on pulmonary vascular endothelium, mice received thoracic radiation of 20 Gy and showed up-regulation of ICAM-1 at 80 days post-irradiation (Epperly et al., 2002). Furthermore, the significant role of ICAM-1 in leukocyte rolling and adherence after irradiation was demonstrated in the study of mesenteric vasculature by intravital microscopy. In this study leukocyte rolling and adherence to endothelium was increased at 2, 4 and 6 h post-irradiation of rat abdomen with 20 Gy (Panes et al., 1995). Gaber *et al.* demonstrated that blockade of ICAM-1 reduced rolling and migration of leukocytes on rat pial vessels after 24 h and 48 h of cranial irradiation with 20 Gy (Gaber et al., 2004).

1.11.1.4 Vascular cell adhesion molecule 1

Vascular cell adhesion molecule 1 (VCAM-1, CD106) is a 110 kDa membrane protein. Like ICAM-1, it is part of the immunoglobulin superfamily (Bevilacqua, 1993; Rice & Bevilacqua, 1989; Rice et al., 1990; Rice et al., 1991) that is important for vasculogenesis and leukocyte adhesion (Storer et al., 2008). Members of the immunoglobulin superfamily share the immunoglobulin domain that consists of $90 - 100$ amino acids (Alzari et al., 1988; Williams & Barclay, 1988) and VCAM-1 has seven immunoglobulin domains (Cybulsky et al., 1991). VCAM-1 mediates the interaction of endothelial cells with monocytes, lymphocytes, (but not neutrophils), eosinophils, and basophils (Bochner et al., 1991; Dobrina et al., 1991; Schleimer et al., 1992). The interaction is through integrin α4β1 (VLA-4; CD49d/CD29) (Graber et al., 1990; Oppenheimer-Marks et al., 1991) and α4β7 that leads to extravasation of the white blood cells from blood vessels.

VCAM-1 expresses predominately on endothelial cells with constitutive expression on tonsils, testis and thyroid endothelial cells (Rice et al., 1991). VCAM-1 is also expressed on bone marrow stromal cells, synovial cells in inflamed joints, dendritic cells of lymph node and skin (Miyake et al., 1991; Rice et al., 1991; Ryan et al., 1991; Simmons et al., 1992), smooth muscle cells (Ardehali et al., 1995), epithelial cells (Cybulsky et al., 1991), and astrocytes following ischaemic stroke (Blann et al., 1999). Unstimulated endothelial cells express VCAM-1 at low levels. However, in the presence of inflammatory stimuli including interleukin-1 (IL-1), interleukin-4 (IL-4), and TNF-α, expression of VCAM-1 increases (Carlos et al., 1990; Schwartz et al., 1990; Wellicome et al., 1990). Oscillatory shear stress stimulates VCAM-1 expression on HUVEC cells (Chappell et al., 1998) however, laminar shear stress has no effect (Nagel et al., 1994). The soluble form of VCAM-1 is present in the blood during aging (Richter et al., 2003) and stages of the menstrual cycle can change the concentration (Bonello & Norman, 2002). Also, there can be a significant elevation in response to malignancy (Alexiou et al., 2003) and vascular diseases (Blann et al., 1999; Kerner et al., 2001).

Radiation has been shown to cause up-regulation of VCAM-1 in organ cultures of normal human skin and HDMEC 24 h after receiving 5 or 10 Gy (Heckmann, 1998). In another study by Haubner *et al.* HDMEC showed increase in VCAM-1 expression 48 h after receiving 6 Gy and 12 Gy (Haubner et al., 2013). In primary cultures of murine pulmonary endothelial cells, 20 Gy radiation caused up-regulation of VCAM-1 after 24 h (Epperly et al., 2002). VCAM-1

expression was up-regulated in murine intestinal venules 14 days after receiving 10 Gy (Mollà et al., 2003). In a study where mice received total lung irradiation with 20 Gy, pulmonary vascular endothelium showed moderate and significant expression of VCAM-1 after 80 and 100 days, respectively (Epperly et al., 2002). The expression of VCAM-1 was examined in a rat AVM model after radiosurgery for 84 days, which showed a 50% increase at 21 days that was sustained for the next 3 weeks until it reduced to baseline at 84 days (Storer et al., 2010).

1.11.2 Phosphatidylserine

Since endothelial CAMs show significant expression differences between normal and irradiated endothelial cells, they have the potential to be good candidates for vascular targeting therapy in the context of AVMs. Similarly, other molecules that appear at the cell surface solely in response to stress may provide novel targets.

Phosphatidylserine (PS) is a negatively charged membrane phospholipid that is synthesised by all cell types and comprises approximately 2 – 10% of the total cellular lipid (Vance & Steenbergen, 2005). This molecule is synthesised in the endoplasmic reticulum (ER), in a subcompartment called the mitochondria-associated membranes (MAM), by phosphatidylserine synthases 1 and 2 (PSS1 and PSS2). Synthesis of PS is carried out by base-exchange from phosphatidylcholine (PC) and phosphatidylethanolamine (PE) via PSS1 and PSS2 respectively (Hermansson et al., 2011; Stone & Vance, 2000). During this calcium dependent reaction, PSS1 replaces the choline group of PC with L-serine and PSS2 replaces the ethanolamine group of PE with L-serine (Vance & Steenbergen, 2005; Vance, 2008). PSS1 and PSS2 also catalyse the reverse reaction of PS synthesis (Hermansson et al., 2011). Brain, kidney and testis are the three organs in the body that have a high capacity to synthesise PS (Sturbois-Balcerzak et al., 2001). PS content in the brain is maintained at a level of 13 – 14% throughout life (Svennerholm, 1968).

Phosphatidylserine regulates the activities of nitric oxide synthase (NOS) (Calderón et al., 1994), rapidly accelerated fibrosarcoma-1(Raf-1) protein kinase (Ghosh et al., 1994), and diglyceride kinase (Sakane et al., 1991) which are involved in cell signalling and can also regulate ligand-receptor interactions (Gagne et al., 1996; Mozzi et al., 2003). Phagocytes that are missing the PS receptor (PSR) are not able to remove apoptotic cells (Li et al., 2003). The PSR has also been reported to be involved in respiratory distress (Li et al., 2003) with an

important function in terminal differentiation of the lung and other vital organs (Böse et al., 2004).

Phosphatidylserine is asymmetrically distributed across the plasma membrane and is strictly located on the cytosolic leaflet of the membrane bilayer in most normal cell types, including the vascular endothelium (Balasubramanian & Schroit, 2003; Smrz et al., 2007). The PS asymmetry is maintained by the energy dependent activity of two enzymes called flippase and floppase. Flippase is responsible for inward-directed transfer of PS and floppase is in charge of outward directed transfer of PS (Bevers et al., 1999; Pomorski & Menon, 2006; Pomorski et al., 2004). Another enzyme called lipid scramblase facilitates bi-directional transfer of PS across the bilayer (Zhou et al., 1997). It has been shown that PS externalisation has a direct relationship with the increase of free cytoplasmic calcium $[Ca^{2+}]$, which regulates lipid translocase activity and enhances randomisation of plasma membrane phospholipids (Bevers et al., 1999; Daleke, 2003; Kunzelmann-Marche et al., 2002).

In response to some stimuli, the PS asymmetry is lost, and PS is translocated to the outer leaflet of the plasma membrane (Zwaal et al., 2005). This has been shown to occur during certain biological processes, such as thrombosis (Zwaal, 1978; Zwaal et al., 1977) phagocytosis and apoptosis (Bratton et al., 1997; Fadok et al., 1992; Savill & Fadok, 2000). Reorientation of PS has been observed with aging erythrocytes, activated macrophages, activated platelets, endothelial cells of tumour blood vessels, infected cells, injured cells, apoptotic bodies, apoptotic cells, senescent, and necrotic cells (Balasubramanian & Schroit, 2003; Brouckaert et al., 2004; Hirt & Leist, 2003; Williamson & Schlegel, 2002), cell derived microparticles, stressed tumour cells, hypoxic cardiomyocytes (Schutters & Reutelingsperger, 2010) and irradiated normal endothelial cells (Zhao et al., 2011). Phosphatidylserine is also externalised in certain developmental stages of the cell (Eijnde et al., 2001) and in the process of immune cell activation by various stimuli, including engagement of immunoreceptors (Blank, 2000; Demo et al., 1999; Dillon et al., 2000; Fischer et al., 2006). The nature of this PS externalisation in response to stress makes this molecule a potential candidate for vascular targeting in irradiated AVMs.

1.12 Arteriovenous malformation animal model

To further investigate the effect of radiation on AVM endothelial cells an AVM animal model is required. The AVM model has to mimic the haemodynamic, histological, morphological,

molecular, and ultrastructural characteristics of human AVM blood vessels. A rat model of AVM was chosen as the most suitable model for this research. It is formed by anastomosing the left common carotid artery (CCA) to the left external jugular vein (EJV). The anastomosis leads to retrograde flow in the jugular vein, with dilated branches forming the model nidus. Drainage is into a single vein. The arterial and vein flow can both be assessed by angiography (Tu et al., 2010). A thorough examination of the AVM rat model showed that the arterialised vein had a maximum flow rate 42 days after fistula creation. At this stage the histological structure of the model nidus was also considered mature and represented many characteristics of human AVM vessels (Tu et al., 2010).

The haemodynamic similarities between the rat AVM model and human AVM include a large arterial inflow, a branching nidus, and a single venous drainage (Karunanyaka et al., 2008). The morphological similarities between the rat and human AVM include hypertrophy of the media of the created nidus vessels and an increase in collagen layers (Karunanyaka et al., 2008). There are also histopathological and ultrastructural similarities between the two, such as elastic lamina splitting, endothelium with multiple layers, heterogeneity in vessel wall thickness and vessel size (Tu et al., 2010).

Molecular similarities between the rat AVM model and human AVM have also been demonstrated, including evidence of immature endothelial cells with fenestration, many filopodia on the luminal surface, cytoplasmic vesicle, lysosomes and vacuoles on the discontinuous endothelial lining (Tu et al., 2010). An advantage of this model is that the nidus is static in its position, which enables precise radiation delivery to the malformation and *in vivo* imaging (Tu et al., 2010).

Although the AVM rat model is not perfect, since it is not located in the brain, its similar characteristics with human AVM vessels and in particular the increase in haemodynamic stress, make it a suitable model for studying the effect of radiation on the AVM-like endothelial cells and validating new candidates for vascular targeting therapies (Tu et al., 2010).

Techniques for studying the molecular changes in the model vessels include immunohistochemistry, polymerase chain reaction (PCR) and proteomics. Another technique that has high potential value in this setting is *in vivo* molecular imaging. This technique can

provide information regarding the anatomical location of expression, quantification of expression, and the ability to repeat measurements over time in the same animal.

1.13 *In vivo* molecular imaging

In vivo molecular imaging is a rapidly emerging research discipline with a potential effect on clinical practice and fundamental biomedical research (Liu et al., 2010; Pierce et al., 2008). The field includes a variety of modalities capable of visualising, characterising and quantifying the molecular and cellular processes that are occurring within intact living systems at a macroscopic level (Gompels et al., 2010). Molecular imaging has immense potential benefits in research, providing real-time information for early diagnosis, facilitating studies of therapeutic activity and accelerating the drug discovery process (Dufort et al., 2010; McLarty & Reilly, 2007; Weber et al., 2008). In the context of this study, *in vivo* molecular imaging presents a suitable tool for the validation of target protein expression *in situ*. This method can detect the expression of protein on the luminal endothelial surface as well as showing specific anatomical localisation of expression.

Molecular imaging modalities include magnetic resonance imaging (MRI), ultrasound (US), computed tomography (CT) positron emission tomography (PET), single photon emission computed tomography (SPECT), and optical imaging (OI) (Gambhir, 2002; Massoud & Gambhir, 2003; Pierce et al., 2008).

Optical imaging rapidly gained popularity in research with immense advantages over other modalities. The advantages include low cost, high sensitivity (10^{-12} M), faster imaging for label detection and imaging at the molecular level and most importantly low risk to the living organism as it uses non-ionising radiation (Wunder et al., 2005). Optical imaging is divided into two groups: bioluminescence imaging (BLI); and fluorescence imaging (Gambhir, 2002; Massoud & Gambhir, 2003). Fluorescence imaging is the only modality that is relevant to this thesis and will be covered in more detail.

1.13.1 Fluorescence imaging

Far-red and near infrared fluorophores (NIRF) (fluorophores in the range of 650 – 900 nm) have several advantages over visible fluorophores for imaging living organisms. Advantages include: (1) low tissue autofluorescence; (2) less photon absorption from haemoglobin, lipid, water and tissue, enabling high transmission through the body and deeper detection (typically

60

1 – 2 cm) (Zhao et al., 2011); and (3) low interference of scattered light used for exciting fluorescence (Hawrysz & Sevick-Muraca, 2000). However, conventional NIRF (organic dyes) have several limitations. Firstly, there is a low quantum yield and detection sensitivity because only a small number of fluorophores attach to a ligand. Secondly, there is an insufficient stability in biological systems that enables long-term molecular imaging. There is also unpredictable toxicity. Currently only one fluorochrome (indocyanine green, ICG) has been approved by the Food and Drug Administration (FDA) for clinical use (Harisinghani et al., 2003; Vetrone & Capobianco, 2008).

Advancements in nanotechnology have introduced a new class of probes for *in vivo* fluorescence imaging called NIRF nanoprobes. Nanoprobes can be classified into two major groups: downconversion (DCN) and upconversion (UCN) NIRF nanoprobes. DCN nanoprobes produce low energy fluorescence when excited by a high energy light, typically within the ultraviolet (UV) short wavelength or visible range. Examples of DCN NIRF nanoparticles include NIRF dye containing nanoparticles, quantum dots (QDs), carbon nanotubes (CNTs) and metal nanoclusters (e.g. gold nanoclusters) (Figure 1.8) (He et al., 2010). UCN nanoprobes are emerging as a new class of fluorescent nanoparticles and biolabels (Vetrone & Capobianco, 2008) that are able to convert excitation light with longer wavelength radiation (low energy) to shorter wavelength fluorescence (high energy) (Auzel, 2004; Jiang et al., 2009; Sivakumar et al., 2007).
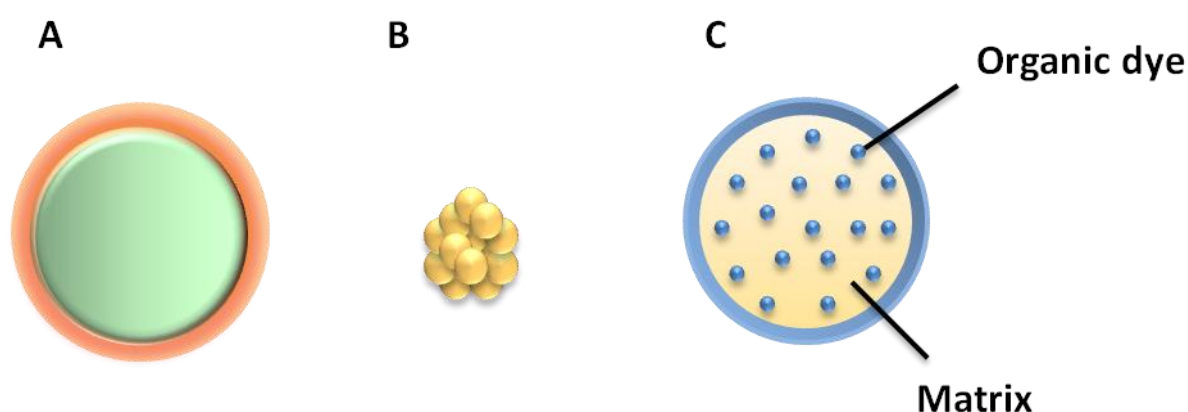
Figure 1.8. Representative nanomaterial-based NIRF nanoprobes for molecular imaging in living subjects (A) Quantum dot. (B) Gold nanocluster. (C) Dye-containing nanoprobes. Adapted from (He et al., 2010).

1.13.2 Fluorescence imaging of PS and endothelial CAMs

A review of the literature suggested that potential candidates for a vascular targeting approach in AVM treatment may include the endothelial CAMs or phosphatidylserine, various probes for these targets were considered for their potential use in fluorescence imaging.

A successful probe for PS molecular imaging would require recognition for PS and binding with great sensitivity and specificity. There are proteins that can bind to externalised PS, namely annexin A5 (annexin V), annexin VI, synaptotagmin I, lactadherin (Krishnan et al., 2008; Smith et al., 2010; Waehrens et al., 2009), T cell immunoglobin mucins and γ-carboxyglutamic acid (GIa) containing proteins (Schutters & Reutelingsperger, 2010). There are also other compounds that can bind to PS including antibodies (He et al., 2009; Luster et al., 2006; Ran et al., 2005), peptides (Burtea et al., 2009; Thapa et al., 2008) and small chemical entities (Hanshaw & Smith, 2005).

Among all ligand proteins, annexin V is a well-known probe for molecular imaging of PS expressing cells due to its availability and molecular weight (36 kDa) (Grosse et al., 2009). Annexin V contains four internal repeats, each including a sequence with a high-affinity calcium-dependent diacyl phosphatidylserine binding site (a K_d in a range of 1.10^{-10} to 7.10^{-9} M-1 has been reported) (Boersma et al., 2005; Ravanat et al., 1992). However, annexin V has some limitations such as biodegradation of the proteins, long residence time in kidneys, and variable degrees of targeting within a single cohort (Beekman et al., 2011; Vanderheyden et al., 2006).

There are commercial antibodies available that are directed against PS (Schutters & Reutelingsperger, 2010). Recently a series of monoclonal antibodies were developed that can bind to externalised PS with higher specificity than annexin V (Luster et al., 2006; Ran & Thorpe, 2002; Ran et al., 2005; Ran et al., 2002). These antibodies are Bavituximab ($K_d \approx 10^{-10}$ M) and PGN635 which are similar in specificity and affinity. They both recognise PS complexed with PS-binding protein, β_2-glycoprotein 1 (β_2GP1) (Luster et al., 2006).

Diannexin (homodimer of annexin V) and Bavituximab are the first PS targeting probes to enter human clinical trials for patients with cancer, HIV, kidney transplant and chronic heptic C virus (Schutters & Reutelingsperger, 2010). Bavituximab is in advanced clinical trials for patients with lung and breast cancer (Digumarti et al., 2010; Tabagari et al., 2009).

Molecular imaging agents, peptides and small chemical entities have the advantage of rapid renal clearance and favourable signal-to-background ratio. However, the disadvantage of these compounds is the low affinity binding for PS. Proteins on the other hand have high affinity for PS but slow clearance from the blood (Schutters & Reutelingsperger, 2010). Also, protein binding probes convey some technical problems, such as poor pharmacokinetics, that limit translation to the clinic (Beekman et al., 2011; Lederle et al., 2011). It is not easy to change the pharmacokinetics of proteins, therefore using low molecular weight imaging probes would be a better option (Xiong et al., 2011; Zheng et al., 2011).

A well-recognised probe that can bind to externalised PS is PSS-794, a zinc (II)-dipicolylamine (Zn^{2+}-DPA) probe (Figure 5.1) containing a near-infrared carbocyanine fluorophore (Hanshaw & Smith, 2005). The Zn^{2+} ions in PSS-974 probe mediate the association of the DPA to the anionic head groups of PS (O'Neil & Smith, 2006). PSS-794 has been used to target PS in a number of rodent models of xenograft tumours, acute muscle damage (Smith et al., 2010; Smith et al., 2011) and thymic atrophy (Smith et al., 2011).

In vivo molecular imaging of ICAM-1 and VCAM-1 was carried out with their specific antibodies conjugated to Xenolight 750, a near infrared fluorescent dye that has been used in the field of *in vivo* molecular imaging for endothelial CAM detection (Gompels et al., 2011).

1.14 Summary

Over one third of AVM patients face the prospect of stroke and have no safe and effective treatment. These patients are in urgent need of new treatment methods. Vascular targeting, with the help of radiosurgery, may open a new path to a successful treatment in this group. The identification and validation of highly discriminating molecular markers on the surface of AVM tissue is required.

Hypothesis

Radiosurgery induces molecular changes on the surface of AVM endothelial cells that are discriminating enough to enable targeting with thrombotic agents to induce localised thrombosis and obliteration of AVM vessels.

Aims

The overall aim of this work is to identify and validate a selection of endothelial surface molecules for their expression after radiation exposure *in vitro* and *in vivo*. The secondary aim is to determine the minimum radiation dose that can induce molecular changes for targeting.

Specific aims for this project were:

Aim 1: To quantify the level of expression of specific cell adhesion molecules (ICAM-1, VCAM-1, E-selectin and P-selectin) in brain microvascular endothelial cells at three different radiation doses of 5, 15 or 25 Gy (*in vitro*) (Chapter 3).

Aim 2: To determine the cellular location of the target molecules (ICAM-1, VCAM-1, P-selectin and E-selectin) after radiation treatment with 5, 15 or 25 Gy (*in vitro*) (Chapter 3).

Aim 3: To determine the anatomical location and level of expression of the most discriminating CAM molecules after irradiation in an animal model of AVM (Chapter 4).

Aim 4: To determine the anatomical location and level of PS externalisation after irradiation in an animal model of AVM (Chapter 5).

Chapter 2. General methods

2.1 Tissue culture experiments

2.1.1 Cell culture

A mouse brain endothelial cell line, bEnd.3 (ATCC, VA, USA), was cultured in Dulbecco's modified Eagle's medium (DMEM) containing 2 mM L-glutamine, sodium pyruvate (110 mg/L), and glucose (4500 mg/L). DMEM was enriched with 10% fetal bovine serum (FBS), penicillin (100 units/mL), and streptomycin (0.1 mg/mL). The cells were maintained at 37ºC in a 5% CO_2 incubator. The cell medium was changed every three days and the cells were passaged with 0.1% Trypsin-EDTA when they reached 80% confluency. All culture supplements were purchased from Sigma-Aldrich, MO, USA.

2.1.2 Linear accelerator irradiation

The cell culture (bEnd.3) was irradiated with X-rays generated by a 6 MV linear accelerator (LINAC) (Elekta Synergy, Crawley, UK) at Macquarie University Hospital (MUH). The cells were irradiated at three different doses (5, 15 or 25 Gy) when they reached 50 – 60% confluence. Cells were irradiated at subconfluence to reflect on the angiogenic characteristic of AVM endothelial cells with an abnormally high proliferative index. The LINAC machine was calibrated according to International Atomic Energy Agency code of practice (IAEA TRS-398). All the cell irradiation work was performed by trained Genesis Care personnel (Ms Jaysree Ukath, Mr Michael Grace, and Mr Yunfei Hu).

Tissue culture vessels (T75 flask, 6-well or 96-well plates or 8-well chamber slides) were filled with culture medium prior to irradiation to enable full scatter conditions. Then the culture vessel was placed on a solid water phantom ($30 \times 30 \times 5$ cm) on the treatment couch and set at the isocentre. The gantry was placed once at 0º and once at 180º to irradiate the samples from both above and below, respectively. The couch was placed in a way that the source to surface distance (SSD) to the couch top and bottom was 100 cm (Figure 2.1). A factor to account for the attenuation of the couch was considered when the calculations for set monitor units (MU) were performed. A 30×30 cm uniform non-modulated field was used. The field was an 'open' field defined by collimators.
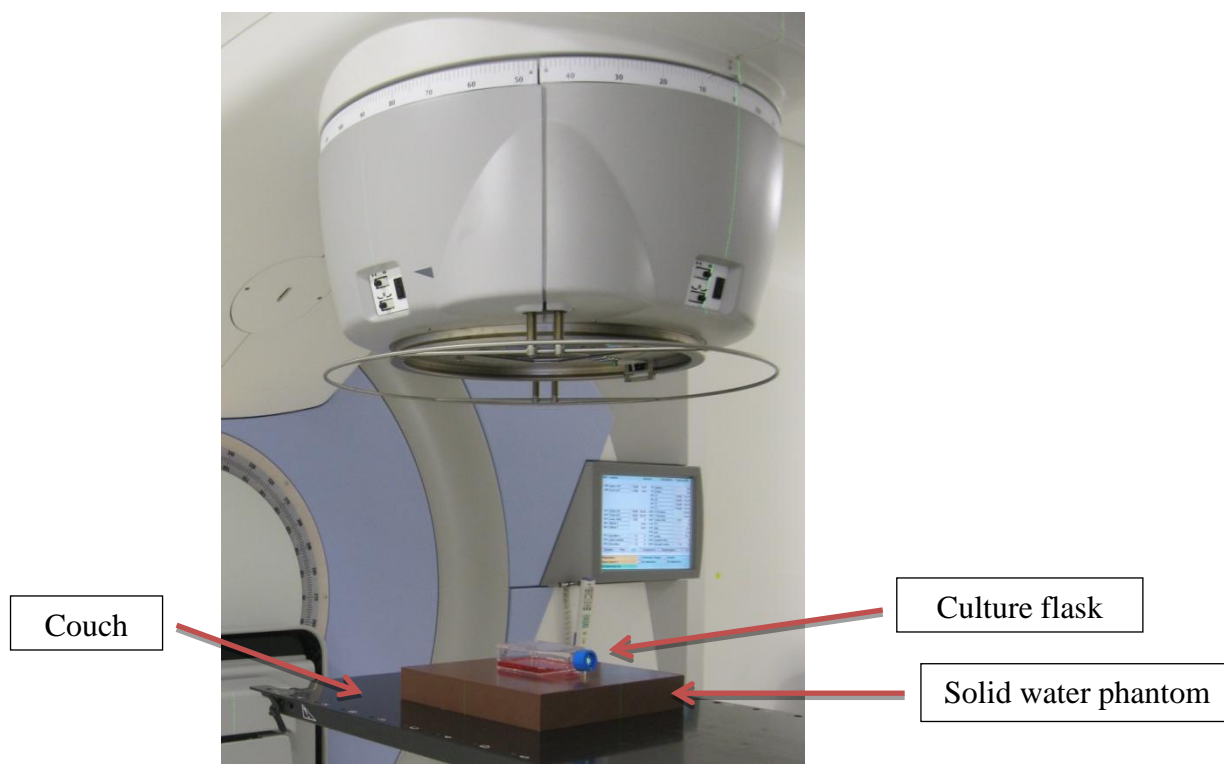
Figure 2.1. Irradiation set up for delivery of 6 MV photons delivered by LINAC machine to a monolayer of bEnd.3 cells in a culture flask.

2.2 Animal experiments

Animal care

2.2.1 Ethics

All animal procedures were approved for animal health, ethics and research by the Macquarie University Animal Ethics Committee (AEC, reference number: $2011/011 - 15$) and were performed in accordance with the Australian Code of Practice for the Care and Use of Animals for Scientific Purposes (8th Edition, 2013).

2.2.2 General

Sprague Dawley rats (n = 62) were received at the age of 5 weeks ($112 - 134$ g) from the Animal Resources Centre (ARC, WA, Australia) and housed at the Central Animal House Facility at Macquarie University. Standard rat cages were used to house a maximum of four rats under a 12 h light-dark cycle with water and food provided *ad libitum.*

2.2.3 Morbidity and mortality

Animals generally tolerated the experimental procedures well. There was no evidence of significant neurological morbidity in any one of the animals. No animal had to be euthanased in the pre-operative or post-operative period.

2.3 Experimental procedures

2.3.1 Anaesthesia and operative care

2.3.1.1 Inhalational anaesthesia and analgesia

Each animal was placed in an anaesthetic induction chamber connected to isoflurane (4%) and oxygen (1 L/min). Anaesthesia was maintained via a nose cone with an anaesthetic concentration of 2 to 3% isoflurane and oxygen flow of 200 mL/min. The hind paw withdrawal and respiration were monitored to ensure the depth of anaesthesia. Animal core body temperature was monitored with a rectal probe and was maintained at 37ºC with a heating pad. During surgery the respiratory rate, core body temperature and response were monitored. At the completion of the surgery a bolus of warm saline (5 mL) was injected intraperitoneally. The isoflurane was turned off while the oxygen was running and buprenorphine (Temgesic, 0.05 mg/kg) was injected subcutaneously.

2.3.1.2 Intraperitoneal anaesthesia

Each animal was anaesthetised with ketamine (75 mg/kg) and medetomidine (0.5 mg/kg) via intraperitoneal injection for either GKS irradiation or *in vivo* fluorescence optical imaging procedures. The animal was sedated 10 min prior to either GKS irradiation or *in vivo* imaging. At the completion of each procedure the reversal drug, atipamazole (1 mg/kg), was injected subcutaneously. Then the animal was moved to the recovery room where it was monitored for the next $1-2$ hours. If there was no sign of morbidity the animal was transferred to the holding room at the Central Animal House Facility at Macquarie University and monitored according to approved protocols. All drugs were purchased from Cenvet, NSW, Australia.

2.3.1.3 Operative and post-procedure care

All the procedures were performed by using aseptic technique in a sterile field. Prior to the surgical procedure, the neck area was shaved and iodine was applied to the area. After the operation the animal was placed in the recovery room on a heating pad and monitored closely for the next one to two hours. The post-operative animal was then returned to the central animal house facility at Macquarie University and monitored twice a day for the first three days followed by once a day for four days, then once a week until the designated endpoint. The monitoring of the animal included recording weight, observing coat appearance, behaviour, breathing, gait, posture, wound site and noting any tenderness on wound palpation. According to the approved protocol, any animal with weight loss of 20% or more of their original body weight would be euthanased. However, none of the animals in this study met this criterion.

2.3.1.4 Arterio-venous fistula (AVF) formation

Surgical creation of the arterio-venous fistula (AVF) was carried out one week after the rats' arrival at the Macquarie University central animal house facility. Using a sterile microsurgical technique and the rat in a supine position, a midline incision was made over the anterior neck and the left sternocleidomastoid muscle identified. Then the left omohyoid muscle was divided in order to expose the left common carotid artery (CCA). The left external jugular vein (EJV) was dissected out from surrounding tissue and one or two small feeding veins were sealed by electrocautery and detached to allow adequate mobilisation of the vein. A ligature was placed across the EJV at its junction with the subclavian vein. After a surgical clip was placed across the rostral EJV, the EJV was transected close to the ligature which was then mobilised to be close to the lateral side of the CCA. Two clips were located proximally and distally on the CCA and a small longitudinal arteriotomoy made on the CCA. The caudal end of the EJV was anastomosed to the side of the CCA with a 10/0 prolene suture (Johnson & Johnson, NJ, USA) with a continuous thread. After the anastomosis the clips were removed and haemostasis was achieved using gentle pressure at the site of the anastomosis. The blood flow through the proximal CCA and EJV was measured by using 1 and 2 mm Doppler probes (Transonic Systems Inc., NY, USA) respectively. The wound area was closed with absorbable sutures (Vicryl Plus Antibacterial, Ethicon; Johnson & Johnson, NJ, USA). (Figure 2.2) and (Figure 2.3) show the vascular arrangement as a result of the fistula creation. Surgical creation

of the AVF was performed by Neurosurgical associates: Dr. Nirav Patel, Dr. David Bervini and Prof. Marcus Stoodley at Macquarie University.
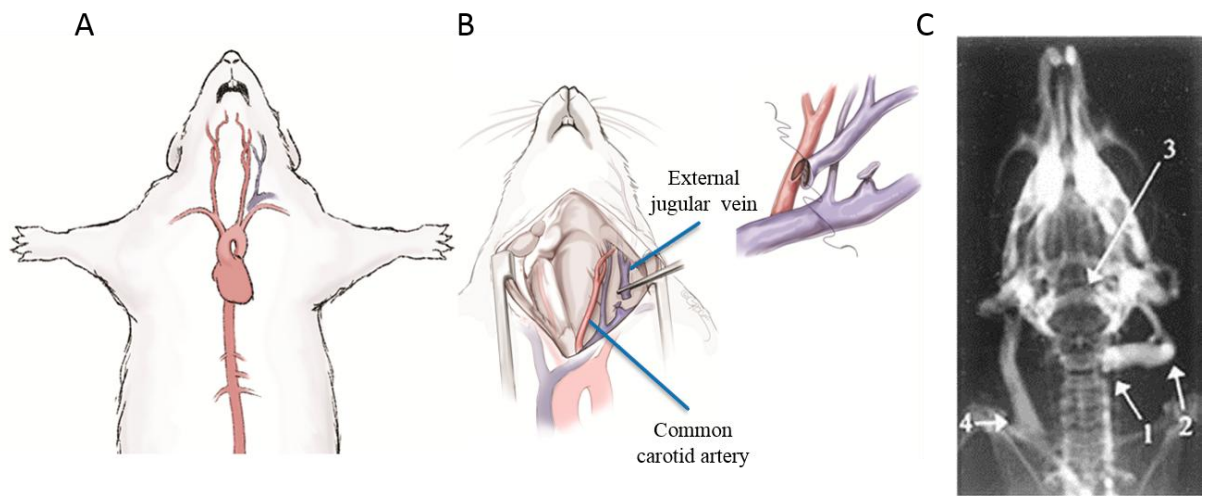
Figure 2.2. Animal model of AVM. (A) Schematic diagram showing the vascular arrangement in normal rat. (B) Fistula creation. (C) Angiogram showing mature AVF. Figure courtesy of Professor Marcus Stoodley.
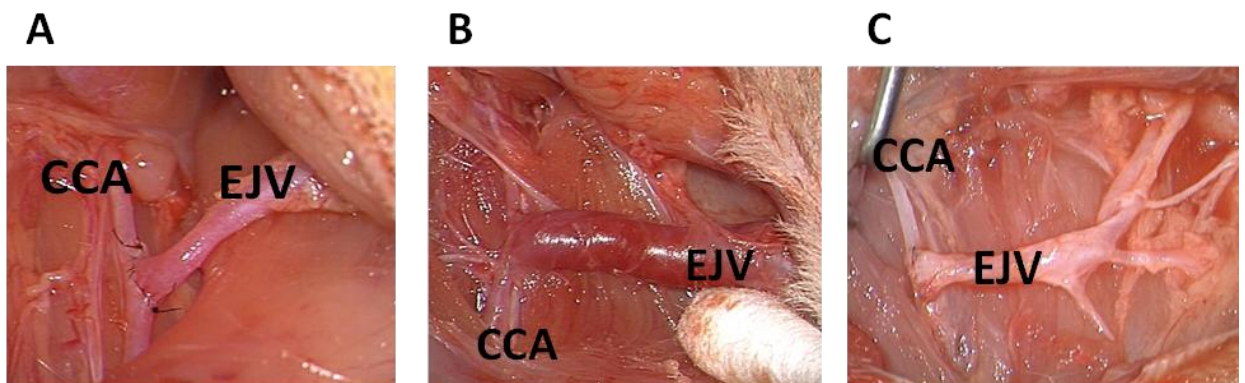
Figure 2.3. Arterio-venous fistula (AVF) formation. (A) Representative image of anastomosed left common carotid artery (CCA) and left external jugular vein (EJV) immediately after creation. (B) The arteriovenous fistula formed after 6 weeks maturation. Note the enlarged size of the EJV. (C) Post-perfusion image of the AVF showing the vessel nidus and branching vessels.

2.3.2 Radiosurgery

2.3.2.1   CT angiography

The AVF was considered ready for radiosurgery six weeks following creation of the fistula. At this stage the model AVM consisted of a feeding artery (common carotid), arterialised veins (external jugular), a nidus (branches of the external juagular vein that reconnected at the skull base), and a draining vein (sigmoid and transverse sinus). Before the radiosurgery

procedure, anaesthesia was induced with ketamine (75 mg/kg) and medetomidine (0.5 mg/kg) via intraperitoneal injection (IP) as described (section 2.3.1.2).

Prior to radiosurgery, a CT scan was performed to allow localisation of the AVF and for radiosurgery dose planning. The rat was restrained in a custom-made frame, positioned supine. The CT scan was carried out at MUH with a Somatom Sensation Open CT instrument (Siemens, Munich, Germany) (Figure 2.4).
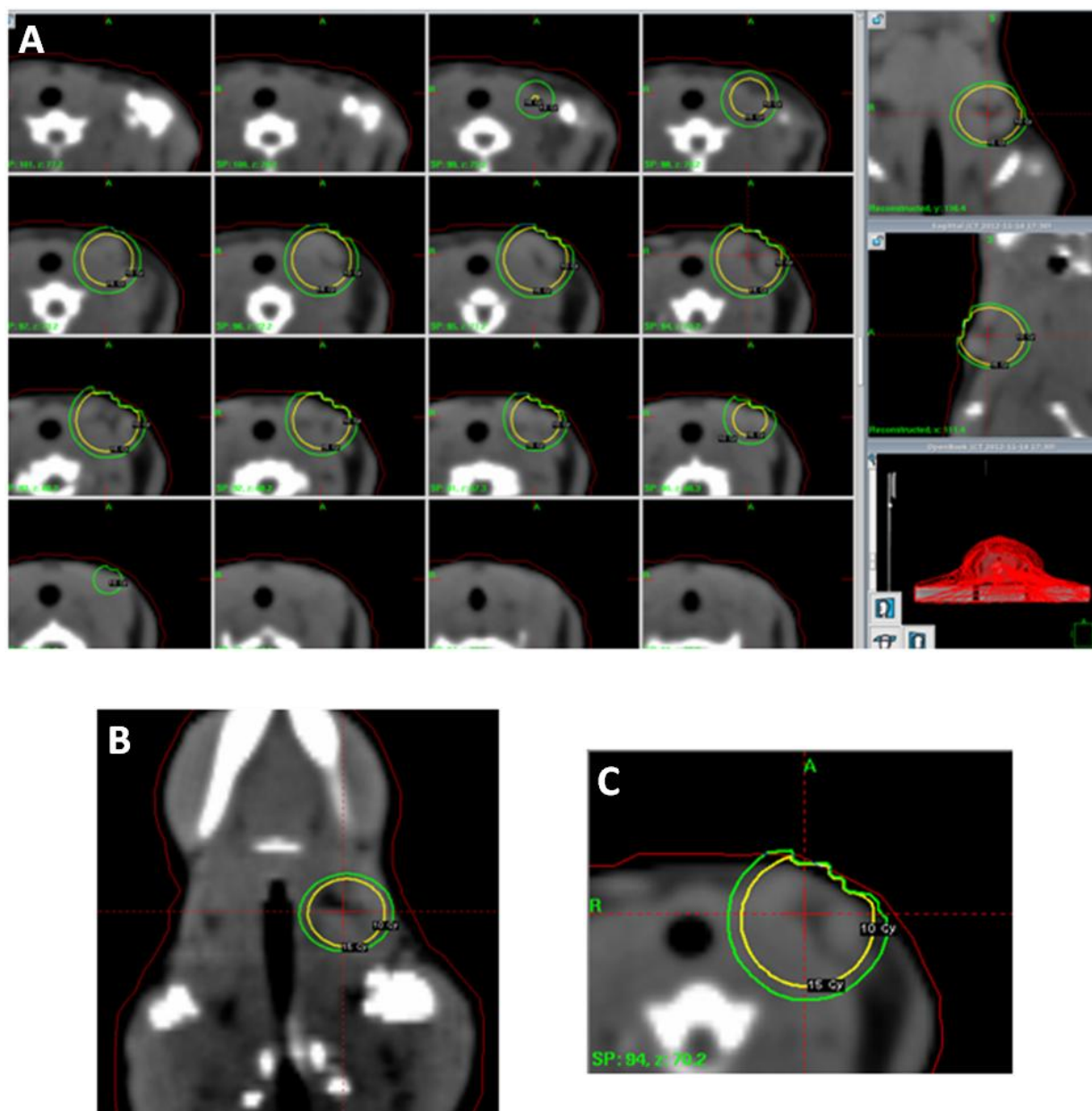
Figure 2.4. CT images of model AVM localisation. (A) CT images used for radiosurgery planning showing transverse, coronal and sagittal sections of rat with the model AVM outlined by 10 Gy (green) and 15 Gy (yellow) isodose lines. (B) Enlarged coronal view of model AVM location. (C) Enlarged transverse view of model AVM.

2.3.2.2 Gamma Knife radiosurgery

A single radiation dose of 15 Gy was delivered to the AVM by a Leksell Gamma Knife (Elekta Instruments, Stockholm, Sweden). The Gamma Knife was calibrated according to International Atomic Energy Agency code of practice (IAEA TRS-398). For dose planning, an Elekta Gamma Plan was used. The treatment parameters were as follows: the dose received by AVM margin 15 Gy; mean maximum dose 30 Gy; mean isodose line 50%; one isocentre; and an 8 mm shot per session. Coverage indices were assessed according to the CT plan and directly targeted. All irradiation was carried out by Mr Michael Grace (GKS-certified Genesis Care personnel, MUH).

At the completion of the radiosurgery procedure the rats were recovered and monitored according to approved protocols (section 2.3.1.2) until the designated endpoints.

2.3.3 Perfusion procedure

Animals underwent *in vivo* imaging as described (see sections 4.2.3 and 5.2.3). At the completion of all *in vivo* procedures 12 weeks after GKS treatment, all animals were perfused as follows:

The animal was anaesthetised with isoflurane (4%) and oxygen (1 L/min) in an induction chamber. Then the rat was moved to the surgery table and anaesthesia was maintained via a nose cone connected to isoflurane (2 − 3%) and oxygen (200 mL/min). The AVM fistula was exposed, followed by laparotomy and bilateral thoracotomy to expose the heart. A haemostat was clamped to the sternum to keep the ribcage up and expose the heart. A cannula (18 gauge needle) was passed through the ascending aorta via the apex of the left ventricle. The cannula was then connected to a peristaltic pump (Cole-Parmer Instruments, IL, USA) and an incision was made in the right atrium to allow outflow. A solution of 0.01 M phosphate buffered saline (PBS, 500 mL) was infused into the aorta with a flow rate of 38 mL/min for 10 min to clear blood. At the completion of perfusion the AVM fistula was extracted and subdivided into left CCA, left EJV and nidus. Also right CCA and right EJV were collected. The fresh extracted tissues were used for *ex vivo* NIR fluorescence imaging (explained in detail in Chapter 4). The perfusion procedures were performed with the assistance of Ms. Vivienne Lee at Macquarie University.

Chapter 3. Quantitative analysis of gene and protein expression of endothelial cell adhesion molecules after radiation

Objectives: Radiosurgery can induce molecular changes on the surface of endothelial cells in the received target volume. Molecular differences between irradiated and normal endothelial cells is the fundamental criterion for successful vascular targeting. Identifying the best radiation dose that can fulfil this goal with the least damage to the surrounding normal cells is important. Determining the best candidate molecule at the luminal surface of endothelial cells for vascular targeting, considering both level of expression and time course of expression, is crucial. The aims of this study were to examine the expression level of endothelial adhesion molecules at three different radiation doses and determine the cellular location of these molecules in a mouse brain endothelial cell line (bEnd.3). A further aim was to identify the lowest possible radiation dose that can induce molecular changes on the surface of bEnd.3 cells.

Methods: Cells (bEnd.3) were irradiated with a LINAC machine at single doses of 5, 15 or 25 Gy. Non-irradiated cells were considered as control cells. Viability was examined at 6, 24, 48 and 72 h by automated trypan blue assay post-irradiation. Gene expression levels of E-selectin, P-selectin, ICAM-1 and VCAM-1 in bEnd.3 cells at 1, 6, 12, 24, 48, 72, 96, 120, 144, 168 h post-irradiation were studied by quantitative real-time polymerase chain reaction (qRT-PCR). Total protein levels of E-selectin, P-selectin, ICAM-1 and VCAM-1 in bEnd.3 were studied by western blot analysis at 24, 72, 120 and 168 h post-irradiation. The externalised protein levels of E-selectin, P-selectin, ICAM-1 and VCAM-1 were examined by enzyme-linked immunosorbent assay (ELISA) at 24, 72, 120 and 168 h post-irradiation. The subcellular location of ICAM-1 and VCAM-1 on bEnd.3 cells was determined at 24, 72, 120 and 168 h post-irradiation by immunocytochemistry (ICC).

Results: Cells irradiated with 5 Gy showed no significant difference in viability to non-irradiated cells while 15 Gy and 25 Gy caused a dose-dependent reduction in cell viability. All endothelial CAMs showed up-regulation at the higher doses (15 Gy and 25 Gy) although differences existed between level of response and time course of expression. Expression of VCAM-1 peaked at 144 h for mRNA (22-fold change) and 72 h for protein (3-fold change) at a dose of 15 Gy. Analysis of VCAM-1 cell surface expression by ICC was highest at 120 h

with a 15 Gy dose. ELISA results for VCAM-1 showed highest level of surface expression at 72 – 120 h with both 15 Gy and 25 Gy. Expression of ICAM-1 at mRNA and protein levels increased with time with a peak at 168 h (5-fold change, mRNA) and 120 h (2.5-fold change, protein) with no significant difference between 15 Gy and 25 Gy doses. However, ICC showed the highest level of surface expression of ICAM-1 was achieved by 25 Gy and ELISA indicated the highest level of surface expression with 15 Gy. For E-selectin, results indicated low levels of induction at mRNA and protein levels (<2-fold) which was reflected at the cell surface in irradiated cells. Low levels of induction for P-selectin were seen at both mRNA and protein levels but significant up-regulation at the cell surface with both 15 Gy and 25 Gy was observed (3 – 6 fold, 72 – 120 h).

Conclusions: Radiation can induce endothelial CAM expression. In this study, the lowest and most efficient dose tested was 15 Gy. The most discriminating increase in surface expression and most promising candidates for vascular targeting were ICAM-1 and VCAM-1, followed by possible consideration of P-selectin.

3.1 Introduction

The constitutive levels of expression of adhesion molecules in AVM endothelial cells are different from normal vessels, however they are not sufficiently different to be used for vascular targeting (Storer et al., 2008). Previous studies have shown that radiosurgery can selectively alter the molecular expression of endothelial cells within the radiation target volume (Storer et al., 2007; Storer et al., 2008; Tu et al., 2006a). Before progressing to vascular targeting studies, it is necessary to identify the most discriminating molecules that are located on the endothelial luminal surface after irradiation. Selecting the most discriminating molecules requires measuring the level of expression, determining the highest time point of expression post-irradiation and comparing the response to a non-irradiated control.

The aims of this study were to use an *in vitro* endothelial cell culture model to examine the level of expression of four endothelial adhesion molecules and their subcellular location (eg. cell surface or plasma membrane) after radiation at three different doses to identify the time point of highest expression and the effect of dose on expression level.

3.2 Materials and methods

3.2.1 Cell viability test

The effect of different radiation doses on cell viability in bEnd.3 cells was examined. Cells were seeded in 6-well plates (In vitro, VIC, Australia) at a density of 5×10^5 cells/well (tissue culture explained in detail in section 2.1.1.). The cells were irradiated with a linear accelerator at doses of 15 or 25 Gy (explained in detail in section 2.1.2). Irradiated (treatment) and non-irradiated (control) cells were analysed for cell death at 6, 24, 48 and 72 h by automated trypan blue assay. Briefly, the cells in 6-well plates were detached by incubation with 0.1% Trypsin-EDTA (200 µL) for 2 min at 37ºC. Then cell culture medium (1 mL) was added, the cells collected and centrifuged at 1200 rpm for 5 min. The supernatant was discarded and the cell pellet was mixed with tissue culture medium (1 mL). The cell suspension (10 µL) was then mixed with trypan blue stain (0.4%, 10 µL, Life Technologies, CA, USA) in a clean eppendorf tube. The mixture (10 µL) was added to the chamber port of a Countess cell counting chamber slide (Invitrogen, CA, USA). The cell counting chamber slide was placed inside the Countess automated cell counter machine (Invitrogen, CA, USA) for automated counting of live and dead cells. The percentages of live and dead cells were determined by the automated counting machine software. The cell pellet was diluted in tissue culture medium in such a way that the total cell concentration measured was between $1 \times 10^4 - 1 \times 10^7$ cells.

3.2.2 Real - Time Polymerase Chain Reaction (qRT - PCR)

The level of gene expression of ICAM-1, VCAM-1, E-selectin and P-selectin molecules after irradiation in bEnd.3 cells was determined by quantitative real-time polymerase chain reaction (qRT-PCR). Relative quantitation was used to determine fold-change in expression of target genes (ICAM-1, VCAM-1, E-selectin, and P-selectin), based on an internal reference gene (hypoxanthine guanine phosphoribosyltransferase (HPRT).

3.2.2.1 Tissue culture and irradiation

The bEnd.3 cells were seeded in 75 cm^2 flasks (In vitro, VIC, Australia) at a density of 2×10^6 cells/flask (tissue culture explained in detail in section 2.1.1). After reaching $50 - 60\%$ confluence, the cells to be treated were irradiated with a linear accelerator instrument at three different doses (5, 15 and 25 Gy) (explained in detail in section 2.1.2). Non-irradiated cells

were used as controls. Post-irradiation at 1, 6, 12, 24, 48, 72, 96, 120, 144, and 168 h, total RNA was extracted from cells in both treatment and control groups.

3.2.2.2   Total RNA extraction

Total RNA extraction was performed using the RNeasy Mini-Kit (QIAGEN, Limburg, Netherlands) according to the manufacturer's instructions. Cells were washed twice with 1X PBS (1 mL), detached from the flask with 0.1% Trypsin-EDTA (1 mL; 2 min at 37ºC), suspended in tissue culture medium (5 mL) and centrifuged (1200 rpm for 5 min). The extracted cell pellet was transferred to a 1.5 mL tube and washed with 1X PBS (1 mL, twice) and lysed on ice with lysing buffer (600 µL; QIAGEN, Limburg, Netherlands) and stored at -80ºC until further processing. When ready the lysate was removed from -80ºC and thawed on ice, then homogenised at least five times by passing through a blunt 20-gauge needle (0.9 mm diameter) fitted to an RNase-free syringe. To the homogenised lysate, 70% ethanol (700 µL) was added and mixed by inversion. The sample was transferred to an RNeasy spin column placed in a 2 mL collection tube and centrifuged. All the centrifugation steps were at 4ºC with a speed of 12000 rpm and duration of 15 s, unless otherwise specified. The flow-through was discarded. To eliminate any genomic DNA contamination, on-column DNase digestion was performed by first washing the spin column by RW1 buffer (350 µL) then adding 80 µL DNase I incubation mix (DNase I stock solution (10 µL) and RDD buffer (70 µL)) to each column and incubating at room temperature (RT) for 15 min. The RNeasy column was washed for the second time with RW1 buffer (350 µL) and centrifuged. The flow-through was discarded. The next wash buffer, RPE (500 µL) was added to the spin column and samples were centrifuged for 15 s. A second wash of buffer RPE (500 µL), was added but this time the samples were centrifuged for 2 min. The RNeasy spin column was placed in a new 2 mL collection tube followed by centrifugation at 13000 rpm for 1 min at 4ºC to dry the membrane. The RNeasy spin column was placed in a new 1.5 mL collection tube. To elute the RNA, RNase-free water (50 µL) was directly added to the spin column membrane and centrifuged at 12000 rpm for 1 min at 4ºC.

3.2.2.3   RNA concentration and quality

The quality of RNA was examined with a NanoDrop 2000 Spectrophotometer (NanoDrop products; Thermo Fisher Scientific Inc., MA, USA). The sample (1 µL) was placed on the lower optical surface of the spectrophotometer and RNA concentration was measured. The

purity of the RNA was determined according to the ratio of absorbance at 260 nm and 280 nm. Only RNA samples with a ratio between 2.0 - 2.1 were considered for the experiments to ensure accurate and reliable qRT-PCR results. The samples were stored at -80ºC for later use to prevent degradation.

3.2.2.4   Reverse transcription PCR (RT–PCR)

Reverse transcription polymerase chain reaction (RT-PCR) was used to synthesise cDNA from the RNA template by reverse transcriptase using the AffinityScript QPCR cDNA Synthesis Kit (Agilent Technologies, Inc., CA, USA, #STG600559). The first-strand of cDNA was synthesised by mixing RNase-free water (5 µL), first strand master mix (10 µL), random primers (0.1 (µg/µL), 3 µL), AffinityScript RT (1.0 µL) and RNA sample (100 (ng/µL), 1 µL) to an RNase-free reaction tube. A no-RT sample was used as a control for cDNA synthesis that contained all the mentioned reagents except the AffinityScript RT. The cDNA synthesis was started by incubating the reaction tubes in a Thermocycler (Analytik Jena, Jena, Germany) for 5 min at 25ºC to allow primer annealing, followed by incubation at 42ºC for 15 min. The reaction was stopped by incubating the tubes at 95ºC for 5 min. The final product, double stranded cDNA, was placed on ice for immediate use or kept at -20ºC for long term storage.

3.2.2.5   Quantitative real-time polymerase chain reaction (qRT-PCR)

The qRT-PCR was carried out using a Rotor-gene 6000 system (Corbett Research, Limburg, Netherlands) with SYBR Green detection method. The primer sequences used are described in Table 3.1 (Weiser et al., 2007). The qRT-PCR reactions were performed in triplicate with a final reaction volume of 25 µL for each replicate. The reaction mixture comprised of 1.0 µL cDNA sample, ImmoMix (12.5 µL; Bioline, MA, USA, #Nio-25020), forward and reverse primers (0.75 µL from each; GeneWorks, MA, USA), SYBR Green (2.5 µL; Life Technologies, CA, USA) and nuclease free PCR-grade water (8.25 µL).

Two different negative controls were included in each run: a no-RT control from the previous step to account for genomic DNA contamination and a control containing no RNA/cDNA to control for general contamination of components.

The thermal cycling conditions for the qRT-PCR consisted of an initial denaturation step at 95ºC for 10 min to activate the ImmoMix, followed by 40 cycles of denaturation at 95ºC for

20 s, annealing at 58ºC for 20 s, and extension at 72ºC for 20 s, with a final hold step at 72ºC for 7 min.

Efficiency curves were generated for all primer sets to ensure that amplification efficiencies were within the 90 – 100% range to allow fold-change comparisons. All real-time PCR runs were followed by melt-curve analysis to ensure single peaks were obtained for all primers without primer-dimers.

Table 3.1. Primer sequences for qRT-PCR

Primer	Forward 5′ → 3′	Reverse 5′ → 3′
HPRT	GCT TTC CCT GGT TAA GCA GTA CA	CAA ACT TGT CTG GAA TTT CAA ATC
E-selectin	TAG CAA GAA GCC CAC GTG TTC	CAA GCT AAA GCC CTC ATT GCA
P-selectin	ATC TGG ACC GGA AAG ACT GGA	GAT TCC TGG ACA CTT GAT GGC
ICAM-1	GCC TCC GGA CTT TCG ATC TT	GTC AGG GGT GTC GAG CTT TG
VCAM-1	GGG AAG CTG GAA CGA AGT ATC C	TCT GGA GCC AAA CAC TTG ACT GT

3.2.2.6 DNA gel electrophoresis

Gel electrophoresis was carried out to confirm primer specificity and assure correct amplicon size. The amplified fragments from the qRT-PCR step were run on a 2% agarose gel at 100 V for 1 h. The agarose gel was prepared with tris-borate-EDTA (TBE) buffer (Thermo Fisher Scientific Inc., MA, USA) containing Gel Red stain (Biotium, CA, USA). The samples were run against a 100 bp DNA ladder (Promega, WI, USA) to determine fragment size. The gel bands were visualised in a Bio-Rad Gel Doc XR system (Bio-Rad Laboratories, CA, USA).

3.2.2.7 qRT-PCR data analysis

Expressions of E-selectin, P-selectin, ICAM-1 and VCAM-1 were normalised to an endogenous control gene, HPRT. The cycle threshold (Ct) values of each reaction were determined using Corbett's Rotor-Gene 6 software (QIAGEN, Limburg, Netherlands). Data were analysed using the comparative Ct method. The HPRT Ct values were subtracted from the Ct value for each gene (to give ΔCt values). These values were used to carry out statistical comparisons between the different time points. For graphical representation, the fold variation was then determined using the $2^{-(\Delta\Delta Ct)}$ method. Fold variation was calculated by determining the difference in ΔCt values between a chosen reference (control group data) and test sample (ΔΔCt value), and applying the $2^{-(\Delta\Delta Ct)}$ formula. The range values were then determined using the formula $2^{-(\Delta\Delta Ct \pm S.D. \Delta Ct)}$ (Livak & Schmittgen, 2001).

3.2.3 Western blot

Western blotting was carried out to determine the level of protein expression of ICAM-1, VCAM-1, E-selectin and P-selectin in whole cell lysates of bEnd.3 cells post-irradiation.

3.2.3.1 Protein extraction

Whole cell protein lysates were prepared from murine bEnd.3 cells. Cells were seeded in 6-well plates (In Vitro, VIC, Australia) at a density of 1×10^5 cells/well (tissue culture explained in detail in section 2.1.1.). As the cells reached $30 - 40\%$ confluence, they were irradiated (treatment) with a LINAC instrument at doses of 5, 15, and 25 Gy (explained in detail in section 2.1.2). Non-irradiated cells were considered as controls. At each time point post-irradiation, both treatment and control cells in wells were washed twice with ice-cold PBS and cells lysed in 120 µL/well of ice-cold RIPA buffer (radioimmunoprecipitation assay buffer; see appendix 1. for recipe) containing 1 x protease inhibitor mix (GE Healthcare, #80-6501-23) and 10 mM EDTA pH 8.0. The cells were then scraped in the lysis buffer and the lysate collected into an eppendorf tube. Multiple wells were pooled for each sample. The lysate was then left on ice for 30 minutes. Cells on ice were sonicated once for 15 s at 40 % power with a Sonic Ruptor 250 with micro-tip (Omni International, Kennesaw, GA, USA) to complete lysis and shear DNA. Lysates were clarified by centrifugation at 4ºC at 12000 rpm for 15 min to pellet debris. Small aliquots were taken for protein measurement. Protein concentrations were determined by the bicinchoninic acid (BCA) assay using bovine serum albumin to create the standard curve (Pierce, Rochford, IL, USA). Samples were stored at - 80ºC until use.

3.2.3.2 Gel electrophoresis and western blotting

Lysates containing equivalent amounts of protein ($10 - 15$ µg loaded per well) were mixed with NuPAGE ® reducing agent, NuPAGE ® LDS sample buffer (Life Technologies, CA, USA) and deionised water to a final volume of 25 µL. Samples were heated at 70ºC for 20 min to denature proteins then transferred to ice for 5 min. Samples were spun briefly to collect any condensate then loaded onto 12-lane 10% NuPAGE ® Novex Bis-Tris Mini Gels (Life Technologies, CA, USA). Novex ® sharp pre-stained protein standard (15 µL) was included in at least one lane to determine band sizes. Gels were run in 1 X NuPAGE MOPS SDS running buffer at 200V for up to 1 h to allow complete separation of bands within the pre-stained ladder. Gel units were disassembled and the gels soaked in NuPAGE Transfer

buffer (Life Technologies, CA, USA) for 20 min to improve transfer of larger molecular weight proteins. The iBLot ® dry blotting system (Life Technologies, CA, USA, 0.2 μm) was used to immunoblot the samples on to a polyvinylidene difluoride (PVDF) membrane. Transfer was at 20 V for 11 minutes. Membranes were then separated from the gel sandwich, dried, activated in 100% ethanol with subsequent washing in deionised water before placement in 5% (w/v) non-fat dry milk powder (in PBS containing 0.1 % v/v Tween 20) and blocked for 60 min at RT (see appendix 1. for recipe). The membranes were then incubated with primary antibodies (listed in Table 3.2) in 5% milk/PBST at 4ºC overnight on a slow rocker. The next day the membranes were washed with PBST (three times, 10 min), followed by incubation for 1 h at RT with goat anti-rabbit horseradish peroxidase (HRP)-conjugated secondary antibody (ab6721, Abcam, Cambridge, UK, 1:20,000). At the completion of the secondary antibody incubation the membranes were washed with PBST (three times, 10 min). The membranes were incubated for 5 min in enhanced chemiluminescence (ECL) solution (Bio-Rad, CA, USA). The excess ECL was blotted and the membranes were visualised with ChemiDoc MP imaging system (Bio-Rad, CA, USA). Glyceraldehyde 3-phosphate dehydrogenase (GAPDH, ab9485, Abcam, Cambridge, UK) was used as the house-keeping protein for all molecules to ensure equal lane loading.

Table 3.2. Primary antibodies used in western blot experiments

Antibody	Antigen recognised	Dilution	Catalogue number Company
Rabbit polyclonal	E-selectin	1:250	ab18981, Abcam, Cambridge, UK
Rabbit polyclonal	ICAM-1	1:1000	sc-1511R, Santa Cruz Biotechnology, TX, USA
Rabbit polyclonal	P-selectin	1:500	sc-25771, Santa Cruz Biotechnology, TX, USA
Rabbit monoclonal	VCAM-1	1:1000	ab134047, Abcam, Cambridge, UK
Rabbit polyclonal	GAPDH	1:2500	ab9485, Abcam, Cambridge, UK

3.2.3.3 Western blot analysis

The signal intensity was quantified using Image J software (Version 1.49, Rasband, W.S., ImageJ, U.S. National Institutes of Health, Bethesda, Maryland, USA, http://imagej.nih.gov/ij/download.html, 1997-2014). In brief, the signal intensity of the background was subtracted from the image. A fixed area was drawn with the rectangle tool

and used to measure signal intensity from the region encompassing each band. Each rectangle was selected sequentially and analysed by plotting the curves and the area under the curve was measured to give an arbitrary value for intensity. Values were then normalised to non-irradiated controls to give relative increase in protein expression (arbitrary units). The western blot analysis was performed with the assistance of Dr. Lucinda McRobb at Macquarie University.

3.2.4 Enzyme-linked immunosorbent assay (ELISA)

Cell ELISA was carried out to determine the level of expression of endothelial cell adhesion molecules (ICAM-1, VCAM-1, E-selectin and P-selectin) on the surface of the bEnd.3 cells after irradiation at 24, 72, 120 and 168 h. ELISA kits were purchased from Biosensis (SA, Australia) for P-selectin (BEK-2091-1P), ICAM-1 (BEK-2024-1P) and VCAM-1 (BEK-2107-1P) and RayBiotech, Inc. (GA, USA) for E-selectin (ELM-ESelectin).

Cells (bEnd.3) were seeded on to 96-well cell culture plates (In vitro, VIC, Australia) at a density of 5×10^3 cells per well (tissue culture explained in detail in section 2.1.1). The cells were irradiated with a linear accelerator at 5, 15 and 25 Gy doses (explained in detail in section 2.1.2). Non-irradiated cells were used as controls. All the incubations were performed at RT. The first ELISA procedure was started 24 h post-irradiation by removing the medium from the plate and washing the cells with 1X PBS (twice, 200 µL per well). Then the cells were fixed with 4% paraformaldehyde for 15 min (200 µL per well). After the fixation step the plate was washed with 1X PBS (three times, 5 min each, 200 µL per well) on a platform rocker. The blocking step was carried out by adding 1% BSA in PBS (200 µL per well) to the plate, and incubating for 1.5 h. After blocking, the cells were washed with 1X PBS (three times, 5 min each, 200 µL per well) with shaking. Biotinylated anti-mouse E-selectin antibody (100 µL per well) was added and the plate was incubated for 2.5 h on a platform rocker. After washing the unbound biotinylated antibody with 1X PBS (three times, 5 min), horseradish peroxidase-conjugated streptavidin (HRP-streptavidin; 100 µL per well) was added. The plate was incubated for 1 h on a platform rocker. After incubation, the cells were washed with 1X PBS (three times, 5 min) followed by addition of 3, 3', 5, 5'- tetramethylbenzidine (TMB; 90 µL per well). TMB colour developer solution was added for 20 min to quantify HRP activity. The reaction was stopped by adding TMB stop solution (100 µL per well) and colour intensity measured with a microplate reader (PHERAstar FS, BMG Labtech, Ortenberg, Germany) at 450 nm. Similar steps were followed for P-selectin,

ICAM-1 and VCAM-1 ELISA except that biotinylated anti-mouse P-selectin, biotinylated anti-mouse ICAM-1, and biotinylated anti-mouse VCAM-1 antibodies were used, respectively.

3.2.4.1   Whole cell staining

The next step was to normalise the HRP signal to Janus Green cell normalisation stain (Sigma-Aldrich, MO, USA) to account for differences in cell confluence.

The plate was emptied and 1X Janus Green stain (50 μL per well) was added and incubated (5 min) at RT. The plate was washed with deionised water for 5 times or more, until the excess dye was removed. After the last wash was removed by blotting, 0.5 M HCl (200 μL per well) was added for 10 min at RT to dissolve the dye precipitate. The colour intensity was measured by microplate reader (PHERAstar FS, BMG Labtech, Ortenberg, Germany) at 595 nm.

3.2.4.2   Data analysis

The raw ELISA signal was corrected for the background signal by subtracting the signal from the well incubated in the absence of primary antibody from the mean signal of wells incubated with both primary and secondary antibodies. To correct for background Janus Green signal, the mean Janus Green signal of wells without cells was subtracted from all other Janus Green readings. Finally, the ELISA signal was normalised by dividing the background-corrected ELISA signal by the background-corrected Janus Green signal. The fold change between the irradiated and non-irradiated cells was considered for the analysis.

3.2.5 Immunocytochemistry

Immunocytochemistry (ICC) was carried out to determine the subcellular location of endothelial adhesion molecules, ICAM-1 and VCAM-1, in bEnd.3 cells at 24, 72, 120 h after irradiation at 5, 15, and 25 Gy doses.

3.2.5.1   Antibody labelling with fluorescent dye

Prior to the immunocytochemistry procedure, anti-ICAM-1 antibody (1 mg/mL) was labelled with Mix-n-Stain^{TM}CF^{TM}555 antibody labelling kit (Sigma-Aldrich, MO, USA, #MX555S100-1KT) according to the following steps. Mix-n-Stain Reaction Buffer vial and Mix-n-Stain Storage Buffer vial were warmed to RT before use. Anti-ICAM-1 antibody

(1 mL) was added to the Mix-n-Stain Reaction Buffer at a ratio of 1:9. The entire solution was added to the CF dye vial and vortexed for a few seconds before incubation for 30 min. The concentration of the CF dye-labelled antibody was approximately the amount of starting antibody divided by the total volume (i.e., ~ 100% labelling yield). The dye bound to the antibody covalently with a degree of labelling of 4 – 6 dye molecules per antibody. $CF^{TM}555$ is a cyanin-based far red fluorescence dye with excitation of 555 nm and emission of 565 nm. The final antibody was divided into aliquots and kept at -20ºC in the dark until use.

Anti-VCAM-1 antibody (1 mg/mL) was labelled in an identical manner but labelled with Mix-n-Stain^{TM}CF^{TM}640 antibody labelling kit (Sigma-Aldrich, MO, USA, #MX640RS100-1KT). $CF^{TM}640$ is a cyanin-based far-red fluorescence dye with excitation of 642 nm and emission of 662 nm.

3.2.5.2 Immunocytochemistry

Adherent bEnd.3 cells were cultured in 8-well chamber slides (80×10^3/cm^2; Thermo Fisher Scientific Inc., MA, USA) (tissue culture explained in detail in section 2.1.1). The cells were irradiated with a linear accelerator at 5, 15 and 25 Gy doses (explained in detail in section 2.1.2). Immunocytochemistry was performed at 24, 72 and 120 h post-irradiation for both irradiated and non-irradiated (control) cells. All the immunostaining procedures were carried out at RT. The culture medium was removed from each chamber and cells were washed twice with 1X PBS (250 µL per chamber). The cells were fixed with 4% paraformaldehyde (250 µl per chamber, 15 min) then washed three times with 1X PBS (250 µl per chamber, 5 min) on a platform rocker. Then the cells were blocked with 5% bovine serum albumin (BSA; 250 µl, 2 h), followed by incubation for 2 h in the dark with labelled ICAM-1 antibody diluted in 1% BSA (1:100, 120 µl per chamber). The cells were washed three times (10 min) by shaking with 1X PBS containing Tween 20 (PBST) (250 µL per chamber). The nuclear stain, 4',6-diamidino-2-phenylindole (DAPI) (1 µg/ml, 200 µl per well, excitation; 358 nm and emission; 461 nm, Life Technologies, CA, USA) was added for 1 – 2 min and then washed with 1X PBS (250 µL per chamber, 2 times). Fluorescent mounting medium (Dako North America, Inc. CA, USA) was used for cover slipping the slides.

The same steps were carried out for VCAM-1 immunocytochemistry with anti-VCAM antibody conjugated with the $CF^{TM}640$ dye.

For both ICAM-1 and VCAM-1 immunocytochemistry, isotype controls were used as negative controls. For ICAM-1 antibody, IgG2b (0.5 mg/mL, #ab18541) conjugated with Mix-n-Stain^{TM}CF^{TM}555 antibody labelling kit was used, and for VCAM-1, IgG1 (1 mg/mL, #ab18407) conjugated with Mix-n-Stain^{TM}CF^{TM}640 antibody labelling kit was used. All the antibodies for the ICC experiments were purchased from Abcam, Cambridge, UK. The slides were observed under a confocal microscope (Leica Microsystems, Wetzlar, Germany).

3.2.5.3 Data analysis

The fluorescence images were analysed with ImageJ (Version 1.49, Rasband, W.S., ImageJ, U.S. National Institutes of Health, Bethesda, Maryland, USA, http://imagej.nih.gov/ij/download.html, 1997-2014). The background was subtracted from each image. A region of interest (ROI) was considered that was used for all the images. The integrated density was calculated for all the selected areas (ROI). The values obtained were used to plot the graphs in GraphPad Prism 6.0 software.

3.2.6 Statistical analysis

All experiments were repeated three times, each time in triplicate. All the values were expressed as mean ± standard error of the mean (SEM). Data were analysed by two-way analysis of variance (ANOVA) with Bonferroni corrections of multiple comparisons. The resulting values were plotted using GraphPad Prism 6.0 software. A probability value of < 0.05 was considered significant.

3.3 Results

3.3.1 Cell viability

3.3.1.1 Effect of irradiation on cell morphology

At different time points after irradiation, the effect of radiation on cellular morphology was assessed with an inverted light microscope (Figure 3.1). After 6 and 24 h post-irradiation, there were no substantial differences in cellular morphology between irradiated and non-irradiated cells at all doses. At 48 h post-irradiation, the irradiated cells (15 Gy and 25 Gy) had a morphology that was enlarged and irregular in shape relative to the non-irradiated cells. At 72 h post-irradiation, both irradiated and non-irradiated bEnd.3 cells reached 100%

confluency, although with different morphology. Non-irradiated cells remained spindle shaped while irradiated cells became star-shaped with increased appearance of lamellipodia and filopodia.

Time post irradiation (h)	Control	15 Gy	25 Gy
6			
24			
48			
72			
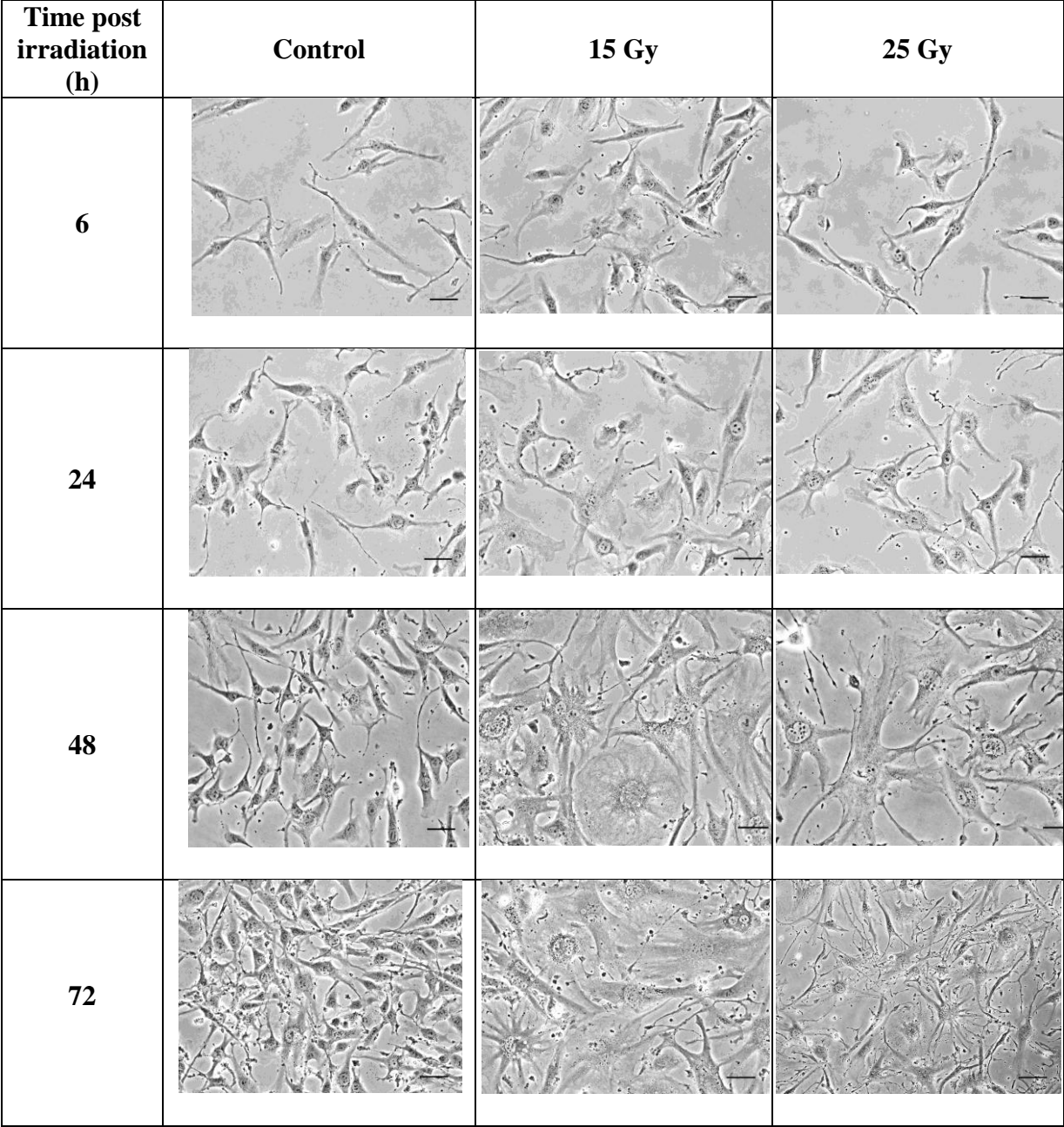
Figure 3.1. Effect of irradiation on bEnd.3 cell morphology. The morphology of irradiated mouse brain endothelial cells (bEnd.3) at 15 Gy and 25 Gy was compared with non-irradiated bEnd.3 control cells at 6, 24, 48 and 72 h after irradiation. Scale bar length = 20 μm.

3.3.1.2 Effect of irradiation on cellular proliferation and viability

The number of viable bEnd.3 cells was determined at 6, 24, 48 and 72 h after irradiation by automated trypan blue assay as described in section 3.2.1. In non-irradiated cells, the number

of live cells continued to increase over the 72 h time period. In contrast, irradiation intensities of 15 Gy and 25 Gy significantly reduced the number of viable cells in comparison to the non-irradiated control cells within the first 24 h (Figure 3.2). There was a significant difference between the number of viable cells in the 15 Gy and 25 Gy treatment groups at 24 and 48 h post-irradiation (Figure 3.2).
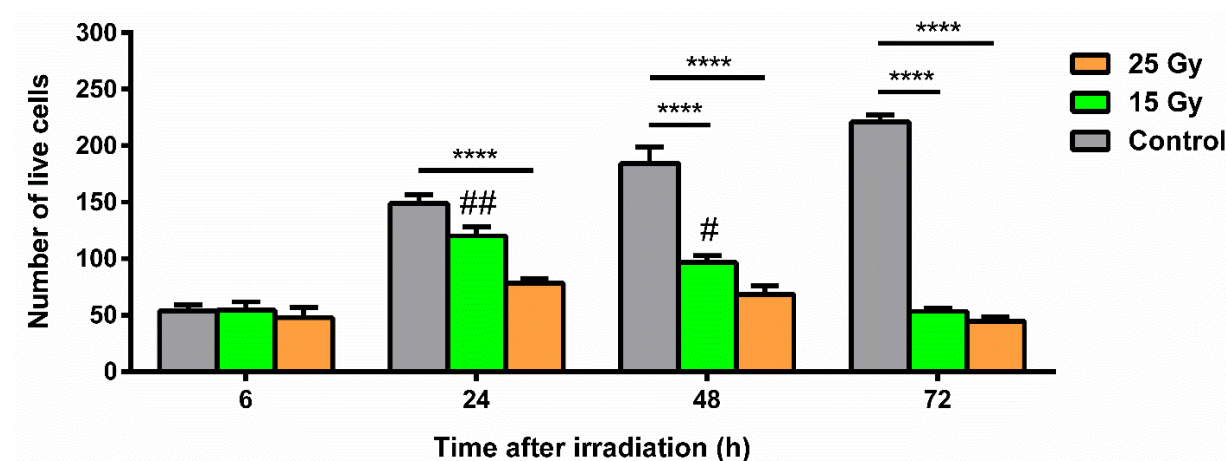
Figure 3.2. Effect of radiation on viability of bEnd.3 cells. Number of viable bEnd.3 cells at 6, 24, 48 and 72 h after irradiation at doses of 15 Gy and 25 Gy compared to non-irradiated control cells. Mean $\pm$ SEM. n = 3. *** $P < 0.001$, **** $P < 0.0001$, *, represents the comparison between irradiated cells (either 15 or 25 Gy) and control cells in the same time point. [#] $P < 0.05$, [##] $P < 0.01$, #, represents the comparison between 15 Gy and 25 Gy in the same time point.

3.3.2 Gene expression levels of endothelial adhesion molecules post-irradiation

Relative gene expression levels of ICAM-1, VCAM-1, E-selectin and P-selectin after irradiation with 5, 15, 25 Gy at 1, 6, 12, 24, 48, 72, 96, 120, 144 and 168 h were studied by quantitative real-time polymerase chain reaction (qRT-PCR). Non-irradiated bEnd.3 cells were considered as controls. The final values gained for the results were normalised to control cell values to show fold change between the treated and non-treated cells.

3.3.2.1 Intercellular adhesion molecule 1 (ICAM-1) relative gene expression

Relative gene expression levels of ICAM-1 increased at all doses over the allotted time period relative to non-irradiated cells and increased in a linear fashion with time (Figure 3.3). Differences became significant after 6 h for 25 Gy and after 24 h for the 5 Gy and 15 Gy doses. The higher the dose, the earlier the increase in relative ICAM-1 gene expression. There was also a significant difference between cells irradiated with 5 Gy and cells irradiated with

15 Gy and 25 Gy. However, there was no significant difference between the cells irradiated with 15 or 25 Gy at any time-point.

Figure 3.3. Relative gene expression of ICAM-1 in bEnd.3 cells post-irradiation. The relative levels of ICAM-1 gene expression were determined by quantitative real-time PCR at 1, 6, 12, 24, 48, 72, 96, 120, 144 and 168 h post-irradiation with LINAC at doses of 5, 15 or 25 Gy. The expression of HPRT gene was used as a housekeeping control. Mean ± SEM. n = 4. *** $P < 0.001$, **** $P < 0.0001$, *, represents the comparison between cells treated with 5 Gy and non-irradiated control. #, represents the comparison between cells treated with 15 Gy and non-irradiated control. +, represents the comparison between 25 Gy treated cells and non-irradiated control.

3.3.2.2   Vascular cell adhesion molecule 1 (VCAM-1) relative gene expression

Examination of relative VCAM-1 gene expression levels after irradiation illustrated no significant change between non-irradiated and cells irradiated with 5 Gy (Figure 3.4). There was no significant difference between the cells irradiated with 15 Gy and 25 Gy. However, there was a significant difference ($P < 0.001$) between cells treated with 15 Gy and 25 Gy and with non-irradiated cells and cells treated with 5 Gy. The increase in relative expression level of VCAM-1 in cells treated with 15 Gy and 25 Gy started 24 h post-irradiation and continued to increase until 168 h, however two peaks were observed at 96 h and 144 h for both the 15 Gy and 25 Gy doses. The highest level of expression of VCAM-1 was reached at 144 h post irradiation at both 15 Gy and 25 Gy with approximate 18- and 15-fold differences, respectively, compared to non-irradiated control cells. The level of expression of VCAM-1 in cells treated with 15 Gy was higher than the cells treated with 25 Gy.
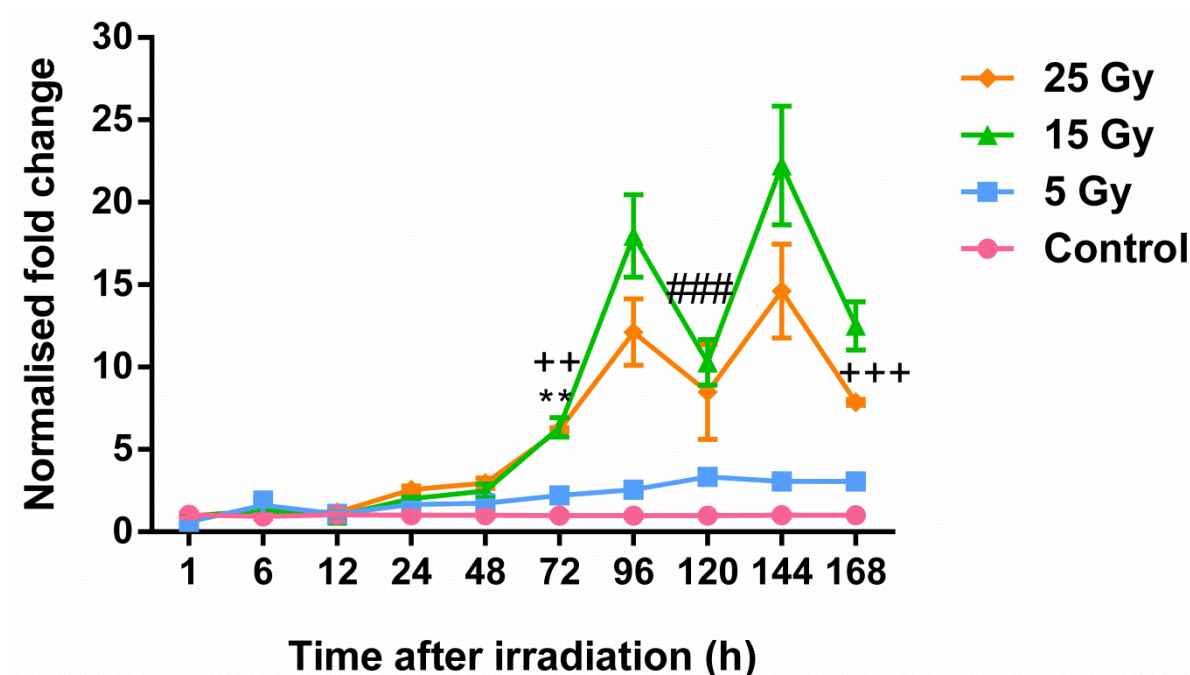
Figure 3.4. Relative gene expression of VCAM-1 in bEnd.3 cells post-irradiation. The relative levels of VCAM-1 gene expression were determined by quantitative real-time PCR at 1, 6, 12, 24, 48, 72, 96, 120, 144 and 168 h post-irradiation with LINAC at 5, 15 or 25 Gy. The fold change between irradiated and non-irradiated cells was considered at all doses. The expression of HPRT gene was used as a housekeeping control. Mean ± SEM. n = 4. ** $P < 0.01$, *** $P < 0.001$, *, represents the comparison between cells treated with 5 Gy and non-irradiated control. #, represents the comparison between cells treated with 15 Gy and non-irradiated control. +, represents the comparison between 25 Gy treated cells and non-irradiated control.

3.3.2.3 E-selectin relative gene expression

The relative levels of E-selectin gene expression after irradiation showed no significant difference between non-irradiated cells and irradiated cells with 5 Gy (Figure 3.5). There was no significant change between the cells irradiated with 15 Gy and 25 Gy. However, there was a significant difference ($P < 0.05$) between cells treated with 15 Gy and non-irradiated cells at the 72 h time point only. In addition, there was a significant difference between irradiated cells (25 Gy) and non-irradiated cells but only at the 96 h time-point. For this gene, fold changes in gene expression were relatively small at each time point while the standard error was relatively large. The peak relative expression level of E-selectin was reached at 96 h with 25 Gy post-irradiation with a 1.6-fold increase compared to control cells.
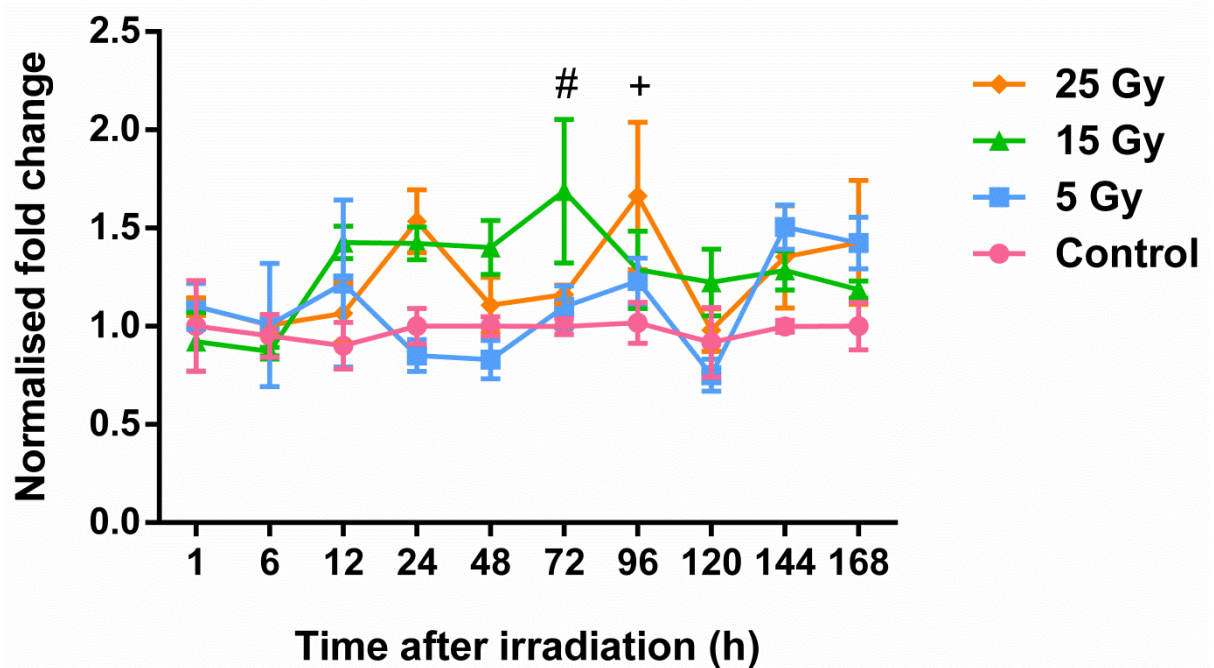
Figure 3.5. Relative gene expression of E-selectin in bEnd.3 cells post-irradiation. The relative levels of E-selectin gene expression were determined by quantitative real-time PCR at 1, 6, 12, 24, 48, 72, 96, 120, 144 and 168 h post-irradiation with LINAC at 5, 15 or 25 Gy. The fold change between irradiated and non-irradiated cells was considered. The expression of HPRT gene was used as a housekeeping control. Mean $\pm$ SEM. n = 4. $^{\#}P < 0.05$, #, represents the comparison between cells treated with 15 Gy and non-irradiated control. +, represents the comparison between 25 Gy treated cells and non-irradiated control.

3.3.2.4   P-selectin relative gene expression

Gene expression levels of P-selectin after irradiation showed no significant change between non-irradiated cells and irradiated cells at a dose of 5 Gy (Figure 3.6). However, there was a significant difference ($P < 0.05$) between irradiated cells at 15 Gy and non-irradiated cells at both 24 h and 96 h post-irradiation. The highest level of relative expression of P-selectin was reached at 24 h in cells treated with 25 Gy with a 1.9-fold difference compared to control ($P < 0.001$). There was no significant difference found between 15 Gy and 25 Gy doses. As for E-selectin, the levels of induction were low (<2-fold) relative to level of error and there was no consistent trend in expression seen as for ICAM-1 and VCAM-1.
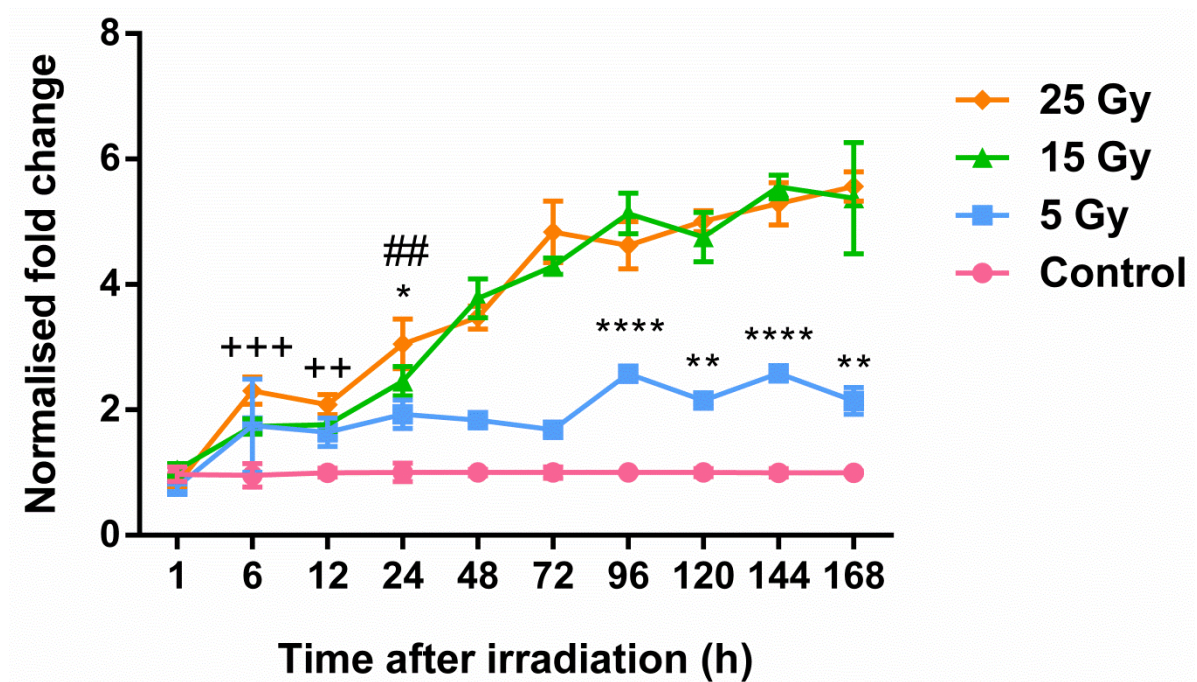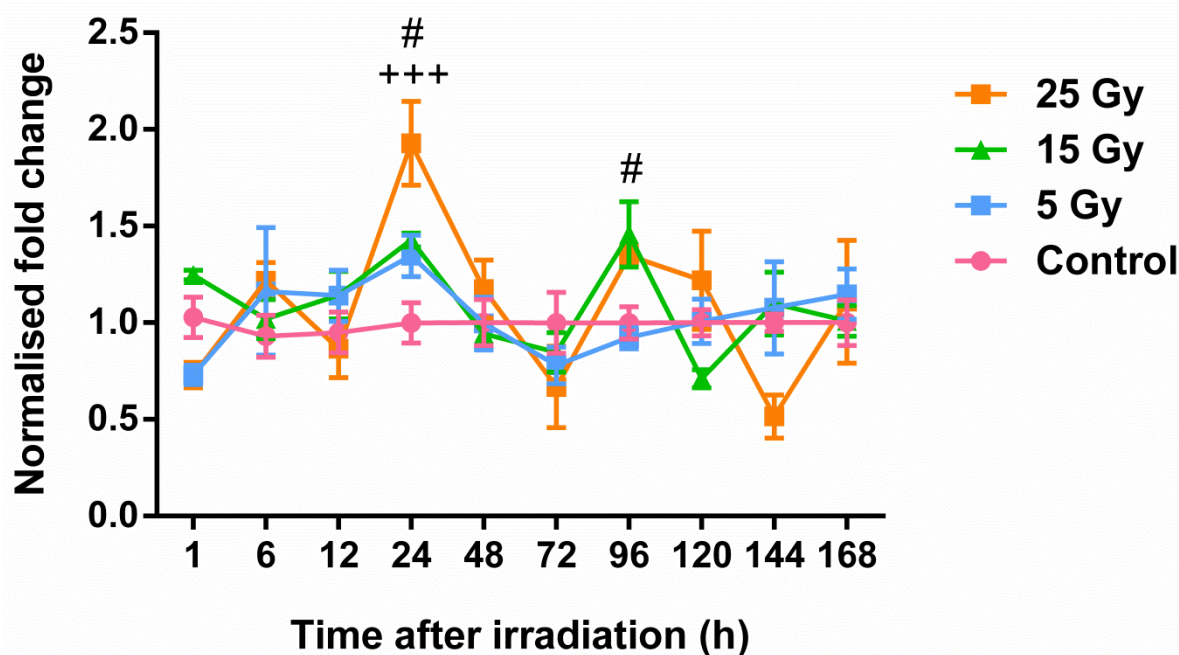
Figure 3.6. Relative gene expression of P-selectin in bEnd.3 cells post-irradiation. The relative levels of P-selectin gene expression were determined by quantitative real-time PCR at 1, 6, 12, 24, 48, 72, 96, 120, 144 and 168 h post-irradiation with LINAC at 5, 15 or 25 Gy. The fold change between irradiated and non-irradiated cells was considered. The expression of HPRT gene was used as a housekeeping control. Mean ± SEM. n = 4. * $P < 0.05$, *** $P < 0.001$, #, represents the comparison between cells treated with 15 Gy and non-irradiated control. +, represents the comparison between cells treated with 25 Gy treated and non-irradiated.

3.3.3 Western analysis of endothelial adhesion molecule expression post-irradiation

Protein expression levels of ICAM-1, VCAM-1, E-selectin and P-selectin, after irradiation with 5, 15, and 25 Gy at 24, 72, and 120 h were studied by western blot analysis. Non-irradiated bEnd.3 cells were considered as controls.

3.3.3.1 Intercellular adhesion molecule 1 (ICAM-1) protein expression

Examination of ICAM-1 protein expression after irradiation with 25 Gy illustrated a time-dependent increase in expression reaching a maximum at the latest time point examined (120 h) (Figure 3.7). At the time of peak expression (120 h), there was a dose-dependent increase in ICAM-1 expression with a significant difference in expression relative to non-irradiated cells at 25 Gy (2.5-fold increase, ** $P < 0.01$) and at 15 Gy (2.1-fold increase, * $P < 0.05$) (Figure 3.8). However, there was no significant difference between irradiated cells with 5 Gy and non-irradiated cells at the 120 h time-point (Figure 3.8). Although there was a

small difference in expression between 15 Gy and 25 Gy doses, this did not reach statistical significance. The protein expression profile for ICAM-1 was reflective of that seen for ICAM-1 gene expression.

| | 0 | 25 | 25 | 25 | Dose (Gy) |
| | 0 | 24 | 72 | 120 | Hour (h) |
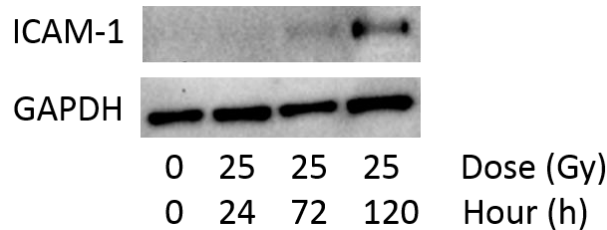
Figure 3.7. Time course of ICAM-1 protein expression in bEnd.3 cells post-irradiation with 25 Gy. The ICAM-1 protein expression was determined by western blot at 24, 72, and 120 h post-irradiation with LINAC at 25 Gy. The expression of GAPDH was used to ensure equal protein loading between samples. n = 1.

ICAM-1 dose-response at 120 h post-irradiation
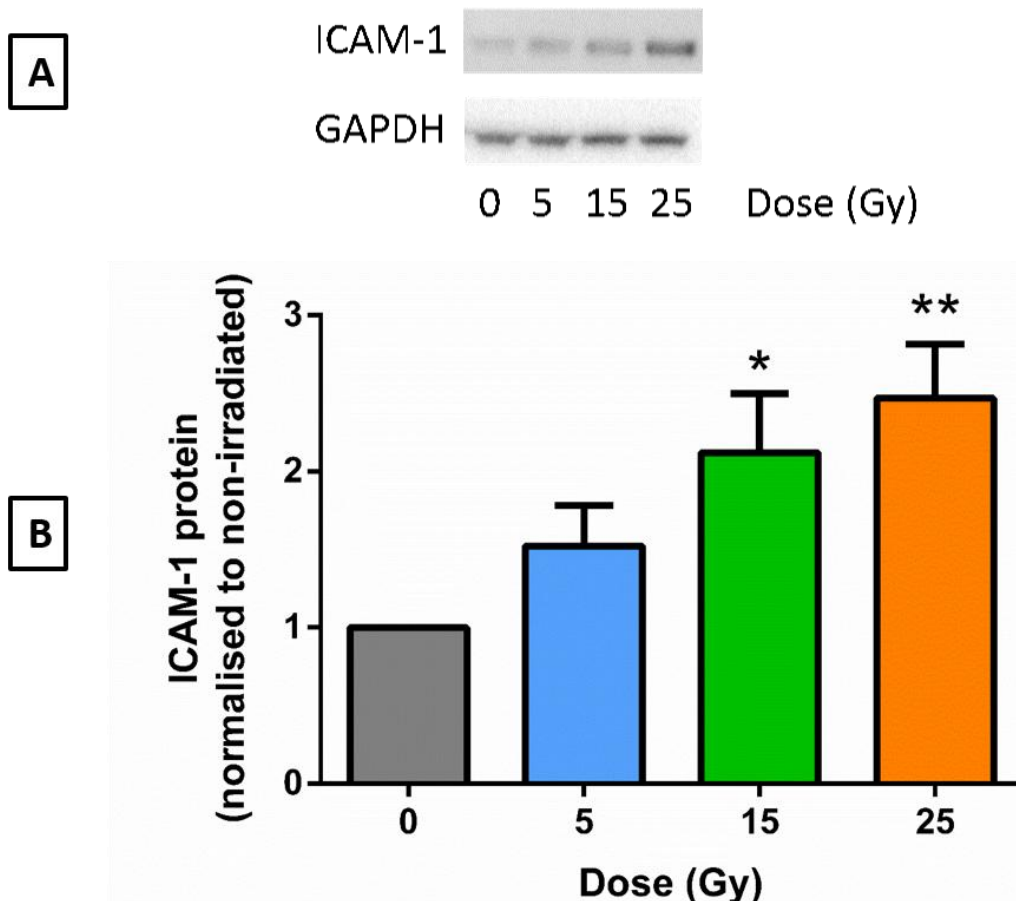
Figure 3.8. Effect of dose on ICAM-1 protein expression in bEnd.3 cells at 120 h post-irradiation. A. Representative western blots of ICAM-1 protein expression at 120 h post-irradiation with LINAC at 5, 15 and 25 Gy. B. Fold-change between irradiated and non-irradiated cells was determined by quantitating band intensity with Image J and normalising to GAPDH to correct for protein loading and non-irradiated cells for fold-change. Mean ± SEM. n = 4. * P < 0.05 vs non-irradiated control, ** P < 0.01 vs non-irradiated control.

3.3.3.2 Vascular cell adhesion molecule 1 (VCAM-1) protein expression

Over the 120 h time period examined, levels of VCAM-1 protein expression peaked at 72 h after irradiation with 25 Gy (Figure 3.9). At the 72 h peak, there was a significant difference between non-irradiated cells and those given a 15 Gy (3.2-fold, ** $P < 0.01$) and 25 Gy (2.7-fold, * $P < 0.05$) dose (Figure 3.10). The level of VCAM-1 protein expression was higher in cells treated with 15 Gy compared to 25 Gy, however this did not reach statistical significance. This finding was consistent with the higher levels of VCAM-1 found earlier for the 15 Gy dose relative to the 25 Gy dose at the gene expression level. The early expression peak followed by a trough at 120 h was also consistent with the pattern of VCAM-1 gene expression described earlier.
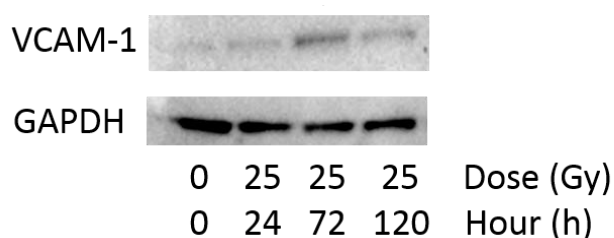
Figure 3.9. Time course of VCAM-1 protein expression in bEnd.3 cells after irradiation with 25 Gy. Representative western blot showing the change in expression of VCAM-1 protein over a 5 day period after 25 Gy radiation. Protein levels of GAPDH were used to ensure equal protein loading between samples.

VCAM-1 dose-response at 72 h post-irradiation
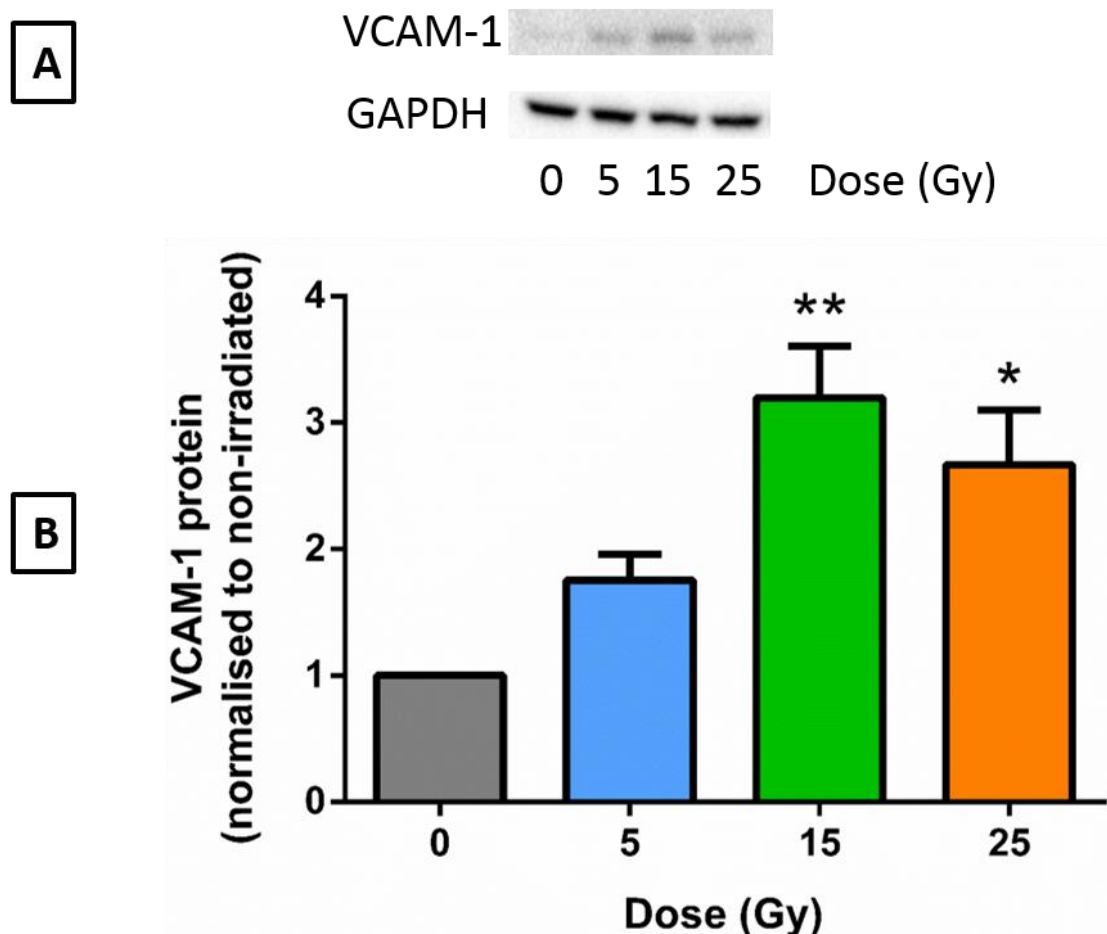
Figure 3.10. Effect of dose on VCAM-1 protein expression in bEnd.3 cells at 72 h post-irradiation. A. Representative western blots of VCAM-1 protein expression at 72 h post-irradiation with LINAC at 5, 15 and 25 Gy. B. Fold-change between irradiated and non-irradiated cells was determined by quantitating band intensity with Image J and normalising to GAPDH to correct for protein loading and non-irradiated cells for fold-change. Mean ± SEM. n = 3. * P < 0.05 vs non-irradiated control, ** P < 0.01 vs non-irradiated control.

3.3.3.3 E-selectin protein expression

Two time points were examined for changes in protein levels for E-selectin. There was no significant difference between irradiated cells with 5, 15, and 25 Gy and non-irradiated cells at both 24 and 72 h post-irradiation (Figure 3.11).
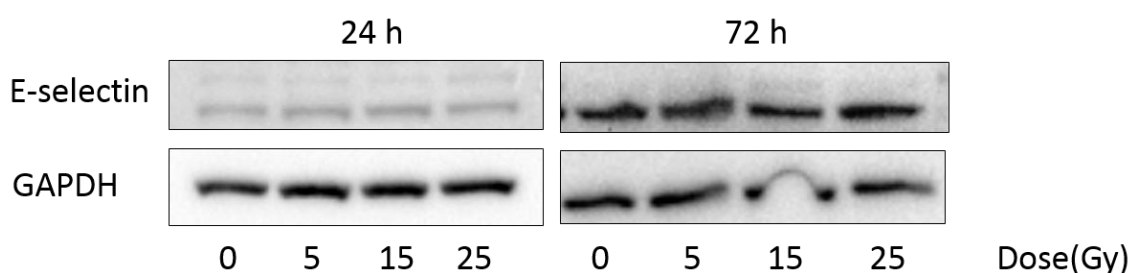
Figure 3.11. Effect of dose on E-selectin protein expression in bEnd.3 cells at 24 h and 72 h post-irradiation. Representative western blots of E-selectin protein expression at 24 h and 72 h post-irradiation with LINAC at different doses (5, 15, and 25 Gy). n = 3.

3.3.3.4 P-selectin protein expression

Protein expression level of P-selectin also showed no significant difference in both irradiated with 5, 15 and 25 Gy and non-irradiated control cells at both 24 and 72 h post-irradiation (Figure 3.12).
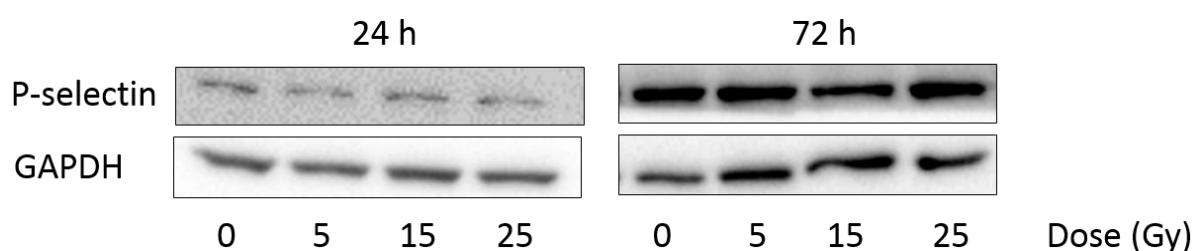
Figure 3.12. Effect of dose on P-selectin protein expression in bEnd.3 cells at 24 h and 72 h post-irradiation. Representative western blots of P-selectin protein expression at 24 h and 72 post-irradiation with LINAC at different doses (5, 15, and 25 Gy). n = 3.

3.3.4 Cell surface expression of endothelial adhesion molecules post-irradiation

The prior analysis of mRNA and protein expression by qRT-PCR and western blotting clarifies the effect of radiation on total cellular expression. However, these data cannot determine the proportion of molecules on the cell surface and their availability for targeting. To examine cell surface localisation and quantification, ICC and ELISA were used to examine ICAM-1 and VCAM-1 after irradiation (5, 15, and 25 Gy) at 24, 72, and 120 h. ELISA was also used for E-selectin and P-selectin, after irradiation (5, 15, and 25 Gy) at 24, 72, and 120 h. Non-irradiated bEnd.3 cells were considered as controls.

3.3.4.1 ELISA quantification of intercellular adhesion molecule 1 (ICAM-1) surface expression

Consistent with the qRT-PCR and western blot results, there was a marked increase in cell surface expression of ICAM-1 in adherent bEnd.3 cells post-irradiation as detected by ICAM-1-specific ELISA (Figure 3.13). The level of expression was increased dramatically in irradiated cells at doses of 15 Gy and 25 Gy compared to non-irradiated cells at all time-points. There was no significant difference between cells irradiated with 5 Gy and non-irradiated control cells. Using this assay, cells irradiated with 15 Gy showed higher surface protein expression at 72 h and 120 h compared to cells irradiated with 25 Gy ($P < 0.05$).
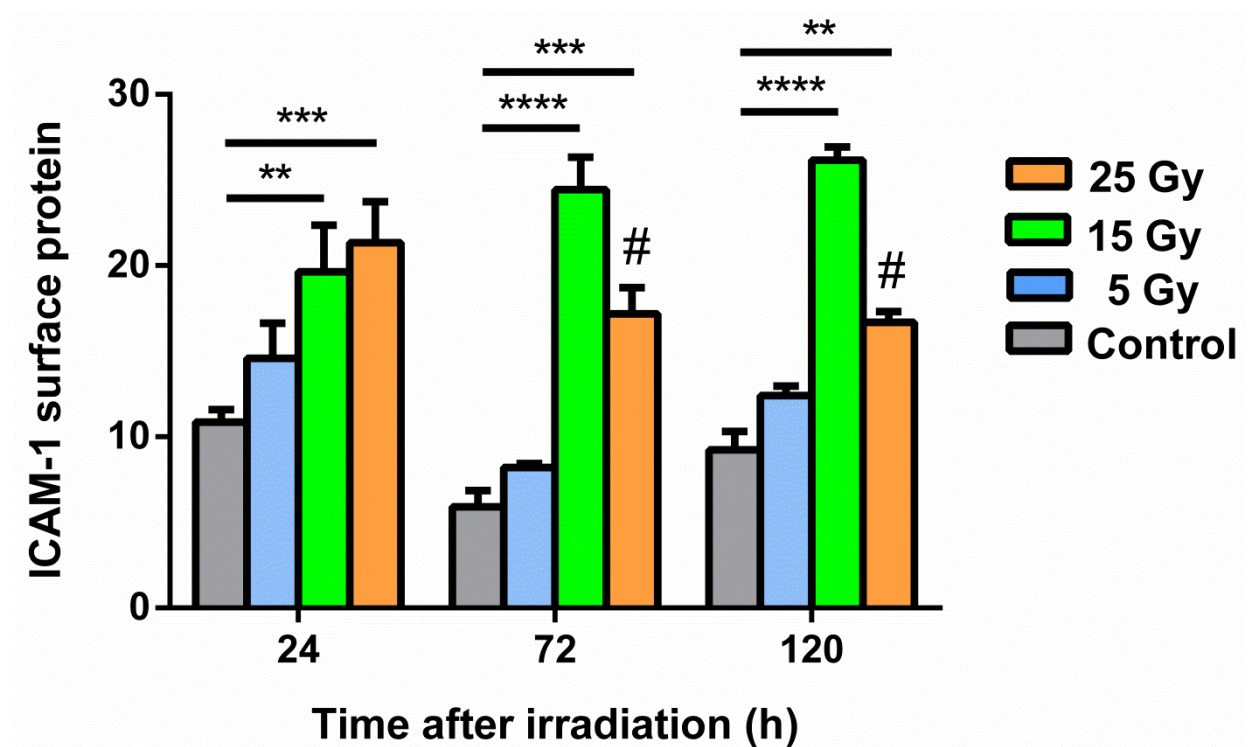
Figure 3.13. ELISA determination of ICAM-1 surface expression in bEnd.3 cells post-irradiation. Surface expression of ICAM-1 was determined by ELISA at 24, 72, and 120 h post-irradiation with 5, 15 and 25 Gy radiation doses. [#]$P < 0.05$, ** $P < 0.01$, *** $P < 0.001$, and **** $P < 0.0001$. *, represent comparisons between irradiated (15 or 25 Gy) and non-irradiated cells; #, represents comparison between 15 Gy and 25 Gy. Data represent mean ± SEM of three independent experiments performed in triplicate. The ELISA absorbance readings were normalised to Janus green absorbance readings.

3.3.4.2 ELISA quantification of vascular cell adhesion molecule 1 (VCAM-1) surface expression

The cell surface protein expression of VCAM-1 was elevated in response to irradiation with 15 Gy and 25 Gy (Figure 3.14). The protein expression level was significantly higher in

irradiated cells with 25 Gy, starting as early as 24 h (P < 0.01) post-irradiation, which continued till the end of the experiment. Marked expression of VCAM-1 occurred with the 15 Gy dose starting at 72 h post-irradiation. No significant increase in expression was evident in cells irradiated with 5 Gy. In addition, there was no significant difference in VCAM-1 expression detected between bEnd.3 cells irradiated with 15 Gy and 25 Gy.
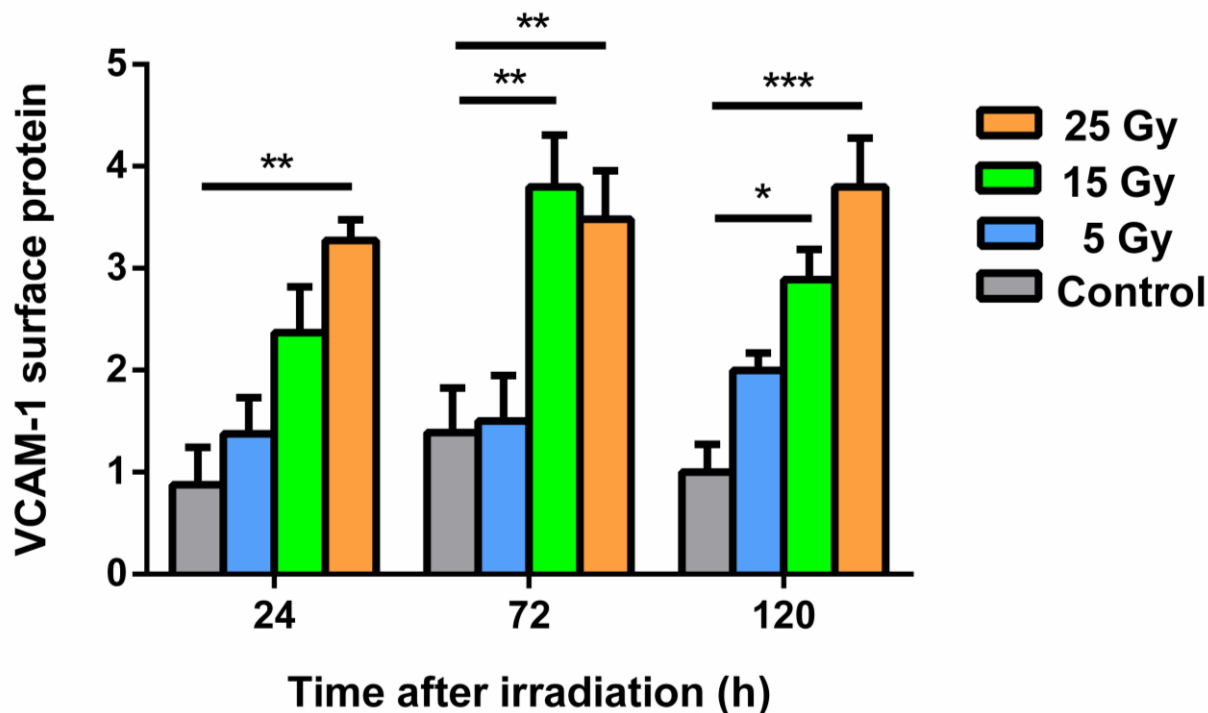
Figure 3.14. ELISA determination of VCAM-1 surface expression in bEnd.3 cells post-irradiation. Surface expression of VCAM-1 was determined by ELISA at 24, 72, and 120 h post-irradiation with 5, 15 and 25 Gy radiation doses. * P < 0.05, ** P < 0.01, and *** P < 0.001. *, represent comparisons between irradiated (15 or 25 Gy) and non-irradiated cells. Data represent mean ± SEM of three independent experiments performed in triplicate. The ELISA absorbance readings were normalised to Janus green absorbance readings.

3.3.4.3 ELISA quantification of E-selectin surface expression

Consistent with earlier qRT-PCR and western analysis, the changes in expression of E-selectin at the cell surface after radiation as determined by ELISA (Figure 3.15) were not as compelling as seen for VCAM-1 and ICAM-1. Although reaching statistical significance, the expression of E-selectin was only 1.3-1.4-fold higher (P < 0.05) in irradiated cells relative to non-irradiated cells with a dose of 25 Gy at 120 h post-irradiation. At the rest of the time-points, there was no significant difference between treated and non-treated cells.
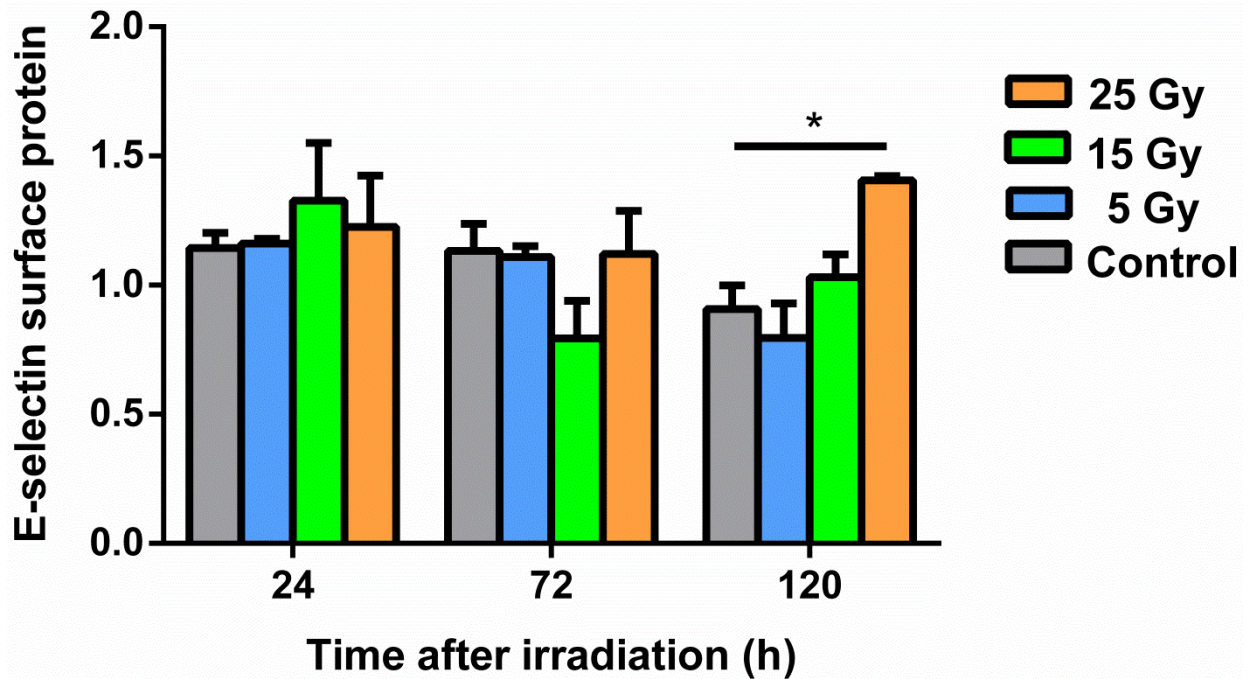
Figure 3.15. ELISA determination of E-selectin surface expression in bEnd.3 cells post-irradiation. Surface expression of E-selectin was determined by ELISA at 24, 72, and 120 h post-irradiation with 5, 15 and 25 Gy radiation doses. * P < 0.05, *, represent comparisons between irradiated (25 Gy) and non-irradiated cells. Data represent mean ± SEM of three independent experiments performed in triplicate. The ELISA absorbance readings were normalised to Janus green absorbance readings.

3.3.4.4 ELISA quantification of P-selectin surface expression

Quantification of P-selectin surface expression by ELISA showed P-selectin expression was significantly elevated after irradiation with either a 15 or 25 Gy dose at all experimental time-points (Figure 3.16). Cells irradiated with 5 Gy showed no up-regulation in protein expression compared to non-irradiated cells. There was no significant difference between bEnd.3 cells irradiated with 15 Gy and 25 Gy at 24 h and 72 h time-points, however expression was greater in cells treated with 15 Gy at 120 h post-irradiation. Surface P-selectin expression appeared to increase rapidly at the 24 h time-point after a dose of 25 Gy then slowly declined over the 120 h. A dose of 15 Gy appeared to result in sustained expression of P-selectin at the cell surface relative to 25 Gy.
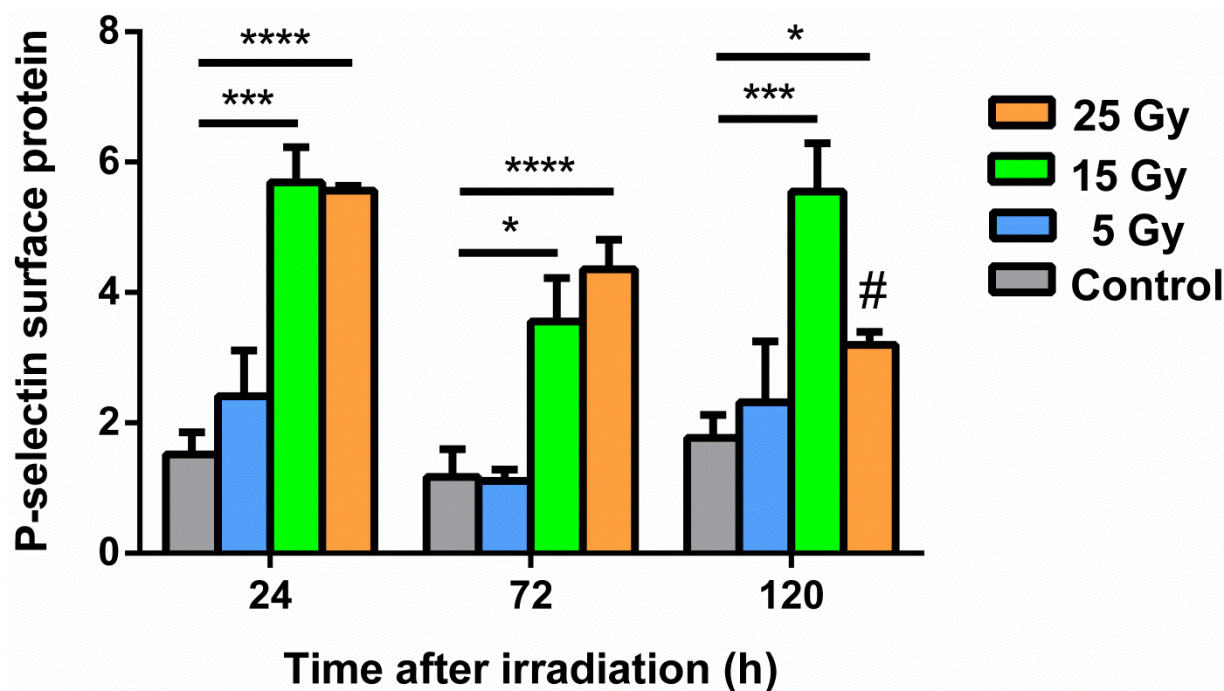
Figure 3.16. ELISA determination of P-selectin surface expression in bEnd.3 cells post-irradiation. Surface expression of P-selectin was determined by ELISA at 24, 72, and 120 h post-irradiation with 5, 15 and 25 Gy radiation doses. * $P < 0.05$, *** $P < 0.001$, and **** $P < 0.0001$. *, represent comparisons between irradiated (15 or 25 Gy) and non-irradiated cells; #, represents comparison between 15 Gy and 25 Gy. Data represent mean ± SEM of three independent experiments performed in triplicate. The ELISA absorbance readings were normalised to Janus green absorbance readings.

3.3.4.5 Immunocytochemical analysis of intercellular adhesion molecule 1 (ICAM-1) and vascular cell adhesion molecule 1 (VCAM-1) expression

Immunocytochemical analysis showed that ICAM-1 was poorly expressed at early time-points and in the absence of radiation treatment but increased over time and with radiation dose at the cell surface (Figure 3.17). Quantitative analysis showed that expression of ICAM-1 increased dramatically in irradiated cells treated with 25 Gy at 72 h ($P < 0.001$) and 120 h ($P < 0.01$) post-irradiation compared to non-irradiated cells (Figure 3.18). Moreover, in cells irradiated with 15 Gy there was a significant elevation at 120 h ($P < 0.0001$) compared to non-irradiated cells. There was no significant difference between irradiated cells treated with 5 Gy and non-irradiated control cells. There was a significant difference between cells irradiated with 15 Gy and 25 Gy ($P < 0.05$) at 72 h and 120 h post-irradiation. It was noted that some of the cells did not express ICAM-1 regardless of time and dose. It is unclear why some cells did not express ICAM-1. The results of this study, western and ELISA analysis thus reflect the average expression across all cells.

Time after irradiation (h)	Control	5 Gy	15 Gy	25 Gy
24				
72				
120				
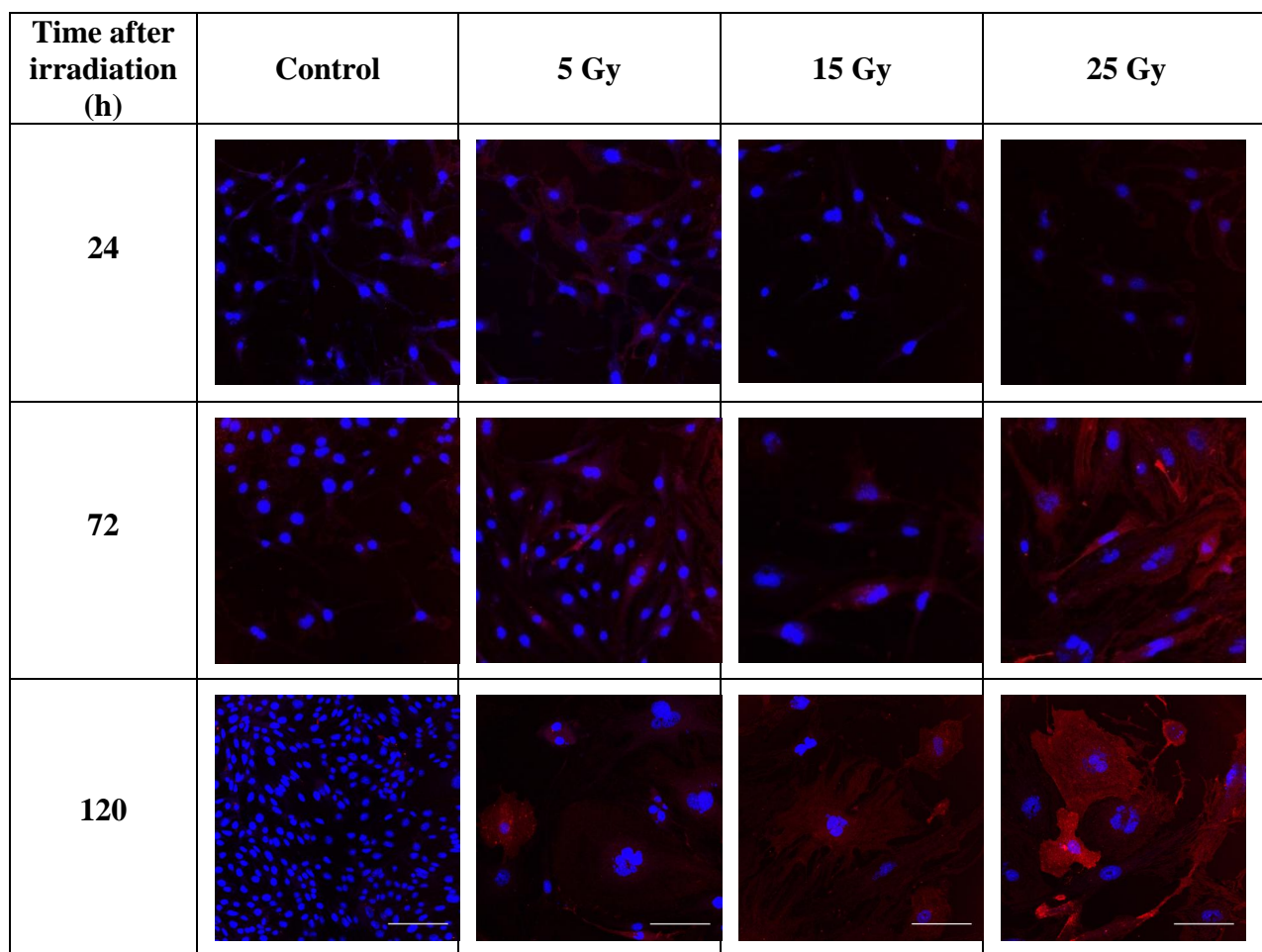
Figure 3.17. Surface localisation of ICAM-1 in irradiated bEnd.3 cells. Immunocytochemistry (ICC) was performed on bEnd.3 cells using CF^{TM}555-conjugated anti-ICAM-1 antibody (red). Cells were counterstained with DAPI (blue) to visualise cell nuclei. Representative images show the CF^{TM}555-conjugated ICAM-1 antibody targeting the cell surface at increasing doses of radiation (5 – 25 Gy) and in a time-dependent manner. Scale bar = 100 µm (Scale bar only shown on the bEnd.3 cell images at 120 h post-irradiation).
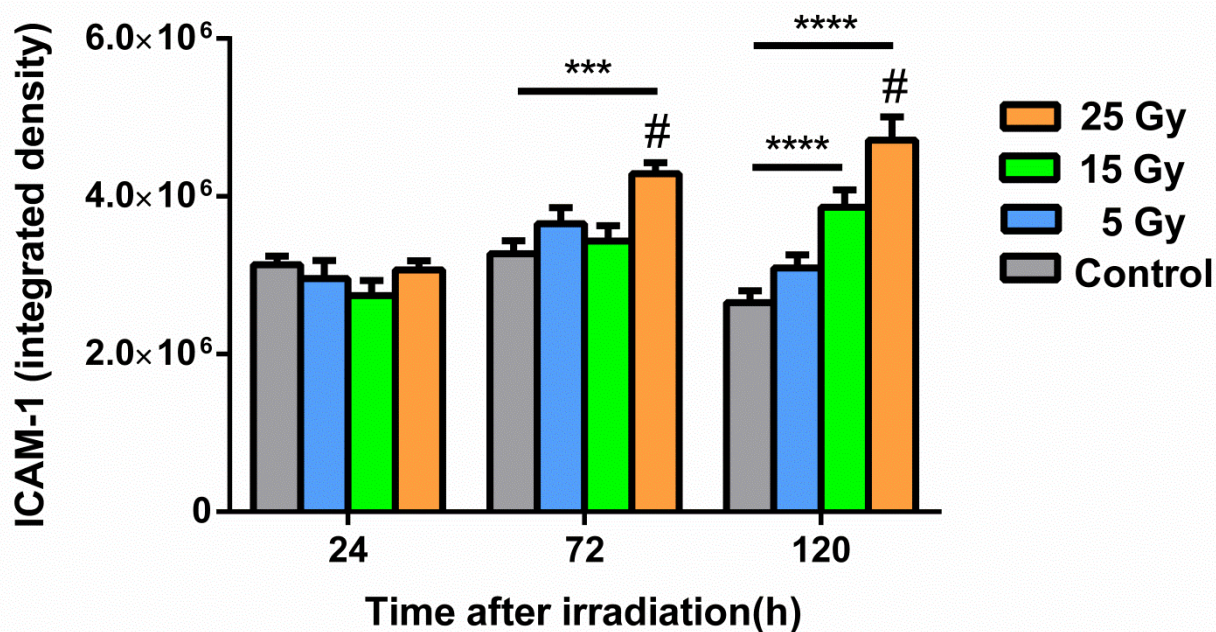
Figure 3.18. Quantification of ICAM-1 surface expression by ICC post-irradiation. Signal intensity in CF[TM]555-ICAM-1 stained bEnd.3 cells at 24, 72, and 120 h post-irradiation (5, 15 and 25 Gy) was quantified using Image J. The same size region of interest (ROI) was considered for all the images. Units of measurement (integrated density = area × intensity) are arbitrary. [#]P < 0.05, *** P < 0.001, and **** P < 0.0001. *, represents comparison between irradiated cells (15 or 25 Gy) and non-irradiated control cells. #, represents comparison between 15 Gy and 25 Gy. Data represent mean ± SEM of three independent experiments performed in triplicate.

Immunocytochemical analysis showed that VCAM-1 was poorly expressed at early time-points and in the absence of radiation treatment but increased with radiation at the cell surface (Figure 3.19). Quantitative analysis showed there was a prominent increase in VCAM-1 cell surface protein expression in bEnd.3 irradiated cells with either 15 or 25 Gy doses compared to non-irradiated cells (Figure 3.20). The cells irradiated with 15 Gy showed marked increases at 24 h (P < 0.01) and 120 h (P < 0.0001) post-irradiation. Moreover, VCAM-1 was elevated in cells irradiated with 25 Gy at 72 h (P < 0.0001) and 120 h (P < 0.01) post-irradiation. Cells irradiated at 5 Gy showed no significant difference to non-irradiated cells. In addition, there was no significant difference between the 15 Gy and 25 Gy irradiated cells at the earlier time points. At the 120 h time-point, VCAM-1 expression was higher in the 15 Gy irradiated cells relative to the 25 Gy treated cells (P < 0.0001). This was consistent with earlier qRT-PCR and western blot analysis of VCAM-1 expression (sections 3.3.2.2 and 3.3.3.2). It was noted that some of the cells did not express VCAM-1 regardless of time and dose. It is unclear why some cells did not express VCAM-1. The results of this study, western and ELISA analysis thus reflect the average expression across all cells.

Time after irradiation (h)	Control	5 Gy	15 Gy	25 Gy
24				
72				
120				
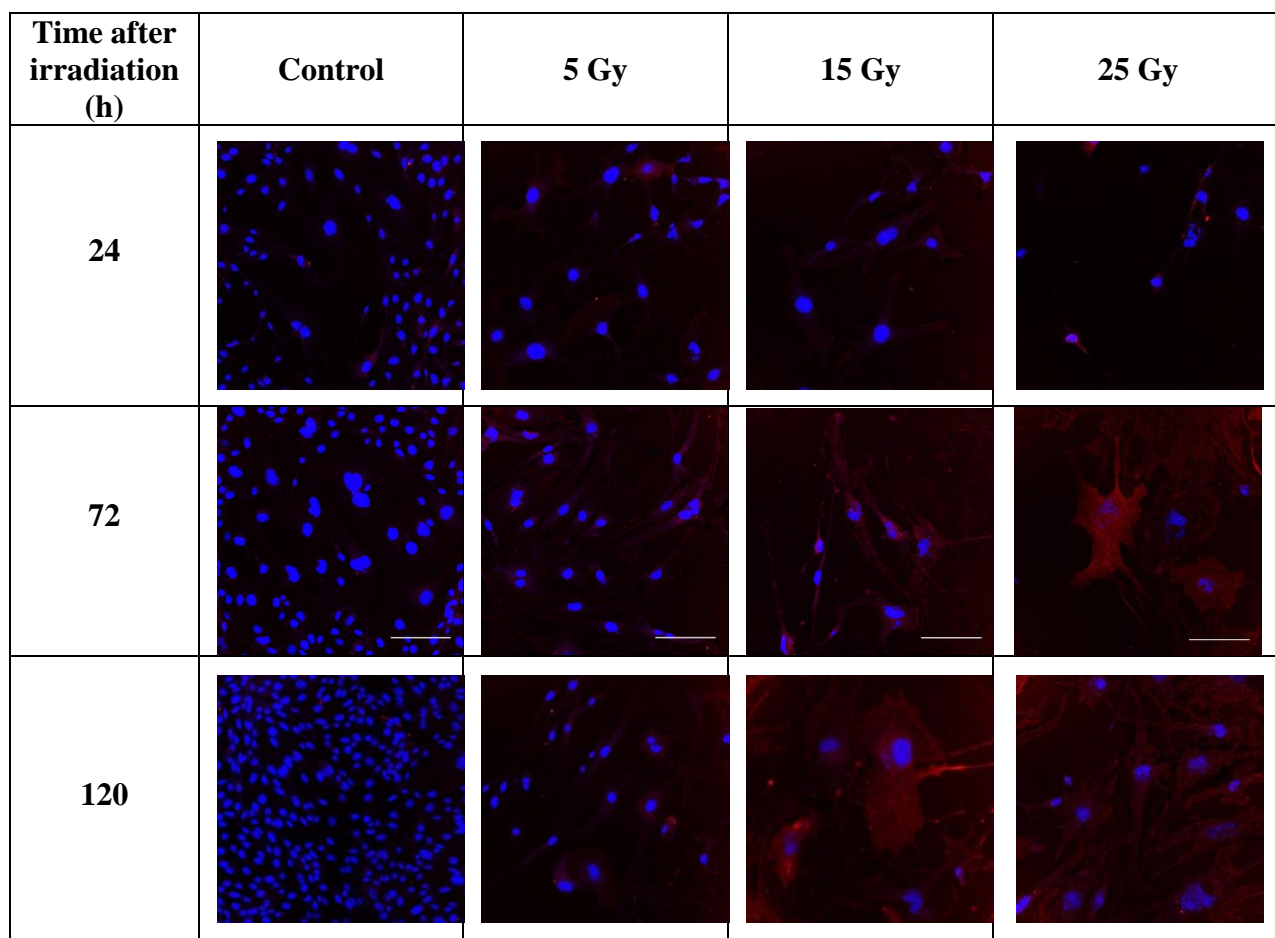
Figure 3.19. Surface localisation of VCAM-1 in irradiated bEnd.3 cells. Immunocytochemistry (ICC) was performed on bEnd.3 cells using CF[TM]640-conjugated anti-VCAM-1 antibody (red). Cells were counterstained with DAPI (blue) to visualise cell nuclei. Representative images show the CF[TM]555-conjugated VCAM-1 antibody targeting the cell surface at increasing doses of radiation (5 – 25 Gy) and in a time-dependent manner. Scale bar = 100 μm (Scale bar only shown on the bEnd.3 cell images at 72 h post-irradiation).
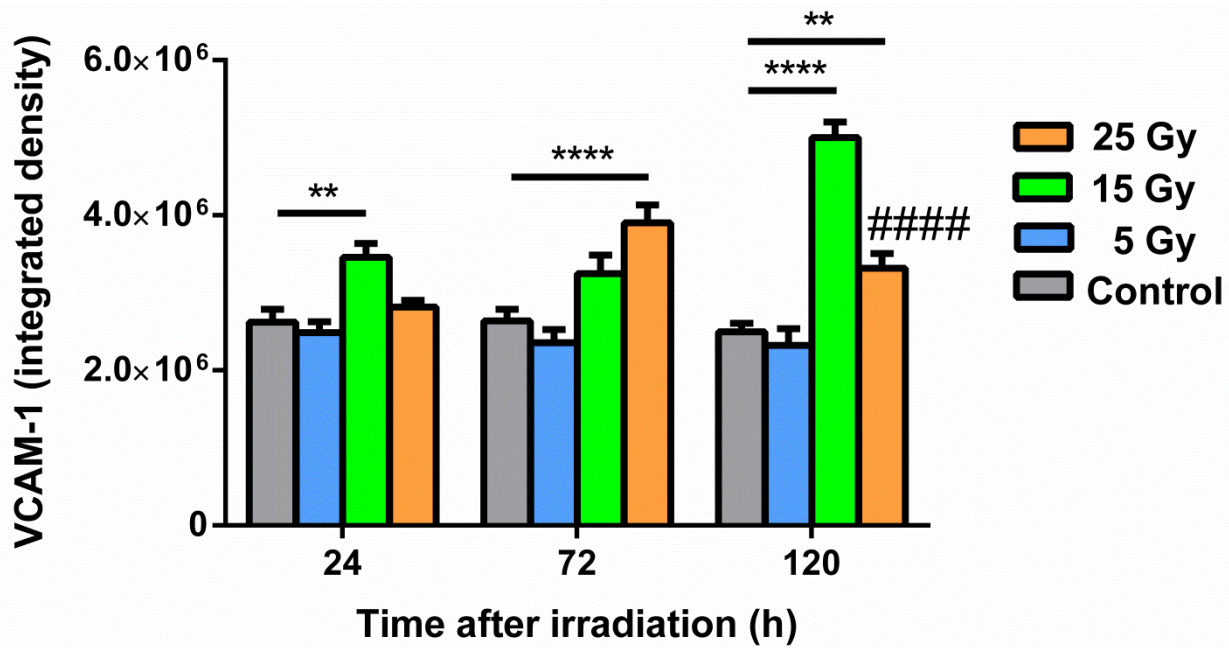
Figure 3.20. Quantification of VCAM-1 surface expression by ICC post-irradiation. Signal intensity in CF^{TM}640-VCAM-1 stained bEnd.3 cells at 24, 72, and 120 h post-irradiation (5, 15 and 25 Gy) was quantified using Image J. The same size region of interest (ROI) was considered for all the images. Units of measurement (integrated density = area × intensity) are arbitrary. ** $P < 0.01$, **** $P < 0.0001$ and $^{####}$ $P < 0.0001$. *, represents comparison between irradiated cells (15 or 25 Gy) and non-irradiated control cells. #, represents comparison between 15 Gy and 25 Gy. Data represent mean ± SEM of three independent experiments performed in triplicate.

3.3.4.6   Validation of CF^{TM}555-ICAM-1 and CF^{TM}640-VCAM-1 specificity with non-targeting CF^{TM}555-isotype and CF^{TM}640-isotype controls

In order to make sure that the CF^{TM}555-ICAM-1 and CF^{TM}640-VCAM-1 antibodies bind specifically to their respective targets, both CF^{TM}555 and CF^{TM}640 dyes conjugated to the appropriate isotype controls (IgG2b isotype for anti-ICAM-1 antibody; IgG1 isotype for anti-VCAM-1 antibody).

The counterstained images with DAPI and CF^{TM}555-isotype (negative control for ICAM-1) showed no fluorescence intensity on the cell surface at any of the irradiation doses. However, the cells counterstained with DAPI and CF^{TM}555-ICAM-1showed high red intensity as the dose of irradiation increased (Figure 3.21). The quantification analysis also showed lower signal intensity in cells stained with CF^{TM}555-isotype compared to the cells stained with CF^{TM}555-ICAM-1 (Figure 3.22).

Irradiation dose	Isotype control	Anti-ICAM probe
Control		
5		
15		
25		
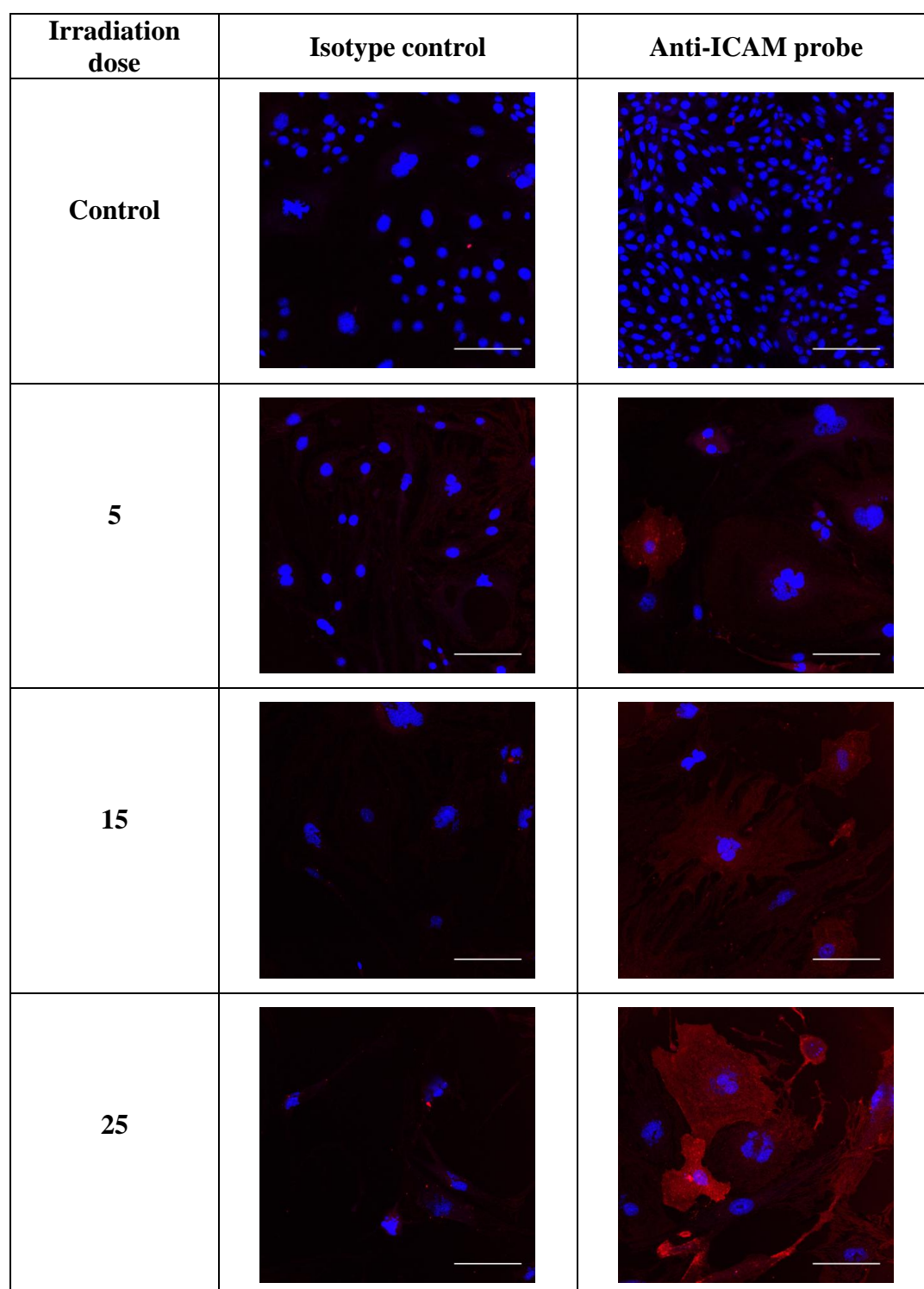
Figure 3.21. Immunocytochemistry (ICC) of CF^{TM}555-isotype and CF^{TM}555-ICAM-1 staining in irradiated bEnd.3 cells. ICC was performed on bEnd.3 cells using CF^{TM}555-conjugated to either isotype or anti-ICAM-1 antibody (red). Cells were counterstained with DAPI (blue) to visualise cell nuclei. Representative images show the CF^{TM}555-conjugated isotype (IgG2b) and CF^{TM}555-conjugated ICAM-1 antibody targeting ICAM-1 at the cell surface 120 h after irradiation (5 – 25 Gy). Scale bar = 100 µm.
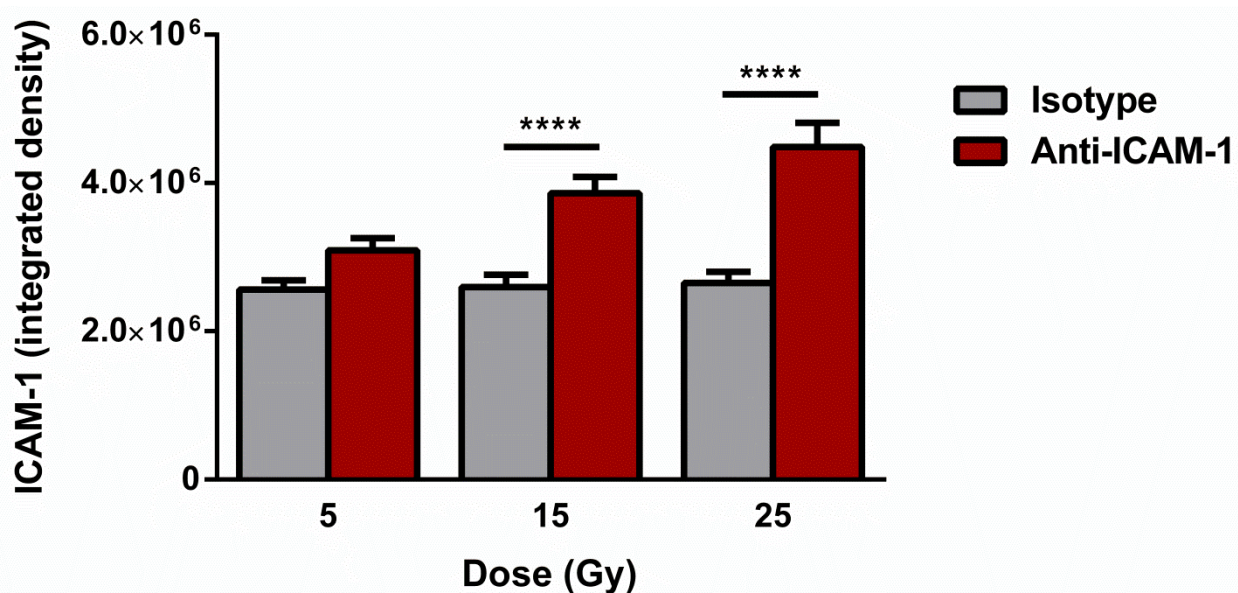
Figure 3.22. Quantification of CF^{TM}555-isotype and CF^{TM}555-ICAM-1 binding on irradiated bEnd.3 cells. Signal intensity in CF^{TM}555-isotype and CF^{TM}555-ICAM-1 stained bEnd.3 cells at 120 h post-irradiation (5, 15 and 25 Gy) was quantified using Image J. The same size region of interest (ROI) was considered for all the images. Units of measurement (integrated density = area × intensity) are arbitrary. Data represent mean ± SEM of three independent experiments performed in triplicate. **** P < 0.0001, *, represents comparison between CF^{TM}555-ICAM-1 and CF^{TM}555-isotype probes at the same dose.

For the VCAM-1 isotype control, the fluorescence images also revealed no fluorescence intensity at the cell surface level in contrast to cells stained with CF^{TM}640-VCAM-1 which showed high red intensity on irradiated cells up to the highest dose (25 Gy) (Figure 3.23). The quantification analysis showed the increase in fluorescence intensity at the cell surface in cells stained with CF^{TM}640-VCAM-1 relative to the CF^{TM}640-isotype (Figure 3.24).

Irradiation dose	Isotype control	Anti-VCAM probe
0		
5		
15		
25		
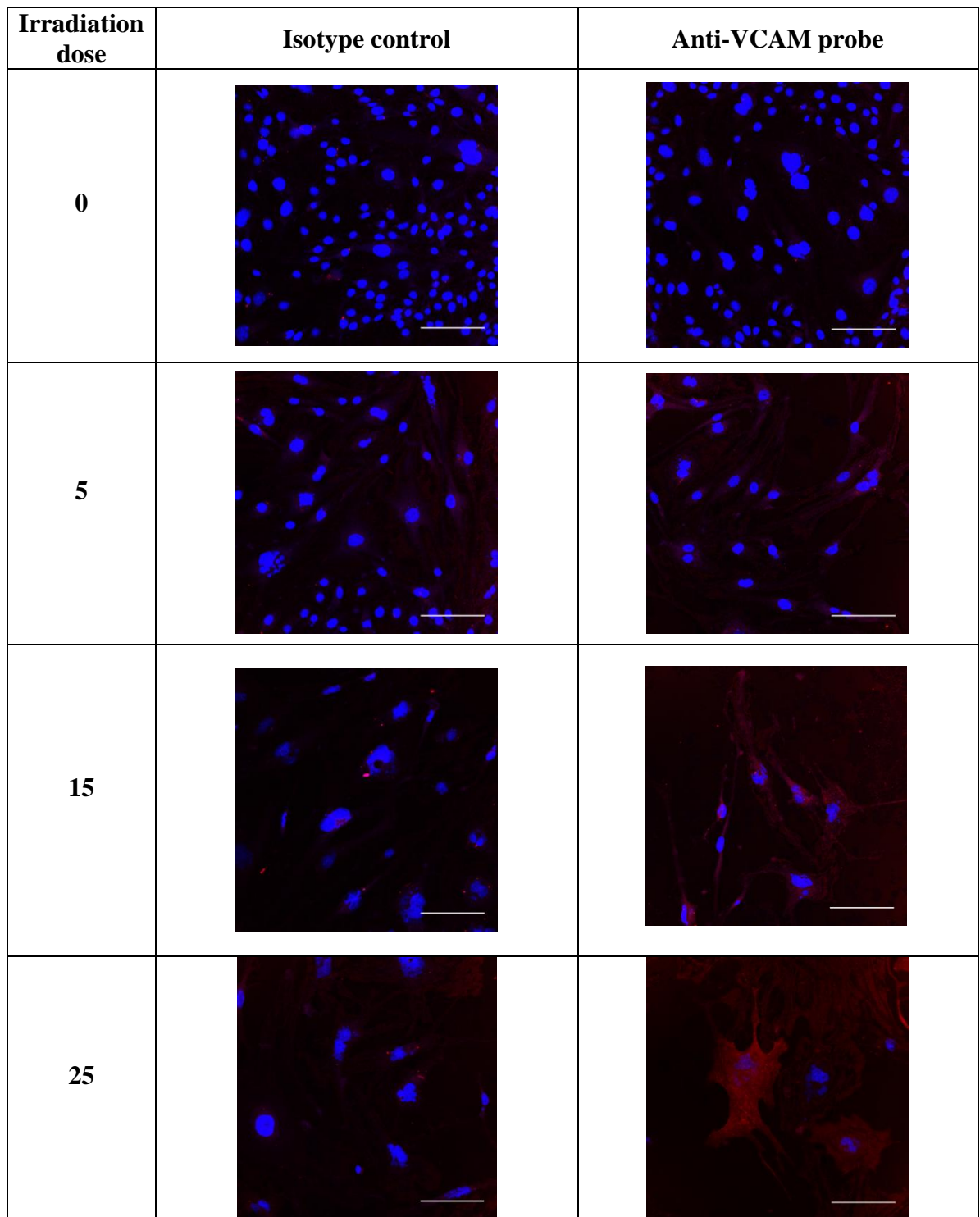
Figure 3.23. Immunocytochemistry (ICC) of $CF^{TM}640$-isotype and $CF^{TM}640$-VCAM-1 staining in irradiated bEnd.3 cells. ICC was performed on bEnd.3 cells using $CF^{TM}640$-conjugated to either isotype or anti-VCAM-1 antibody (red). Cells were counterstained with DAPI (blue) to visualise cell nuclei. Representative images show the $CF^{TM}640$-conjugated isotype (IgG1) and $CF^{TM}640$-conjugated VCAM-1 antibody targeting VCAM-1 at the cell surface 72 h after irradiation (5 − 25 Gy). Scale bar = 100 μm.
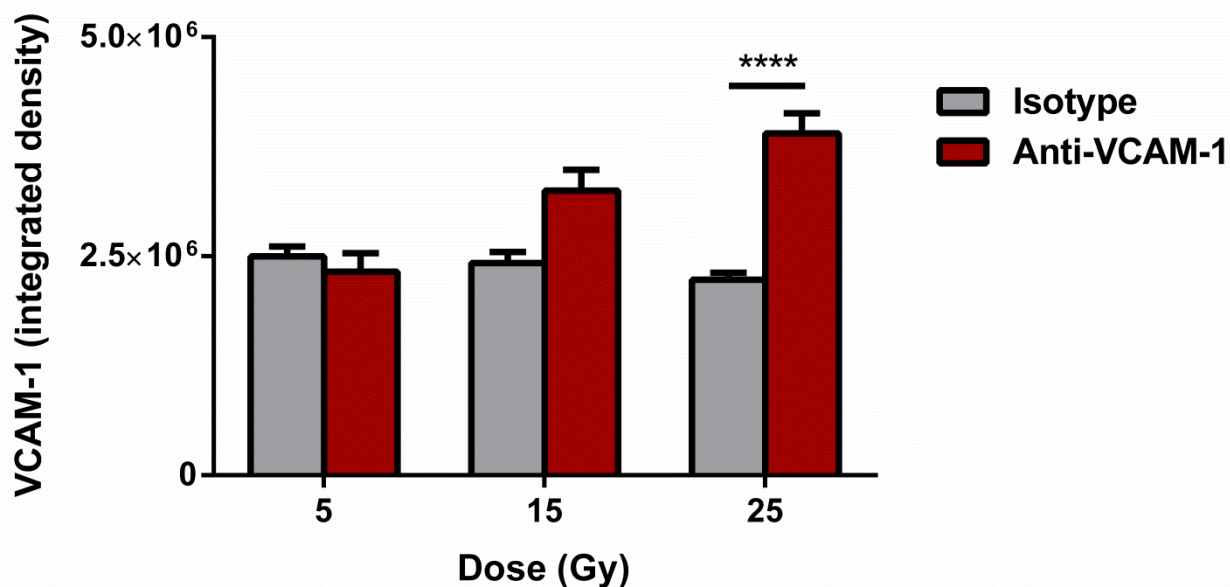
Figure 3.24. Quantification of CF^{TM}640-isotype and CF^{TM}640-VCAM-1 binding on irradiated bEnd.3 cells. Signal intensity in CF^{TM}640-isotype and CF^{TM}640-VCAM-1 stained bEnd.3 cells at 72 h post-irradiation (5, 15 and 25 Gy) was quantified using Image J. The same size region of interest (ROI) was considered for all the images. Units of measurement (integrated density = area × intensity) are arbitrary. Data represent mean ± SEM of three independent experiments performed in triplicate. **** $P < 0.0001$, *, represents comparison between CF^{TM}640-VCAM-1 and CF^{TM}640-isotype probes at the same dose.

3.4 Discussion

The effect of irradiation at three different doses was examined on endothelial cell adhesion molecules (CAMs) both at the gene and protein levels. The investigation was leading toward the selection of the best candidate for vascular targeting treatment of AVMs. The ideal candidate should be highly discriminating in the AVM irradiated tissue compared to the normal tissue to be appropriate for selection. Radiation doses of 15 Gy and 25 Gy showed induction in expression of all considered endothelial CAMs during the study time period. Among the four candidates, E-selectin showed only moderate expression post-irradiation suggesting this molecule is not the optimal choice for vascular targeting. In contrast, ICAM-1 and VCAM-1 examination post-irradiation indicated enhanced induction with increased surface expression. Similarly, increased surface expression of P-selectin suggests these three molecules have potential for selection for vascular targeting in irradiated AVMs.

3.4.1 Radiation effect on cell growth and morphology

As well as showing alterations to cell surface molecule expression, radiation had a significant effect on endothelial cell proliferation and morphology. With respect to cell growth there was a negative relationship between irradiation dose and cell count. At the higher doses, cell numbers decreased over time. Similar results were obtained by Henning *et al.* who irradiated human endothelial cells with doses up to 16 Gy (Henning et al., 2004). In this study, the remaining adherent cells became enlarged and flattened, with a shape reminiscent of senescent cells that can no longer divide. Yentrapalli *et al.* also reported premature senescence post-irradiation in HUVECs and studies on vascular endothelial cells by Igarashi and Miura showed similar results (Igarashi & Miura, 2008; Yentrapalli et al., 2013). In response to radiation and depending on the level of damage, cells normally go through any of these three pathways: cell cycle arrest, DNA lesion repair, or apoptosis (Eriksson & Stigbrand, 2010; Li et al., 2001). Cells are relatively radiosensitive in the G1 and G2 phases of the cell cycle compared to S phase (Brown & Rzucidlo, 2011). Cells are also radiosensitive at M phase as the DNA is packaged tightly and there is a high chance that ionising radiation causes lethal DNA double-stranded breaks (Brown & Rzucidlo, 2011). Fareh *et al.* reported G1 arrest in human coronary artery endothelial cells in response to irradiation at 2 Gy with no apoptosis induction (Fareh et al., 1999). Recent studies performed at Macquarie University have shown by flow cytometry that irradiated bEnd.3 cells show a G2/M peak after irradiation with 25 Gy (Zhao et al., 2015). In the current study, automated cell counter results and microscopic observations did not indicate complete apoptosis in any of the experimental conditions.

3.4.2 Radiation effect on ICAM-1 expression

The experiments described here at the level of mRNA and protein revealed up-regulation of ICAM-1 post-irradiation in a time- and a dose-dependent manner. There was no significant difference between 15 Gy and 25 Gy at the mRNA and protein level indicated by qRT-QPCR and western blot techniques, respectively. Induction of ICAM-1 in irradiated bEnd.3 cells as measured by ELISA and ICC techniques, suggested the cell surface expression of ICAM-1 after irradiation was proportional to the level of transcription and translation. Cell surface expression of ICAM-1 on endothelial cells is an important characteristic that the target molecule should have for the future vascular targeting of AVMs.

Radiation is well known to induce ICAM-1 expression in various cells and tissue types. In a study by Gaugler *et al.*, an increase in expression of ICAM-1 was reported in HUVEC cells

with a range of doses from 2 to 10 Gy. The results obtained from their study were based on both northern blot analysis (mRNA) and flow cytometry (surface expression) and were consistent with the current study showing a proportional change between transcription and surface expression (Gaugler et al., 1997). Similarly, northern blot analysis and flow cytometry on HDMEC indicated ICAM-1 mRNA up-regulation and cell surface expression at 24 h after exposure to 5 Gy or 10 Gy (Heckmann et al., 1998). In another study by Haubner *et al.*, ELISA analysis of HDMEC revealed significant up-regulation of ICAM-1 at 48 h after receiving 12 Gy (Haubner et al., 2013). An increase in ICAM-1 surface protein expression in HUVEC cells was also reported 72 h post-irradiation with 10 Gy by flow cytometry (Van Der Meeren, 1999). Other studies have also shown increased surface expression of ICAM-1 by ELISA. Another study by Gaugler *et al.*, showed ICAM-1 up-regulation on the surface of transformed human bone marrow endothelial cells by ELISA with 2 Gy (Gaugler et al., 1998). In another study by ELISA on human brain endothelial cell line 24 h after receiving 50 Gy, the cells demonstrated up-regulation of ICAM-1 expression over 4-fold which returned to baseline by 72 h (Sharp et al., 2003). The expression of ICAM-1 in the current study is in agreement with previous studies, although the differences in time of peak expression may be a feature of primary cell cultures versus immortalised cell lines, radiation dose and type or other experimental conditions. ICAM-1 showed a significant induction of surface expression in response to radiation and may be an ideal candidate for vascular targeting.

3.4.3 Radiation effect on VCAM-1 expression

In regards to VCAM-1 expression post-irradiation, this study showed significant up-regulation at both the level of mRNA and protein after irradiation with both 15 Gy and 25 Gy. The methodologies showed a similar trend in expression over time and dose. There was no significant difference between the cells irradiated with 15 Gy and 25 Gy, showing 15 Gy is as effective as 25 Gy to induce VCAM-1 expression on endothelial cells.

Irradiation has been shown to cause induction of VCAM-1 expression in different cell types and tissues. In a study by Heckmann *et al.*, an increase in VCAM-1 expression in HDMEC cells was shown by northern blot analysis and flow cytometry, 24 h after receiving either 5 or 10 Gy doses (Heckmann, 1998). In the latter study, both VCAM-1 mRNA expression and cell surface up-regulation showed a time- and dose-dependent increase (Heckmann, 1998). Haubner *et al.*, also showed significant elevation of VCAM-1 in HDMEC 48 h after receving

6 Gy and 12 Gy, by ELISA analysis (Haubner et al., 2013). In another study by Epperly *et al.*, on primary cultures of murine pulmonary endothelial cells, VCAM-1 expression was increased 24 h after receiving 20 Gy (Epperly et al., 2002). Both of these studies are in agreement with the current results for VCAM-1 expression in bEnd.3 cells that demonstrated up-regulation post-irradiation with 15 or 25 Gy, although with different times of peak expression.

Interestingly, the level and time of peak expression of VCAM-1 in irradiated cells was different to ICAM-1 which suggests that these two molecules are regulated by different mechanisms in response to radiation. The exact mechanisms or signalling pathways that cause VCAM-1 and ICAM-1 expression post-irradiation are unknown. It has been postulated that reactive oxygen species (ROS) generated during irradiation (Riley, 1994) can activate NFκB (nuclear factor kappa-light-chain-enhancer of activated B cells) (Schreck et al., 1991). The NFκB protein complex regulates DNA transcription affecting cytokine production, inflammation and cell survival (Brasier, 2006). However, both ICAM-1 and VCAM-1 are regulated by NFκB (Min et al., 2005; Paxton et al., 1997) hence the radiation-induced signals to these genes must be multifactorial and differ for the two adhesion molecules. The sustained expression of ICAM-1 may be associated with the senescence-like cell morphology observed in irradiated cells at later time points, as senescent cells are known to express high levels of ICAM-1 in a p53-dependent but an NFκB-independent manner (Gorgoulis et al., 2005; Zhou et al., 2006). Overall, as for ICAM-1, VCAM-1 is a potential candidate molecule for vascular targeting.

3.4.4 Radiation effect on E-selectin expression

E-selectin revealed a small increase in expression at the mRNA level post-irradiation. Although significant, there was less than two-fold difference between irradiated and non-irradiated control cells at 72 h and 96 h. There was also a very marginal increase in E-selectin cell surface expression post-irradiation indicated by ELISA with the highest radiation dose at 120 h. Western analysis showed there was a high basal level of E-selectin expression in these endothelial cells that was not altered with irradiation. Studies have shown that expression of E-selectin *in vitro* requires *de novo* synthesis of both RNA and protein (Nelson & Bevilacqua, 1993). Thus, it is unclear why there is some discrepancy between the methods used here, but this may be due to the very low levels of induction as well as the sensitivity of each method.

Regardless, the cell surface expression level of E-selectin seems limited in this study and does not fulfil our goal for considering this molecule for vascular targeting.

To further understand the effect of irradiation on E-selectin, several *in vitro* studies have focused on the expression of E-selectin on cultured endothelial cells in response to radiation. The literature concerning E-selectin time course of expression post-irradiation on endothelial cells is inconsistent (Prabhakarpandian et al., 2001). Hallahan's group reported up-regulation of E-selectin on HUVEC surface at 4 h post-irradiation with 0.5 Gy by immunofluorescence (Hallahan et al., 1997; Hallahan et al., 1996). Heckman and colleagues reported elevation of E-selectin mRNA levels at 6 h and 24 h post-irradiation with either 5 or 10 Gy in HDMECs by northern blot and flow cytometric analysis (Heckmann, 1998). In another study, up-regulation of E-selectin on HDMECs at 5 h and 24 h post-irradiation with 10 Gy was revealed with flow cytometric analysis (Prabhakarpandian et al., 2001). They also demonstrated a low level of expression of E-selectin in non-irradiated HDMEC cells compared to irradiated cells (Prabhakarpandian et al., 2001). In contrast, Sharpe *et al.* demonstrated significant up-regulation of E-selectin in a human brain endothelial cell line 72 h after irradiation with 50 Gy by ELISA (Sharp et al., 2003) which is most consistent with the data presented here. The discrepancy in peak of expression of E-selectin in different tissues post-irradiation may be due to the different characteristics of primary cell cultures and immortal cell lines, experimental conditions, and/or different radiation dose. In the current study, E-selectin did not show a high level of expression at either the mRNA or protein level post-irradiation, which suggests it may not be a good candidate for vascular targeting. However, previous studies showed that proliferating subconfluent bovine capillary endothelial cells exhibit constitutive levels of E-selectin expression compared to quiescent confluent cultures (Bischoff et al., 1997). Similar results were achieved with human microvascular endothelial cells (Luo et al., 1999). Thus, the small increase in E-selectin in the current study may have been due to high constitutive levels expressed in the subconfluent, proliferating cells. However, this may reflect the higher proliferative activity of AVM endothelial cells. Further experiments could re-examine expression of this molecule using irradiation of confluent ECs.

3.4.5 Radiation effect on P-selectin expression

In regards to P-selectin expression, this study revealed moderate up-regulation of this molecule at the mRNA level at early time points post-irradiation but only with 15 Gy and 25 Gy (i.e. at 24 h and 72 h). There was no significant increase in P-selectin at the total

protein level indicated by western blot however this analysis indicated a high endogenous level in total cell protein. In contrast, P-selectin exhibited significant cell surface expression post-irradiation with 15 Gy and 25 Gy as determined by ELISA. The ELISA technique was an informative method to more specifically elucidate the cell surface expression of P-selectin compared to western blot analysis. These results were expected as P-selectin is normally produced and stored intracellularly in the Weibel-Palade bodies of vascular endothelial cells and upon activation is merged with the plasma membrane and migrates to the cell surface (Pinsky et al., 1996; Vestweber & Blanks, 1999).

Irradiation has been shown to cause induction in the expression level of P-selectin in endothelial cells both *in vitro* and *in vivo.* In a study by Hallahan and Virudachalam, immunofluorescence studies of HUVECs revealed significant up-regulation of P-selectin after receiving 2 Gy irradiation (Hallahan & Virudachalam, 1999). In another study by Hariri *et al.*, P-selectin expression was increased in HUVECs after irradiation with 3 Gy (Hariri et al., 2008).

Most studies examing the effect of radiation on P-selectin expression on endothelial cells are *in vivo*. In an immunohistochemical study on thoracic irradiation of mice with doses between 2 – 20 Gy, P-selectin was expressed within 30 min in the vascular lumen with subsequent accumulation in endothelial cells of larger vessels in the pulmonary vascular system (Hallahan & Virudachalam, 1997). Immunohistochemistry studies on endothelial cells of lung larger vessels (veins and arteries) of mice showed P-selectin up-regulation 14 day post-irradiation with 9 Gy. Also Van der Meeren and her colleagues studied P-selectin expression at the mRNA level with qRT-PCR which showed 3-fold increase in expression after 10 to 18 days post-irradiation (Van der Meeren et al., 2003). Also, Molla *et al*. reported P-selectin up-regulation at different time-points depending on the irradiation doses of 4 or 10 Gy on rat mesenteric vessels measured by the radiolabeled antibody technique. P-selectin expression was significantly increased on small-bowel endothelium 24 h after receiving 4 Gy, however when higher dose of 10 Gy was administered the up-regulation was reached as early as 2 h post-irradiation with further increases at 6 h and 24 h. It was also shown that P-selectin was expressed on the intestinal vascular endothelium of non-irradiated mice at low levels compared to irradiated (Molla et al., 1999; Molla et al., 2001). As P-selectin showed moderate expression at mRNA and protein level post-irradiation it suggests it cannot be a good candidate for vascular targeting.

3.4.6 Dose radiation effect on endothelial CAM expression

The secondary aim of this study was to determine the lowest effective dose for induction of molecular changes on the endothelial cells for future vascular targeting. With respect to cell growth, 15 Gy and 25 Gy reduced cell growth significantly compared to control cells. The 25 Gy reduced the cell number significantly compared to 15 Gy, which might have put more cells in either cell cycle arrest, DNA damage or apoptosis. These outcomes suggested that 15 Gy is a better radiation dose than 25 Gy as this dose could induce vascular target but would pose less risk *in vivo* to damage surrounding cells.

Examination of endothelial CAM induction with three different irradiation doses suggested that there was no significant induction with a dose of 5 Gy when compared to non-irradiated cells. The situation was different however when the cells were irradiated with 15 Gy and 25 Gy. The results showed significant up-regulation of endothelial CAM molecules when the cells were irradiated with either 15 or 25 Gy. Most importantly, results indicated no significant difference in ICAM-1, E-selectin and P-selectin induction in cells irradiated with either 15 or 25 Gy. Since there was no significant difference between the 15 Gy and 25 Gy, and in the case of VCAM-1 where there was some indication that 15 Gy has a higher level of expression than 25 Gy, it can be suggested that 15 Gy may be a reasonable option to proceed with in future targeting experiments. Applying a lower radiation dose has many clinical advantages. For example, reducing the dose will increase the size of AVM lesions that are able to be treated. Thus, this may provide some hope for patients with AVMs currently classed as untreatable because of size. Lower dose also reduces the possibility of radiation damage on normal cells surrounding the AVM tissue. It must be kept in mind that choosing 15 Gy from this set of *in vitro* experiments does not necessarily indicate that this will be ideal or sufficient to induce molecular changes *in vivo* in either the AVM animal model or in a clinical context. Therefore, to further study the effect of 15 Gy irradiation dose on induction of endothelial CAMs, the AVM animal model was examined in the next two chapters.

3.5 Limitations and future directions

The immortal mouse brain endothelial cell line used in this study was the best available option at the commencement of this study for examining the effect of irradiation on endothelial cells. Obviously these are not human cells and this may have some limitation if there are species-specific differences. Ideally, irradiation of endothelial cells isolated directly

from human AVM tissue would be the most relevant. In general, *in vitro* work has its limitations, as it does not provide the exact environmental condition as *in vivo*, e.g. there is no interaction between different cell types and no macrophages to remove dead cells. However, this *in vitro* work can still generate valuable results to be taken forward to a more complicated pre-clinical *in vivo* environment. Considering all these, an ideal model to study the effect of irradiation on AVM tissue would be an AVM animal model that would resemble the human AVM. Therefore, in the next chapter the effect of irradiation on the AVM animal model will be studied to further investigate the effect of irradiation on the possible two best candidate molecules, ICAM-1 and VCAM-1.

3.6 Summary and Conclusions

The results from these studies indicated that radiation induces molecular changes on the surface of endothelial cells. Some changes occurred as a result of transcriptional regulation while others occurred at the level of protein localisation to the cell surface. Among the endothelial CAMs, ICAM-1 and VCAM-1 in radiated cells with 15 Gy and 25 Gy indicated the highest increase in surface expression compared to non-irradiated cells. P-selectin showed a moderate increase at the cell surface. E-selectin demonstrated limited up-regulation and cell surface expression after irradiation. These outcomes point to ICAM-1 and VCAM-1 as the most discriminating candidates for vascular targeting treatment in future investigations. P-selectin is also a promising candidate as it showed high levels of induction on the cell surface.

The second aim of this study was to determine the lowest radiation dose to induce these molecular changes on the surface of endothelial cells. The results indicated that 5 Gy showed no significant difference in induction of endothelial CAMs compared to non-irradiated cells. Radiating the cells with 15 Gy and 25 Gy led to a reduction in the number of live cells with a greater reduction in cells irradiated with 25 Gy. As radiation with 25 Gy resulted in more cells going through either cell cycle arrest, DNA damage or apoptosis, the cell proliferation study suggested the lower dose of 15 Gy was a better option than the 25 Gy, given the primary desired outcome is high expression, not cell death. The study of molecular changes on endothelial cells with 15 Gy and 25 Gy suggested that 15 Gy not only caused the same expression level in endothelial CAMs, but with respect to VCAM-1, generated a higher level of expression compared to 25 Gy.

These results indicated that ICAM-1 and VCAM-1 are the best candidates for further study in the AVM animal model in response to a radiation dose of 15 Gy.

Chapter 4. Anatomical localisation and quantification of post-radiosurgery ICAM-1 and VCAM-1 expression in an AVM animal model

Objectives: Intercellular adhesion molecule 1 (ICAM-1) and vascular cell adhesion molecule 1 (VCAM-1) play essential roles in inflammatory processes. Their expression has been shown to increase in response to irradiation. The aims of this experiment were to identify the level of expression of ICAM-1 and VCAM-1 and their anatomical location in an animal model of AVM and to examine whether they may be potential candidates for vascular targeting post-irradiation.

Methods: Six week old, male Sprague-Dawley rats (n = 48) had creation of an AVF. Six weeks later, the AVM area in 24 rats was irradiated with Gamma Knife at 15 Gy while the remaining 24 received no radiation. Xenolight 750 conjugated with ICAM-1 or VCAM-1 antibody was used to detect surface ICAM-1 and VCAM-1 expression, respectively, during fluorescence optical *in vivo* imaging. Fluorescence intensity was measured at 1, 7, 21, 42, 63 and 84 days post-irradiation.

Results: Fluorescent signal determining the expression of ICAM-1 was high in both irradiated and non-irradiated AVM rats at all time-points. The fluorescent signal was localised solely to the AVM area indicative of accessible ICAM-1 expression in this area. The ICAM-1 signal was not significantly different between control and irradiated rats at any time point despite a trend to increasing fluorescence intensity over time in irradiated animals. The fluorescent signal indicating luminal expression of VCAM-1 was also high both in irradiated and non-irradiated rats at all time-points. The signal was localised specifically at the AVM area. The VCAM-1 expression peaked at day 21 in irradiated animals however, there was no significant difference between irradiated and non-irradiated rats.

Conclusions: Vessels in the rat model AVM express high levels of ICAM-1 and VCAM-1 compared to normal vessels. A single dose of 15 Gy gamma radiation does not significantly increase surface expression of ICAM-1 and VCAM-1. At this dose, ICAM-1 and VCAM-1 may not be ideal candidates for a vascular targeting approach.

4.1 Introduction

Intercellular adhesion molecule 1 (ICAM-1) and vascular cell adhesion molecule 1 (VCAM-1) are part of the immunoglobulin superfamily of membrane proteins (Bevilacqua, 1993; Rice & Bevilacqua, 1989; Rice et al., 1990; Rice et al., 1991). Both ICAM-1 and VCAM-1 play key roles in inflammatory processes by mediating firm and irreversible adhesion of leukocytes to the endothelium (Springer, 1990). ICAM-1 also contributes to thrombosis and haemostasis (Bombeli et al., 1998; Etienne et al., 1998; Thompson et al., 2002). Both VCAM-1 and ICAM-1 are expressed at low levels on the surface of unstimulated endothelial cells. Expression is increased in the presence of inflammatory stimuli, radiation, and shear stress (Pohlman et al., 1986).

In the previous chapter it was shown that the expression of inflammatory molecules was up-regulated post-irradiation in mouse brain endothelial cells at doses of 15 Gy and 25 Gy. *In vitro* studies cannot competely replicate the *in vivo* environment, thus to elucidate further the response of ICAM-1 and VCAM-1 post-irradiation in an *in vivo* context, an AVM animal model was considered. The specific aims of this study were to determine the time course and anatomical location of expression of ICAM-1 and VCAM-1 in the animal model of AVM after irradiation at a dose of 15 Gy, to evaluate their suitability as vascular targeting candidates.

4.2 Materials and methods

4.2.1 AVM rat Model

In vivo fluorescence optical imaging was performed to localise and quantify the level of expression of ICAM-1 and VCAM-1 in the AVM model. Six week old male Sprague Dawley rats (Animal Resources Centre, WA, Australia, 162 – 188 g, n = 48) had the creation of an anastomosis between the left carotid artery and left jugular vein to form the animal model of arteriovenous malformation (AVM) (explained in detail in section 2.3.1.4.). Six weeks after the formation of the model AVM the rats were irradiated with a Leksell Gamma Knife (explained in detail in section 2.3.2.).

Animals (n = 48) were randomly divided into groups as shown in Table 4.1 Out of the total number of rats, three groups were considered, each group with two cohorts of irradiated and

non-irradiated rats. The first group of animals (n = 2, each cohort) were used for Xenolight 750-ICAM-1/VCAM-1 dye concentration optimisation. The second group of animals (n = 6, each cohort) were used as negative controls to account for non-specific binding of Xenolight 750-ICAM-1/VCAM-1. This group of rats was shared between ICAM-1, VCAM-1 and phosphatidylserine experiments (Chapter 5) as a negative control for each NIR dye. The third group of animals (n = 7, each cohort) formed the experimental group for ICAM-1/VCAM-1 detection over the 84 day period. A separate group of six week old male rats (n = 6, total) without any AVM creation or radiation treatment were also considered as controls for AVM formation.

Table 4.1. Rat usage and number

Experimental group	Number of AVM irradiated rats	Number of AVM non-irradiated rats
ICAM-1 dye optimisation	n = 2	n = 2
ICAM-1/VCAM-1 negative control	n = 6	n = 6
ICAM-1 detection	n = 7	n = 7
VCAM-1 dye optimisation	n = 2	n = 2
VCAM-1 detection	n = 7	n = 7
Control AVM (No creation of AVF)	n = 6	

4.2.2 Near Infrared (NIR) dye preparation

Prior to NIR fluorescence optical *in vivo* imaging at each time point, the NIR probes for ICAM-1 and VCAM-1 detection were prepared fresh. Purified mouse anti-rat ICAM-1 (CD54, 0.5 mg/mL, #554967), purified mouse anti-rat VCAM-1 (CD 106, 0.5 mg/mL, #559165) and control mouse IgG1 isotype (1 mg/mL, #553447) antibodies were labelled with the NIR dye. The antibodies were free of BSA. They contained $\leq 0.09\%$ sodium azide in aqueous buffered solution that was removed by size filtration during the labelling procedure. All the antibodies were purchased from BD Biosciences, CA, USA.

The NIR dye used for *in vivo* molecular optical imaging was Xenolight CF750 (Caliper Life Sciences, Inc., MA, USA; #PK1125674). Xenolight CF750 has maximum absorption at 755 nm and maximum emission at 775 nm. The dye probe was prepared by conjugating Xenolight CF750 to either ICAM-1 or VCAM-1 or IgG1 isotype control antibodies. The resulting probe was formed by a stable amide linkage that connected the succinimidyl ester

group of the dye to the amine group of the protein (i.e., lysine side-chain amine). The NIR dye was sufficient to label 1 – 2 mg of IgG antibody. At the completion of the labelling reaction the unconjugated dye was removed from the final NIR dye by ultrafiltration.

Conjugation steps were as follows: ICAM-1 antibody (CD54, 0.5 mg/mL, 1 mL) was added to 1 M pH 8.3 sodium bicarbonate (0.2 mL). A vial of CF 750 SE (0.1 μmole) dye was warmed to room temperature then dissolved with anhydrous dimethyl sulfoxide (DMSO, 25 μL). The prepared dye stock (25 μL) was mixed with the prepared antibody solution. The antibody/dye solution was protected from light by aluminium foil and incubated for 1 h on a platform rocker at room temperature. Then 0.3 mL of this antibody/dye solution was added to the upper chamber of a NanoSep membrane filtration vial. The vial was centrifuged at 13,000 rpm for 5 min. The centrifugation step was repeated until all of the solution was transferred. The NanoSep membrane was permeable to molecules with molecular weight of less than ~ 10,000 Daltons. Thus, small molecules such as the unconjugated free dye and phosphates could pass through the membrane. Conjugated dye with molecular weight of 150,000 Daltons remained on the upper side of the NanoSep membrane. At this stage, the upper chamber of the NanoSep membrane contained the labelled antibody and the collection tube contained the free dye, which was discarded. To the upper chamber 1X PBS was added (300 μL) and mixed gently to fully dissolve the labelled dye, which was then centrifuged at 13,000 rpm for 5 min. This step was repeated two more times until the collection tube contained an almost clear solution. The clear solution indicated that the free dye was completely removed from the labelled antibody. To the upper side of the NanoSep membrane, 1X PBS (2 mL) was added to reach a 1 mg/mL concentration for the labelled antibody. Then the labelled antibody solution was filtered into a sterile storage vial by a syringe attached to a filter. According to the manufacturer's protocol, the typical yield for preparing the CF Xenolight dye-labelled antibody was 80 – 90%.

The final concentration of the labelled antibody was calculated by the following formula:
[conjugate] (mg/mL) = {[A_{280} − (A_{max} × CF)] / 1.4} × dilution factor

"Dilution factor" is the fold of dilution used for spectral measurement. "A_{280}" is the absorbance reading of the labelled antibody at 280 nm and "A_{max}" is the absorption maximum (~ 755 nm). "CF" is the absorbance correction factor for Xenolight 750 which is 0.03. The value 1.4 is the extinction coefficient of whole (H + L) IgG. Finally, the degree of labelling (DOL) was calculated according to the following formula:

$$DOL = (A_{max} \times Mwt \times dilution\ factor) / (\varepsilon \times [conjugate])$$

In the above formula, "Mwt" is the molecular weight of IgG: ~ 150,000 and "ε" is the molar extinction coefficient of Xenolight 750: ~ 250,000. The labelled antibody was protected from light and stored at 4ºC, ready to be used for fluorescence optical *in vivo* imaging.

For NIR labelling of the VCAM-1 antibody (CD 106, 0.5 mg/mL) and IgG1 isotype antibody (1 mg/mL), the same steps were followed. Conjugated antibodies will be referred to as Xenolight 750-ICAM-1, Xenolight 750-VCAM-1 and Xenolight 750-isotype throughout this chapter.

4.2.3 NIR fluorescence optical *in vivo* imaging

The anaesthetised rat was placed in an In-Vivo Multispectral Imaging System FX cabinet (Carestream, NY, USA) with the shaved neck facing the glass platen surface. The rat was positioned face down to maximise AVM proximity for signal intensity. Anaesthesia was maintained via a nose cone with isoflurane ($2 - 3$ Vol.%) in oxygen (200 mL/min).

Three different *in vivo* images were taken. Prior to Xenolight 750-ICAM-1/VCAM-1 injection, an image in the same NIR fluorescence channel as Xenolight 750 dye (excitation filter, 730 nm; emission filter, 790 nm; exposure time, 60 s; bin = 2×2; f-stop = 2.80; field of view = 120 mm) was taken. This image was used to obtain a background reading for the fluorescence image taken after Xenolight 750-ICAM-1/VCAM-1 injection. Then Xenolight 750-ICAM-1/VCAM-1 was injected via the tail vein, followed by a NIR fluorescence image (excitation filter, 730 nm; emission filter, 790 nm; exposure time, 60 s; bin = 2×2; f-stop = 2.80; field of view = 120 mm). Immediately following the NIR image, an X-ray image (exposure time, 60 s; f-stop = 2.5; field of view = 120 mm) was taken to allow identification of the anatomical location of the fluorescence signal. At each experimental time point, new Xenolight 750 conjugated dye was prepared.

4.2.3.1 Dose optimisation of NIR-conjugated dye

The most important step at this stage was to optimise the concentration of the conjugated Xenolight 750-ICAM-1/VCAM-1 according to the signal intensity and dye clearance from the body. The rats (n = 2, each cohort) at day 1 post-irradiation were considered for this experiment. The animals received an intravenous (IV) injection of Xenolight 750-ICAM-

1/VCAM-1 (60 µg/kg or 120 µg/kg) via the tail vein. The dye was allowed to circulate for a total of 144 h and sequential images were taken at 1, 12, 24, 48, 72, 96, 120 and 144 h post-injection (excitation filter, 730 nm; emission filter, 790 nm; exposure time, 60 s; bin = 2 × 2; f-stop = 2.80; field of view = 120 mm).

It was determined that the optimum time to take the *in vivo* fluorescence image (excitation filter, 730 nm; emission filter, 790 nm; exposure time, 60 s; bin = 2 × 2; f-stop = 2.80; field of view = 120 mm) after Xenolight 750-ICAM-1/VCAM-1 injection was at 12 h with a 120 µg/kg concentration. This step was carried out separately for both Xenolight 750-ICAM-1 and Xenolight 750-VCAM-1 dyes.

4.2.3.2   Administration of NIR-conjugated isotype control

The negative control group (n = 6, each cohort) received Xenolight 750-isotype dye via the tail vein (240 µg/kg) on day 21 post-irradiation. The same mouse isotype IgG1 antibody was used as negative control for both ICAM-1 and VCAM-1. The *in vivo* fluorescence image was taken 12 h post-injection of the dye in the same fluorescence channel and same parameters as the Xenolight 750-ICAM-1/VCAM-1 conjugates.

4.2.3.3   NIR-conjugate administration in AVF-free animals

The untreated rats (n = 6, total) that had no surgical creation of an AVF and no irradiation were injected with Xenolight 750-ICAM-1 and Xenolight 750-VCAM-1 (120 µg/kg) via the tail vein at 7 and 21 days post-irradiation, respectively.

4.2.3.4   NIR-conjugate ICAM-1 and VCAM-1 detection

On days 1, 7, 21, 42, 63 and 84 post-irradiation the ICAM-1 and VCAM-1 detection group (n = 7, each cohort) received Xenolight 750-ICAM-1 and Xenoligh 750-VCAM-1 injection via the tail vein as described (section 4.2.3.1).

All three different *in vivo* images were considered for all experimental groups (NIR fluorescence background image pre-injection of antibody-conjugate, X-ray image and NIR fluorescence image post antibody-conjugate injection).

4.2.4 *Ex Vivo* **fluorescence imaging**

Immediately after the last set of images were taken at day 84 post-irradiation, perfusion was carried out (explained in detail at section 2.3.3). After perfusion, selected tissues were excised and *ex vivo* NIR fluorescence imaging was performed with the same protocol as Xenolight 750 dye (excitation filter, 730 nm; emission filter, 790 nm; exposure time, 60 s; bin = 2×2; f-stop = 2.80; field of view = 120 mm) (see section 4.2.3.). Selected tissues considered were left CCA (AVM); AVM nidus; left EJV (AVM); right CCA (contralateral vessel); and right EJV (contralateral vessel). The right CCA and right EJV (non-irradiated contralateral vessels) were used as controls for the created fistula. All the tissues were placed on a petri dish and located on the glass platen surface of the In-Vivo Multispectral Imaging System FX.

4.2.5 **Analysis of** *in vivo* **fluorescence imaging**

Image analysis was performed with ImageJ (Version 1.49, Rasband, W.S., ImageJ, U.S. National Institutes of Health, Bethesda, Maryland, USA, http://imagej.nih.gov/ij/download.html, 1997-2014). The original images were exported as 16-bit files which were opened in sequence, converted to stack and then the rolling ball algorithm (pixel = 1024) was used to subtract the background. The images were artificially coloured as "Fire" (under the "Lookup Table" menu). The stacked images were converted to montage with a scale showing high (yellow) and low (purple) fluorescent signal intensity.

A region of interest (ROI) was depicted around the AVM area in both treated and control rats. The ROI drawn around the AVM area was considered as the "Target" area and also a "Non-target" area was chosen. The non-target area was the average of the ROI depicted around an area at the upper side of the two forelimbs of the rat. In addition, the ROI was drawn around the AVM area for pre-injection images and used for background calculation. The same size ROI was used for all the images and different steps. The mean fluorescence intensity (MFI) for each image was calculated by the following formula:

T/NT = (Target ROI – background ROI) / (Non-target ROI – background ROI)

Optimisation experiments express the data as MFI and are given in arbitrary units. The fluorescence image of each rat was co-registered onto its X-ray image taken concurrently, to identify the anatomical location of the fluorescence signal.

For *ex vivo* NIR fluorescence images a ROI was drawn around the blood vessels to calculate the MFI.

4.2.6 Statistical analysis

The T/NT ratios (or MFIs) were calculated and the results were expressed as mean ± standard error of the mean (SEM). The non-parametric Kruskal-Wallis test with Dunn's post-hoc analysis for multiple comparisons was performed to determine the significance of differences between ICAM/VCAM conjugates and negative controls due to the large differences in variance as established by F-tests. Parametric data were analysed by repeated measures two-way analysis of variance (ANOVA) to consider the effects of treatment and time as values at each time point were collected sequentially from the same animal. The final ROI values were plotted using GraphPad Prism 6.0 software. P values less than or equal to 0.05 were considered significant.

4.3 Results

4.3.1 Optimisation of Xenolight 750 dose

Preliminary *in vivo* imaging experiments examined Xenolight 750-ICAM-1/VCAM-1 intensity and clearance from the body prior to any subsequent dosing as described (section 4.2.3.1). One day after irradiation, the probes were injected and fluorescence intensity monitored periodically to examine peak intensity and rate of probe clearance. A dose of 120 µg/kg was determined to be optimal for both Xenolight 750-ICAM-1 and Xenolight 750-VCAM-1 and was used in all subsequent experimental animals. At this dose, Xenolight 750-ICAM-1 fluorescence intensity increased until 12 h post-injection, which then decreased and slowly reached a plateau 48 h post-injection (Figure 4.1; other dose not shown). The 12 h time point was therefore considered as the optimal time to take the *in vivo* optical image after administration of 120 µg/kg Xenolight 750-ICAM-1(60 µg/kg dose not shown).
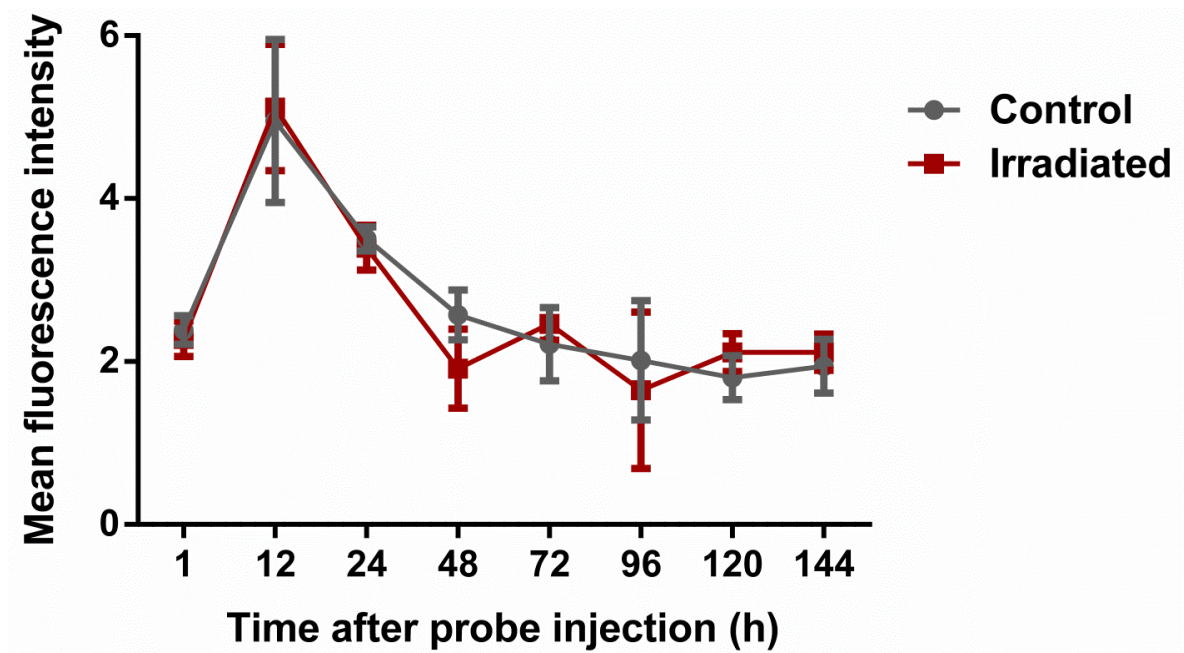
Figure 4.1. Signal intensity and clearance of Xenolight 750-ICAM-1. *In vivo* quantification of externalised ICAM-1 with Xenolight 750-ICAM-1 probe (120 µg/kg) in control and irradiated AVM rats at different time points. Consecutive images taken after one injection of the probe at the start of the experiment. Rats were injected at day 1 post-irradiation. Mean ± SEM. n = 2 per cohort.

For Xenolight 750-VCAM-1, fluorescent intensity peaked at 12 h, then gradually decreased over the following days until it reached the base-line level 144 h after injection (Figure 4.2). Therefore, the 12 h time-point was considered as the optimal time to take the *in vivo* optical image after applying Xenolight 750-VCAM-1 (120 µg/kg). At this dose, clearance time was sufficient to allow re-injection and imaging every 1 – 3 weeks.
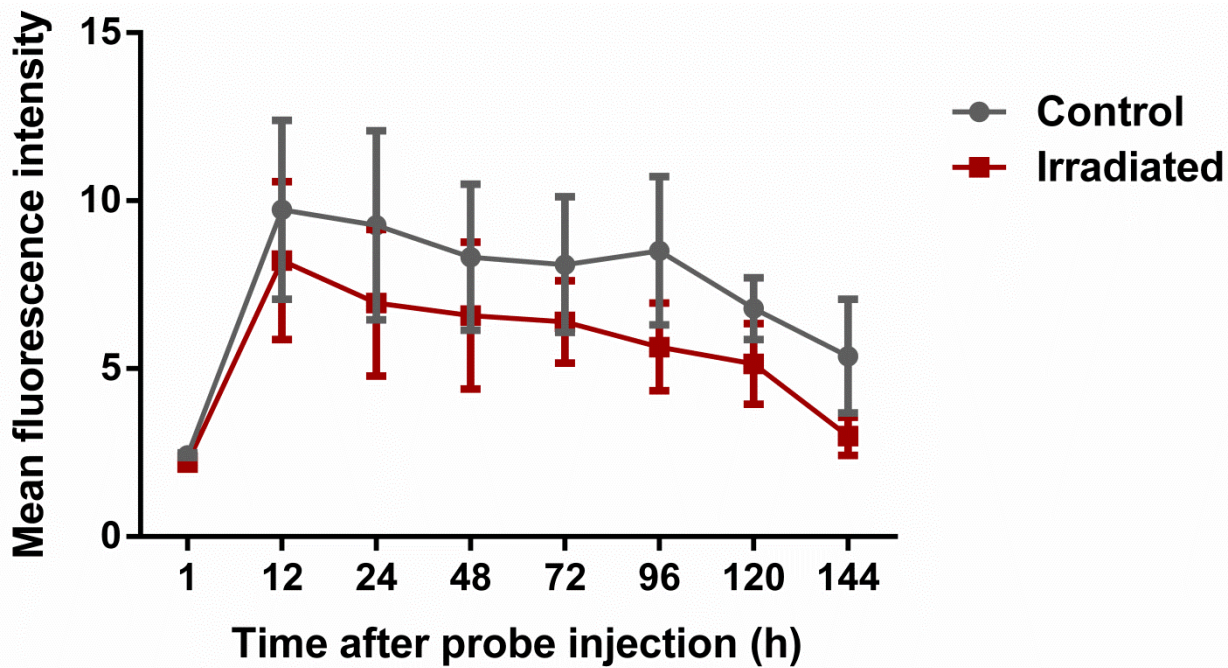
Figure 4.2. Signal intensity and clearance of Xenolight 750-VCAM-1. *In vivo* quantification of externalised VCAM-1 with Xenolight 750-VCAM-1 probe (120 µg/kg) in control and irradiated AVM rats at different time points. Consecutive images taken after one injection of the probe at the start of the experiment. Rats were injected at day 1 post-irradiation. Mean ± SEM. n = 2 per cohort.

4.3.2 Validation of Xenolight 750-ICAM/VCAM specificity with non-targeting Xenolight 750-isotype control

In order to make sure that the Xenolight 750 conjugated ICAM-1/VCAM-1 antibodies bind specifically to their respective targets, Xenolight 750 conjugated to an isotype control (mouse IgG1) was used. The Xenolight 750-isotype was injected at day 21 post-irradiation to both irradiated and non-irradiated groups (n = 6, each cohort; 120 µg/kg). The overlaid images of X-ray and fluorescence indicated no fluorescent signal anywhere in the body. Figure 4.3 represents the overlaid images of X-ray and fluorescence of Xenolight 750-isotype injected in an irradiated rat after 21 days. To reduce the unnecessary use of animal numbers in this study, only one time-point was used to examine the lack of binding of this non-targeting probe and to establish the validity of the ICAM/VCAM targeting probes.

Figure 4.3. *In vivo* near-infrared fluorescence of Xenolight 750-isotype antibody in the rat AVM model. Representative montage of *in vivo* near-infrared fluorescence of Xenolight 750-isotype and X-ray in an irradiated AVM rat at 21 days post-irradiation. (A) X-ray, (B) fluorescence and (C) overlaid image of X-ray and fluorescence. No fluorescent signal was seen in the AVM area. Identical results were recorded in non-irradiated animals.

In contrast to the non-targeting probe, Figure 4.4 indicates the presence of fluorescent signal localised to the AVM area both in non-irradiated and irradiated animals injected at day 21 post-irradiation with Xenolight 750-ICAM-1. The signal intensity of the probe indicates expression of ICAM-1 only in the AVM area. Quantification of *in vivo* fluorescence intensity of Xenolight 750-isotype and Xenolight 750-ICAM-1 in non-irradiated and irradiated rats injected with the probes at day 21 post-irradiation is depicted in Figure 4.5. The results indicated a 4.3- and 4.5-fold increase in fluorescence intensity in non-irradiated and irradiated rats, respectively, injected with Xenolight 750-ICAM-1, compared to rats injected with Xenolight 750-isotype.
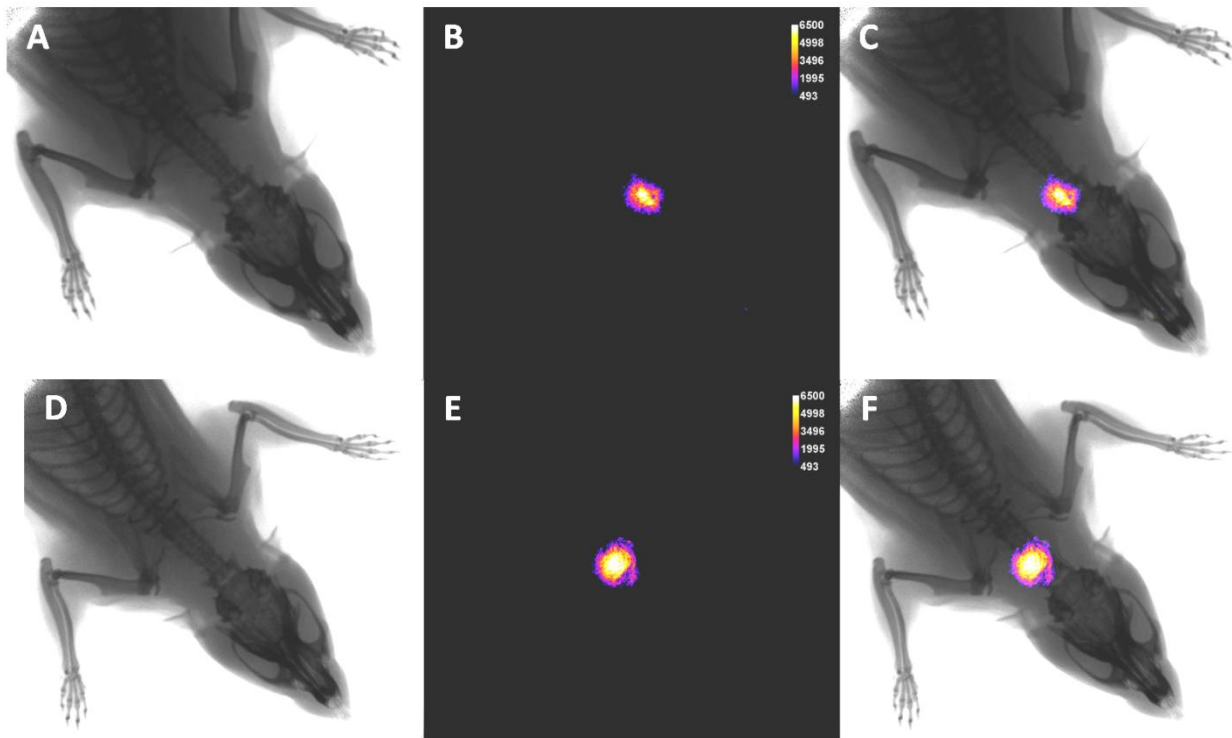
Figure 4.4. *In vivo* near-infrared fluorescence of Xenolight 750-ICAM-1 antibody in the AVM rat model. Representative montage of *in vivo* near-infrared fluorescence of Xenolight 750-ICAM-1 and X-ray in an AVM non-irradiated rat (A-C) and irradiated AVM rat (D-F) at day 21 post-irradiation. (A, D) X-ray; (B, E) fluorescence; and (C, F) overlaid image of X-ray and fluorescence.
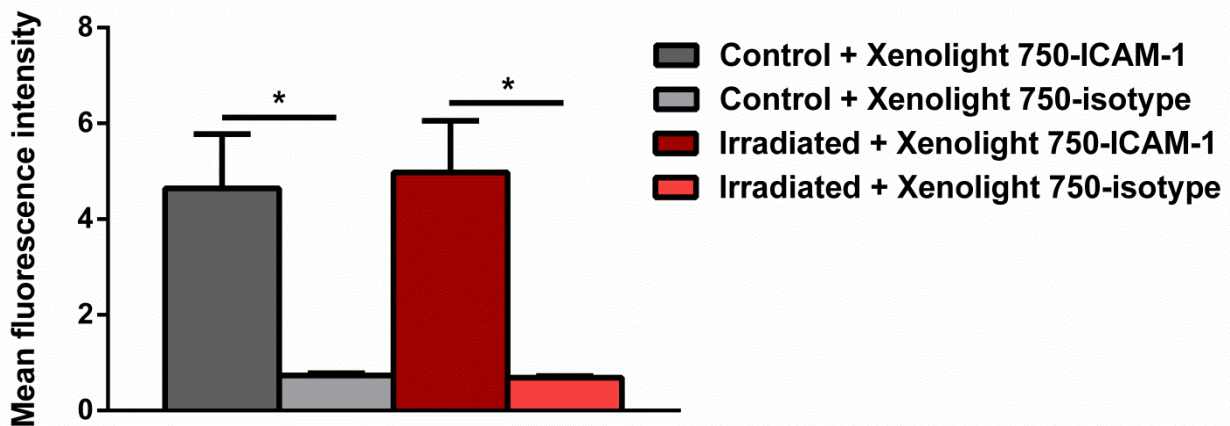
Figure 4.5. Quantification of Xenolight 750-ICAM-1 and Xenolight 750-isotype probe binding in AVM animal model. Images taken at day 21 post-irradiation in both AVM non-irradiated and irradiated rats were quantitated for probe binding and fluorescence intensity using ImageJ. Mean ± SEM. n = 6 per cohort. * $P < 0.05$. Kruskal-Wallis with Dunn's post-hoc analysis.

For the Xenolight 750-VCAM-1 probe injected in non-irradiated and irradiated rats at day 21 post-irradiation, fluoresence accumulated at the AVM area as found for ICAM-1 (Figure 4.6). The presence of signal at the AVM area indicated the cell surface expression of VCAM-1 protein only in this region. *In vivo* quantification of fluorescence intensity of Xenolight 750-

isotype and Xenolight 750-VCAM-1 in irradiated and non-irradiated rats at day 21 post-irradiation is shown in Figure 4.6. The results showed 11- and 14-fold increases in fluorescence intensity at the AVM area in non-irradiated and irradiated rats, respectively, injected with Xenolight 750-VCAM-1, compared to rats injected with Xenolight 750-isotype (Figure 4.7).

Figure 4.6. *In vivo* near-infrared fluorescence of Xenolight 750-VCAM-1 antibody in the AVM rat model. Representative montage of *in vivo* near-infrared fluorescence of Xenolight 750-VCAM-1 and X-ray in an AVM irradiated rat (A-C) and non-irradiated AVM rat (D-F) at day 21 post-irradiation. (A, D) X-ray; (B, E) fluorescence; and (C, F) overlaid image of X-ray and fluorescence.
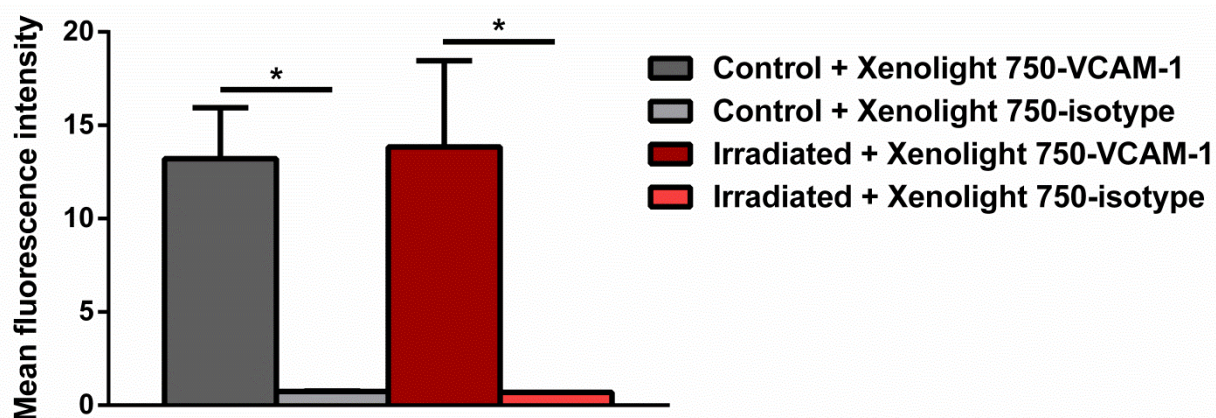
Figure 4.7. Quantification of Xenolight 750-VCAM-1 and Xenolight 750-isotype probe binding in AVM animal model. Images taken at day 21 post-irradiation in both AVM non-irradiated and irradiated rats that were quantitated for probe binding and fluorescence intensity using ImageJ. Mean ± SEM. n = 6 per cohort. * P < 0.05. Kruskal-Wallis with Dunn's post-hoc analysis.

4.3.3 Time course of ICAM-1 expression in the rat AVM after irradiation

To study the level of cell surface expression of ICAM-1 and VCAM-1 at different time points post-irradiation in non-irradiated and irradiated AVM rats, Xenolight 750-ICAM-1 and Xenolight 750-VCAM-1 were utilised, respectively, and rats were imaged with the In-Vivo Multispectral Imaging System FX. Examining the MFI levels, the level of ICAM-1 expression was higher in the irradiated animals at days 7 and 84 compared to non-irradiated rats however there was no statistically significant difference at any of the time points. The non-irradiated rats also showed ICAM-1 expression on the cell surface of AVM endothelial cells; the level of expression was almost the same for all time points (Figure 4.8).
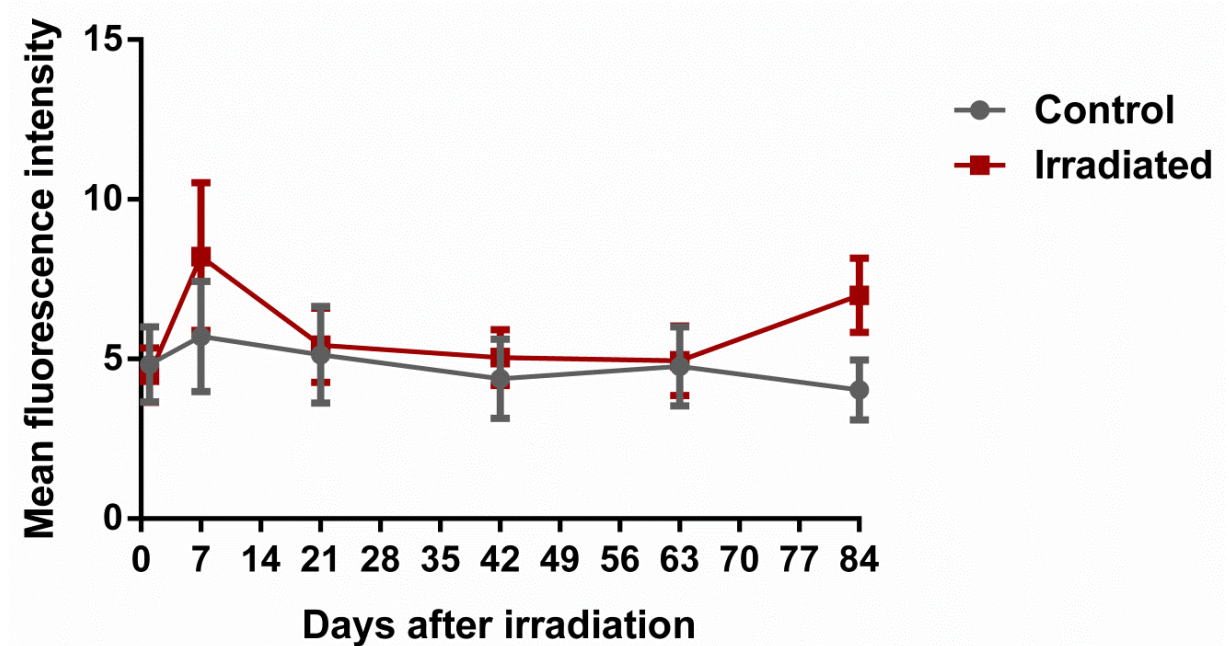
Figure 4.8. ICAM-1 expression in model AVM (MFI). *In vivo* quantification of cell surface expression of ICAM-1 with Xenolight 750-ICAM-1 probe (120 µg/kg) in control and irradiated rat AVMs at different time points. Data shown represent mean fluorescence intensity (MFI) of Xenolight 750-ICAM-1 probe in animals. Mean ± SEM. n = 7 per cohort. Repeated measures two-way ANOVA with Holm-Sidak correction. No significant differences were determined.

In order to reduce intra-animal variability the mean fluorescence intensity was normalised for each animal to day 1 MFI to see whether there was an increase in expression over time. There was a high level of expression of ICAM-1 at all time-points post-irradiation compared to day 1 in irradiated AVM rats (Figure 4.9). By day 7, ICAM-1 increased 1.6-fold and remained relatively stable between 1.6- and 2-fold higher than day 1. In non-irradiated AVM rats, the level of surface expression of ICAM-1 increased 1.5-fold by day 21 then remained relatively unchanged. However, repeated measures analysis did not reveal any significant effect of time or treatment on ICAM-1 expression.
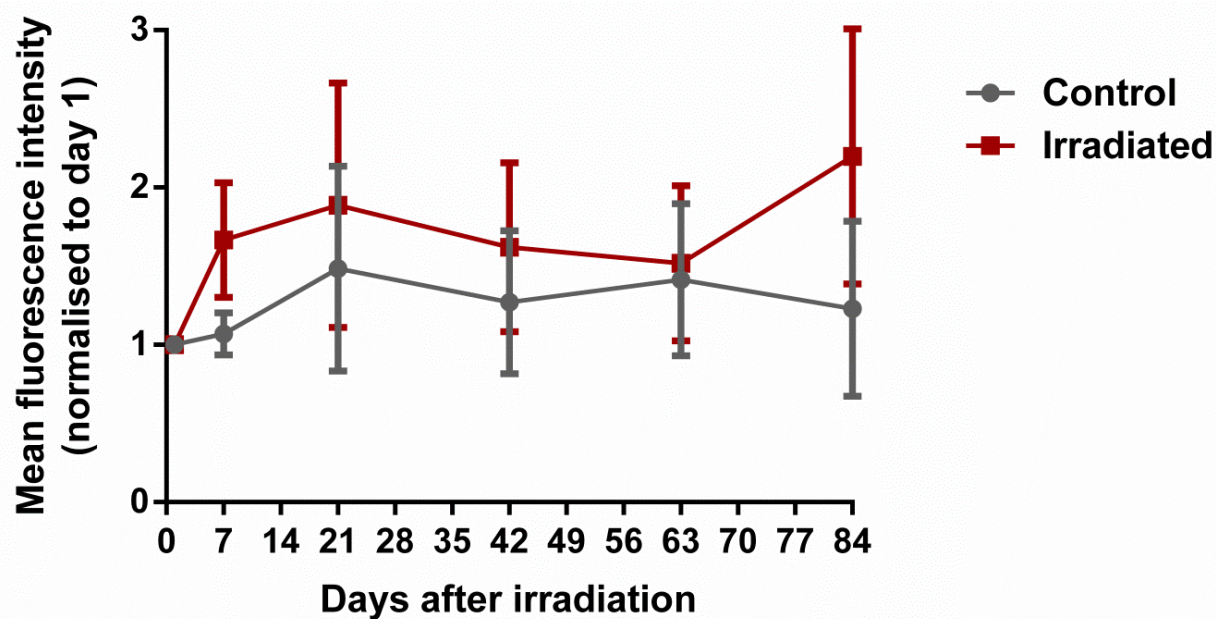
Figure 4.9. ICAM-1 expression in model AVM (normalised MFI). *In vivo* quantification of cell surface expression of ICAM-1 with Xenolight 750-ICAM-1 probe (120 µg/kg) in control and irradiated rat AVMs at different time points normalised to expression at day 1 for each individual animal. Mean ± SEM. n = 7 per cohort. Repeated measures two-way ANOVA with Holm-Sidak correction. No significant differences were determined.

4.3.4 Time course of VCAM-1 expression in AVM rat after irradiation

The level of surface expression of VCAM-1 was high in both irradiated and non-irradiated rat AVMs (Figure 4.10). In control rats, the level of VCAM-1 increased up to day 21 then slowly decreased over the 84 days. In irradiated rats, expression also peaked at day 21. Mean MFI was greater in irradiated rats at day 1 and day 21, however the difference was not statistically significant.
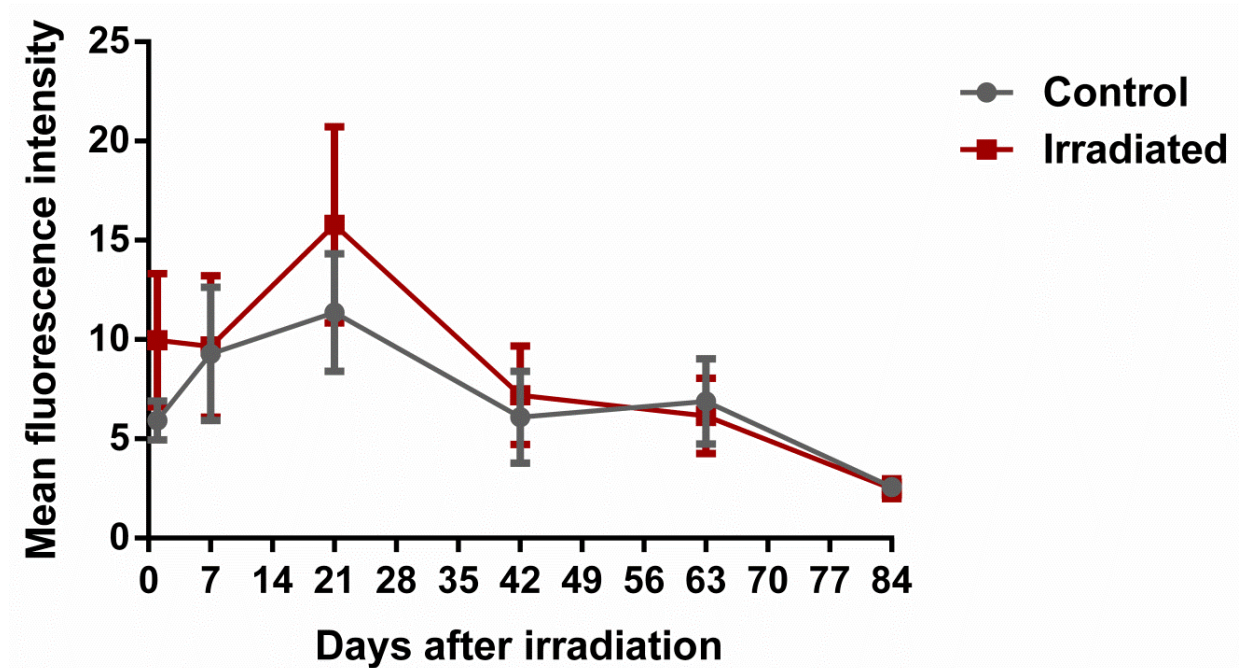
Figure 4.10. VCAM-1 expression in model AVM (MFI). *In vivo* quantification of cell surface expression of VCAM-1 with Xenolight 750-VCAM-1 probe (120 µg/kg) in control and irradiated AVM rat models at different time points. Data shown represent mean fluorescence intensity (MFI) of Xenolight 750-VCAM-1 probe in animals. Mean ± SEM. n = 7 per cohort. Repeated measures two-way ANOVA with Holm-Sidak correction. No significant differences were determined.

As performed for ICAM-1, the mean fluorescence intensity (MFI) was normalised to day 1 MFI for each animal to reduce intra-animal variability. Expression still peaked at day 21 for both irradiated and control rats at a level 2.5-fold higher than day 1, with a slow decrease until day 84 to basal levels. There was no significant difference between the irradiated and non-irradiated rats at any time point (Figure 4.11). Repeated measures analysis did not reveal any significant effect of time or treatment on ICAM-1 expression.
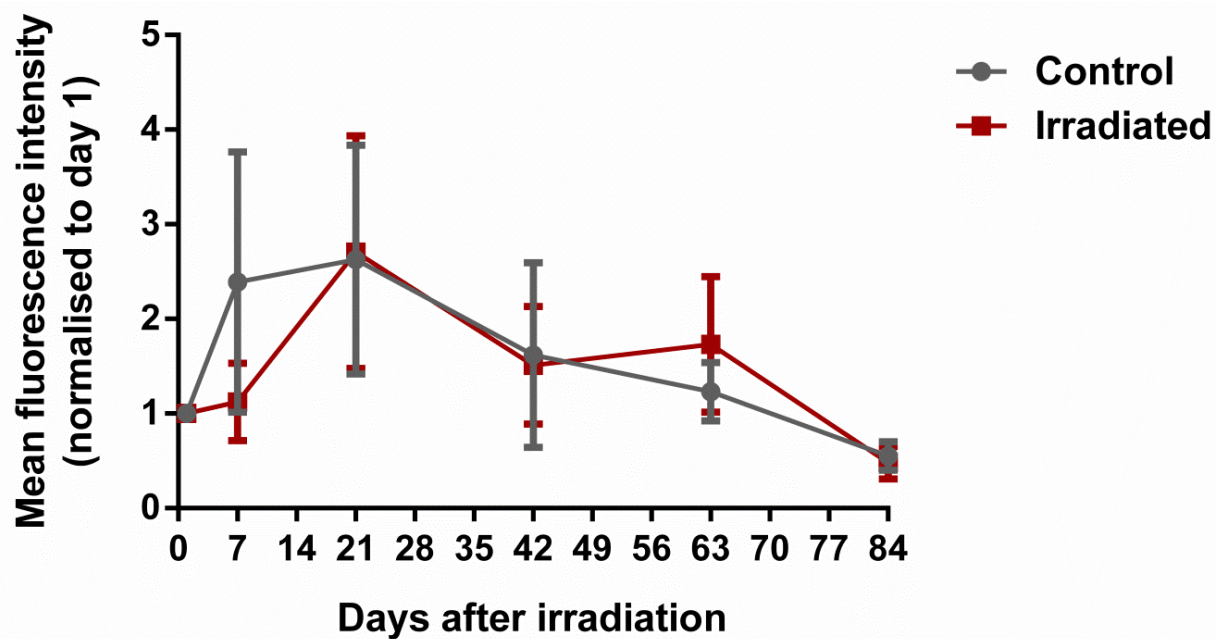
Figure 4.11. VCAM-1 expression in model AVM (normalised MFI). *In vivo* quantification of cell surface expression of VCAM-1 with Xenolight 750-VCAM-1 probe (120 µg/kg) in control and irradiated rat AVMs at different time points normalised to expression at day 1 for each individual animal. Mean ± SEM. n = 7 per cohort. Repeated measures two-way ANOVA with Holm-Sidak correction. No significant differences were determined.

4.3.5 In vivo imaging of non-AVM rats

To validate the location of expression of ICAM-1 and VCAM-1 at the AVM area, control rats with no AVF creation and no radiation (n = 6, total) were injected with Xenolight 750-ICAM-1 and Xenolight 750-VCAM-1 (120 µg/kg) at 7 and 21 days post-irradiation, respectively. There was no fluorescent signal present at the neck area of the rats as indicated with the overlaid images of X-ray and fluorescence. Figure 4.12 shows a representative set of images after Xenolight 750-ICAM-1 administration in a non-AVM rat.
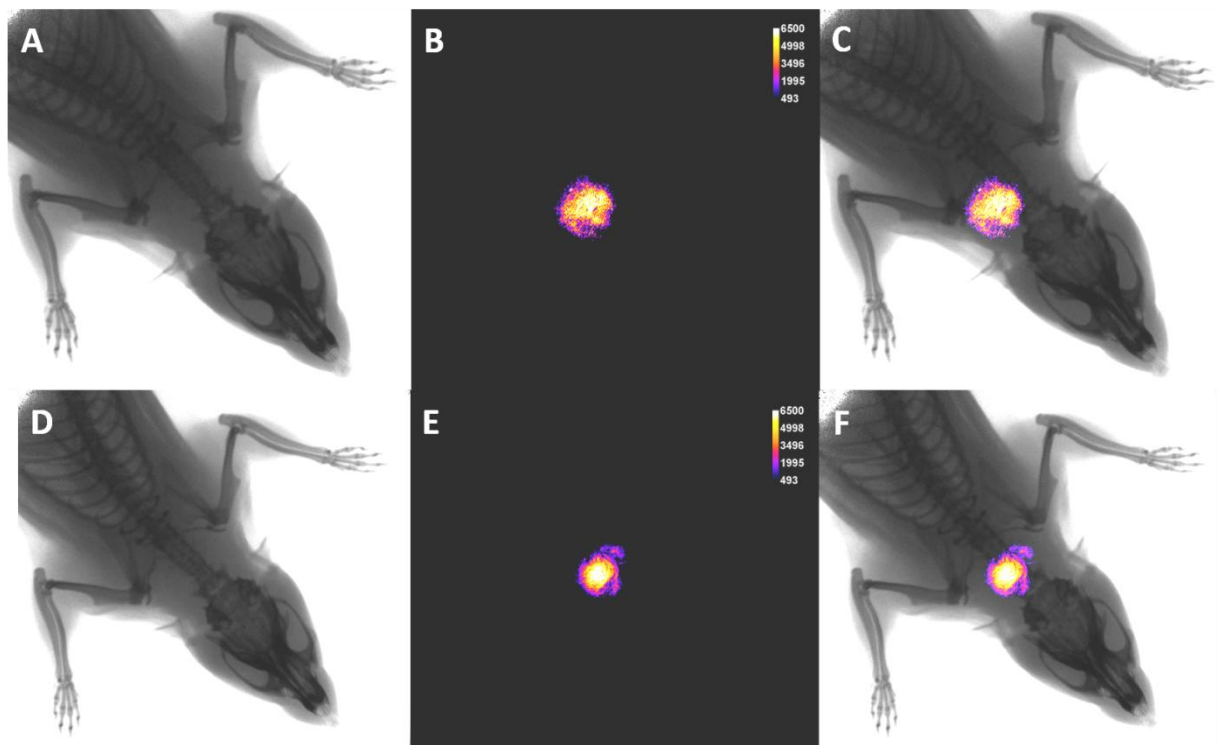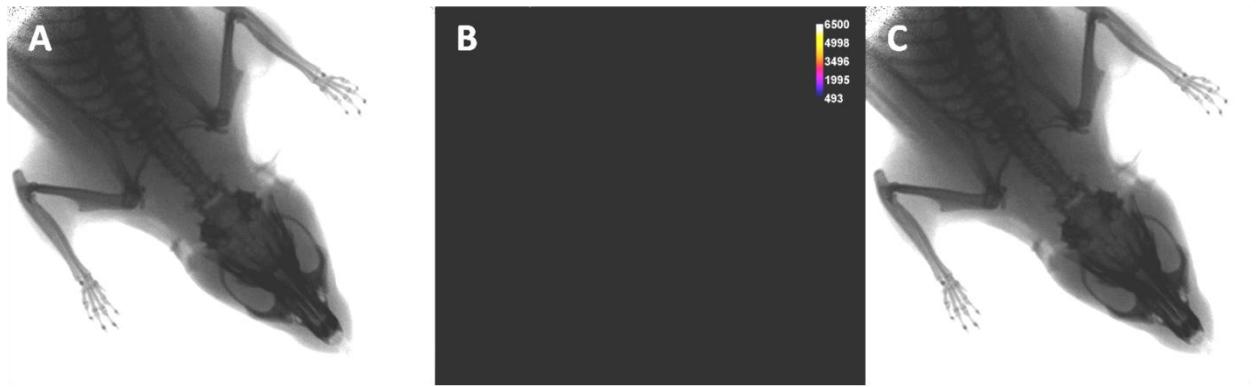
Figure 4.12. *In vivo* near-infrared fluorescence of Xenolight 750-ICAM-1 antibody in the normal rat. Representative montage of *in vivo* near-infrared fluorescence of Xenolight 750-ICAM-1 and X-ray in a non-AVM rat. (A) X-ray, (B) fluorescence and (C) overlay image of X-ray and fluorescence. No fluorescent signal was seen in the neck area, where the AVM is normally created. Identical results for non-AVM rats injected with Xenolight 750-VCAM-1 were achieved.

4.3.6 *Ex vivo* **near-infrared fluorescence imaging**

Immediately after the last live animal imaging at day 84, the rats were perfused and AVM vessels and control vessels were removed. Excised vessels (left/right CCA, left/right EJV and nidus) were imaged using In-Vivo Multispectral Imaging System FX. The mean fluorescence intensity (MFI) of Xenolight 750-ICAM-1/VCAM-1 for each vessel was considered by depicting a ROI around the vessel. The quantitative analysis of *ex vivo* imaging of the vessels showed there was no significant difference in ICAM-1 expression between irradiated and non-irradiated vessels in each vessel type. However, there was enhanced Xenolight 750-ICAM-1 uptake in the AVM vessels (left EJV and CCA) compared to the normal, non-irradiated contralateral vessels (right EJVand CCA) that reached significance only in EJV vessels ($P < 0.05$). The ICAM-1 expression was twice as high in AVM EJV vessels compared to control EJV vessels (Figure 4.13).
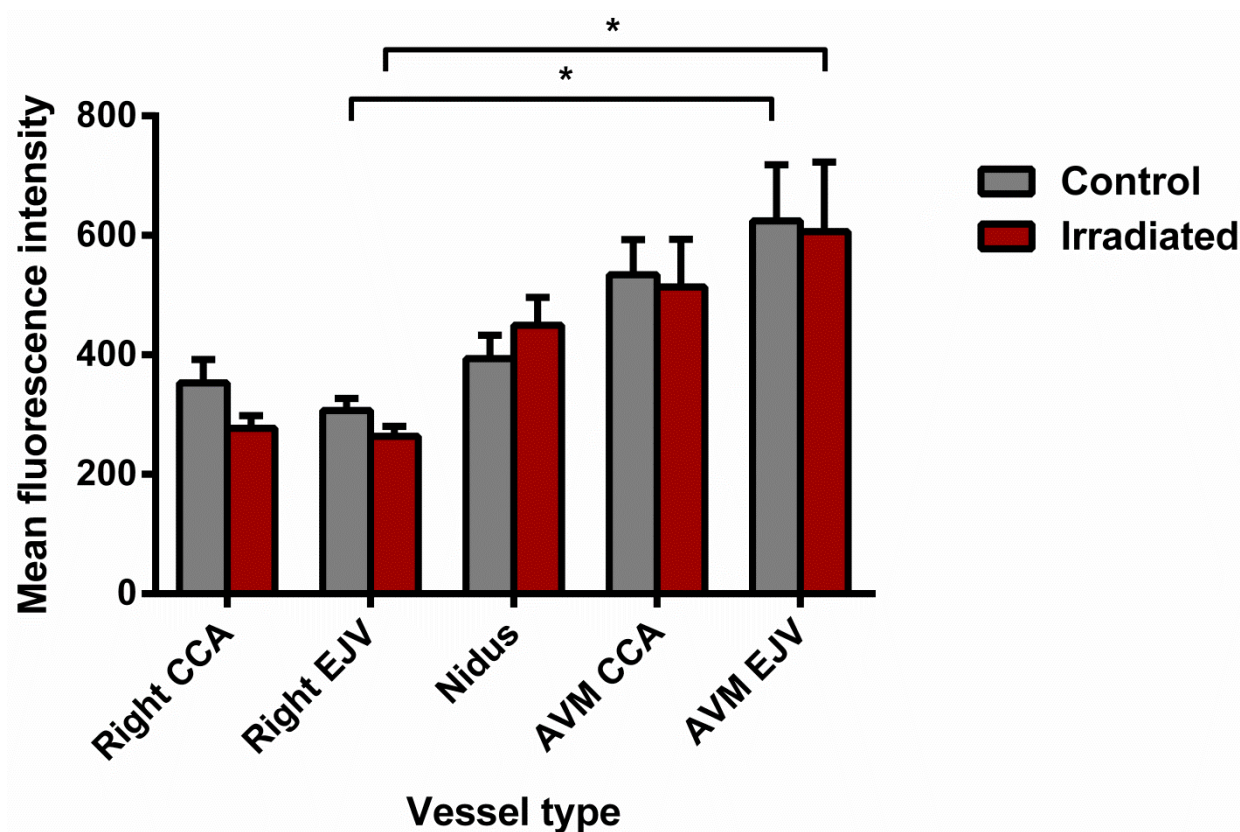
Figure 4.13. Ex *vivo* quantification of Xenolight 750-ICAM-1 probe in AVM and contralateral vessels of irradiated and non-irradiated AVM model rats. The *ex vivo* images were taken after *in vivo* imaging at day 84 post-irradiation. Mean ± SEM. n = 7 per cohort. * P < 0.05.

In rats injected with Xenolight 750-VCAM-1 there was no significant difference between irradiated and non-irradiated vessels in each vessel type. Although there was a significant difference in VCAM-1 expression between both AVM vessels (left EJV and CCA) and normal, non-irradiated contralateral vessels (right EJV and CCA) (Figure 4.14).
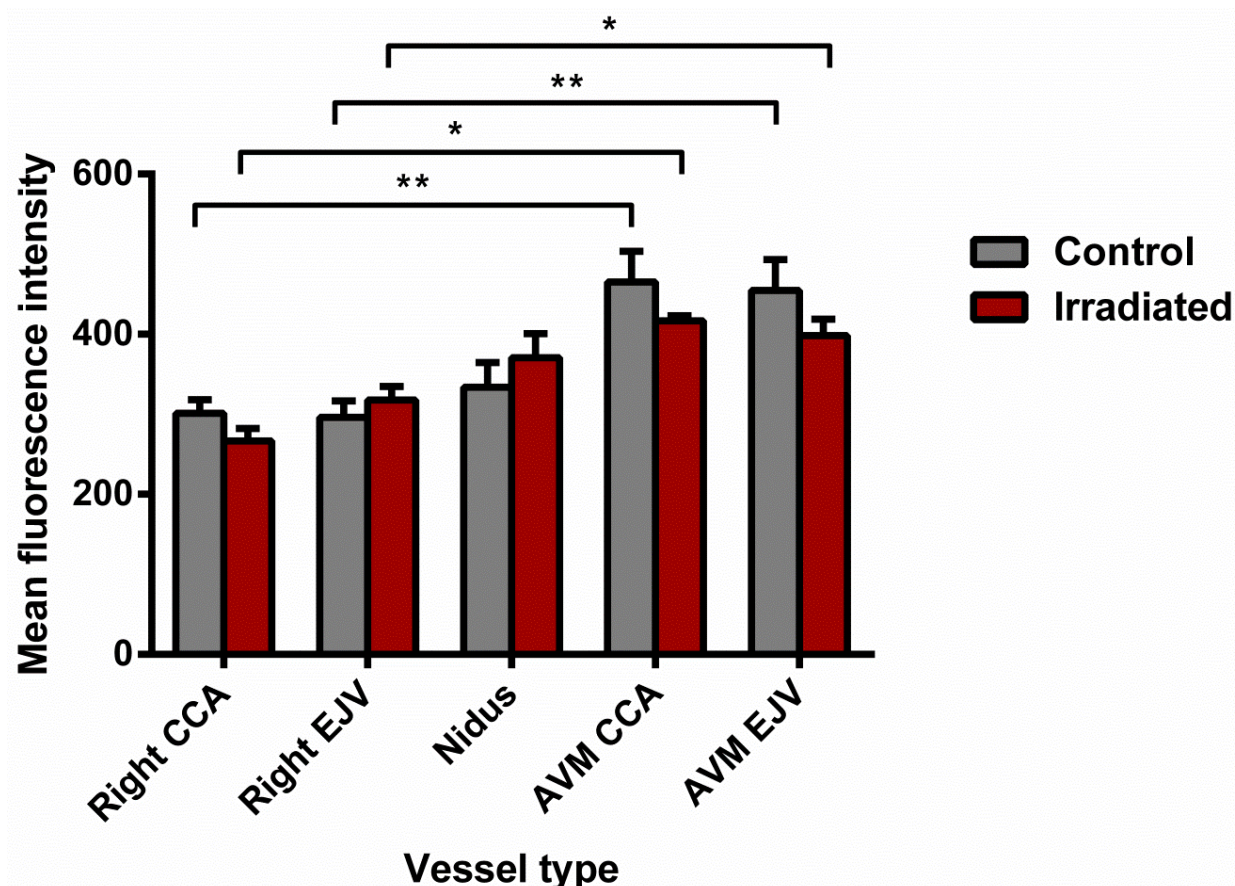
Figure 4.14. Ex *vivo* quantification of Xenolight 750-VCAM-1 probe in AVM and contralateral vessels of irradiated and non-irradiated AVM model rats. The *ex vivo* images were taken after *in vivo* imaging at day 84 post-irradiation. Mean ± SEM. n = 7 per cohort. * P < 0.05 and ** P < 0.01.

4.4 Discussion

In this chapter, the effect of irradiation on ICAM-1 and VCAM-1 expression in the AVM rat model was investigated using Xenolight 750-ICAM-1/VCAM-1 probes. The high expression level of ICAM-1 and VCAM-1 was present solely on vessels within the AVM region. The results revealed increased expression levels of ICAM-1 and VCAM-1 in AVM vessels of both non-irradiated and irradiated rats compared to the normal vasculature. The level of expression of ICAM-1 and VCAM-1 in the model AVM was not significantly increased in response to irradiation. Therefore, ICAM-1 and VCAM-1 may not be good candidates for vascular targeting in AVMs.

Previous studies have provided evidence for ICAM-1 and VCAM-1 expression post-irradiation on endothelial cells. In mice pulmonary microvascular endothelium, ICAM-1 expression was increased 24 h after receiving radiation as low as 2 Gy that was sustained for

several days. Immunohistochemical analysis showed ICAM-1 expression on pulmonary capillary endothelium with minimal expression on the endothelium of larger vessels (Hallahan & Virudachalam, 1997). In a similar study, mice received thoracic radiation of 20 Gy and showed up-regulation of ICAM-1 and VCAM-1 on the pulmonary vascular endothelium at 100 days post-irradiation by immunohistochemistry (Epperly et al., 2002). Irradiation of a three-dimensional skin organ model and skin biopsies revealed ICAM-1 expression by immunohistochemistry after 48 h (Müller et al., 2006). Molla et al. showed up-regulation of ICAM-1 in intestinal venules 24 h after receiving 10 Gy radiation with VCAM-1 expression increased after 14 days (Mollà et al., 2003).

The failure of the current *in vivo* study to show a significant effect of radiation on ICAM-1 and VCAM-1 expression, consistent with previous studies, may be a result of the non-irradiated AVM vessels already expressing a high level of ICAM-1 and VCAM-1 on their endothelial surface relative to the normal vasculature. There is a possibility that in response to haemodynamic changes in the AVM, the expression level of both ICAM-1 and VCAM-1 reached saturation prior to the radiation procedure, thus radiation caused no further effect. Previous studies have revealed that oscillatory shear stress stimulates ICAM-1 and VCAM-1 expression in HUVEC cells (Chappell et al., 1998) while laminar shear stress stimulates ICAM-1 but not VCAM-1 expression (Nagel et al., 1994). Previous studies on rat AVMs have shown that creation of the AVF causes significant haemodynamic changes almost immediately and maintenance of a high flow state that may be responsible for the increased adhesion molecule expression (Yassari et al., 2004).

Previous immunohistochemical studies performed with the rat AVM model showed an increase in VCAM-1 staining by day 21 after treatment with a 25 Gy dose of radiation, which decreased to the baseline level by day 84 (Storer et al., 2010). This was consistent with the increase in VCAM-1 seen at day 21 in this study, however this occurred in both irradiated and non-irradiated AVMs. The dose of 15 Gy, rather than 25 Gy, used in the current study may have reduced the significance of the effect on the expression level of ICAM-1 or VCAM-1 *in vivo*, even though this dose significantly increased expression of ICAM-1 and VCAM-1 *in vitro*. In the *in vivo* environment, there are high basal levels of ICAM-1 and VCAM-1 expression on AVM endothelial cells in response to altered blood flow, and also the influence of other cell-types. These factors are not replicated in the *in vitro* environment. Therefore, despite the findings of significant induction of VCAM-1 and ICAM-1 *in vitro*, a dose of

15 Gy does not induce a discriminatory effect on the expression level of ICAM-1 and VCAM-1 on rat AVM endothelial cells *in vivo*.

The created AVM animal model has similarities in haemodynamic, histological, molecular and ultrastructural characteristics to human AVMs (Kashba et al., 2015; Yassari et al., 2004). The AVM model consists of a large arterial input, and a nidus with branching vessels that all drain into a single draining vein. These findings support the use of this model to study human AVMs. Where *in vitro* studies cannot replicate the altered flow conditions and other complexities of the human AVM, the rat AVM model can replicate many of these factors. In previous studies, faint to moderate expression of ICAM-1 and VCAM-1 by immunohistochemistry in human AVMs was shown (Storer et al., 2008). Elevated expression of ICAM-1 and VCAM-1 in AVM tissue could be a result of increased levels of shear stress (Nagel et al., 1994), ischaemia (Frijns & Kappelle, 2002), high levels of vascular endothelial growth factor (VEGF) or a range of cytokines (Shenkar et al., 2003). The expression of these adhesion molecules in human AVMs is consistent with the elevated basal expression in the rat AVM. It is difficult to determine, however, if the level expressed in human AVMs would be sufficient to discriminate them from normal vessels, as appeared to be the case for the rat AVMs, even without radiation. It may be a limitation of the model that the VCAM-1 and ICAM-1 expression is overtly high relative to a human AVM, but this is difficult to determine absolutely. Taking this under consideration, to ensure that the candidate protein under investigation may be useful in downstream studies, the main criterion in the context of this study must be to have a significantly higher level of ICAM-1 and VCAM-1 expression after irradiation than the basal level on AVM endothelial vessels. An ideal candidate protein would perhaps have very low basal expression in either the human or rat AVM prior to radiation.

4.5 Limitations

The failure to see a significant increase in ICAM-1 or VCAM-1 expression in response to radiation may lie primarily with the high basal level of expression found in the rat AVM. However, other technical limitations that increase the statistical error may have contributed to the inability to show a significant effect. In the current study, the Xenolight 750-conjugated dye was not prepared for all the experimental rats as a single batch. A limited number of rats could be irradiated with Gamma Knife at any one time, due to restrictions on availability of the Gamma Knife machine. Therefore, the Xenolight 750-conjugated dye had to be prepared

anew for each group of rats that were irradiated. Hence, the labelling efficiency may have been slightly different at each preparation, although care was taken during the labelling procedure.

It would have been useful if the current work could have been validated further with other semi-quantitative assays such as immunofluorescence analysis at each time-point, as was performed in the study by Storer (Storer et al., 2010). In this study however, it was not possible to do this, as the same animal was used for all the experimental time-points until day 84.

As discussed above, the AVM animal model used in the current study has several similarities with human AVMs, however it is not congenital and is not formed in the brain. The AVM animal model does however provide an important intermediate between *in vitro* cell culture studies and human applications. While this study demonstrated that irradiation does not increase the level of ICAM-1 and VCAM-1 in the AVM animal model, at least at a dose of 15 Gy, it has shown that these molecules can be targeted with a probe via the blood circulation, an important step to show that we can potentially test antibody-thrombotic conjugates in this model.

4.6 Summary and Conclusions

In vivo imaging demonstrated that AVM rat models express high levels of ICAM-1 and VCAM-1 at the AVM area relative to the normal vasculature. High basal levels of ICAM-1 and VCAM-1 in rat AVMs are not significantly increased by a single 15 Gy radiation dose. Based on these current findings, ICAM-1 and VCAM-1 are not ideal candidates for a vascular targeting approach to treat AVMs, at least at a dose of 15 Gy. However, given the high basal levels of expression of these molecules in the animal model may not wholly reflect that found in a human AVM, further experiments to validate their potential are warranted.

Chapter 5. Phosphatidylserine translocation and anatomical location post-irradiation in an AVM animal model

Objective: Phosphatidylserine (PS) is asymmetrically distributed throughout the plasma membrane, located predominantly on the cytoplasmic side in normal healthy cells. Under certain cellular conditions, such as apoptosis, PS is translocated to the cell surface, where it plays an important role in thrombosis and phagocytosis. Externalisation of PS is known to occur in cells exposed to radiation. The aims of this study were to examine PS translocation and anatomical location after radiosurgery in an AVM animal model and to determine whether PS may be a potential candidate for post-irradiation vascular targeting.

Methods: An arteriovenous fistula was created in 6-week old, male Sprague-Dawley rats (n = 30). Six weeks following AVM creation, animals were divided into two groups. The first group received a single 15 Gy dose of ionising radiation. The second group were used as controls and did not receive any radiation treatment. Externalisation of PS was examined by intravenous (IV) injection of a PS-specific fluorescent probe, PSVue-794, and *in vivo* fluorescence optical imaging. Fluorescence intensity was measured at 1, 7, 21, 42, 63 and 84 days post-irradiation.

Results: Fluorescent signal indicative of PS translocation to the luminal cell surface was seen in AVM vessels both irradiated and non-irradiated at all time-points examined. Fluorescent signal was specifically localised to the AVM region in all rats and was not present in any other anatomical location. The level of externalised PS increased over time in the AVM vessels of irradiated rats but not in control animals. The difference in PS externalisation between irradiated and non-irradiated AVMs reached significance at day 84.

Conclusions: Vessels within the mature rat AVM demonstrate elevated PS externalisation compared to normal vessels. A single dose of ionising radiation can increase PS externalisation in a time-dependent manner. Strict localisation of PS externalisation within the AVM region suggests that PS may be a suitable candidate molecule for vascular-targeting approaches for AVM treatment.

5.1 Introduction

Phosphatidylserine (PS) is an aminophospholipid that plays a key role in cell signalling, haemostasis (Zwaal & Schroit, 1997) and thrombosis (Zwaal, 1978; Zwaal et al., 1977). PS is asymmetrically distributed throughout the plasma membrane in healthy cells, being located predominately in the inner leaflet (cytoplasmic side) of the plasma membrane (Schutters & Reutelingsperger, 2010). However, during certain biological processes, PS translocates to the outer leaflet of the plasma membrane where it plays an important role in phagocytosis and blood coagulation (Schutters & Reutelingsperger, 2010). Externalisation of PS to the cell surface is known to occur in apoptotic cells (Bennett et al., 1995; Fadok et al., 1992), tumorigenic cells (Utsugi et al., 1991), irradiated cells, activated platelets, and activated macrophages (Schutters & Reutelingsperger, 2010).

The appearance of PS on the cell surface has been exploited in many diseases as a target for molecular imaging (diagnosis) and targeted drug delivery (therapy) by the use of ligands that bind selectively and with affinity to PS (Schutters & Reutelingsperger, 2010). The aims of this study were to determine the level and anatomical location of PS after radiation in an animal model of AVM and evaluate its suitability as a vascular targeting candidate.

5.2 Materials and methods

5.2.1 AVM rat Model

To examine the translocation of phosphatidylserine (PS) *in vivo* post-irradiation, fluorescent *in vivo* imaging was carried out. A fistula was created (explained in detail in section 2.3.1.4.) in six week old male Sprague Dawley rats (Animal Resources Centre, WA, Australia, 162 – 188 g, n = 30, Table 5.1). Six weeks after fistula formation the rats were given a single 15 Gy dose of radiation with a Leksell Gamma Knife (explained in detail in section 2.3.2.).

Animals (n = 30) were randomly divided into three groups as shown in Table 5.1. Out of the total number of rats, three groups were considered, each group with two cohorts of irradiated and non-irradiated. The first animal group (n = 2, each cohort) was used for PSVue-794 probe concentration optimisation. The second animal group (n = 6, each cohort) was used as a negative control to account for any non-specific binding of the PSVue-794 probe. This group of rats was shared between ICAM-1, VCAM-1 (Chapter 4) and phosphatidylserine

experiments as a negative control for each NIR dye. The third group of animals (n = 7, each cohort) formed the experimental group for PS detection post-irradiation over the 84 day period.

Table 5.1. Rat usage and number

Experimental group	Number of AVM irradiated rats	Number of AVM non-irradiated rats
PSVue-794 probe optimisation	n = 2	n = 2
Negative control	n = 6	n = 6
PS detection	n = 7	n = 7

5.2.2 Near infrared (NIR) dye preparation

Prior to *in vivo* molecular imaging, the NIR dye for PS detection was prepared. The PS-specific PSS-794 dye is commercially available as "PSVue-794" (#P-1001) and the non-specific, non-targeting PSS-794 control dye as "PSVue-794 control" (#P-1007) (Molecular Targeting Technologies, Inc. MTTI, PA, USA). The dyes are referred to as "PSVue-794" and "PSVue-794 control" throughout this chapter.

PSVue-794 has a molecular formula of $C_{83}H_{95}N_{13}O_{23}S_2Zn_2$ and a molecular weight of 1837.6 g/mol. The extinction coefficient of PSVue-794 in water is 1.1×10^5 $M^{-1} cm^{-1}$ and its quantum yield is 0.14 (higher in organic solvent). PSVue-794 has a maximum excitation of 794 nm and a maximum emission of 810 nm (PSVue-794 data sheet, Molecular Targeting Technologies). The chemical structures of the PSVue-794 probe and its precursor apo-PSS794 are shown in Figure 5.1.
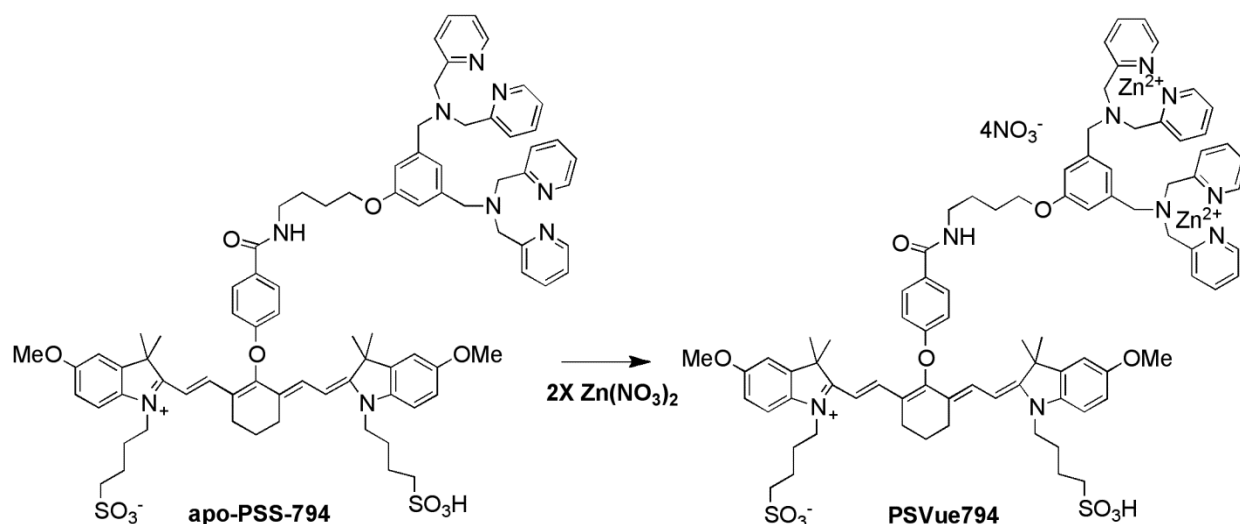
Figure 5.1. Chemical structures of precursor apo-PSS794 and PSVue-794 (PSVue-794 data sheet, Molecular Targeting Technologies).

The PSVue-794 control probe was used as a non-targeting control probe for PSVue-794. It contains the same fluorophore as PSVue-794, but it does not have the zinc-dipicolylamine (Zn^{2+}-DPA) targeting moiety. The PSVue-794 control probe has a molecular formula of $C_{47}H_{55}N_2O_{11}S_2Na$ and a molecular weight of 911.1 g/mol with an extinction coefficient of 1.751×10^5 M^{-1} cm^{-1} (in water). The structure of the PSVue-794 control probe is shown in Figure 5.2. The fluorescent probe has a maximum excitation and emission of 787 nm and 808 nm respectively (PSVue-794 control data sheet, Molecular Targeting Technologies).
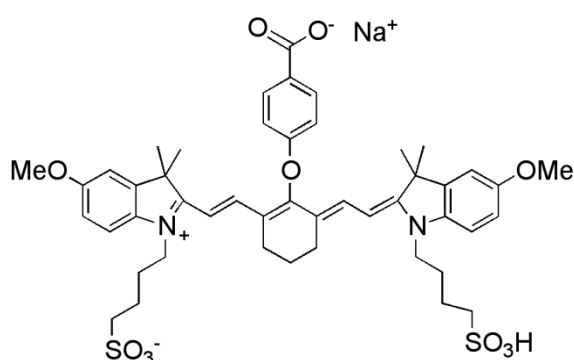
Figure 5.2. Chemical structure of the PSVue-794 control probe (PSVue-794 control probe data sheet, Molecular Targeting Technologies).

The PSVue-794 dye was prepared in two steps, immediately before the *in vivo* imaging procedure. Diluent X (410 μL) was added to the precursor apo-PSS solid powder (1.2 mg) in a 2 mL vial to prepare a 2 mM solution (2.92 mg/mL). A solution of zinc nitrate (4.2 mM, 410 μL) was added to the first solution to prepare and activate the PSVue-794 dye (1 mM).

The final solution was placed in a water bath at 40ºC for 30 min and mixed frequently until a clear green solution was obtained. The 1 mM stock solution of PSVue-794 control dye in water (600 nmoles) was purchased ready-to-use from Molecular Targeting Technologies, Inc. (MTTI, PA, USA).

5.2.3 NIR fluorescence optical in vivo imaging

On the day of *in vivo* fluorescence imaging, the rats (treatment and control groups) were sedated with an intraperitoneal injection of ketamine (75 mg/kg) and medetomidine (0.5 mg/kg) and the necks were shaved in preparation for imaging. The anaesthetised rat was placed in the In-Vivo Multispectral Imaging System FX instrument face down on the glass platen surface.

The first image taken prior to injection of the NIR dye was an image in the same fluorescence channel as PSVue-794 (excitation filter, 760 nm; emission filter, 830 nm; exposure time, 60 s; bin = 4 × 4; f-stop = 2.50; field of view = 120 mm). After rats received IV injection of PSVue-794 (27 µg/kg), two sets of images were taken; an X-ray image (exposure time, 60 s; f-stop = 2.5; field of view = 120 mm) and a fluorescence image (excitation filter, 760 nm; emission filter, 830 nm; exposure time, 60 s; bin = 4 × 4; f-stop = 2.50; field of view = 120 mm). At each experimental time point, new PSVue-794 dye was prepared.

5.2.3.1   Dose optimisation of NIR-conjugated dye

The crucial step at this stage was to optimise the concentration of the PSVue-794 dye. The dye concentration of 27 µg/kg was optimised based on the dye clearance from the body and signal intensity post-injection in the rats (n = 2, each cohort). Consecutive *in vivo* fluorescence images were taken at time points of 5, 15, and 30 min, 1, 24, 72, and 120 h after PSVue-794 injection in irradiated and non-irradiated rats at day 1. It was determined that the optimum time to take *in vivo* fluorescence image after PSVue-794 (27 µg/kg; excitation filter, 760 nm; emission filter, 830 nm; exposure time, 60 s; bin = 4 × 4; f-stop = 2.50; field of view = 120 mm) injection was 30 min. Therefore, all the subsequent NIR fluorescence images were taken 30 min after NIR dye injection at each time point post-irradiation. For each *in vivo* imaging time point, a fresh dye solution was prepared and injected.

5.2.3.2 Administration of NIR control dye

The negative control group (n = 6, each cohort) received an IV injection of PSVue-794 control dye (27 µg /kg) on day 84 post-irradiation. *In vivo* fluorescence image was taken 30 min post injection of the dye in the same fluorescence channel as PSVue-794 dye (excitation filter, 760 nm; emission filter, 830 nm; exposure time, 60 s; bin = 4 × 4; f-stop = 2.50; field of view = 120 mm).

5.2.3.3 Phosphatidylserine detection

On days 1, 7, 21, 42, 63 and 84 post-irradiation the PS detection group (n = 7, each cohort) received PSVue-794 dye (27 µg /kg) injection via the tail vein.

All three types of *in vivo* images were taken for all experimental groups (NIR fluorescence background image pre-injection of PSVue-794, X-ray image and NIR fluorescence image post PSVue-794 injection).

After the completion of all imaging, rats received a subcutaneous injection of atipamazole (1 mg/kg) to reverse the sedative effects of medetomidine as described in section 2.3.1.2.

5.2.4 Analysis of in vivo fluorescence imaging

In vivo fluorescence imaging analysis was performed with ImageJ (Version 1.49, Rasband, W.S., ImageJ, U.S. National Institutes of Health, Bethesda, Maryland, USA, http://imagej.nih.gov/ij/download.html, 1997-2014) as described in detail in section 4.2.5. The original images were exported as 16-bit files which were opened in sequence, converted to stack and then the rolling ball algorithm (pixel = 1024) was used to subtract the background. The images were artificially coloured as "Fire" (under the "Lookup Table" menu). A region of interest (ROI) was depicted around the AVM area in both treated and control rats. The stacked images were converted to montage with a scale showing high (yellow) and low (purple) fluorescent signal intensity. The ROI drawn around the AVM area was considered as the "Target" area and also a "Non-target" area was chosen. The non-target area was the average of the ROI depicted around an area at the upper side of the two forelimbs of the rat. In addition, the same size ROI was drawn around the AVM area for pre-injection images and used for background calculation. The mean fluorescence intensity (MFI) for each image was calculated by the following formula:

T/NT = (Target ROI - background ROI) / (Non-target ROI – background ROI)

Optimisation experiments express the data as MFI and are given in arbitrary units.

In the experimental animals, to compare the change in fluorescence intensity over time and to reduce the intra-subject variability, MFI values determined for each animal at each time point were divided by the same animals' specific MFI at day 1 to provide an induction ratio. To determine the anatomical location of any fluorescent signal, the fluorescence image was montaged with the X-ray image taken simultaneously.

5.2.5 Statistical analysis

The T/NT ratios or MFI were calculated and the results depicted as mean ± standard error of the mean (SEM). The statistical analysis was assessed using the Student's unpaired t-test to compare two groups. As values at each time point were collected sequentially from the same animal, data were analysed by repeated measures two-way ANOVA to consider the effects of treatment and time. The resulting ROI values were plotted using GraphPad Prism 6.0 software. A probability value of ≤0.05 was considered significant.

5.3 Results

5.3.1 Optimisation of PSVue-794 dose

Preliminary *in vivo* imaging experiments examined the level of externalised PS with PSVue-794 probe at various concentrations to determine a dose that would clear the animal within 5 days prior to any subsequent dosing. The concentration of PSVue-794 probe for injection was optimised based on the highest intensity of the probe and the optimum clearance of the probe from the body. A dose of 27 µg/kg was determined to be optimal and used in all experimental animals. At this dose, the level of fluorescence decreased from the time of injection for 30 min before stabilising for 30 min (Figure 5.3; other doses not shown). The intensity then continued to decrease over several days until no fluorescence was detected by day 5. The 30 min time point was henceforth considered as the optimal time to image animals after administration of 27 µg/kg PSVue-794.
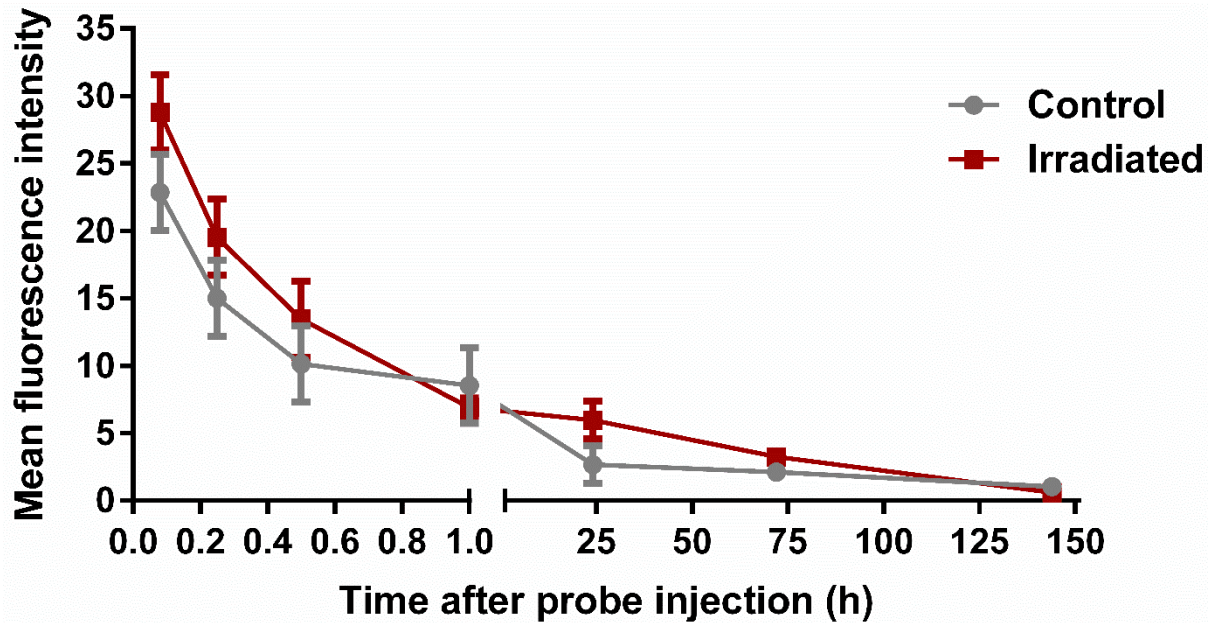
Figure 5.3. Signal intensity and clearance of PSVue-794. *In vivo* quantification of exposed phosphatidylserine with the PSVue-794 probe (27 μg/kg) in control and irradiated rat AVMs. The course of fluorescence intensity and clearance was monitored by taking consecutive images at designated time points after one injection of the probe at time zero. The considered rats were at day 1 post-irradiation. Mean ± SEM. n = 2 per cohort.

5.3.2 Validation of PSVue-794 specificity with non-targeting PSVue-794 control

To ensure that the fluorescent probe was not binding non-specifically, PSVue-794 control dye was administered to animals at the same dose rate as determined for PSVue-794, 27 μg/kg, and *in vivo* imaging performed. The control probe was injected into animals only at the 84 day time-point in both irradiated and non-irradiated animals (n = 6, each cohort). The overlaid images of X-ray and fluorescence showed no fluorescent signal at the AVM area in either treatment group. Figure 5.4 shows overlaid images representative of PSVue-794 control administration in an irradiated rat after 84 days.

Figure 5.4. *In vivo* near-infrared fluorescence of PSVue-794 control in the AVM rat model. Representative montage of *in vivo* near-infrared fluorescence of PSVue-794 control (27 µg/kg) and X-ray in an irradiated AVM rat at 84 days post-irradiation (A) X-ray, (B) fluorescence and (C) overlay image of X-ray and fluorescence. No fluorescent signal was seen in the AVM area. Identical images were recorded for non-irradiated animals.

In contrast to the non-targeting control probe, Figure 5.5 shows that when the PSVue-794 probe was injected to both non-irradiated and irradiated rats at day 84 post-irradiation, fluorescent signal of the PS-targeting probe (PSVue-794) accumulated at the AVM area. The results suggested the externalisation of PS is specific to the AVM area. *In vivo* quantification of PSVue-794 and control probes injected to both non-irradiated and irradiated AVM rats at 84 days post-irradiation are depicted in Figure 5.6 The fluorescence intensity of PSVue-794 at the AVM area in non-irradiated and irradiated rats was approximately 6- and 7-fold higher, respectively, than the PSVue-794 control.
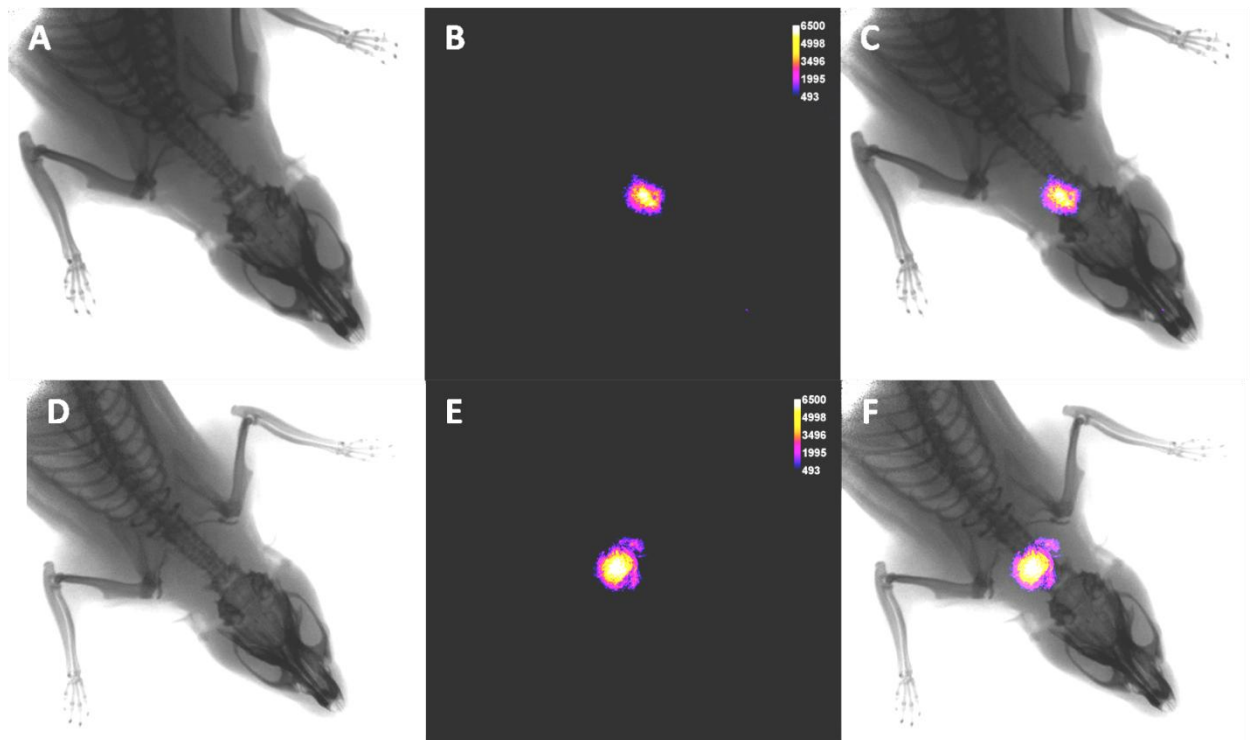
Figure 5.5. *In vivo* near-infrared fluorescence of PSVue-794 in the AVM rat model. Representative montage of *in vivo* near-infrared fluorescence of PSVue-794 and X-ray in an AVM non-irradiated rat (A-C) and irradiated AVM rat (D-F) at day 84 post-irradiation. (A, D) X-ray; (B, E) fluorescence; and (C, F) overlay image of X-ray and fluorescence.
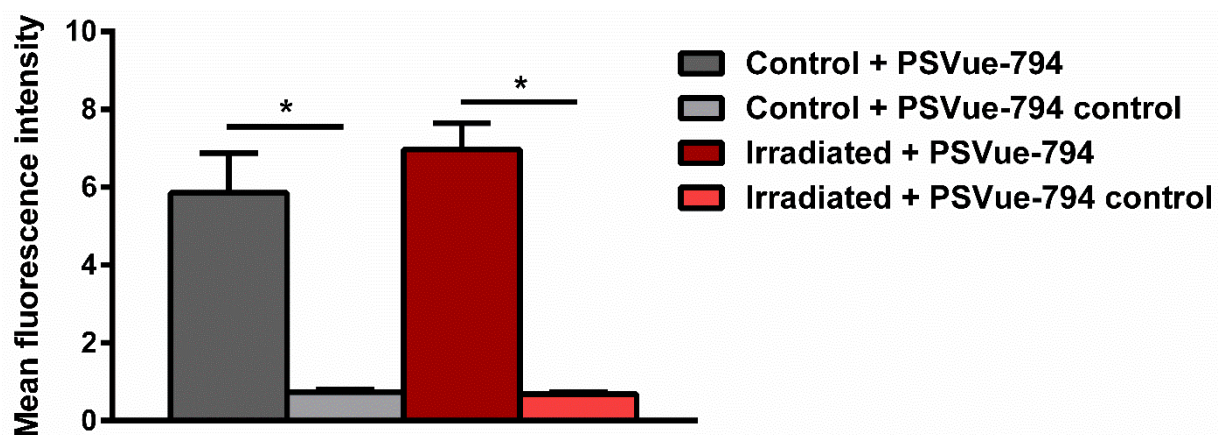
Figure 5.6. Quantification of PSVue-794 and PSVue-794 control probe binding in the AVM animal model. Images taken at day 84 post-irradiation in both AVM non-irradiated and irradiated rats that were quantified for probe binding and fluorescence intensity using ImageJ. Mean ± SEM. n = 6 per cohort. * $P < 0.01$.

5.3.3 Time course of PS externalisation in rat AVMs after irradiation

To examine the time course of PS externalisation after irradiation, the PSVue-794 probe was administered to non-irradiated and irradiated AVM rats at various time points and imaging

performed. The results revealed a time-dependent increase in PS externalisation on AVM endothelial cells post-irradiation with a significant difference at the three last time points. In addition, there was an increase in PS externalisation in non-irradiated rats, which increased until day 7 and then displayed a linear trend until the end of the experiment (Figure 5.7). At later time points, the irradiated rats showed a higher increase in externalised PS compared to non-irradiated rats, although these differences were not significant.

To reduce intra-animal variability, mean fluorescence intensity at each time point was normalised to day 1 for each animal. The data presented in Figure 5.8 indicate that irradiation increased the level of exposed PS on the surface of AVM endothelial cells in a time dependent manner. There was a significant difference between day 1 and days 42, 63 and 84 in AVM irradiated rats. In contrast, while PS externalisation was present in non-irradiated AVM vessels, this did not increase over the 84 day period. The level of PS externalisation in the AVM was higher at all time-points in the irradiated rats compared to non-irradiated rats however; this only reached statistical significance at day 84.
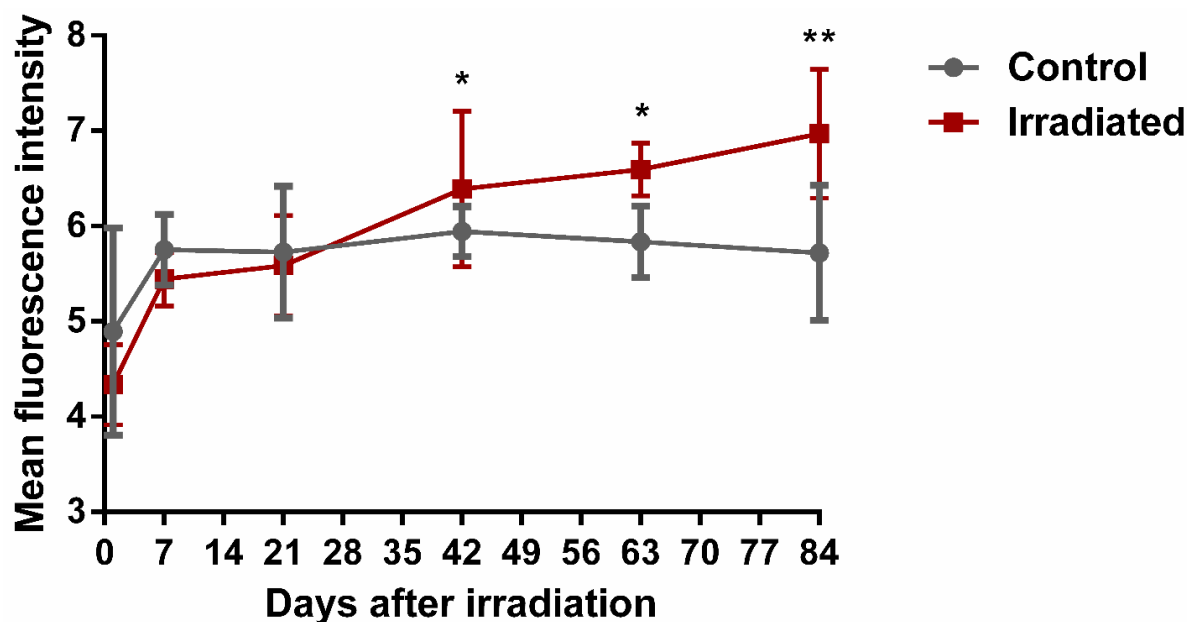
Figure 5.7. Phosphatidylserine exposure in the rat model AVM (MFI). *In vivo* quantification of exposed phosphatidylserine with PSVue-794 probe in control and irradiated AVM rat models at different time points. Mean ± SEM. n = 7 per cohort. * P < 0.05 and * P < 0.01, * represents the comparison between different time points in the same group.
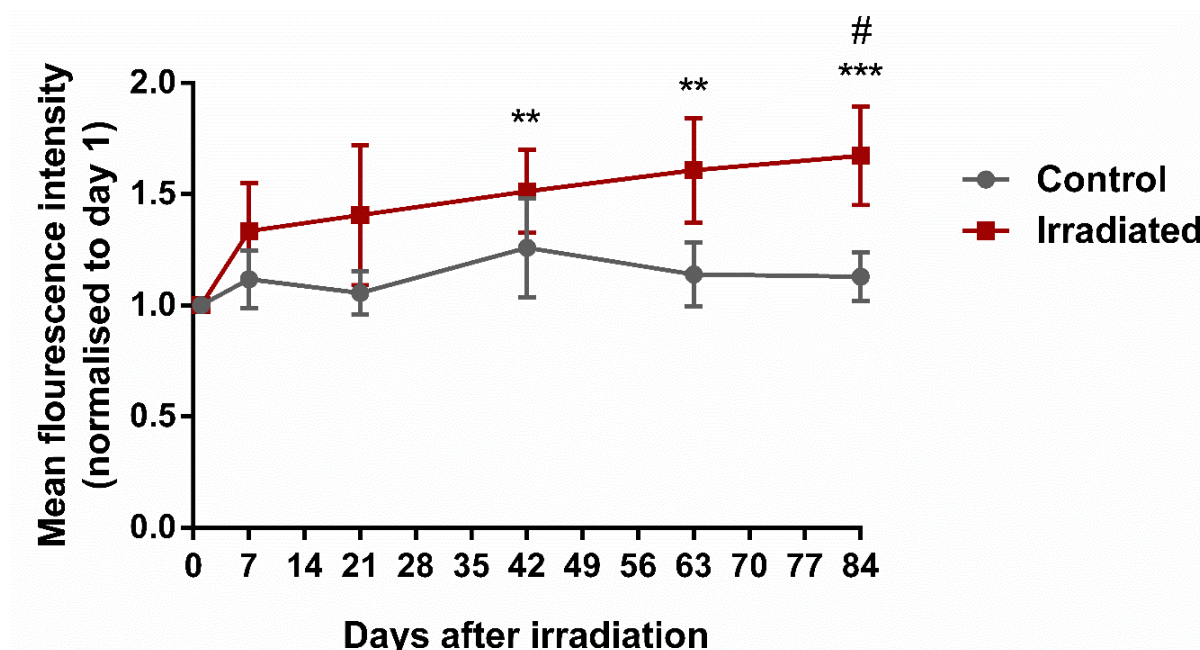
Figure 5.8. Phosphatidylserine exposure in the rat model AVM (normalised MFI). *In vivo* quantification of exposed phosphatidylserine with PSVue-794 probe in control and irradiated AVM rat models at different time points compared to day 1 as a ratio. Mean ± SEM. n = 7 per cohort. ** P < 0.001 and *** P < 0.001, * represents the comparison between different time points in the same group. # represents comparison between the irradiated and control groups. # P < 0.05.

5.4 Discussion

This study examined the effect of irradiation on PS translocation in the rat AVM model using the PS-specific PSVue-794 probe and the In-Vivo Multispectral Imaging System FX instrument. Binding of PSVue-794 demonstrated that externalisation of PS was evident in non-irradiated animals within AVM vessels. Gamma Knife irradiation caused a further significant increase in PS externalisation which was also localised solely within the irradiated AVM region. The specific localisation of PS externalisation, the increase observed with radiation treatment, as well as the sustained surface expression seen in this model, indicates that PS has potential as a candidate for vascular targeting of AVMs with thrombotic agents.

One of the primary requirements of a potential candidate for vascular targeting is that its surface expression must be significantly discriminatory between target and normal vessels. This allows the targeted thrombotic ligand to bind only at the designated region to drive thrombosis and reduces the risk of off-target thrombosis in vessels of other organs, which may have serious consequences for the patient. The targeting of PS in this study and in earlier

151

vascular targeting studies (Hanshaw & Smith, 2005; Reshef et al., 2010) is based on the premise that normal healthy vessels maintain PS on the inner leaflet of the plasma membrane and that translocation to the outer surface occurs in response to injury or abnormal conditions often associated with disease. Reorientation of PS has been observed in aging erythrocytes, activated platelets, activated macrophages, many viable tumours (Kirszberg et al., 2009; Riedl et al., 2011), endothelial cells of tumour blood vessels, infected cells, injured cells, apoptotic cells, senescent and necrotic cells (Balasubramanian & Schroit, 2003; Brouckaert et al., 2004; Hirt & Leist, 2003; Williamson & Schlegel, 2002), cell-derived microparticles, stressed tumour cells and irradiated normal endothelial cells (Zhao et al., 2011). There are also many stimuli that can cause translocation of PS to the exoplasmic leaflet of the plasma membrane (Zwaal et al., 2005) including inflammatory cytokines, thrombin, hypoxia/reoxygenation and viral infection (Ran et al., 2002). Irradiation is well known to stimulate PS externalisation both *in vitro* and *in vivo* (Ran et al., 2002; Zhao et al., 2011). For example, in a mouse glioma model, it was demonstrated that PS was translocated to the cell surface after irradiation in both endothelial cells and tumour cells with maximum tumour-to-normal tissue ratio (TNR) being obtained at 24 h post-irradiation (Zhao et al., 2011). Consistent with the literature, the results of the current study have now shown that Gamma Knife irradiation of AVM vessels can increase PS externalisation at the luminal surface and further show that this is targetable with PS binding probe injected in blood.

Interestingly, there was a significant level of PSVue-794 probe binding in the AVMs from non-irradiated animals in this study. Previous *ex vivo* studies in our group that examined immunohistological staining of PS in the rat AVM also demonstrated that PS was translocated to the surface of AVM endothelial cells in both sham and irradiated rats (PhD Thesis, 2006, Kingsley P. Storer, "Cerebral arteriovenous malformations: molecular biology and enhancement of radiosurgical treatment"). In the latter study, PS expression was deemed higher in AVM sections from irradiated rats relative to non-irradiated rats, consistent with the current *in vivo* findings. The same study also, reported faint to moderate expression of PS on the endothelial cells of high flow vessels of sham-irradiated rats located ipsilateral and contralateral to the fistula. The molecular changes that occur in response to altered flow in the rat AVM, as postulated for VCAM-1 and ICAM-1 in the previous chapter, may result in cellular proliferation in the cell wall in early stages of development followed by apoptosis of cells in later stages when the AVM is considered mature and vessel growth/expansion has

reached an equilibrium. Such apoptotic cells may be expected to have PS exposure on the surface, which may explain the increased basal exposure of PS seen in this study.

Whether this endogenous level of PS externalisation is evident in human AVMs has not been investigated. The AVM animal model used in this experiment has been shown to demonstrate similar haemodynamic, angiographic, and morphological characteristics to human AVMs (Yassari et al., 2004). It has been demonstrated previously that vessels in human AVMs have increased levels of cellular apoptosis (as determined by active caspase-3 staining and DNA fragmentation assays) (Chen et al., 2012) and thus would be assumed to have increased levels of PS externalisation. However, this staining was predominantly evident in the smooth muscle cell layer in the human AVMs and not specifically in the endothelial cells. Consequently, irradiation of human AVMs may show an even greater induction of PS externalisation on the endothelium than seen here in the rat model.

This is the first study that has looked at the effect of Gamma Knife on PS translocation in an AVM rat model by *in vivo* fluorescence imaging. *In vivo* fluorescence imaging provides a non-invasive visualisation of biological processes that are occurring at the molecular and cellular level (Biswal et al., 2007) in the live AVM animal model. It is also an ideal technique to track molecular changes that occur *in vivo* to elucidate AVM pathogenesis with the requirement of sensitive NIR probes for detection. In this case, to fully exploit PS as a candidate molecule for vascular targeting, a good molecule that can selectively bind with high affinity to externalised PS is required. The most widely used protein for PS binding with high affinity is Annexin-V. Despite its popularity for PS detection, it has previously demonstrated non-specific binding to tissue and a suboptimal pharmacokinetics profile (Reshef et al., 2010). Also, annexin has a high molecular weight that leads to slower clearance rates from the circulation compared to small chemical compounds and peptides (Schutters & Reutelingsperger, 2010). High affinity probes with less molecular weight have the more favourable signal-to-background ratio (Schutters & Reutelingsperger, 2010). Therefore among all the PS-binding compounds reported in the literature, PSVue-794 overall showed significant advantages. PSVue-794 can quickly and efficiently be cleared from the blood circulation due to its relatively small molecular weight (Schutters & Reutelingsperger, 2010; Smith et al., 2011). It binds with high affinity to negatively charged PS through its cation complex (zinc(II)-dipicolylamine; Zn-DPA) (Hanshaw & Smith, 2005). PSVue-794 probe has targeted PS in a number of rodent models of xenograft tumours, acute muscle damage and

thymic atrophy (Smith et al., 2012; Smith et al., 2011). Thus, PSVue-794 has boosted research and development of non-invasive *in vivo* fluorescence imaging of externalised PS. In the current experiments, PSVue-794 was cleared from the animal in less than 5 days allowing consecutive images to be taken over a defined time period in the one animal to reduce inter-subject variation. This probe also demonstrated high fluorescence intensity and high specificity at the AVM area. The ability to use a consistent batch of labelled probe for PS, as opposed to that for the ICAM-1 and VCAM-1 imaging in Chapter 4, also contributed to an improvement in statistical error allowing detection of significant differences between the treatment groups.

5.5 Limitations

This work would be strengthened by further validation with an immunofluorescence study at each time point. As for the ICAM-1 and VCAM-1 imaging study, this was not possible in this set of experiments as the same animal was used for the whole period of the experiment. Further examination of the apoptotic state of the cells by examining active caspase-3 expression and DNA fragmentation might have demonstrated how many of the PS-positive cells were associated with apoptosis. As mentioned above, the model has many overlaps with human AVMs but it is limited by the fact that the AVM is not formed in the brain and is not congenital. However, this model represents an important intermediate between the *in vitro* context and human studies, and has now demonstrated that irradiation can induce PS externalisation on the endothelium of a model AVM and that this can be targeted with a probe via the circulation.

5.6 Summary and Conclusions

This study demonstrated that PS was externalised at the AVM area in the AVM rat model relative to the normal vasculature. Radiation (15 Gy) further promoted PS externalisation in the rat AVM in a time-dependent manner. PS may be a valid candidate for a vascular targeting approach to treat AVMs at a reduced radiation dose.

Chapter 6. General discussion and future directions

Arteriovenous malformations in the brain are the leading cause of stroke in children and young adults. Small and superficial AVMs are manageable with the current treatment methods although there are over one third of AVM patients with large and deep lesions that cannot be safely and effectively treated. Therefore, a new treatment method for these patients with life-threatening AVMs is required. A biological technique that can be applied to increase the rate of thrombosis or occlusion is highly attractive. In the field of cancer therapy the technique of vascular targeting has been employed (Neri & Bicknell, 2005). This technique relies on molecular markers that differentiate the cancer vascular cells from normal vascular cells. The molecular markers are recognised by specific antibodies that carry a thrombotic agent to induce thrombosis inside the tumour vessels and eventually lead to tumour cell death as a result of ischaemia (Thorpe, 2004). In the case of AVMs, specific markers that differentiate the AVM vessels from the normal vasculature are required to fulfil this goal. Studies to date have failed to find expression of surface molecules that are sufficiently discriminatory in AVMs. Highly focused irradiation is therefore proposed as a priming agent to induce molecular changes on the surface of AVM endothelial cells. Previous studies have shown that radiation can induce molecular changes on the surface of endothelial cells such as phosphatidylserine (PS) translocation and up-regulation of CAMs, including ICAM-1, VCAM-1, E-selectin and P-selectin (Hallahan et al., 1997; Prabhakarpandian et al., 2001; Ran et al., 2002; Zhao et al., 2011). Therefore, the aims of the current study were to identify the most discriminating endothelial marker from this selection of targets with the minimum radiation dose (5, 15, or 25 Gy) and to study those molecules further in a rat AVM model as potential targets in AVM treatment. Reducing the radiation dose is important from a clinical perspective, as a lower dose of radiation will be safer for large AVM treatment and also reduces the risk of off-target radiation damage to normal cells.

The primary findings of the current study indicate that irradiation as low as 15 Gy produces significant induction in the expression of the molecular markers in brain microvascular endothelial cells *in vitro*. The molecules that showed the highest level of expression on the endothelial cell surface were ICAM-1 and VCAM-1. *In vivo*, the rat AVM was shown to express high basal levels of these molecules within the AVM, relative to the normal vasculature, however, 15 Gy induced no further significant changes in the level of expression. Further studies demonstrated that rat AVMs also expressed high basal levels of PS relative to

the normal vasculature, but increased externalisation of PS was evident post-irradiation in the AVM animal model in response to a 15 Gy dose of radiation.

One of the aims of the current study was to determine the lowest dose that induced significant molecular changes on the surface of endothelial cells for a future vascular targeting approach. In the existing approach to AVM treatment with radiosurgery, doses of $16 - 25$ Gy are considered reliably able to induce AVM occlusion through fibrosis and vessel remodelling (Lunsford et al., 2008). Using radiosurgery as a primer for vascular targeting is not intended to induce vessel occlusion directly, but simply to stimulate cell surface expression of a discriminatory molecule. A lower radiation dose may therefore be acceptable. This would reduce the risk of off-target radiation effects and may allow targeting of large, currently untreatable AVMs, which would typically need doses that would be considered unsafe. The current *in vitro* studies demonstrated that irradiation doses of 15 Gy and 25 Gy, but not 5 Gy, showed significant induction in the expression level of CAMs. Among the CAMs, ICAM-1 and VCAM-1 showed the highest level of expression post-irradiation followed by P-selectin with a moderate increase at the cell surface. E-selectin showed limited up-regulation and cell surface expression. As ICAM-1 and VCAM-1 had the highest level of expression among other CAMs, they were examined further in the AVM animal model with a selected dose for *in vivo* studies of 15 Gy. This however was insufficient to significantly up-regulate the surface expression of either molecule *in vivo*. Therefore, the results indicated that the 15 Gy radiation dose is not high enough to induce discriminating expression, at least in this rat model. In previous studies using the AVM animal model, a significant induction of CAM expression in the AVM was achieved by 20 Gy and 25 Gy doses. In an *ex vivo* study examining ICAM-1 expression by immunofluorescence (IF), high expression of ICAM-1 was revealed post-irradiation with 20 Gy at day 1 (PhD Thesis, 2015, Saleh. Kashba, "Cerebral arteriovenous malformations: radiosurgery-enhanced molecular targeting therapy"). In another *ex vivo* study by Storer et al., VCAM-1 expression was reported to be up-regulated on the rat AVM endothelium at day 21 post-irradiation by 25 Gy (Storer et al., 2010). The discrepancy in results between the studies may be due to the differences in dose. However, it cannot be excluded that there were some differences to the quantitation of expression between the IF staining method and *in vivo* imaging. In the IF studies, little expression of ICAM-1 or VCAM-1 was displayed on the non-irradiated rat AVM endothelium by IF, unlike the high level found in the current study. This may have been artificially captured in the images by altering the gain and exposure time. Secondly, a limitation of IF performed on fixed tissue is

that it cannot determine whether the increased expression detected is at the cell surface or whether the increase occurs predominantly in the cytoplasm, that is, it can only localise expression at the cellular, not subcellular, level. The use of *in vivo* imaging in this study has shown firstly, that we can target these antibody-conjugates specifically to the AVM via intravenous administration. Secondly, this technique demonstrates that the antibody-conjugates are specifically targeting surface expression of these molecules. It must be considered that the results obtained by each method may differ for this reason. The *in vivo* imaging technique is a far more accurate way to establish whether candidates are exposed at the luminal surface of the endothelium. Further experiments are required to establish whether increasing the dose would indeed increase surface expression of ICAM-1 or VCAM-1 in line with the IF studies (Storer et al., 2010; PhD Thesis, 2015, Saleh. Kashba, "Cerebral arteriovenous malformations: radiosurgery-enhanced molecular targeting therapy").

Improvements could certainly be made to increase the sensitivity of the *in vivo* imaging procedure. If the conjugated dyes for ICAM-1 and VCAM-1 could have been prepared at the same time for all the experimental rats this may have reduced variability. Due to the limited number of gamma irradiated rats that could be accommodated for each Gamma Knife irradiation session this was not possible. Using the available pre-conjugated PSVue-794 dye appeared advantageous in this study over conjugating the dye with an antibody as it leads to slightly different labelling efficiencies. *In vivo* imaging could be improved perhaps by conjugating the ICAM-1 and VCAM-1 antibodies with NIRF nanoparticles such as quantum dots, carbon nanotubes and metal nanoclusters which have been used in an array of studies associated with inflammatory disease (Jayagopal et al., 2007; Rossin et al., 2007). Positron emission tomography (PET) is a highly sensitive approach to examine *in vivo* expression giving a 3-dimensional image of the target (Cherry & Gambhir, 2001; Liang et al., 2007). PET typically has sensitivities within the 10^{-11} mol/L to 10^{-12} mol/L concentration range (Chatziioannou et al., 2001). PET has previously been used for example to examine vascular expression of ICAM-1 after LPS injection with ^{64}Cu-labeled nanoparticles coated with anti-ICAM-1 antibodies (Rossin et al, 2007). This would be a more sensitive and accurate way to examine expression within the vessels of AVMs and better localise the target area.

Considering the high level of basal expression of CAM and PS molecules in the AVM in the non-irradiated rats is important. Previous studies that have examined the effect of radiation on the vasculature and subsequent expression of ICAM-1 and VCAM-1, used "normal" vascular

158

endothelium that typically have low basal levels of expression of these two molecules (Epperly et al., 2002; Mollà et al., 2003; Müller et al., 2006). The elevated expression of ICAM-1 and VCAM-1 found on the AVM endothelium is most likely a result of the changes in flow and shear stress caused by the anastomosis (Nagel et al., 1994). It is possible that the high CAM expression evident in non-irradiated rats may have reached saturation before irradiation, hence radiation at 15 Gy did not have any additive effect nor induce any further increase in the level of expression of CAMs. This would explain the lack of cohesion between the *in vitro* and *in vivo* results in this study and reinforces the limitations of *in vitro* work in general. In this case, the effect of altered flow on the endothelial cells was not replicated in culture, nor the presence of other cell types and factors present in blood that would normally influence the expression of such molecules on endothelial cells *in situ*. This is consistent with the fact that many of the previous studies suggest that endothelial cells are more radiosensitive in an *in vitro* environment than in an *in vivo* environment (Haimovitz-Friedman & Fuks, 1998), potentially due to a lower basal state of induction *in vitro*. In this sense, the rat AVM model represents an important pre-clinical model to test vascular targets. Considering the rat AVM carries a nidus structure that is static in its position, it was an attractive model to study the effect of Gamma Knife irradiation on AVM endothelial cells.

What was demonstrated quite clearly in this study was that the rat AVMs did have significantly increased expression of ICAM-1 and VCAM-1, and increased translocation of PS, compared to the normal vasculature of the rat. The localisation of CAM expression and PS translocation was specifically at the AVM area. This might suggest that these molecules would be highly expressed in human AVMs even without irradiation since the AVM animal model has been shown to be similar in haemodynamic, ultrastructural, molecular and histological characteristics to human AVMs (Tu et al., 2010). However, perhaps this very high level of expression is an artefact of the surgical creation of the anastomosis and the subsequent arterialisation of the vein. Human AVMs once detected are often considered static and not undergoing further growth (Rangel-Castilla et al., 2014). Although the rat AVM is left to mature for 6 weeks after creation, perhaps this length of time is not sufficient for the stabilisation of expression of all molecules on the endothelial surface. For instance in this study, VCAM-1 expression continued to increase up to day 21 in both control and irradiated rat AVMs. In human AVMs, faint to moderate ICAM-1 and VCAM-1 expression was evident by IF in comparison to expression in other brain vascular malformations (Storer et al., 2008). This is consistent with the elevated levels in the rat model. However, it is hard to compare the

absolute levels of expression between the two models and whether radiation may further induce CAM expression in a human AVM. Also in human AVM vessels, increased levels of cellular apoptosis (as determined by active caspase-3 staining and DNA fragmentation assays) have been detected (Chen et al., 2012) and therefore would be assumed to have increased PS externalisation (Fadok et al., 1992). However, this staining was found predominantly in the AVM smooth muscle cells and not specifically in the endothelium. Consequently, this may further suggest that ICAM-1/VCAM-1 targeting may not be ideal, however irradiation of human AVM vessels may lead to a higher level of PS externalisation on the endothelium compared to that found in the rat model in response to radiation.

Further work is required to determine whether these studies can be extrapolated to human AVMs. PS is among the list of the candidate molecules that seems to have the greatest potential to be progressed further for vascular targeting. As we have shown that intravenous delivery of PSVue-794 to PS can work *in vivo* in the rat AVM model, conjugates to this molecule or antibodies targeting PS that are carrying pro-thrombotic agents such as tissue factor can be prepared to promote thrombosis inside the rat AVM vessels after irradiation. Performing such experiments to compare doses of both 15 Gy and 25 Gy would further strengthen whether this molecule could be taken further for development and at what potential dose.

6.1 Final Conclusions

In conclusion, based on the results obtained in this study, PS seems to be the molecule with the most potential to study further as a vascular targeting candidate. The dose considered for the future irradiations in the AVM animal model should be higher than 15 Gy to be effective enough for vascular targeting. Further consideration must be given to understanding the molecular differences between human and rat AVMs to improve testing of candidate molecules and to find an ideal target to translate this approach to the clinical setting.

References

Abdulrauf, S. I., Malik, G. M., & Awad, I. A. (1999). Spontaneous angiographic obliteration of cerebral arteriovenous malformations. *Neurosurgery*, *44*(2), 280–7; discussion 287–8.

Achrol, A. ., Kim, H., Pawlikowska, L., Trudy Poon, K., McCulloch, C. E., & Ko, N. U. (2007). Association of tumor necrosis factore α–238G>A and apolipoprotein E2 polymorphisms with intracranial hemorrhage after brain arteriovenous malformation treatment. *Neurosurgery*, *61*(4), 731–740.

Achrol, A. S., Guzman, R., Varga, M., Adler, J. R., Steinberg, G. K., & Chang, S. D. (2009). Pathogenesis and radiobiology of brain arteriovenous malformations: implications for risk stratification in natural history and posttreatment course. *Neurosurgical Focus*, *26*(5), E9.

Achrol, A. S., Pawlikowska, L., McCulloch, C. E., Poon, K. Y. T., Ha, C., Zaroff, J. G., … Young, W. L. (2006). Tumor necrosis factor-alpha-238G>A promoter polymorphism is associated with increased risk of new hemorrhage in the natural course of patients with brain arteriovenous malformations. *Stroke*, *37*(1), 231–4.

Aird, W. C. (2007). Phenotypic heterogeneity of the endothelium: I. Structure, function, and mechanisms. *Circulation Research*, *100*(2), 158–73.

Alexander, M. J., & Tolbert, M. E. (2006). Targeting cerebral arteriovenous malformations for minimally invasive therapy. *Neurosurgery*, *59*(5 Suppl 3), S178–83; discussion S3–13.

Alexiou, D., Karayiannakis, A. J., Syrigos, K. N., Zbar, A., Sekara, E., Michail, P., … Diamantis, T. (2003). Clinical significance of serum levels of E-selectin, intercellular adhesion molecule-1, and vascular cell adhesion molecule-1 in gastric cancer patients. *The American Journal of Gastroenterology*, *98*(2), 478–85.

Al-Jarallah, A., Al-Rifai, M. T., Riela, A. R., & Roach, E. S. (2000). Nontraumatic Brain Hemorrhage in Children: Etiology and Presentation. *Journal of Child Neurology*, *15*(5), 284–289.

Allt, G., & Lawrenson, J. G. (2001). Pericytes: cell biology and pathology. *Cells, Tissues, Organs*, *169*(1), 1–11.

Al-Shahi, R., Bhattacharya, J. J., Currie, D. G., Papanastassiou, V., Ritchie, V., Roberts, R. C., … Warlow, C. P. (2003). Prospective, population-based detection of intracranial vascular malformations in adults: the Scottish Intracranial Vascular Malformation Study (SIVMS). *Stroke*, *34*(5), 1163–9.

Al-Shahi, R., Fang, J. S. Y., Lewis, S. C., & Warlow, C. P. (2002). Prevalence of adults with brain arteriovenous malformations: a community based study in Scotland using capture-recapture analysis. *Journal of Neurology, Neurosurgery, and Psychiatry*, *73*(5), 547–51.

Al-Shahi, R., & Warlow, C. (2001). A systematic review of the frequency and prognosis of arteriovenous malformations of the brain in adults. *Brain : A Journal of Neurology*, *124*(Pt 10), 1900–26.

Alzari, P. M., Lascombe, M. B., & Poljak, R. J. (1988). Three-dimesional structure of antibodies. *Annual Review of Immunology*, *6*, 555–580.

Andaluz, N., Myseros, J. S., Sathi, S., Crone, K. R., & Tew, J. M. (2004). Recurrence of

cerebral arteriovenous malformations in children: report of two cases and review of the literature. *Surgical Neurology*, *62*(4), 324–30; discussion 330–1.

Andrade-Souza, Y. M., Ramani, M., Scora, D., Tsao, M. N., TerBrugge, K., & Schwartz, M. L. (2007). Embolization before radiosurgery reduces the obliteration rate of arteriovenous malformations. *Neurosurgery*, *60*(3), 443–51; discussion 451–2.

ApSimon, H. T., Reef, H., Phadke, R. V., & Popovic, E. a. (2002). A Population-Based Study of Brain Arteriovenous Malformation: Long-Term Treatment Outcomes. *Stroke*, *33*(12), 2794–2800.

Ardehali, A., Laks, H., Drinkwater, D. C., Ziv, E., & Drake, T. A. (1995). Vascular cell adhesion molecule-1 is induced on vascular endothelia and medial smooth muscle cells in experimental cardiac allograft vasculopathy. *Circulation*, *92*(3), 450–6.

Asa, D., Raycroft, L., Ma, L., Aeed, P. A., Kaytes, P. S., Elhammer, A. P., & Geng, J. G. (1995). The P-selectin glycoprotein ligand functions as a common human leukocyte ligand for P- and E-selectins. *The Journal of Biological Chemistry*, *270*(19), 11662–70.

Auzel, F. (2004). Upconversion and anti-Stokes processes with f and d ions in solids. *Chemical Reviews*, *104*(1), 139–73.

Balasubramanian, K., & Schroit, A. J. (2003). Aminophospholipid asymmetry: A matter of life and death. *Annual Review of Physiology*, *65*, 701–34.

Barr, J. C., & Ogilvy, C. S. (2012). Selection of treatment modalities or observation of arteriovenous malformations. *Neurosurgery Clinics of North America*, *23*(1), 63–75.

Beekman, C. a C., Buckle, T., van Leeuwen, A. C., Valdés Olmos, R. a, Verheij, M., Rottenberg, S., & van Leeuwen, F. W. B. (2011). Questioning the value of (99m)Tc-HYNIC-annexin V based response monitoring after docetaxel treatment in a mouse model for hereditary breast cancer. *Applied Radiation and Isotopes*, *69*(4), 656–62.

Bennett, M. R., Gibson, D. F., Schwartz, S. M., & Tait, J. F. (1995). Binding and Phagocytosis of Apoptotic Vascular Smooth Muscle Cells Is Mediated in Part by Exposure of Phosphatidylserine. *Circulation Research*, *77*(6), 1136–1142.

Bevers, E. M., Comfurius, P., Dekkers, D. W. ., & Zwaal, R. F. . (1999). Lipid translocation across the plasma membrane of mammalian cells. *Biochimica et Biophysica Acta (BBA)*, *1439*(3), 317–330.

Bevilacqua, M., Butcher, E., Furie, B., Furie, B., Gallatin, M., Gimbrone, M., … Zimmerman, G. (1991). Selectins: a familiy of adhesion receptors. *Cell*, *67*(2), 233.

Bevilacqua, M. P. (1993). Endothelial-leukocyte adhesion molecules. *Annual Review of Immunology*, *11*, 767–804.

Bevilacqua, M. P., Stengelin, S., Gimbrone, M. A., & Seed, B. (1989). Endothelial Leukocyte Adhesion Moleculae 1: An Inducible Receptor for Neutrophils Related to Complement Regulatory Proteins and Lectins. *Science*, *243*(4895), 1160–1165.

Bevilacqua, M., Pober, J., Mendrick, D., Cotran, R., & Gimbrone, M. (1987). Identification of an inducible endothelial-leukocyte adhesion molecule. *Proceedings of the National Academy of Sciences*, *84*(24), 9238–9242.

Bewes, J. M., Suchowerska, N., Jackson, M., Zhang, M., & McKenzie, D. R. (2008). The radiobiological effect of intra-fraction dose-rate modulation in intensity modulated

radiation therapy (IMRT). *Physics in Medicine and Biology*, *53*(13), 3567–78.

Bischoff, J., Brasel, C., Kräling, B., & Vranovska, K. (1997). E-selectin is upregulated in proliferating endothelial cells in vitro. *Microcirculation (New York, N.Y. : 1994)*, *4*(2), 279–87.

Biswal, S., Resnick, D. L., Hoffman, J. M., & Gambhir, S. S. (2007). Molecular imaging: integration of molecular imaging into the musculoskeletal imaging practice. *Radiology*, *244*(3), 651–671.

Blamek, S., Tarnawski, R., & Miszczyk, L. (2011). Linac-based stereotactic radiosurgery for brain arteriovenous malformations. *Clinical Oncology*, *23*(8), 525–531.

Blann, A., Kumar, P., Krupinski, J., McCollum, C., Beevers, D. G., & Lip, G. Y. (1999). Soluble intercelluar adhesion molecule-1, E-selectin, vascular cell adhesion molecule-1 and von Willebrand factor in stroke. *Blood Coagulation & Fibrinolysis*, *10*(5), 277–84.

Bochner, B. S., Luscinskas, F. W., Gimbrone, M. A., Newman, W., Sterbinsky, S. A., Derse-Anthony, C. P., … Schleimer, R. P. (1991). Adhesion of human basophils, eosinophils, and neutrophils to interleukin 1-activated human vascular endothelial cells: contributions of endothelial cell adhesion molecules. *The Journal of Experimental Medicine*, *173*(6), 1553–7.

Boersma, H. H., Kietselaer, B. L. J. H., Stolk, L. M. L., Bennaghmouch, A., Hofstra, L., Narula, J., … Reutelingsperger, C. P. M. (2005). Past , Present , and Future of Annexin A5 : From Protein Discovery to Clinical Applications. *Journal of Nuclear Medicine*, *46*(12), 2035–50.

Bollet, M. A., Anxionnat, R., Buchheit, I., Bey, P., Cordebar, A., Jay, N., … Picard, L. (2004). Efficacy and morbidity of arc-therapy radiosurgery for cerebral arteriovenous malformations: a comparison with the natural history. *International Journal of Radiation Oncology, Biology, Physics*, *58*(5), 1353–63.

Bombeli, T., Schwartz, B. R., & Harlan, J. M. (1998). Adhesion of activated platelets to endothelial cells: evidence for a GPIIbIIIa-dependent bridging mechanism and novel roles for endothelial intercellular adhesion molecule 1 (ICAM-1), alphavbeta3 integrin, and GPIbalpha. *The Journal of Experimental Medicine*, *187*(3), 329–39.

Bonello, N., & Norman, R. J. (2002). Soluble adhesion molecules in serum throughout the menstrual cycle. *Human Reproduction*, *17*(9), 2272–8.

Böse, J., Gruber, A. D., Helming, L., Schiebe, S., Hafner, M., Beales, M., & Köntgen, F. (2004). The phosphatidylserine receptor has essential functions during embryogenesis but not in apoptotic cell removal. *Journal of Biology*, *3*(4), 15.

Brant-Zawadzki, M., Anderson, M., DeArmond, S. J., Conley, F. K., & Jahnke, R. W. (1980). Radiation-induced large intracranial vessel occlusive vasculopathy. *American Journal of Roentgenology*, *134*(1), 51–5.

Brasier, A. R. (2006). The NF-κB Regulatory Network. *Cardiovascular Toxicology*, *6*(2), 111–130.

Bratton, D. L., Fadok, V. a., Richter, D. a., Kailey, J. M., Guthrie, L. a., & Henson, P. M. (1997). Appearance of Phosphatidylserine on Apoptotic Cells Requires Calcium-mediated Nonspecific Flip-Flop and Is Enhanced by Loss of the Aminophospholipid Translocase. *Journal of Biological Chemistry*, *272*(42), 26159–26165.

Brouckaert, G., Kalai, M., Krysko, D. V, Saelens, X., Vercammen, D., Ndlovu, M., … Vandenabeele, P. (2004). Phagocytosis of Necrotic Cells by Macrophages Is Phosphatidylserine Dependent and Does Not Induce Inflammatory Cytokine Production. *Molecular Biology of the Cell*, *15*(3), 1089–1100.

Brown, K. R., & Rzucidlo, E. (2011). Acute and chronic radiation injury. *Journal of Vascular Surgery*, *53*(1 Suppl), 15S–21S.

Brown, R. D., Wiebers, D. O., Forbes, G., O'Fallon, W. M., Piepgras, D. G., Marsh, W. R., & Maciunas, R. J. (1988). The natural history of unruptured intracranial arteriovenous malformations. *Journal of Neurosurgery*, *68*(3), 352–357.

Brown, R. D., Wiebers, D. O., & Forbes, G. S. (1990). Unruptured intracranial aneurysms and arteriovenous malformations: frequency of intracranial hemorrhage and relationship of lesions. *Journal of Neurosurgery*, *73*(6), 859–63.

Brown, R. D., Wiebers, D. O., Torner, J. C., & O'Fallon, W. M. (1996). Frequency of intracranial hemorrhage as a presenting symptom and subtype analysis: a population-based study of intracranial vascular malformations in Olmsted Country, Minnesota. *Journal of Neurosurgery*, *85*(1), 29–32.

Brown, R. D., Wiebers, D., Torner, J. C., & Fallon, W. M. O. (1996). Incidence and prevalence of intracranial vascular malformations in Olrnsted County , Minnesota , 1965 to 1992. *Journal of Neurology*, *46*(4), 949–952.

Burchiel, K. J., Clarke, H., Ojemann, G. a, Dacey, R. G., & Winn, H. R. (1989). Use of stimulation mapping and corticography in the excision of arteriovenous malformations in sensorimotor and language-related neocortex. *Journal of Neurosurgery*, *24*(3), 322–7.

Burtea, C., Laurent, S., Lancelot, E., Ballet, S., Murariu, O., Rousseaux, O., … Muller, R. N. (2009). Peptidic targeting of phosphatidylserine for the MRI detection of apoptosis in atherosclerotic plaques. *Molecular Pharmaceutics*, *6*(6), 1903–19.

Butterworth, K. T., Mcgarry, C. K., Sullivan, J. M. O., Hounsell, A. R., & Kevin, M. (2010). A study of the biological effects of modulated 6 MV radiation fields. *Journal of Physics in Medicine and Biology*, *55*(6), 1607–1618.

Calderón, C., Huang, Z., Gage, D., Sotomayor, E., & Lopez, D. (1994). Isolation of a Nitric Oxide Inhibitor from Mammary Tumor Cells and its Characterization as Phosphatidyl Serine. *Journal of Experimental Medicine*, *180*(3), 945–958.

Carlos, T., Kovach, N., Schwartz, B., Rosa, M., Newman, B., Wayner, E., … Harlan, J. (2014). Human monocytes bind to two cytokine-induced adhesive ligands on cultured human endothelial cells: endothelial-leukocyte adhesion molecule-1 and vascular cell adhesion molecule-1. *Blood*, *77*(10), 2266–2271.

Carlos, T. M., & Harlan, J. M. (1994). Leukocyte-endothelial adhesion molecules. *Blood*, *84*(7), 2068–101.

Carlos, T. M., Schwartz, B. R., Kovach, N. L., Yee, E., Rosa, M., Osborn, L., … Rosso, M. (1990). Vascular cell adhesion molecule-1 mediates lymphocyte adherence to cytokine-activated cultured human endothelial cells. *Blood*, *76*(5), 965–70.

Carmeliet, P., & Tessier-Lavigne, M. (2005). Common mechanisms of nerve and blood vessel wiring. *Nature*, *436*(7048), 193–200.

Carmichael, S. T., Vespa, P. M., Saver, J. L., Coppola, G., Geschwind, D. H., Starkman, S.,

… Martin, N. a. (2008). Genomic profiles of damage and protection in human intracerebral hemorrhage. *Journal of Cerebral Blood Flow and Metabolism*, *28*(11), 1860–75.

Chang, S. D., Marcellus, M. L., Marks, M. P., Levy, R. P., Do, H. M., & Steinberg, G. K. (2007). Multimodality treatment of giant intracranial arteriovenous malformations. *Neurosurgery*, *61*(1 Suppl), 432–42; discussion 442–4.

Chang, T.-C., Shirato, H., Aoyama, H., Ushikoshi, S., Kato, N., Kuroda, S., … Miyasaka, K. (2004). Stereotactic irradiation for intracranial arteriovenous malformation using stereotactic radiosurgery or hypofractionated stereotactic radiotherapy. *International Journal of Radiation Oncology, Biology, Physics*, *60*(3), 861–70.

Chappell, D. C., Varner, S. E., Nerem, R. M., Medford, R. M., & Alexander, R. W. (1998). Oscillatory shear stress stimulates adhesion molecule expression in cultured human endothelium. *Circulation Research*, *82*(5), 532–9.

Chatziioannou, A., Tai, Y. C., Doshi, N., & Cherry, S. R. (2001). Detector development for microPET II: a 1 microl resolution PET scanner for small animal imaging. *Physics in Medicine and Biology*, *46*(11), 2899–910.

Chen, G., Zheng, M., Shu, H., Zhan, S., Wang, H., Zhou, D., … Feng, L. (2012). Macrophage migration inhibitory factor reduces apoptosis in cerebral arteriovenous malformations. *Neuroscience Letters*, *508*(2), 84–88.

Cherry, S. R., & Gambhir, S. S. (2001). Use of positron emission tomography in animal research. *ILAR Journal / National Research Council, Institute of Laboratory Animal Resources*, *42*(3), 219–32.

Chiu, J.-J., Lee, P.-L., Chen, C.-N., Lee, C.-I., Chang, S.-F., Chen, L.-J., … Chien, S. (2004). Shear stress increases ICAM-1 and decreases VCAM-1 and E-selectin expressions induced by tumor necrosis factor-[alpha] in endothelial cells. *Arteriosclerosis, Thrombosis, and Vascular Biology*, *24*(1), 73–9.

Choi, J. H., & Mohr, J. P. (2005). Brain arteriovenous malformations in adults. *The Lancet. Neurology*, *4*(5), 299–308.

Clark, P., Jordan, F., Pearson, C., Walker, I. D., Sattar, N., Ellison, J., & Greer, I. A. (2003). Intercellular adhesion molecule-1 (ICAM-1) expression is upregulated by thrombin in human monocytes and THP-1 cells in vitro and in pregnant subjects in vivo. *Thrombosis and Haemostasis*, *89*(6), 1043–51.

Colombo, F., Pozza, F., Chierego, G., Casentini, L., De Luca, G., & Francescon, P. (1994). Linear accelerator radiosurgery of cerebral arteriovenous malformations: an update. *Neurosurgery*, *34*(1), 14–20; discussion 20–1.

Corre, I., Guillonneau, M., & Paris, F. (2013). Membrane signaling induced by high doses of ionizing radiation in the endothelial compartment. Relevance in radiation toxicity. *International Journal of Molecular Sciences*, *14*(11), 22678–96.

Crawford, P. M., West, C. R., Chadwick, D. W., & Shaw, M. D. (1986). Arteriovenous malformations of the brain: natural history in unoperated patients. *Journal of Neurology, Neurosurgery, and Psychiatry*, *49*(1), 1–10.

Crone, C., & Olesen, S. P. (1982). Electrical resistance of brain microvascular endothelium. *Brain Research*, *241*(1), 49–55.

Cybulsky, M. I., Fries, J. W., Williams, A. J., Sultan, P., Eddy, R., Byers, M., … Collins, T. (1991). Gene structure, chromosomal location, and basis for alternative mRNA splicing of the human VCAM1 gene. *Proceedings of the National Academy of Sciences of the United States of America*, *88*(17), 7859–63.

Cybulsky, M. I., & Gimbrone, M. A. (1991). Endothelial expression of a mononuclear leukocyte adhesion molecule during atherogenesis. *Science*, *251*(4995), 788–791.

Da Costa, L., Wallace, M. C., Ter Brugge, K. G., O'Kelly, C., Willinsky, R. a., & Tymianski, M. (2009). The natural history and predictive features of hemorrhage from brain arteriovenous malformations. *Stroke*, *40*(1), 100–105.

Daleke, D. L. (2003). Regulation of transbilayer plasma membrane phospholipid asymmetry. *Journal of Lipid Research*, *44*(2), 233–42.

Darland, D. C., & D'Amore, P. A. (1999). Blood vessel maturation: vascular development comes of age. *The Journal of Clinical Investigation*, *103*(2), 157–8.

Dawson, R. C., Tarr, R. W., Hecht, S. T., Jungreis, C. A., Lunsford, L. D., Coffey, R., & Horton, J. A. (1990). Treatment of arteriovenous malformations of the brain with combined embolization and stereotactic radiosurgery: results after 1 and 2 years. *American Journal of Neuroradiology*, *11*(5), 857–64.

del Zoppo, G. J. (2006). Stroke and neurovascular protection. *The New England Journal of Medicine*, *354*(6), 553–555.

Demo, S. D., Masuda, E., Rossi, a B., Throndset, B. T., Gerard, a L., Chan, E. H., … Fisher, J. M. (1999). Quantitative measurement of mast cell degranulation using a novel flow cytometric annexin-V binding assay. *Cytometry*, *36*(4), 340–8.

Denekamp, J. (1982). Endothelial cell proliferation as a novel approach to targeting tumour therapy. *British Journal of Cancer*, *45*(1), 136–9.

Denekamp, J. (1990). Vascular attack as a therapeutic strategy for cancer. *Cancer Metastasis Reviews*, *9*(3), 267–82.

Denekamp, J. (1993). Review article: angiogenesis, neovascular proliferation and vascular pathophysiology as targets for cancer therapy. *The British Journal of Radiology*, *66*(783), 181–96.

Deruty, R., Pelissou-Guyotat, I., Mottolese, C., Bascoulergue, Y., & Amat, D. (1993). The combined management of cerebral arteriovenous malformations. Experience with 100 cases and review of the literature. *Acta Neurochirurgica*, *123*(3-4), 101–12.

Diamond, M. S., & Springer, T. A. (1993). A subpopulation of Mac-1 (CD11b/CD18) molecules mediates neutrophil adhesion to ICAM-1 and fibrinogen. *The Journal of Cell Biology*, *120*(2), 545–56.

Digumarti, R., Suresh, A. V, Bhattacharyya, G. S., Dasappa, L., & Shan, J. (2010). Phase II study of bavituximab plus paclitaxel and carboplatin in untreated locally advanced or metastatic non-small cell lung cancer: Interim results. | 2010 ASCO Annual Meeting | Abstracts | Meeting Library. *Journal of Clinical Oncology*, *28 (15s)*.

Dillon, S. R., Mancini, M., Rosen, A., & Schlissel, M. S. (2000). Annexin V Binds to Viable B Cells and Colocalizes with a Marker of Lipid Rafts upon B Cell Receptor Activation. *The Journal of Immunology*, *164*(3), 1322–1332.

Dobrina, A., Menegazzi, R., Carlos, T. M., Nardon, E., Cramer, R., Zacchi, T., … Patriarca, P. (1991). Mechanisms of eosinophil adherence to cultured vascular endothelial cells. Eosinophils bind to the cytokine-induced ligand vascular cell adhesion molecule-1 via the very late activation antigen-4 integrin receptor. *The Journal of Clinical Investigation*, *88*(1), 20–6.

Dufort, S., Sancey, L., Wenk, C., Josserand, V., & Coll, J. L. (2010). Optical small animal imaging in the drug discovery process. *Biochimica et Biophysica Acta*, *1798*(12), 2266–73.

Duong, D. H., Young, W. L., Vang, M. C., Sciacca, R. R., Mast, H., Koennecke, H.-C., … Pile-Spellman, J. (1998). Feeding Artery Pressure and Venous Drainage Pattern Are Primary Determinants of Hemorrhage From Cerebral Arteriovenous Malformations. *Stroke*, *29*(6), 1167–1176.

Dustin, M. L., Rothlein, R., Bhan, A. K., Dinarello, C. A., & Springer, T. A. (1986). Induction by IL 1 and interferon-γ: tissue distribution, biochemistry, and function of a natural adherence molecule (ICAM-1). *The Journal of Immunology*, *137*(1).

Dustin, M. L., & Springer, T. A. (1988). Lymphocyte function-associated antigen-1 (LFA-1) interaction with intercellular adhesion molecule-1 (ICAM-1) is one of at least three mechanisms for lymphocyte adhesion to cultured endothelial cells. *The Journal of Cell Biology*, *107*(1), 321–31.

Dustin, M. L., Staunton, D. E., & Springer, T. A. (1988). Supergene families meet in the immune system. *Immunology Today*, *9*(7-8), 213–5.

Eijnde, S. M. Van Den, Hoff, M. J. B. Van Den, Reutelingsperger, C. P. M., Heerde, W. L. Van, Henfling, M. E. R., Vermeij-keers, C., … Ramaekers, F. C. S. (2001). Transient expression of phosphatidylserine at cell-cell contact areas is required for myotube formation. *Journal of Cell Science*, *114*(Pt 20), 3631–42.

Elkind, M., & Whitmore, G. (1967). *The radiobiology of cultured mammalian cells*. New York: Gordon and Breach.

Epperly, M. W., Sikora, C. A., DeFilippi, S. J., Gretton, J. E., Bar-Sagi, D., Archer, H., … Greenberger, J. S. (2002). Pulmonary irradiation-induced expression of VCAM-I and ICAM-I is decreased by manganese superoxide dismutase-plasmid/liposome (MnSOD-PL) gene therapy. *Biology of Blood and Marrow Transplantation*, *8*(4), 175–87.

Eriksson, D., & Stigbrand, T. (2010). Radiation-induced cell death mechanisms. *Tumor Biology*, *31*(4), 363–372.

Ernst, E., Matrai, A., & Paulsen, F. (1987). Leukocyte rheology in recent stroke. *Stroke*, *18*(1), 59–62.

Etienne, S., Adamson, P., Greenwood, J., Strosberg, A. D., Cazaubon, S., & Couraud, P. O. (1998). ICAM-1 signaling pathways associated with Rho activation in microvascular brain endothelial cells. *Journal of Immunology*, *161*(10), 5755–61.

Etingin, O. R., Silverstein, R. L., & Hajjar, D. P. (1991). Identification of a monocyte receptor on herpesvirus-infected endothelial cells. *Proceedings of the National Academy of Sciences of the United States of America*, *88*(16), 7200–3.

Fadok, V. a, Voelker, D. R., Campbell, P. a, Cohen, J. J., Bratton, D. L., & Henson, P. M. (1992). Exposure of phosphatidylserine on the surface of apoptotic lymphocytes triggers specific recognition and removal by macrophages. *Journal of Immunology*, *148*(7),

2207–16.

Fajardo, L. (1998). The endothelial cell is a unique target of radiation: an overview. In D. B. Rubin (Ed.), *The radiation biology of the vascular endothelium.* (pp. 1–12). CRC Press, Boca Raton.

Fajardo, L. F. (1989). The complexity of endothelial cells. A review. *American Journal of Clinical Pathology*, *92*(2), 241–50.

Fajardo, L. F., & Berthrong, M. (1988). Vascular lesions following radiation. *Pathology Annual*, *23 Pt 1*, 297–330.

Fareh, J., Martel, R., Kermani, P., & Leclerc, G. (1999). Cellular effects of beta-particle delivery on vascular smooth muscle cells and endothelial cells: a dose-response study. *Circulation*, *99*(11), 1477–1484.

Farhood, A., McGuire, G. M., Manning, A. M., Miyasaka, M., Smith, C. W., & Jaeschke, H. (1995). Intercellular adhesion molecule 1 (ICAM-1) expression and its role in neutrophil-induced ischemia-reperfusion injury in rat liver. *Journal of Leukocyte Biology*, *57*(3), 368–74.

Ferch, R. D., & Morgan, M. K. (2002). High-grade arteriovenous malformations andtheir management. *Journal of Clinical Neuroscience*, *9*(1), 37–40.

Fischer, K., Voelkl, S., Berger, J., Andreesen, R., Pomorski, T., & Mackensen, A. (2006). Antigen recognition induces phosphatidylserine exposure on the cell surface of human CD8+ T cells. *Blood*, *108*(13), 4094–101.

Fisher, M. (2008). Injuries to the vascular endothelium: vascular wall and endothelial dysfunction. *Reviews in Neurological Diseases*, *5 Suppl 1*, S4–11.

Fleetwood, I. G., & Steinberg, G. K. (2002). Arteriovenous malformations. *Lancet*, *359*(9309), 863–73.

Flickinger, J. C., Kondziolka, D., Lunsford, L. D., Kassam, A., Phuong, L. K., Liscak, R., & Pollock, B. (2000). Development of a model to predict permanent symptomatic postradiosurgery injury for arteriovenous malformation patients. Arteriovenous Malformation Radiosurgery Study Group. *International Journal of Radiation Oncology, Biology, Physics*, *46*(5), 1143–8.

Flickinger, J. C., Kondziolka, D., Lunsford, L. D., Pollock, B. E., Yamamoto, M., Gorman, D. A., … Liscak, R. (1999). A multi-institutional analysis of complication outcomes after arteriovenous malformation radiosurgery. *International Journal of Radiation Oncology, Biology, Physics*, *44*(1), 67–74.

Flickinger, J. C., Kondziolka, D., Maitz, A. H., & Dade Lunsford, L. (2002). An analysis of the dose–response for arteriovenous malformation radiosurgery and other factors affecting obliteration. *Radiotherapy and Oncology*, *63*(3), 347–354.

Flickinger, J. C., Kondziolka, D., Maitz, A. H., & Lunsford, L. D. (1998). Analysis of neurological sequelae from radiosurgery of arteriovenous malformations: how location affects outcome. *International Journal of Radiation Oncology, Biology, Physics*, *40*(2), 273–8.

Flickinger, J. C., Kondziolka, D., Pollock, B. E., Maitz, A. H., & Lunsford, L. D. (1997). Complications from arteriovenous malformation radiosurgery: multivariate analysis and risk modeling. *International Journal of Radiation Oncology, Biology, Physics*, *38*(3),
169

485–90.

Flickinger, J. C., Lunsford, L. D., Kondziolka, D., Maitz, A. H., Epstein, A. H., Simons, S. R., & Wu, A. (1992). Radiosurgery and brain tolerance: an analysis of neurodiagnostic imaging changes after gamma knife radiosurgery for arteriovenous malformations. *International Journal of Radiation Oncology, Biology, Physics*, *23*(1), 19–26.

Fournier, D., Terbrugge, K., Rodesch, G., & Lasjaunias, P. (1990). Revascularization of brain arteriovenous malformations after embolization with brucrylate. *Neuroradiology*, *32*(6), 497–501.

Frenette, P. S., Johnson, R. C., Hynes, R. O., & Wagner, D. D. (1995). Platelets roll on stimulated endothelium in vivo: an interaction mediated by endothelial P-selectin. *Proceedings of the National Academy of Sciences of the United States of America*, *92*(16), 7450–4.

Friedlander, R. M. (2007). Arteriovenous Malformations of the Brain. *The New England Journal of Medicine*, *356*(26), 2704–2712.

Friedman, M., Ryan, U. S., Davenport, W. C., Chaney, E. L., Strickland, D. L., & Kwock, L. (1986). Reversible alterations in cultured pulmonary artery endothelial cell monolayer morphology and albumin permeability induced by ionizing radiation. *Journal of Cellular Physiology*, *129*(2), 237–49.

Friedman, W. A., Bova, F. J., Bollampally, S., & Bradshaw, P. (2003). Analysis of factors predictive of success or complications in arteriovenous malformation radiosurgery. *Neurosurgery*, *52*(2), 296–307; discussion 307–8.

Friedman, W. A., Bova, F. J., & Mendenhall, W. M. (1995). Linear accelerator radiosurgery for arteriovenous malformations: the relationship of size to outcome. *Journal of Neurosurgery*, *82*, 180–189.

Gaber, M. W., Yuan, H., Killmar, J. T., Naimark, M. D., Kiani, M. F., & Merchant, T. E. (2004). An intravital microscopy study of radiation-induced changes in permeability and leukocyte-endothelial cell interactions in the microvessels of the rat pia mater and cremaster muscle. *Brain Research. Brain Research Protocols*, *13*(1), 1–10.

Gabryś, D., Greco, O., Patel, G., Prise, K. M., Tozer, G. M., & Kanthou, C. (2007). Radiation effects on the cytoskeleton of endothelial cells and endothelial monolayer permeability. *International Journal of Radiation Oncology, Biology, Physics*, *69*(5), 1553–62.

Gagne, J., Giguere, C., Tocco, G., Ohayon, M., Thompson, R. F., Baudry, M., & Massicotte, G. (1996). Effect of phosphatidylserine on the binding properties of glutamate receptors in brain sections from adult and neonatal rats. *Brain Research*, *740*(1-2), 337–345.

Gahmberg, C. G., Valmu, L., Kotovuori, A., Kotovuori, P., Hilden, T. J., Fagerholm, S., … Tian, L. (1999). Leukocyte adhesion--an integrated molecular process at the leukocyte plasma membrane. *Bioscience Reports*, *19*(4), 273–81.

Gambhir, S. S. (2002). Molecular imaging of cancer with positron emission tomography. *Nature Reviews. Cancer*, *2*(9), 683–93.

Gaugler, M. H., Squiban, C., Claraz, M., Schweitzer, K., Weksler, B., Gourmelon, P., & Van der Meeren, a. (1998). Characterization of the response of human bone marrow endothelial cells to in vitro irradiation. *British Journal of Haematology*, *103*(4), 980–989.

Gaugler, M. H., Squiban, C., van der Meeren, A., Bertho, J. M., Vandamme, M., & Mouthon, M. A. (1997). Late and persistent up-regulation of intercellular adhesion molecule-1 (ICAM-1) expression by ionizing radiation in human endothelial cells in vitro. *International Journal of Radiation Biology*, *72*(2), 201–9.

Gaugler, M.-H. (2005). A unifying system: does the vascular endothelium have a role to play in multi-organ failure following radiation exposure? *The British Journal of Radiology*, *27*(1), 100–105.

Geng, J. G., Bevilacqua, M. P., Moore, K. L., McIntyre, T. M., Prescott, S. M., Kim, J. M., … McEver, R. P. (1990). Rapid neutrophil adhesion to activated endothelium mediated by GMP-140. *Nature*, *343*(6260), 757–60.

Gerber, H. P., Senter, P. D., & Grewal, I. S. (2009). Antibody drug-conjugates targeting the tumor vasculature Current and future developments. *mAbs*, *1*(3), 247–253.

Ghosh, S., Quest, A. F. G., Mabrouks, G. M., Strum, J. C., & Bell, R. M. (1994). The Cysteine-rich Region of Raf-1 Kinase Contains Zinc , Is Adjacent to a Segment Translocates to Liposomes , and That Binds GTP-Ras. *The Journal of Biological Chemistry*, *269*(2), 10000–10007.

Gobin, Y. P., Laurent, A., Merienne, L., Schlienger, M., Aymard, A., Houdart, E., … Merland, J. J. (1996). Treatment of brain arteriovenous malformations by embolization and radiosurgery. *Journal of Neurosurgery*, *85*(1), 19–28.

Goelz, S. E., Hession, C., Goff, D., Griffiths, B., Tizard, R., Newman, B., … Lobb, R. (1990). ELFT : A Gene That Directs the Expression of an ELAM-1 Ligand. *Cell*, *63*(6), 1349–1356.

Gompels, L. L., Lim, N. H., Vincent, T., & Paleolog, E. M. (2010). In vivo optical imaging in arthritis--an enlightening future? *Rheumatology*, *49*(8), 1436–46.

Gompels, L. L., Madden, L., Lim, N. H., Inglis, J. J., McConnell, E., Vincent, T. L., … Paleolog, E. M. (2011). In vivo fluorescence imaging of E-selectin: quantitative detection of endothelial activation in a mouse model of arthritis. *Arthritis and Rheumatism*, *63*(1), 107–17.

Gonzalez, F., Bristol, R., Porter, R., & Spetzler, R. (2005). De novo presentation of an arteriovenous malformation. *Journal of Neurosurgery*, *102*(4), 726–729.

Gorgoulis, V. G., Pratsinis, H., Zacharatos, P., Demoliou, C., Sigala, F., Asimacopoulos, P. J., … Kletsas, D. (2005). p53-Dependent ICAM-1 overexpression in senescent human cells identified in atherosclerotic lesions. *Laboratory Investigation*, *85*(4), 502–511.

Graber, N., Gopal, T. V., Wilson, D., Beall, L. D., & Polte, T. O. M. (1990). T cells bind to cytokine-activated endothelial cells via a novel, inducible sialoglycoprotein and endothelial leukocyte adhesion molecule-1. *The Journal of Immunology*, *145*(3).

Graf, C. J., Perret, G. E., & Torner, J. C. (1983). Bleeding from cerebral arteriovenous malformations as part of their natural history. *Journal of Neurosurgery*, *58*(3), 331–7.

Graham, M., & Peterson, L. (1998). Functional measures of endothelial integrity and pharmacologic modifications of radiation injury. In D. B. Rubin (Ed.), *The radiation biology of the vascular endothelium.* (pp. 39–64). CRC Press, Boca Raton.

Granger, D. N., & Kubes, P. (1994). The microcirculation and inflammation: modulation of leukocyte-endothelial cell adhesion. *Journal of Leukocyte Biology*, *55*(5), 662–75.

Gross, B. a, & Du, R. (2013). Natural history of cerebral arteriovenous malformations: a meta-analysis. *Journal of Neurosurgery*, *118*(2), 437–43.

Grosse, J., Grimm, D., Westphal, K., Ulbrich, C., Moosbauer, J., Pohl, F., … Schoenberger, J. (2009). Radiolabeled annexin V for imaging apoptosis in radiated human follicular thyroid carcinomas--is an individualized protocol necessary? *Nuclear Medicine and Biology*, *36*(1), 89–98.

Guo, S., Kim, W. J., Lok, J., Lee, S.-R., Besancon, E., Luo, B.-H., … Lo, E. H. (2008). Neuroprotection via matrix-trophic coupling between cerebral endothelial cells and neurons. *Proceedings of the National Academy of Sciences of the United States of America*, *105*(21), 7582–7.

Guo, W. Y., Wikholm, G., Karlsson, B., Lindquist, C., Svendsen, P., & Ericson, K. (1993). Combined embolization and gamma knife radiosurgery for cerebral arteriovenous malformations. *Acta Radiologica*, *34*(6), 600–6.

Haimovitz-Friedman, A., & Fuks, Z. (1998). Signaling in the radiation response of endothelial cells. In D. B. Rubin (Ed.), *The radiation biology of the vascular endothelium.* (pp. 101–127). CRC Press, Boca Raton.

Halim, A. X., Johnston, S. C., Singh, V., McCulloch, C. E., Bennett, J. P., Achrol, A. S., … Young, W. L. (2004). Longitudinal risk of intracranial hemorrhage in patients with arteriovenous malformation of the brain within a defined population. *Stroke*, *35*(7), 1697–702.

Hall, E., & Giaccia, A. (2006). *Radiobiology for the Radiologist*. Philadelphia: Lippincott William & Wilkins.

Hallahan, D., Clark, E. T., Kuchibhotla, J., Gewertz, B. L., & Collins, T. (1995). E-Selectin Gene Induction by Ionizing Radiation Is Independent of Cytokine Induction. *Biochemical and Biophysical Research Communications*, *217*(3), 784–795.

Hallahan, D. E., Chen, A. Y., Teng, M., & Cmelak, A. J. (1999). Drug-radiation interactions in tumor blood vessels. *Oncology*, *13*(10 Suppl 5), 71–7.

Hallahan, D. E., Kuchibhotla, J., & Wyble, C. (1997). Sialyl Lewis X mimetics attenuate E-selectin-mediated adhesion of leukocytes to irradiated human endothelial cells. *Radiation Research*, *147*(1), 41–7.

Hallahan, D. E., & Virudachalam, S. (1997). Ionizing radiation mediates expression of cell adhesion molecules in distinct histological patterns within the lung. *Cancer Research*, *57*(11), 2096–9.

Hallahan, D. E., & Virudachalam, S. (1999). Accumulation of P-selectin in the lumen of irradiated blood vessels. *Radiation Research*, *152*(1), 6–13.

Hallahan, D., Kuchibhotla, J., & Wyble, C. (1996). Cell Adhesion Molecules Mediate Radiation-induced Leukocyte Adhesion to the Vascular Endothelium. *Cancer Research*, *56*(22), 5150–5155.

Hamel, E., Nicolakakis, N., Aboulkassim, T., Ongali, B., & Tong, X.-K. (2008). Oxidative stress and cerebrovascular dysfunction in mouse models of Alzheimer's disease. *Experimental Physiology*, *93*(1), 116–20.

Hamilton, M. G., & Spetzler, R. F. (1994). The prospective application of a grading system for arteriovenous malformations. *Neurosurgery*, *34*(1), 2–6; discussion 6–7.

172

Han, P. P., Ponce, F. a, & Spetzler, R. F. (2003). Intention-to-treat analysis of Spetzler-Martin grades IV and V arteriovenous malformations: natural history and treatment paradigm. *Journal of Neurosurgery*, *98*(1), 3–7.

Handschel, J., Prott, F. J., Sunderkötter, C., Metze, D., Meyer, U., & Joos, U. (1999). Irradiation induces increase of adhesion molecules and accumulation of β2-integrin-expressing cells in humans. *International Journal of Radiation Oncology Biology Physics*, *45*(2), 475–481.

Hanshaw, R. G., & Smith, B. D. (2005). New reagents for phosphatidylserine recognition and detection of apoptosis. *Bioorganic & Medicinal Chemistry*, *13*(17), 5035–42.

Hara, M., Nakamura, M., Shiokawa, Y., Sawa, H., Sato, E., Koyasu, H., & Saito, I. (1998). Delayed cyst formation after radiosurgery for cerebral arteriovenous malformation: two case reports. *Minimally Invasive Neurosurgery : MIN*, *41*(1), 40–5.

Harisinghani, M. G., Barentsz, J., Hahn, P. F., Deserno, W. M., Tabatabaei, S., van de Kaa, C. H., … Weissleder, R. (2003). Noninvasive detection of clinically occult lymph-node metastases in prostate cancer. *The New England Journal of Medicine*, *348*(25), 2491–9.

Hartmann, A., Mast, H., Mohr, J. P., Koennecke, H. C., Osipov, A., Pile-Spellman, J., … Young, W. L. (1998). Morbidity of intracranial hemorrhage in patients with cerebral arteriovenous malformation. *Stroke*, *29*(5), 931–4.

Hartmann, A., Pile-Spellman, J., Stapf, C., Sciacca, R. R., Faulstich, A., Mohr, J. P., … Mast, H. (2002). Risk of Endovascular Treatment of Brain Arteriovenous Malformations. *Stroke*, *33*(7), 1816–1820.

Hashimoto, T., Lam, T., Boudreau, N. J., Bollen, A. W., Lawton, M. T., & Young, W. L. (2001). Abnormal balance in the angiopoietin-tie2 system in human brain arteriovenous malformations. *Circulation Research*, *89*(2), 111–3.

Hashimoto, T., Mesa-Tejada, R., Quick, C. M., Bollen, A., Joshi, S., Pile-spellman, J., … Young, W. L. (2001). Evidence of Increased Endothelial Cell Turnover in Brain Arteriovenous Malformations. *Neurosurgery*, *49*(1), 124–31.

Hattori, R., Hamilton, K. K., Fugate, R. D., McEver, R. P., & Sims, P. J. (1989). Stimulated secretion of endothelial von Willebrand factor is accompanied by rapid redistribution to the cell surface of the intracellular granule membrane protein GMP-140. *The Journal of Biological Chemistry*, *264*(14), 7768–71.

Hatva, E., Jääskeläinen, J., Hirvonen, H., Alitalo, K., & Haltia, M. (1996). Tie endothelial cell-specific receptor tyrosine kinase is upregulated in the vasculature of arteriovenous malformations. *Journal of Neuropathology and Experimental Neurology*, *55*(11), 1124–33.

Haubner, F., Leyh, M., Ohmann, E., Pohl, F., Prantl, L., & Gassner, H. G. (2013). Effects of external radiation in a co-culture model of endothelial cells and adipose-derived stem cells. *Radiation Oncology*, *8*(1), 66.

Haw, C. S., TerBrugge, K., Willinsky, R., & Tomlinson, G. (2006). Complications of embolization of arteriovenous malformations of the brain. *Journal of Neurosurgery*, *104*(2), 226–32.

Hawkins, B. T., & Davis, T. P. (2005). The blood-brain barrier/neurovascular unit in health and disease. *Pharmacological Reviews*, *57*(2), 173–85.

Hawrysz, D. J., & Sevick-Muraca, E. M. (2000). Developments toward diagnostic breast cancer imaging using near-infrared optical measurements and fluorescent contrast agents. *Neoplasia*, *2*(5), 388–417.

Hayashi, S., Watanabe, N., Nakazawa, K., Suzuki, J., Tsushima, K., Tamatani, T., … Isobe, M. (2000). Roles of P-selectin in inflammation, neointimal formation, and vascular remodeling in balloon-injured rat carotid arteries. *Circulation*, *102*(14), 1710–1717.

He, J., Yin, Y., Luster, T. a, Watkins, L., & Thorpe, P. E. (2009). Antiphosphatidylserine antibody combined with irradiation damages tumor blood vessels and induces tumor immunity in a rat model of glioblastoma. *Clinical Cancer Research : An Official Journal of the American Association for Cancer Research*, *15*(22), 6871–80.

He, X., Gao, J., Gambhir, S. S., & Cheng, Z. (2010). Near-infrared fluorescent nanoprobes for cancer molecular imaging: status and challenges. *Trends in Molecular Medicine*, *16*(12), 574–83.

He, X., Wang, K., & Cheng, Z. (2010). In vivo near-infrared fluorescence imaging of cancer with nanoparticle-based probes. *Wiley Interdisciplinary Reviews. Nanomedicine and Nanobiotechnology*, *2*(4), 349–66.

Heckmann, M. (1998). Vascular Activation of Adhesion Molecule mRNA and Cell Surface Expression by Ionizing Radiation. *Experimental Cell Research*, *238*(1), 148–154.

Henkes, H., Nahser, H. C., Berg-Dammer, E., Weber, W., Lange, S., & Kühne, D. (1998). Endovascular therapy of brain AVMs prior to radiosurgery. *Neurological Research*, *20*(6), 479–92.

Henning, E., Dittmann, H., Wiskirchen, J., Bantleon, R., Kehlbach, R., Claussen, C. D., & Duda, S. H. (2004). Dose dependent effects of the combined beta-gamma-emitter 188Rhenium on the growth of human vessel wall cells. *RöFo : Fortschritte Auf Dem Gebiete Der Röntgenstrahlen Und Der Nuklearmedizin*, *176*(3), 404–8.

Hermansson, M., Hokynar, K., & Somerharju, P. (2011). Mechanisms of glycerophospholipid homeostasis in mammalian cells. *Progress in Lipid Research*, *50*(3), 240–57.

Heros, R. C., Korosue, K., & Diebold, P. M. (1990). Surgical excision of cerebral arteriovenous malformations: late results. *Neurosurgery*, *26*(4), 570–7; discussion 577–8.

Herzig, R., Burval, S., Vladyka, V., Janouskova, L., Krivanek, P., Krupka, B., & Vlachova, I. (2000). Familial occurrence of cerebral arteriovenous malformation in sisters : case report and review of the literature. *European Journal of Neurology*, *7*(1), 95–100.

Hirt, U. a, & Leist, M. (2003). Rapid, noninflammatory and PS-dependent phagocytic clearance of necrotic cells. *Cell Death and Differentiation*, *10*(10), 1156–64.

Hladky, J. P., Lejeune, J. P., Blond, S., Pruvo, J. P., & Dhellemmes, P. (1994). Cerebral arteriovenous malformations in children: report on 62 cases. *Child's Nervous System : ChNS*, *10*(5), 328–33.

Hogg, N., Henderson, R., Leitinger, B., McDowall, A., Porter, J., & Stanley, P. (2002). Mechanisms contributing to the activity of integrins on leukocytes. *Immunological Reviews*, *186*, 164–71.

Hopewell, J. (1983). Radiation effects on vascular tissue. In C. Potten & J. Hendry (Eds.), *Cytotoxic Insult to Tissue: Effects on Cell Lineages* (pp. 228–257). Churchill Livingstone, Edinburgh.

Houtteville, J.-P. (1997). Brain Cavernoma: A Dynamic Lesion. *Surgical Neurology*, *48*(6), 610–614.

Hu, P., Yan, J., Sharifi, J., Bai, T., Khawli, L. A., & Epstein, A. L. (2003). Comparison of Three Different Targeted Tissue Factor Fusion Proteins for Inducing Tumor Vessel Thrombosis. *Cancer Research*, *63*(16), 5046–5053.

Igarashi, K., & Miura, M. (2008). Inhibition of a radiation-induced senescence-like phenotype: a possible mechanism for potentially lethal damage repair in vascular endothelial cells. *Radiation Research*, *170*(4), 534–9.

Inoue, H. K. (2006). Long-term results of Gamma Knife surgery for arteriovenous malformations: 10- to 15-year follow up in patients treated with lower doses. *Journal of Neurosurgery*, *105 Suppl*, 64–8.

Inoue, H. K., & Ohye, C. (2002). Hemorrhage risks and obliteration rates of arteriovenous malformations after gamma knife radiosurgery. *Journal of Neurosurgery*, *97*(5 Suppl), 474–6.

Iwama, T., Hayashida, K., Takahashi, J. C., Nagata, I., & Hashimoto, N. (2002). Cerebral hemodynamics and metabolism in patients with cerebral arteriovenous malformations: an evaluation using positron emission tomography scanning. *Journal of Neurosurgery*, *97*(6), 1314–21.

Izawa, M., Chernov, M., Hayashi, M., Iseki, H., Hori, T., & Takakura, K. (2009). Combined management of intracranial arteriovenous malformations with embolization and gamma knife radiosurgery: comparative evaluation of the long-term results. *Surgical Neurology*, *71*(1), 43–52; discussion 52–3.

Jabbour, M. N., Elder, J. B., Samuelson, C. G., Khashabi, S., Hofman, F. M., Giannotta, S. L., & Liu, C. Y. (2009). Aberrant Angiogenic Characteristics of Human Brain Arteriovenous Malformation Endothelial Cells. *Neurosurgery*, *64*(1), 139–148.

Jain, R. K. (2003). Molecular regulation of vessel maturation. *Nature Medicine*, *9*(6), 685–93.

Jain, R. K. (2005). Normalization of tumor vasculature: an emerging concept in antiangiogenic therapy. *Science*, *307*(5706), 58–62.

Jameson, M. B., Thompson, P. I., Baguley, B. C., Evans, B. D., Harvey, V. J., Porter, D. J., … Kestell, P. (2003). Clinical aspects of a phase I trial of 5,6-dimethylxanthenone-4-acetic acid (DMXAA), a novel antivascular agent. *British Journal of Cancer*, *88*(12), 1844–50.

Jayagopal, A., Russ, P. K., & Haselton, F. R. (2007). Surface engineering of quantum dots for in vivo vascular imaging. *Bioconjugate Chemistry*, *18*(5), 1424–1433.

Jayaraman, M. V, Marcellus, M. L., Do, H. M., Chang, S. D., Rosenberg, J. K., Steinberg, G. K., & Marks, M. P. (2007). Hemorrhage rate in patients with Spetzler-Martin grades IV and V arteriovenous malformations: is treatment justified? *Stroke*, *38*(2), 325–9.

Jeffree, R. L., & Stoodley, M. a. (2009). Postnatal development of arteriovenous malformations. *Pediatric Neurosurgery*, *45*(4), 296–304.

Jiang, S., Zhang, Y., Lim, K. M., Sim, E. K. W., & Ye, L. (2009). NIR-to-visible upconversion nanoparticles for fluorescent labeling and targeted delivery of siRNA. *Nanotechnology*, *20*(15), 155101.

Johnson, L. K., Longenecker, J. P., & Fajardo, L. F. (1982). Differential radiation response of

cultured endothelial cells and smooth myocytes. *Analytical and Quantitative Cytology*, *4*(3), 188–98.

Jordan, L. C., & Hillis, A. E. (2007). Hemorrhagic stroke in children. *Pediatric Neurology*, *36*(2), 73–80.

Kadoya, C., Momota, Y., Ikegami, Y., Urasaki, E., Wada, S., & Yokota, A. (1994). Central nervous system arteriovenous malformations with hereditary hemorrhagic telangiectasia: report of a family with three cases. *Surgical Neurology*, *42*(3), 234–9.

Kaido, T., Hoshida, T., Uranishi, R., Akita, N., Akihira, K., Nishi, N., & Sakaki, T. (2001). Radiosurgery-induced brain tumor. *Journal of Neurosurgery*, *95*(4), 710–713.

Kalogeris, T. J., Kevil, C. G., Laroux, F. S., Coe, L. L., Phifer, T. J., Alexander, J. S., … Alexander, S. (1999). Differential monocyte adhesion and adhesion molecule expression in venous and arterial endothelial cells. *The American Journal of Physiology*, *276*(1 Pt 1), 9–19.

Karlsson, B., Lax, I., & Söderman, M. (2001). Risk for hemorrhage during the 2-year latency period following gamma knife radiosurgery for arteriovenous malformations. *International Journal of Radiation Oncology, Biology, Physics*, *49*(4), 1045–51.

Karlsson, B., Lindquist, C., & Steiner, L. (1997). Prediction of obliteration after gamma knife surgery for cerebral arteriovenous malformations. *Neurosurgery*, *40*(3), 425–30; discussion 430–1.

Karlsson, B., Lindqvist, M., Blomgren, H., Wan-Yeo, G., Söderman, M., Lax, I., … Bailes, J. (2005). Long-term results after fractionated radiation therapy for large brain arteriovenous malformations. *Neurosurgery*, *57*(1), 42–9; discussion 42–9.

Karunanyaka, A., Tu, J., Watling, A., Storer, K. P., Windsor, A., & Stoodley, M. A. (2008). Endothelial molecular changes in a rodent model of arteriovenous malformation. *Journal of Neurosurgery*, *109*(6), 1165–72.

Kashba, S. R., Patel, N. J., Grace, M., Lee, V. S., Raoufi-Rad, N., Amal Raj, J. V, … Stoodley, M. (2015). Angiographic, hemodynamic, and histological changes in an animal model of brain arteriovenous malformations treated with Gamma Knife radiosurgery. *Journal of Neurosurgery*, *123*(4), 954–60.

Kennedy, S., McPhaden, A. R., Wadsworth, R. M., & Wainwright, C. L. (2000). Correlation of leukocyte adhesiveness, adhesion molecule expression and leukocyte-induced contraction following balloon angioplasty. *British Journal of Pharmacology*, *130*(1), 95–103.

Kerner, T., Ahlers, O., Reschreiter, H., Bührer, C., Möckel, M., & Gerlach, H. (2001). Adhesion molecules in different treatments of acute myocardial infarction. *Critical Care*, *5*(3), 145–50.

Kerr, D. J., Kaye, S. B., Graham, J., Cassidy, J., Harding, M., Setanoians, A., … Forrest, G. (1986). Phase I and pharmacokinetic study of LM985 (flavone acetic acid ester). *Cancer Research*, *46*(6), 3142–6.

Khan, F. M. (1994). *The physics of radiation therapy*. Baltimore, Williams & Wilkins.

Khan, B. V, Parthasarathy, S. S., Alexander, R. W., & Medford, R. M. (1995). Modified low density lipoprotein and its constituents augment cytokine-activated vascular cell adhesion molecule-1 gene expression in human vascular endothelial cells. *The Journal of*

Clinical Investigation, *95*(3), 1262–70.

Khaw, a V, Mohr, J. P., Sciacca, R. R., Schumacher, H. C., Hartmann, A., Pile-Spellman, J., … Stapf, C. (2004). Association of infratentorial brain arteriovenous malformations with hemorrhage at initial presentation. *Stroke*, *35*(3), 660–3.

Kihlstrom, L., Guo, W., Karlsson, B., Lindquist, C., & Lindquist, M. (1997). Magnetic resonance imaging of obliterated arteriovenous malformations up to 23 years after radiosurgery. *Journal of Neurosurgery*, *86*(4), 589–593.

Kiliç, T., Pamir, M. N., Küllü, S., Eren, F., Ozek, M. M., & Black, P. M. (2000). Expression of structural proteins and angiogenic factors in cerebrovascular anomalies. *Neurosurgery*, *46*(5), 1179–91; discussion 1191–2.

Kirszberg, C., Lima, L. G., Da Silva de Oliveira, A., Pickering, W., Gray, E., Barrowcliffe, T. W., … Monteiro, R. Q. (2009). Simultaneous tissue factor expression and phosphatidylserine exposure account for the highly procoagulant pattern of melanoma cell lines. *Melanoma Research*, *19*(5), 301–8.

Kjellberg RN, Hanamura T, Davis KR, Lyons SL, A. R. (2010). Bragg-peak proton-beam therapy for arteriovenous malformations of the brain. *The New England Journal of Medicine*, *309*(5), 269–274.

Klinger, M. H. (1997). Platelets and inflammation. *Anatomy and Embryology*, *196*(1), 1–11.

Kniesel, U., & Wolburg, H. (2000). Tight junctions of the blood-brain barrier. *Cellular and Molecular Neurobiology*, *20*(1), 57–76.

Koizumi, T., Shiraishi, T., Hagihara, N., Tabuchi, K., Hayashi, T., & Kawano, T. (2002). Expression of vascular endothelial growth factors and their receptors in and around intracranial arteriovenous malformations. *Neurosurgery*, *50*(1), 117–24; discussion 124–6.

Kokura, S., Wolf, R. E., Yoshikawa, T., Granger, D. N., & Aw, T. Y. (2000). T-Lymphocyte-Derived Tumor Necrosis Factor Exacerbates Anoxia-Reoxygenation-Induced Neutrophil-Endothelial Cell Adhesion. *Circulation Research*, *86*(2), 205–213.

Krishnan, A. S., Neves, A. A., de Backer, M. M., Hu, D.-E., Davletov, B., Kettunen, M., & Brindle, K. M. (2008). Detection of cell death in tumors by using MR imaging and a gadolinium-based targeted contrast agent. *Radiology*, *246*(3), 854–62.

Kukielka, G. L., Hawkins, H. K., Michael, L., Manning, A. M., Youker, K., Lane, C., … Anderson, D. C. (1993). Regulation of Intercellular Adhesion Molecule-I (ICAM-1) in Ischemic and Reperfused Canine Myocardium. *Journal of Clinical Investigation*, *92*(3), 1504–1516.

Kunzelmann-Marche, C., Freyssinet, J.-M., & Martínez, M. C. (2002). Loss of plasma membrane phospholipid asymmetry requires raft integrity. Role of transient receptor potential channels and ERK pathway. *The Journal of Biological Chemistry*, *277*(22), 19876–81.

Kwock, L., Blackstock, A., & Friedman, M. (1998). Effect of ionizing radiation on endothelial cell plasma membrane processes. In D. B. Rubin (Ed.), *The radiation biology of the vascular endothelium.* (pp. 129–145). CRC Press, Boca Raton.

Laakso, A., & Hernesniemi, J. (2012). Arteriovenous malformations: epidemiology and clinical presentation. *Neurosurgery Clinics of North America*, *23*(1), 1–6.

Labatts, S., Tumor, B., England, N., Knife, G., Hospital, R. I., & Island, R. (2001). Glioblastoma multiforme occurring in a patient treated with gamma knife surgery. *Journal of Neurosurgery*, *94*(5), 816–821.

Languino, L. R., Duperray, A., Joganic, K. J., Fornaro, M., Thornton, G. B., & Altieri, D. C. (1995). Regulation of leukocyte-endothelium interaction and leukocyte transendothelial migration by intercellular adhesion molecule 1-fibrinogen recognition. *Proceedings of the National Academy of Sciences of the United States of America*, *92*(5), 1505–9.

Larsen, E., Celi, A., Gilbert, G. E., Furie, B. C., Erban, J. K., Bonfanti, R., … Furie, B. (1989). PADGEM protein: a receptor that mediates the interaction of activated platelets with neutrophils and monocytes. *Cell*, *59*(2), 305–12.

Lasjaunias, P. (1996). *Vascular Diseases in Neonates, Infants, and Children: Interventional Neuroradiology Management*. Berlin: Springer-Verlag.

Lasky, L. A. (1991). Lectin Cell Adhesion Molecules (LEC-CAMs): A New family of Cell Adhesion Proteins Involved with Inflammation. *Journal of Cellular Biochemistry*, *146*(1991), 139–146.

Lasky, L. A. (1992). Selectins: interpreters of cell-specific carbohydrate information during inflammation. *Science*, *258*(5084), 964–9.

Latchaw, R. E., Hu, X., Ugurbil, K., Hall, W. A., Madison, M. T., & Heros, R. C. (1995). Functional magnetic resonance imaging as a management tool for cerebral arteriovenous malformations. *Neurosurgery*, *37*(4), 619–25; discussion 625–6.

Lawrence, M. B., Kansas, G. S., Kunkel, E. J., & Ley, K. (1997). Threshold levels of fluid shear promote leukocyte adhesion through selectins (CD62L,P,E). *The Journal of Cell Biology*, *136*(3), 717–27.

Lawrence, M., & Springer, T. (1991). Leukocytes Roll on a Selectin at Physiologic Flow Rates : Distinction from and Prerequisite for Adhesion through Integrins. *Cell*, *65*(5), 859–873.

Lederle, W., Arns, S., Rix, A., Gremse, F., Doleschel, D., Schmaljohann, J., … Palmowski, M. (2011). Failure of annexin-based apoptosis imaging in the assessment of antiangiogenic therapy effects. *EJNMMI Research*, *1*(1), 26.

Ledezma, C. J., Hoh, B. L., Carter, B. S., Pryor, J. C., Putman, C. M., & Ogilvy, C. S. (2006). Complications of cerebral arteriovenous malformation embolization: multivariate analysis of predictive factors. *Neurosurgery*, *58*(4), 602–11; discussion 602–11.

Leksell, L. (1951). The stereotaxic method and radiosurgery of the brain. *Acta Chirurgica Scandinavica*, *102*(4), 316–9.

Ley, K. (2001). Functions of selectins. *Results and Problems in Cell Differentiation*, *33*, 177–200.

Li, L., Story, M., & Legerski, R. J. (2001). Cellular responses to ionizing radiation damage. *International Journal of Radiation Oncology, Biology, Physics*, *49*(4), 1157–1162.

Li, M. O., Sarkisian, M. R., Mehal, W. Z., Rakic, P., & Flavell, R. a. (2003). Phosphatidylserine receptor is required for clearance of apoptotic cells. *Science*, *302*(5650), 1560–3.

Liang, H., Yang, Y., Yang, K., Wu, Y., Boone, J. M., & Cherry, S. R. (2007). A microPET/CT system for in vivo small animal imaging. *Physics in Medicine and*

Biology, *52*(13), 3881–94.

Lim, M., Cheshier, S., & Steinberg, G. K. (2006). New vessel formation in the central nervous system during tumor growth, vascular malformations, and Moyamoya. *Current Neurovascular Research*, *3*(3), 237–45.

Liu, H., Ren, G., Miao, Z., Zhang, X., Tang, X., Han, P., … Cheng, Z. (2010). Molecular optical imaging with radioactive probes. *PloS One*, *5*(3), e9470.

Livak, K. J., & Schmittgen, T. D. (2001). Analysis of relative gene expression data using real-time quantitative PCR and the 2-ΔΔCT method. *Methods*, *25*(4), 402–408.

Lunsford, L. D., Niranjan, A., Kondziolka, D., Sirin, S., & Flickinger, J. C. (2008). Arteriovenous malformation radiosurgery: a twenty year perspective. *Clinical Neurosurgery*, *55*, 108–19.

Luo, J., Paranya, G., & Bischoff, J. (1999). Noninflammatory expression of E-selectin is regulated by cell growth. *Blood*, *93*(11), 3785–91.

Luster, T. a, He, J., Huang, X., Maiti, S. N., Schroit, A. J., de Groot, P. G., & Thorpe, P. E. (2006). Plasma protein beta-2-glycoprotein 1 mediates interaction between the anti-tumor monoclonal antibody 3G4 and anionic phospholipids on endothelial cells. *The Journal of Biological Chemistry*, *281*(40), 29863–71.

Lutz, W., Winston, K. R., & Maleki, N. (1988). A system for stereotactic radiosurgery with a linear accelerator. *International Journal of Radiation Oncology, Biology, Physics*, *14*(2), 373–81.

Maciunas, R. J. (1996). Stereotactic Radiosurgery. *Nature Medicine*, *2*, 712–713.

Major et al. (2002). Effect of a single high-dose gamma irradiation on cultured cells in human cerebral arteriovenous malformation, *97*(Suppl 5), 459–463.

Mandybur, T. I., & Nazek, M. (1990). Cerebral arteriovenous malformations. A detailed morphological and immunohistochemical study using actin. *Archives of Pathology & Laboratory Medicine*, *114*(9), 970–3.

Mansmann, U., Meisel, J., Brock, M., Rodesch, G., Alvarez, H., & Lasjaunias, P. (2000). Factors associated with intracranial hemorrhage in cases of cerebral arteriovenous malformation. *Neurosurgery*, *46*(2), 272–9; discussion 279–81.

Martens, C. L., Cwirla, S. E., Lee, R. Y.-W., Whitehorn, E., Chen, E. Y.-F., Bakker, A., … Barrett, R. W. (1995). Peptides Which Bind to E-selectin and Block Neutrophil Adhesion. *Journal of Biological Chemistry*, *270*(36), 21129–21136.

Martin, S., Gregoire, I., Poncet, P., David, B., Arock, M., & Blank, U. (2000). Immunologic Stimulation of Mast Cells Leads to the Reversible Exposure of Phosphatidylserine in the Absence of Apoptosis. *International Archives of Allergy and Immunology*, *123*(3), 249–258.

Maruyama, K., Kawahara, N., Shin, M., Tago, M., Kishimoto, J., Kurita, H., … Kirino, T. (2005). The risk of hemorrhage after radiosurgery for cerebral arteriovenous malformations. *The New England Journal of Medicine*, *352*(2), 146–53.

Massoud, T. F., & Gambhir, S. S. (2003). Molecular imaging in living subjects: seeing fundamental biological processes in a new light. *Genes & Development*, *17*(5), 545–80.

Mast, H., Young, W. L., Koennecke, H. C., Sciacca, R. R., Osipov, A., Pile-Spellman, J., …

Mohr, J. P. (1997). Risk of spontaneous haemorrhage after diagnosis of cerebral arteriovenous malformation. *Lancet*, *350*(9084), 1065–8.

Mathis, J. A., Barr, J. D., Horton, J. A., Jungreis, C. A., Lunsford, L. D., Kondziolka, D. S., … Pentheny, S. (1995). The efficacy of particulate embolization combined with stereotactic radiosurgery for treatment of large arteriovenous malformations of the brain. *AJNR. American Journal of Neuroradiology*, *16*(2), 299–306.

McCormick, P., & Schochet, S. (1976). *Atlas of cerebrovascular disease*. Philadelphia: WB Saunders.

McCourt, P. A., Ek, B., Forsberg, N., & Gustafson, S. (1994). Intercellular adhesion molecule-1 is a cell surface receptor for hyaluronan. *The Journal of Biological Chemistry*, *269*(48), 30081–4.

McEver, R. P. (1997). Selectin-carbohydrate interactions during inflammation and metastasis. *Glycoconjugate Journal*, *14*(5), 585–91.

McLarty, K., & Reilly, R. M. (2007). Molecular imaging as a tool for personalized and targeted anticancer therapy. *Clinical Pharmacology and Therapeutics*, *81*(3), 420–4.

Meder, J., Nataf, F., Delvat, D., Ghossoub, M., Trystram, D., Nagi, S., … Frédy, D. (1998). Radioanatomie des malformations artérioveineuses cérébrales - EM|consulte. *Cancer Radiotherapy*, *2*(2), 173–179.

Milliat, F., François, A., Tamarat, R., & Benderitter, M. (2008). [Role of endothelium in radiation-induced normal tissue damages]. *Annales de Cardiologie et D'angéiologie*, *57*(3), 139–48.

Min, J.-K., Kim, Y.-M., Kim, S. W., Kwon, M.-C., Kong, Y.-Y., Hwang, I. K., … Kwon, Y.-G. (2005). TNF-Related Activation-Induced Cytokine Enhances Leukocyte Adhesiveness: Induction of ICAM-1 and VCAM-1 via TNF Receptor-Associated Factor and Protein Kinase C-Dependent NF- B Activation in Endothelial Cells. *The Journal of Immunology*, *175*(1), 531–540.

Miyachi, S., Negoro, M., Okamoto, T., Kobayashi, T., Kida, Y., Tanaka, T., & Yoshida, J. (2000). Embolisation of cerebral arteriovenous malformations to assure successful subsequent radiosurgery. *Journal of Clinical Neuroscience : Official Journal of the Neurosurgical Society of Australasia*, *7 Suppl 1*, 82–5.

Miyake, K., Medina, K., Ishihara, K., Kimoto, M., Auerbach, R., & Kincade, P. W. (1991). A VCAM-like adhesion molecule on murine bone marrow stromal cells mediates binding of lymphocyte precursors in culture. *The Journal of Cell Biology*, *114*(3), 557–65.

Miyawaki, L., Dowd, C., Wara, W., Goldsmith, B., Albright, N., Gutin, P., … Larson, D. (1999). Five year results of LINAC radiosurgery for arteriovenous malformations: outcome for large AVMS. *International Journal of Radiation Oncology, Biology, Physics*, *44*(5), 1089–106.

Moftakhar, P., Hauptman, J. S., Malkasian, D., & Martin, N. a. (2009). Cerebral arteriovenous malformations. Part 1: cellular and molecular biology. *Neurosurgical Focus*, *26*(5), 1–15.

Mohr, J. (1999). The Arteriovenous Malformation Study Group: Arteriovenous malformations of the brain in adults. *The New England Journal of Medicine*, (340), 1812–1818.

Mohr, J., Stein, B., & Pile-Spellman, J. (1998). Arteriovenous malformation. In *Barnett, J. Mohr, J. Stein, B. Yatsu, F. eds. Stroke. Pathophysiology, diagnosis, and management* (3rd ed., pp. 725–50). Philadelphia: Churchill Livingstone.

Mollà, M., Gironella, M., Miquel, R., Tovar, V., Engel, P., Biete, A., … Panés, J. (2003). Relative roles of ICAM-1 and VCAM-1 in the pathogenesis of experimental radiation-induced intestinal inflammation. *International Journal of Radiation Oncology, Biology, Physics*, *57*(1), 264–73.

Molla, M., Gironella, M., Salas, A., Miquel, R., Perez-del-Pulgar, S., Conill, C., … Panes, J. (2001). Role of P-selectin in radiation-induced intestinal inflammatory damage. *International Journal of Cancer*, *96*(2), 99–109.

Molla, M., Panes, J., Casadevall, M., Salas, A., Conill, C., Biete, A., … Pique, J. M. (1999). Influence of dose-rate on inflammatory damage and adhesion molecule expression after abdominal radiation in the rat. *International Journal of Radiation Oncology, Biology, Physics*, *45*(4), 1011–8.

Montgomery, K. F., Osbornt, L., Hessiont, C., Tizardt, R., Gofft, D., Vassallot, C., … Pohlman, T. H. (1991). Activation of endothelial-leukocyte adhesion molecule 1 (ELAM-1) gene transcription. *Proceedings of the National Academy of Sciences of the United States of America*, *88*(15), 6523–6527.

Mozzi, R., Buratta, S., & Goracci, G. (2003). Metabolism and Functions of Phosphatidylserine in Mammalian Brain. *Neurochemical Research*, *28*(2), 195–214.

Mullan, S., Mojtahedi, S., Johnson, D. L., & Macdonald, R. L. (1996). Embryological basis of some aspects of cerebral vascular fistulas and malformations. *Journal of Neurosurgery*, *85*(1), 1–8.

Müller, K., Köhn, F.-M., Port, M., Abend, M., Molls, M., Ring, J., … Abend. (2006). Intercellular adhesion molecule-1 : a consistent inflamma- tory marker of the cutaneous radiation reaction both in vitro and in vivo. *British Journal of Dermatology*, *155*(4), 670–679.

Murray, J. (1998). Inflammatory cytokines, radiation and endothelial gene products: a common role for reactive oxygen intermediates. In D. B. Rubin (Ed.), *The radiation biology of the vascular endothelium.* (pp. 147–160). CRC Press, Boca Raton.

Nagel, T., Resnick, N., Atkinson, W. J., Dewey, C. F., & Gimbrone, M. A. (1994). Shear stress selectively upregulates intercellular adhesion molecule-1 expression in cultured human vascular endothelial cells. *The Journal of Clinical Investigation*, *94*(2), 885–91.

Nelson, M. D., Gonzalez-Gomez, I., & Gilles, F. H. (1991). Dyke Award. The search for human telencephalic ventriculofugal arteries. *American Journal of Neuroradiology*, *12*(2), 215–22.

Nelson, R. M., & Bevilacqua, M. P. (1993). Selectins. *Journal of Clinical Investigation*, *91*(41), 379–387.

Nelson, R. M., Venot, A., & Linhardt, R. M. (1995). Carbohydrate-Protein Interactions in Vascular Biology. *Annual Review of Cell and Developmental Biology*, *11*(1), 601–631.

Neri, D., & Bicknell, R. (2005). Tumour vascular targeting. *Nature Reviews. Cancer*, *5*(6), 436–46.

Nihei, Y., Suzuki, M., Okano, A., Tsuji, T., Akiyama, Y., Tsuruo, T., … Sato, Y. (1999).

Evaluation of antivascular and antimitotic effects of tubulin binding agents in solid tumor therapy. *Japanese journal of cancer research*, *90*(12), 1387–95.

Nomura, S., Tandon, N. N., Nakamura, T., Cone, J., Fukuhara, S., & Kambayashi, J. (2001). High-shear-stress-induced activation of platelets and microparticles enhances expression of cell adhesion molecules in THP-1 and endothelial cells. *Atherosclerosis*, *158*(2), 277–87.

O'Connor, M. M., & Mayberg, M. R. (2000). Effects of radiation on cerebral vasculature: a review. *Neurosurgery*, *46*(1), 138–49; discussion 150–1.

O'Neil, E. J., & Smith, B. D. (2006). Anion recognition using dimetallic coordination complexes. *Coordination Chemistry Reviews*, *250*(23-24), 3068–3080.

Ogilvy, C. S. (1990). Radiation therapy for arteriovenous malformations: a review. *Neurosurgery*, *26*(5), 725–35.

Ogilvy, C. S., Stieg, P. E., Awad, I., Brown, R. D., Kondziolka, D., Rosenwasser, R., … Hademenos, G. (2001). Recommendations for the Management of Intracranial Arteriovenous Malformations. *Stroke*, *32*(6), 1458–1471.

Ogino, H., Shibamoto, Y., Sugie, C., & Ito, M. (2005). Biological Effects of Intermittent Radiation in Cultured Tumor Cells : Influence of Fraction Number and Dose Per Fraction. *Journal of Radiation Research*, *46*(4), 401–406.

Oh, C. W., Bump, E. A., Kim, J. S., Janigro, D., & Mayberg, M. R. (2001). Induction of a senescence-like phenotype in bovine aortic endothelial cells by ionizing radiation. *Radiation Research*, *156*(3), 232–40.

Oldendorf, W. H., Cornford, M. E., & Brown, W. J. (1977). The large apparent work capability of the blood-brain barrier: a study of the mitochondrial content of capillary endothelial cells in brain and other tissues of the rat. *Annals of Neurology*, *1*(5), 409–17.

Ondra, S., Troupp, H., George, E., & Schwab, K. (1990). The natural history of symptomatic arteriovenous malformations of the brain: a 24-year follow-up assessment. *Journal Neurosurgery*, *73*(3), 387–391.

Onoda, J. M., Kantak, S. S., & Diglio, C. A. (1999). Radiation induced endothelial cell retraction in vitro: correlation with acute pulmonary edema. *Pathology Oncology Research : POR*, *5*(1), 49–55.

Oppenheimer-Marks, N., Davis, L. S., Bogue, D. T., Ramberg, J., & Lipsky, P. E. (1991). Differential utilization of ICAM-1 and VCAM-1 during the adhesion and transendothelial migration of human T lymphocytes. *Journal of Immunology*, *147*(9), 2913–21.

Padget, D. (1956). The cranial venous system in man in reference to development, adult configuration, and relation to the arteries. *The American Journal of Anatomy*, *98*(3), 307–55.

Pan, H.-C., Sheehan, J., Stroila, M., Steiner, M., & Steiner, L. (2005). Late cyst formation following gamma knife surgery of arteriovenous malformations. *Journal of Neurosurgery*, *102 Suppl*, 124–7.

Panes, J., Anderson, D. C., Miyasaka, M., & Neil Granger, D. (1995). Role of leukocyte-endothelial cell adhesion in radiation-induced microvascular dysfunction in rats. *Gastroenterology*, *108*(6), 1761–1769.

Paris, F. (2001). Endothelial Apoptosis as the Primary Lesion Initiating Intestinal Radiation Damage in Mice. *Science*, *293*(5528), 293–297.

Park, S. O., Wankhede, M., Lee, Y. J., Choi, E., Fliess, N., Choe, S., … Oh, S. P. (2009). Real-time imaging of de novo arteriovenous malformation in a mouse model of hereditary hemorrhagic telangiectasia. *Journal of Clinical Investigation*, *119*(11), 3487–96.

Parkinson, D., & Bachers, G. (1980). Arteriovenous malformations. *Journal of Neurosurgery*, *53*(3), 285–299.

Patel, K. D., Zimmerman, G. A., Prescott, S. M., McEver, R. P., & McIntyre, T. M. (1991). Oxygen radicals induce human endothelial cells to express GMP-140 and bind neutrophils. *The Journal of Cell Biology*, *112*(4), 749–59.

Paxton, L. L., Li, L. J., Secor, V., Duff, J. L., Naik, S. M., Shibagaki, N., & Caughman, S. W. (1997). Flanking sequences for the human intercellular adhesion molecule-1 NF-kappaB response element are necessary for tumor necrosis factor alpha-induced gene expression. *The Journal of Biological Chemistry*, *272*(25), 15928–15935.

Pena, L. A., Fuks, Z., & Kolesnick, R. N. (2000). Radiation-induced Apoptosis of Endothelial Cells in the Murine Central Nervous System: Protection by Fibroblast Growth Factor and Sphingomyelinase Deficiency. *Cancer Research*, *60*(2), 321–327.

Perret, G., & Nishioka, H. (1969). Arteriovenous malformations: an analysis of 545 cases of cranio-cerebral arteriovenous malformations and fistulae reported to the cooperative study. In A. Sahs, G. Perret, H. Locksley, & H. Nishioka (Eds.), *Intracranial aneurysms and subarachnoid hemorrhage: a cooperative study.* (pp. 200–22). Philadelphia: JB Lippincott.

Phillips, M. H., Stelzer, K. J., Griffin, T. W., Mayberg, M. R., & Winn, H. R. (1994). Stereotactic radiosurgery: a review and comparison of methods. *Journal of Clinical Oncology*, *12*(5), 1085–99.

Phillips, M. L., Nudelman, E., Gaeta, F. C. A., Perez, M., Anil, K., Hakomori, S., … Singhal, A. K. (1990). ELAM-1 Mediates Cell Adhesion by Recognition of a Carbohydrate Ligand , Sialyl-Lex, *250*(4984), 1130–1132.

Pierce, M. C., Javier, D. J., & Richards-Kortum, R. (2008). Optical contrast agents and imaging systems for detection and diagnosis of cancer. *International Journal of Cancer*, *123*(9), 1979–90.

Pile-Spellman, J., Young, W. L., Joshi, S., Duong, H., Vang, M. C., Hartmann, A., … Ostapkovich, N. D. (1999). Adenosine-induced cardiac pause for endovascular embolization of cerebral arteriovenous malformations: technical case report. *Neurosurgery*, *44*(4), 881–6; discussion 886–7.

Pinsky, D. J., Naka, Y., Liao, H., Oz, M. C., Wagner, D. D., Mayadas, T. N., … Stern, D. M. (1996). Hypoxia-induced exocytosis of endothelial cell Weibel-Palade bodies. A mechanism for rapid neutrophil recruitment after cardiac preservation. *The Journal of Clinical Investigation*, *97*(2), 493–500.

Pober, J. S., Gimbrone, M. A., Lapierre, L. A., Mendrick, D. L., Fiers, W., Rothlein, R., & Springer, T. A. (1986). Overlapping patterns of activation of human endothelial cells by interleukin 1, tumor necrosis factor, and immune interferon. *Journal of Immunology*, *137*(6), 1893–6.

Podgorsak, E. B., Pike, G. B., Olivier, A., Pla, M., & Souhami, L. (1989). Radiosurgery with high energy photon beams: a comparison among techniques. *International Journal of Radiation Oncology, Biology, Physics*, *16*(3), 857–65.

Pohlman, T. H., Stanness, K. A., Beatty, P. G., Ochs, H. D., & Harlan, J. M. (1986). An endothelial cell surface factor(s) induced in vitro by lipopolysaccharide, interleukin 1, and tumor necrosis factor increases neutrophil adherence by a CDW 18-dependent mechanism. *The Journal of Immunology*, *136*(12), 4548–4553.

Pollock, B. E., & Brown, R. D. (2001). Management of cysts arising after radiosurgery to treat intracranial arteriovenous malformations. *Neurosurgery*, *49*(2), 259–64; discussion 264–5.

Pollock, B. E., & Flickinger, J. C. (2002). A proposed radiosurgery-based grading system for arteriovenous malformations. *Journal of Neurosurgery*, *96*(1), 79–85.

Pollock, B. E., Flickinger, J. C., Lunsford, L. D., Bissonette, D. J., & Kondziolka, D. (1996). Factors That Predict the Bleeding Risk of Cerebral Arteriovenous Malformations. *Stroke*, *27*(1), 1–6.

Pollock, B. E., Flickinger, J. C., Lunsford, L. D., Bissonette, D. J., & Kondziolka, D. (1996). Hemorrhage risk after stereotactic radiosurgery of cerebral arteriovenous malformations. *Neurosurgery*, *38*(4), 652–9; discussion 659–61.

Pollock, B. E., Flickinger, J. C., Lunsford, L. D., Maitz, A., & Kondziolka, D. (1998). Factors associated with successful arteriovenous malformation radiosurgery. *Neurosurgery*, *42*(6), 1239–44; discussion 1244–7.

Pollock, B. E., Gorman, D. a., & Coffey, R. J. (2003). Patient Outcomes after Arteriovenous Malformation Radiosurgical Management: Results Based on a 5- to 14-year Follow-up Study. *Neurosurgery*, *52*(6), 1291–1297.

Pollock, B. E., Kline, R. W., Stafford, S. L., Foote, R. L., & Schomberg, P. J. (2000). The rationale and technique of staged-volume arteriovenous malformation radiosurgery. *International Journal of Radiation Oncology Biology Physics*, *48*(3), 817–824.

Pollock, B. E., Kondziolka, D., Flickinger, J. C., Patel, A. K., Bissonette, D. J., & Lunsford, L. D. (1996). Magnetic resonance imaging: an accurate method to evaluate arteriovenous malformations after stereotactic radiosurgery. *Journal of Neurosurgery*, *85*(6), 1044–9.

Pomorski, T., Holthuis, J. C. M., Herrmann, A., & van Meer, G. (2004). Tracking down lipid flippases and their biological functions. *Journal of Cell Science*, *117*(Pt 6), 805–13.

Pomorski, T., & Menon, A. K. (2006). Lipid flippases and their biological functions. *Cellular and Molecular Life Sciences : CMLS*, *63*(24), 2908–21.

Potter, J. M. (1955). Angiomatous malformations of the brain: their nature and prognosis. *Annals of the Royal College of Surgeons of England*, *16*(4), 227–43.

Prabhakarpandian, B., Goetz, D. J., Swerlick, R. a., Chen, X., & Kiani, M. F. (2001). Expression and Functional Significance of Adhesion Molecules on Cultured Endothelial Cells in Response to Ionizing Radiation. *Microcirculation*, *8*(5), 355–364.

Prionas, S. D., Kowalski, J., Fajardo, L. F., Kaplan, I., Kwan, H. H., & Allison, A. C. (1990). Effects of X irradiation on angiogenesis. *Radiation Research*, *124*(1), 43–9.

Prise, K. M., & O'Sullivan, J. M. (2009). Radiation-induced bystander signalling in cancer therapy. *Nature Reviews. Cancer*, *9*(5), 351–60.

Putman, C. M., Chaloupka, J. C., Fulbright, R. K., Awad, I. a, White, R. I., & Fayad, P. B. (1996). Exceptional multiplicity of cerebral arteriovenous malformations associated with hereditary hemorrhagic telangiectasia (Osler-Weber-Rendu syndrome). *AJNR. American Journal of Neuroradiology*, *17*(9), 1733–42.

Quarmby, S., Kumar, P., & Kumar, S. (1999). Radiation-induced normal tissue injury: role of adhesion molecules in leukocyte-endothelial cell interactions. *International Journal of Cancer.*, *82*(3), 385–95.

Ran, S., Downes, A., Thorpe, P. E., & Vessels, B. (2002). Increased Exposure of Anionic Phospholipids on the Surface of Tumor Blood Vessels. *Cancer Research*, *62*(21), 6132–6140.

Ran, S., He, J., Huang, X., Soares, M., Scothorn, D., & Thorpe, P. E. (2005). Antitumor Effects of a Monoclonal Antibody that Binds Anionic Phospholipids on the Surface of Tumor Blood Vessels in Mice. *Clinical Cancer Research*, *11*(4), 1551–1562.

Ran, S., & Thorpe, P. E. (2002). Phosphatidylserine is a marker of tumor vasculature and a potential target for cancer imaging and therapy. *Radiation Oncology Biology Physics*, *54*(5), 1479–1484.

Rangel-Castilla, L., Russin, J. J., Martinez-Del-Campo, E., Soriano-Baron, H., Spetzler, R. F., & Nakaji, P. (2014). Molecular and cellular biology of cerebral arteriovenous malformations: a review of current concepts and future trends in treatment. *Neurosurgical Focus*, *37*(3), E1.

Ravanat, C., Archipoff, G., Beretz, A., Freund, G., & Cazenave, J. (1992). Use of annexin-V to demonstrate the role of phosphatidylserine exposure in the maintenance of haemostatic balance by endothelial cells. *The Biochemical Journal*, *282*(Pt 1), 7–13.

Raymond, J., Iancu, D., Weill, A., Guilbert, F., Bahary, J. P., Bojanowski, M., & Roy, D. (2005). Embolization as one modality in a combined strategy for the management of cerebral arteriovenous malformations. *Journal of Interventional Neuroradiology*, *11*(Suppl 1), 57–62.

Read, M. A., Neish, A. S., Luscinskas, F. W., Palombella, V. J., Maniatis, T., & Collins, T. (1995). The proteasome pathway is required for cytokine-induced endothelial-leukocyte adhesion molecule expression. *Immunity*, *2*(5), 493–506.

Reinhold, H. S., & Hopewell, J. W. (1980). Late changes in the architecture of blood vessels of the rat brain after irradiation. *The British Journal of Radiology*, *53*(631), 693–6.

Reshef, A., Shirvan, A., Akselrod-Ballin, A., Wall, A., & Ziv, I. (2010). Small-molecule biomarkers for clinical PET imaging of apoptosis. *Journal of Nuclear Medicine*, *51*(6), 837–40.

Rice, G. E., & Bevilacqua, M. P. (1989). An inducible endothelial cell surface glycoprotein mediates melanoma adhesion. *Science*, *246*(4935), 1303–6.

Rice, G. E., Munro, J. M., & Bevilacqua, M. P. (1990). Inducible cell adhesion molecule 110 (INCAM-110) is an endothelial receptor for lymphocytes. A CD11/CD18-independent adhesion mechanism. *The Journal of Experimental Medicine*, *171*(4), 1369–74.

Rice, G. E., Munro, J. M., Corless, C., & Bevilacqua, M. P. (1991). Vascular and nonvascular expression of INCAM-110. A target for mononuclear leukocyte adhesion in normal and inflamed human tissues. *The American Journal of Pathology*, *138*(2), 385–93.

Richling, B., Killer, M., Al-Schameri, A. R., Ritter, L., Agic, R., & Krenn, M. (2006). Therapy of brain arteriovenous malformations: multimodality treatment from a balanced standpoint. *Neurosurgery*, *59*(5 Suppl 3), S148–57; discussion S3–13.

Richter, V., Rassoul, F., Purschwitz, K., Hentschel, B., Reuter, W., & Kuntze, T. (2003). Circulating vascular cell adhesion molecules VCAM-1, ICAM-1, and E-selectin in dependence on aging. *Gerontology*, *49*(5), 293–300.

Riedl, S., Rinner, B., Asslaber, M., Schaider, H., Walzer, S., Novak, A., … Zweytick, D. (2011). In search of a novel target - phosphatidylserine exposed by non-apoptotic tumor cells and metastases of malignancies with poor treatment efficacy. *Biochimica et Biophysica Acta*, *1808*(11), 2638–45.

Riley, P. A. (1994). Free radicals in biology: oxidative stress and the effects of ionizing radiation. *International Journal of Radiation Biology*, *65*(1), 27–33.

Rizzo, M. T., & Leaver, H. A. (2010). Brain endothelial cell death: modes, signaling pathways, and relevance to neural development, homeostasis, and disease. *Molecular Neurobiology*, *42*(1), 52–63.

Roebuck, K. A., & Finnegan, A. (1999). Regulation of intercellular adhesion molecule-1 (CD54) gene expression. *Journal of Leukocyte Biology*, *66*(6), 876–88.

Ross, M. H., Romrell, L. J., & Kaye, G. (1995). *Histology: A Text and Atlas* (3rd ed.). Baltimore: Williams & Wilkins.

Rossin, R., Muro, S., Welch, M. J., Muzykantov, V. R., & Schuster, D. P. (2007). In Vivo Imaging of 64Cu-Labeled Polymer Nanoparticles Targeted to the Lung Endothelium. *Journal of Nuclear Medicine*, *49*(1), 103–111.

Rothbart, D., Awad, I. A., Lee, J., Kim, J., Harbaugh, R., & Criscuolo, G. R. (1996). Expression of angiogenic factors and structural proteins in central nervous system vascular malformations. *Neurosurgery*, *38*(5), 915–24; discussion 924–5.

Rousseau, M., Gaugler, M.-H., Rodallec, A., Bonnaud, S., Paris, F., & Corre, I. (2011). RhoA GTPase regulates radiation-induced alterations in endothelial cell adhesion and migration. *Biochemical and Biophysical Research Communications*, *414*(4), 750–755.

Ryan, D. H., Nuccie, B. L., Abboud, C. N., & Winslow, J. M. (1991). Vascular cell adhesion molecule-1 and the integrin VLA-4 mediate adhesion of human B cell precursors to cultured bone marrow adherent cells. *The Journal of Clinical Investigation*, *88*(3), 995–1004.

Sakane, F., Yamada, K., Imai, S., & Kanohz, H. (1991). Porcine 80-kDa Diacylglycerol Kinase Is a Calcium-binding and Calcium/Phospholipid-dependent Enzyme and Undergoes Calcium-dependent Translcation. *The Journal of Biological Chemistry*, *266*(11), 7096–7100.

Sanno, N., Hayashi, S., Shimura, T., Maeda, S., & Teramoto, A. (2004). Intracranial Osteosarcoma After Radiosurgery. *Neurologia Medico-Chirurgica*, *44*(1), 29–32.

Savill, J., & Fadok, V. (2000). Corpse clearance defines the meaning of cell death. *Nature*, *407*(6805), 784–8.

Scalia, R., Appel, J. Z., & Lefer, A. M. (1998). Leukocyte-endothelium interaction during the early stages of hypercholesterolemia in the rabbit: role of P-selectin, ICAM-1, and VCAM-1. *Arteriosclerosis, Thrombosis, and Vascular Biology*, *18*(7), 1093–100.

Schaller, C., Schramm, J., & Haun, D. (1998). Significance of factors contributing to surgical complications and to late outcome after elective surgery of cerebral arteriovenous malformations. *Journal of Neurology, Neurosurgery, and Psychiatry*, *65*(4), 547–54.

Schlachter, L. B., Fleischer, A. S., Faria, M. A., & Tindall, G. T. (1980). Multifocal intracranial arteriovenous malformations. *Neurosurgery*, *7*(5), 440–4.

Schleimer, R. P., Sterbinsky, S. A., Kaiser, J., Bickel, C. A., Klunk, D. A., Tomioka, K., … McIntyre, B. W. (1992). IL-4 induces adherence of human eosinophils and basophils but not neutrophils to endothelium. Association with expression of VCAM-1. *Journal of Immunology*, *148*(4), 1086–92.

Schneider, B. F., Eberhard, D. A., & Steiner, L. E. (1997). Histopathology of arteriovenous malformations after gamma knife radiosurgery. *Journal of Neurosurgery*, *87*(3), 352–357.

Schreck, R., Rieberl, P., & Baeuerle, P. a. (1991). Reactive oxygen intermediates as apparently widely used messengers in the activation of the NF-kappa B transcription factor and HIV-1. *The EMBO Journal*, *10*(8), 2247–2258.

Schutters, K., & Reutelingsperger, C. (2010). Phosphatidylserine targeting for diagnosis and treatment of human diseases. *Apoptosis*, *15*(9), 1072–82.

Schwartz, B. R., Wayner, E. A., Carlos, T. M., Ochs, H. D., & Harlan, J. M. (1990). Identification of surface proteins mediating adherence of CD11/CD18-deficient lymphoblastoid cells to cultured human endothelium. *The Journal of Clinical Investigation*, *85*(6), 2019–22.

Sedlakova, R., Shivers, R. R., & Del Maestro, R. F. (1999). Ultrastructure of the blood-brain barrier in the rabbit. *Journal of Submicroscopic Cytology and Pathology*, *31*(1), 149–61.

See, A. P., Raza, S., Tamargo, R. J., & Lim, M. (2012). Stereotactic radiosurgery of cranial arteriovenous malformations and dural arteriovenous fistulas. *Neurosurgery Clinics of North America*, *23*(1), 133–46.

Shankar, R., de la Motte, C., Poptic, E., & DiCorleto, P. (1994). Thrombin receptor-activating peptides differentially stimulate platelet- derived growth factor production, monocytic cell adhesion, and E- selectin expression in human umbilical vein endothelial cells. *The Journal of Biological Chemistry*, *269*(19), 13936–13941.

Sharp, C. D., Jawahar, A., Warren, A. C., Elrod, J. W., Nanda, A., & Alexander, J. S. (2003). Gamma Knife Irradiation Increases Cerebral Endothelial Expression of Intercellular Adhesion Molecule 1 and E-selectin. *Neurosurgery*, *53*(1), 154–161.

Shebuski, R. J., & Kilgore, K. S. (2002). Role of inflammatory mediators in thrombogenesis. *The Journal of Pharmacology and Experimental Therapeutics*, *300*(3), 729–35.

Shen, Q., Goderie, S. K., Jin, L., Karanth, N., Sun, Y., Abramova, N., … Temple, S. (2004). Endothelial Cells Stimulate Self-Renewal and Expand Neurogenesis of Neural Stem Cells. *Science*, *304*(5675), 1338–1340.

Shen, W. Y., Yu, M. J., Barry, C. J., Constable, I. J., & Rakoczy, P. E. (1998). Expression of cell adhesion molecules and vascular endothelial growth factor in experimental choroidal neovascularisation in the rat. *The British Journal of Ophthalmology*, *82*(9), 1063–71.

Shibamoto, Y., Ito, M., Sugie, C., Ogino, H., & Hara, M. (2004). Recovery from sublethal damage during intermittent exposures in cultured tumor cells: implications for dose

modification in radiosurgery and IMRT. *International Journal of Radiation Oncology, Biology, Physics*, *59*(5), 1484–90.

Shimizu, T. S., Ugawara, K. S., Osaka, M. T., Mai, H. I., Oya, K. H., Akeuchi, T. T., & Asaki, T. S. (2006). Nestin Expression in Vascular Malformations : A Novel Marker for Proliferative Endothelium. *Neurologia Medico-Chirurgica*, *46*(3), 111–7.

Simmons, P. J., Masinovsky, B., Longenecker, B. M., Berenson, R., Torok-Storb, B., & Gallatin, W. M. (1992). Vascular cell adhesion molecule-1 expressed by bone marrow stromal cells mediates the binding of hematopoietic progenitor cells. *Blood*, *80*(2), 388–395.

Sisti, M. B., Kader, A., & Stein, B. M. (1993). Microsurgery for 67 intracranial arteriovenous malformations less than 3 cm in diameter. *Journal of Neurosurgery*, *79*(5), 653–60.

Sivakumar, S., van Veggel, F. C. J. M., & May, P. S. (2007). Near-infrared (NIR) to red and green up-conversion emission from silica sol-gel thin films made with La(0.45)Yb(0.50)Er(0.05)F(3) nanoparticles, hetero-looping-enhanced energy transfer (Hetero-LEET): a new up-conversion process. *Journal of the American Chemical Society*, *129*(3), 620–5.

Skjøth-Rasmussen, J., Roed, H., Ohlhues, L., Jespersen, B., & Juhler, M. (2010). Complications following linear accelerator based stereotactic radiation for cerebral arteriovenous malformations. *International Journal of Radiation Oncology, Biology, Physics*, *77*(2), 542–7.

Smith, B. a, Akers, W. J., Leevy, W. M., Lampkins, A. J., Xiao, S., Wolter, W., … Smith, B. D. (2010). Optical Imaging of Mammary and Prostate Tumors in Living Animals using a Synthetic Near Infrared Zinc (II) -Dipicolylamine Probe for Anionic Cell Surfaces. *Journal of the American Chemical Society*, *132*(1), 67–69.

Smith, B. a, Xiao, S., Wolter, W., Wheeler, J., Suckow, M. a, & Smith, B. D. (2011). In vivo targeting of cell death using a synthetic fluorescent molecular probe. *Apoptosis : An International Journal on Programmed Cell Death*, *16*(7), 722–31.

Smith, B. A., Xie, B., Beek, E. R. Van, Que, I., Blankevoort, V., Xiao, S., … Smith, B. D. (2012). Multicolor Fluorescence Imaging of Traumatic Brain Injury in a Cryolesion Mouse Model. *ACS Chemical Neuroscience*, *3*(7), 530–537.

Smith, B., Gammon, S., Xiao, S., Wang, W., Chapman, S., McDermott, R., … Leevy, M. (2011). In vivo optical imaging of acute cell death using a near-infrared fluorescent zincdipicolylamine probe. *Molecular Pharmaceutics*, *127*(2), 358–366.

Smith, C., Mehta, R., Gibson, D. F., Levashova, Z., Blankenberg, F. G., & Tait, J. F. (2010). Characterization of a recombinant form of annexin VI for detection of apoptosis. *Bioconjugate Chemistry*, *21*(8), 1554–8.

Smith, C. W., & Anderson, D. C. (1991). PMN adhesion and extravasation as a paradigm for tumor cell dissemination. *Cancer Metastasis Reviews*, *10*(1), 61–78.

Smrz, D., Dráberová, L., & Dráber, P. (2007). Non-apoptotic phosphatidylserine externalization induced by engagement of glycosylphosphatidylinositol-anchored proteins. *The Journal of Biological Chemistry*, *282*(14), 10487–97.

Söderman, M., Andersson, T., Karlsson, B., Wallace, M. C., & Edner, G. (2003). Management of patients with brain arteriovenous malformations. *European Journal of Radiology*, *46*(3), 195–205.

Sonstein, W. J., Kader, A., Michelsen, W. J., Llena, J. F., Hirano, A., & Casper, D. (1996). Expression of vascular endothelial growth factor in pediatric and adult cerebral arteriovenous malformations: an immunocytochemical study. *Journal of Neurosurgery*, *85*(5), 838–45.

Spetzler, R. F., & Martin, N. a. (1986). A proposed grading system for arteriovenous malformations. *Journal of Neurosurgery*, *65*(4), 476–83.

Springer, T. A. (1990). Adhesion receptors of the immune system. *Nature*, *346*, 425–434.

Springer, T. A. (1994). Traffic signals for lymphocyte recirculation and leukocyte emigration: the multistep paradigm. *Cell*, *76*(2), 301–14.

Springer, T. A., Dustin, M. L., Kishimoto, T. K., & Marlin, S. D. (1987). The lymphocyte function-associated LFA-1, CD2, and LFA-3 molecules: cell adhesion receptors of the immune system. *Annual Review of Immunology*, *5*, 223–52.

Stapf, C., Khaw, a V, Sciacca, R. R., Hofmeister, C., Schumacher, H. C., Pile-Spellman, J., … Hartmann, A. (2003). Effect of age on clinical and morphological characteristics in patients with brain arteriovenous malformation. *Stroke*, *34*(11), 2664–9.

Stapf, C., Mast, H., Sciacca, R. R., Berenstein, A., Nelson, P. K., Gobin, Y. P., … Mohr, J. P. (2003). The New York Islands AVM Study: design, study progress, and initial results. *Stroke; a Journal of Cerebral Circulation*, *34*(5), e29–33.

Stapf, C., Mohr, J. P., Pile-Spellman, J., Solomon, R. a, Sacco, R. L., & Connolly, E. S. (2001). Epidemiology and natural history of arteriovenous malformations. *Neurosurgical Focus*, *11*(5), e1.

Stapf, C., Mohr, J. P., Sciacca, R. R., Hartmann, A., Aagaard, B. D., Pile-Spellman, J., & Mast, H. (2000). Incident Hemorrhage Risk of Brain Arteriovenous Malformations Located in the Arterial Borderzones. *Stroke*, *31*(10), 2365–2368.

Steinberg, D. (1987). Lipoproteins and the pathogenesis of atherosclerosis. *Circulation*, *76*(3), 508–14.

Steiner, L. (1986). *Radiosurgery in cerebral arteriovenous malformations*. (E. Flamm & J. Fein, Eds.). Berlin: Springer, 1161–1215.

Steiner, L., Leksell, L., Greitz, T., Forster, D. M., & Backlund, E. O. (1972). Stereotaxic radiosurgery for cerebral arteriovenous malformations. Report of a case. *Acta Chirurgica Scandinavica*, *138*(5), 459–64.

Steiner, L., & Lindquist, C. (1987). Radiosurgery in cerebral arteriovenous malformation. In *Stereotactic Surgery* (Tasker RR, pp. 329–336). Philadelphia, Hanley and Belfus, Inc.

Stone, S. J., & Vance, J. E. (2000). Phosphatidylserine synthase-1 and -2 are localized to mitochondria-associated membranes. *The Journal of Biological Chemistry*, *275*(44), 34534–40.

Stoolman, L. M. (1989). Adhesion Molecules Controlling Lymphocyte Migration Minireview. *Cell*, *56*(6), 907–910.

Storer, K. P., Tu, J., Karunanayaka, A., Morgan, M. K., & Stoodley, M. a. (2007). Thrombotic molecule expression in cerebral vascular malformations. *Journal of Clinical Neuroscience*, *14*(10), 975–80.

Storer, K. P., Tu, J., Karunanayaka, A., Morgan, M. K., & Stoodley, M. a. (2008).

Inflammatory molecule expression in cerebral arteriovenous malformations. *Journal of Clinical Neuroscience*, *15*(2), 179–84.

Storer, K. P., Tu, J., Stoodley, M. A., & Smee, R. I. (2010). Expression of endothelial adhesion molecules after radiosurgery in an animal model of arteriovenous malformation. *Neurosurgery*, *67*(4), 976–83; discussion 983.

Sturbois-Balcerzak, B., Stone, S. J., Sreenivas, A., & Vance, J. E. (2001). Structure and expression of the murine phosphatidylserine synthase-1 gene. *The Journal of Biological Chemistry*, *276*(11), 8205–12.

Sun, D. Q., Carson, K. a, Raza, S. M., Batra, S., Kleinberg, L. R., Lim, M., … Rigamonti, D. (2011). The radiosurgical treatment of arteriovenous malformations: obliteration, morbidities, and performance status. *International Journal of Radiation Oncology, Biology, Physics*, *80*(2), 354–61.

Sure, U., Butz, N., Schlegel, J., Siegel, A. M., Wakat, J. P., Mennel, H. D., … Bertalanffy, H. (2001). Endothelial proliferation, neoangiogenesis, and potential de novo generation of cerebrovascular malformations. *Journal of Neurosurgery*, *94*(6), 972–7.

Suzuki, H., Abe, K., Tojo, S., Kimura, K., Mizugaki, M., & Itoyama, Y. (1998). A change of P-selectin immunoreactivity in rat brain after transient and permanent middle cerebral artery occlusion. *Neurological Research*, *20*(5), 463–9.

Svennerholm, L. (1968). Distribution and fatty acid composition of phosphoglycerides in normal human brain. *Journal of Lipid Research*, *9*(5), 570–579.

Tabagari, D., Nemsadze, G., Janjalia, M., Jincharadze, M., & Shan, J. (2009). Phase II study of bavituximab plus docetaxel in locally advanced or metastatic breast cancer. *Journal of Clinical Oncology*, *27 (15s)*.

Taylor, C. L., Dutton, K., Rappard, G., Pride, G. L., Replogle, R., Purdy, P. D., … Samson, D. S. (2004). Complications of preoperative embolization of cerebral arteriovenous malformations. *Journal of Neurosurgery*, *100*(5), 810–812.

Thapa, N., Kim, S., So, I.-S., Lee, B.-H., Kwon, I.-C., Choi, K., & Kim, I.-S. (2008). Discovery of a phosphatidylserine-recognizing peptide and its utility in molecular imaging of tumour apoptosis. *Journal of Cellular and Molecular Medicine*, *12*(5A), 1649–60.

Thompson, P. W., Randi, A. M., & Ridley, A. J. (2002). Intercellular adhesion molecule (ICAM)-1, but not ICAM-2, activates RhoA and stimulates c-fos and rhoA transcription in endothelial cells. *Journal of Immunology*, *169*(2), 1007–13.

Thorpe, P. E. (2004). Vascular Targeting Agents as Cancer Therapeutics. *Clinical Cancer Research*, *10*(214), 415–427.

Thorpe, P. E., Chaplin, D. J., & Blakey, D. C. (2003). The First International Conference on Vascular Targeting: Meeting Overview. *The Journal of Cancer Research*, *63*(5), 1144–1147.

Todaka, T., Hamada, J., Kai, Y., Morioka, M., & Ushio, Y. (2003). Analysis of mean transit time of contrast medium in ruptured and unruptured arteriovenous malformations: a digital subtraction angiographic study. *Stroke*, *34*(10), 2410–4.

Tu, J., Karunanayaka, A., Windsor, A., & Stoodley, M. a. (2010). Comparison of an animal model of arteriovenous malformation with human arteriovenous malformation. *Journal*

of Clinical Neuroscience, *17*(1), 96–102.

Tu, J., Stoodley, M. a, Morgan, M. K., & Storer, K. P. (2006a). Responses of arteriovenous malformations to radiosurgery: ultrastructural changes. *Neurosurgery*, *58*(4), 749–58; discussion 749–58.

Tu, J., Stoodley, M. A., Morgan, M. K., & Storer, K. P. (2006b). Ultrastructure of perinidal capillaries in cerebral arteriovenous malformations. *Neurosurgery*, *58*(5), 961–70; discussion 961–70.

Turjman, F., Massoud, T. F., Vinuela, F., Sayre, J. W., Guglielmi, G., & Duckwiler, G. (1994). Aneurysms related to cerebral arteriovenous malformations: Superselective angiographic assessment in 58 patients. *American Journal of Neuroradiology*, *15*(9), 1601–1605.

Utsugi, T., Schroit, A. J., Connor, J., Bucana, C., & Fidler, I. J. (1991). Elevated Expression of Phosphatidylserine in the Outer Membrane Leaflet of Human Tumor Cells and Recognition by Activated Human Blood Monocytes1. *Cancer Research*, *51*, 3062–3067.

Van de Stolpe, A., & Van der Saag, P. T. (1996). Intercellular adhesion molecule-1. *Journal of Molecular Medicine*, *74*(1), 13–33.

Van Der Meeren, A., Squiban, C., Gourmelon, P., Lafont, H., & Gaugler, M. H. (1999). Differential regulation by IL-4 and IL-10 of radiation-induced IL-6 and IL-8 production and ICAM-1 expression by human endothelial cells. *Cytokine*, *11*(11), 831–838.

Van der Meeren, A., Vandamme, M., Squiban, C., Gaugler, M.-H., & Mouthon, M.-A. (2003). Inflammatory reaction and changes in expression of coagulation proteins on lung endothelial cells after total-body irradiation in mice. *Radiation Research*, *160*(6), 637–646.

Vance, J. E. (2008). Phosphatidylserine and phosphatidylethanolamine in mammalian cells: two metabolically related aminophospholipids. *Journal of Lipid Research*, *49*(7), 1377–87.

Vance, J. E., & Steenbergen, R. (2005). Metabolism and functions of phosphatidylserine. *Progress in Lipid Research*, *44*(4), 207–34.

Vanderheyden, J.-L., Liu, G., He, J., Patel, B., Tait, J. F., & Hnatowich, D. J. (2006). Evaluation of 99mTc-MAG3-annexin V: influence of the chelate on in vitro and in vivo properties in mice. *Nuclear Medicine and Biology*, *33*(1), 135–44.

Vestweber, D., & Blanks, J. E. (1999). Mechanisms that regulate the function of the selectins and their ligands. *Physiological Reviews*, *79*(1), 181–213.

Vetrone, F., & Capobianco, J. A. (2008). Lanthanide-doped fluoride nanoparticles: luminescence, upconversion, and biological applications. *International Journal of Nanotechnology*, *5*(9-12), 1306.

Veznedaroglu, E., Andrews, D. W., Benitez, R. P., Downes, M. B., Werner-Wasik, M., Rosenstock, J., … Rosenwasser, R. H. (2008). Fractionated stereotactic radiotherapy for the treatment of large arteriovenous malformations with or without previous partial embolization. *Neurosurgery*, *62 Suppl 2*, 763–75.

Waehrens, L. N., Heegaard, C. W., Gilbert, G. E., & Rasmussen, J. T. (2009). Bovine lactadherin as a calcium-independent imaging agent of phosphatidylserine expressed on the surface of apoptotic HeLa cells. *The Journal of Histochemistry and Cytochemistry*,

57(10), 907–14.

Ward, D., Molteni, J., & Ts'ao, C. (1998). Endothelial-oriented strategies to spare normal tissues. In D. B. Rubin (Ed.), *The radiation biology of the vascular endothelium.* (pp. 185–208). CRC Press, Boca Raton.

Weber, W. A., Czernin, J., Phelps, M. E., & Herschman, H. R. (2008). Technology Insight: novel imaging of molecular targets is an emerging area crucial to the development of targeted drugs. *Nature Clinical Practice. Oncology*, *5*(1), 44–54.

Weber, W., Kis, B., Siekmann, R., & Kuehne, D. (2007). Endovascular treatment of intracranial arteriovenous malformations with onyx: technical aspects. *AJNR. American Journal of Neuroradiology*, *28*(2), 371–7.

Weibel, E. R., & Palade, G. E. (1964). New cytoplasmic components in arterial endothelia. *The Journal of Cell Biology*, *23*, 101–112.

Weiser, S., Miu, J., Ball, H. J., & Hunt, N. H. (2007). Interferon-gamma synergises with tumour necrosis factor and lymphotoxin-alpha to enhance the mRNA and protein expression of adhesion molecules in mouse brain endothelial cells. *Cytokine*, *37*(1), 84–91.

Wellicome, S. M., Thornhill, M. H., Pitzalis, C., Thomas, D. S., Lanchbury, J. S., Panayi, G. S., & Haskard, D. O. (1990). A monoclonal antibody that detects a novel antigen on endothelial cells that is induced by tumor necrosis factor, IL-1, or lipopolysaccharide. *Journal of Immunology*, *144*(7), 2558–65.

Wilkins, R. H. (1985). Natural history of intracranial vascular malformations: a review. *Neurosurgery*, *16*(3), 421–30.

Williams, A. F., & Barclay, A. N. (1988). The immunoglobulin superfamily--domains for cell surface recognition. *Annual Review of Immunology*, *6*, 381–405.

Williamson, P., & Schlegel, R. a. (2002). Transbilayer phospholipid movement and the clearance of apoptotic cells. *Biochimica et Biophysica Acta (BBA) - Molecular and Cell Biology of Lipids*, *1585*(2-3), 53–63.

Willinsky, R. A., Lasjaunias, P., Terbrugge, K., & Burrows, P. (1990). Multiple cerebral arteriovenous malformations (AVMs). Review of our experience from 203 patients with cerebral vascular lesions. *Neuroradiology*, *32*(3), 207–10.

Wong, J. H., Awad, I. A., & Kim, J. H. (2000). Ultrastructural pathological features of cerebrovascular malformations: a preliminary report. *Neurosurgery*, *46*(6), 1454–9.

Wunder, a, Straub, R. H., Gay, S., Funk, J., & Müller-Ladner, U. (2005). Molecular imaging: novel tools in visualizing rheumatoid arthritis. *Rheumatology*, *44*(11), 1341–9.

Xiong, C., Brewer, K., Song, S., Zhang, R., Lu, W., Wen, X., & Li, C. (2011). Peptide-based imaging agents targeting phosphatidylserine for the detection of apoptosis. *Journal of Medicinal Chemistry*, *54*(6), 1825–35.

Xu, H., Gonzalo, J. A., St Pierre, Y., Williams, I. R., Kupper, T. S., Cotran, R. S., … Gutierrez-Ramos, J. C. (1994). Leukocytosis and resistance to septic shock in intercellular adhesion molecule 1-deficient mice. *The Journal of Experimental Medicine*, *180*(1), 95–109.

Yao, L., Setiadi, H., Xia, L., Laszik, Z., Taylor, F. B., & McEver, R. P. (1999). Divergent inducible expression of P-selectin and E-selectin in mice and primates. *Blood*, *94*(11),

3820–8.

Yasargil, M. (1987). *AVM of the Brain, History, Embryology, Pathological Considerations, Hemodynamics, Diagnostic Studies, Microsurgical Anatomy*. New York, Thieme.

Yassari, R., Sayama, T., Jahromi, B. S., Aihara, Y., Stoodley, M., Macdonald, R. L., & Morgan, M. K. (2004). Angiographic, hemodynamic and histological characterization of an arteriovenous fistula in rats. *Acta Neurochirurgica*, *146*(5), 495–504.

Yen, C.-P., & Steiner, L. (2011). Gamma knife surgery for brainstem arteriovenous malformations. *World Neurosurgery*, *76*(1-2), 87–95; discussion 57–8.

Yentrapalli, R., Azimzadeh, O., Barjaktarovic, Z., Sarioglu, H., Wojcik, A., Harms-Ringdahl, M., … Tapio, S. (2013). Quantitative proteomic analysis reveals induction of premature senescence in human umbilical vein endothelial cells exposed to chronic low-dose rate gamma radiation. *Proteomics*, *13*(7), 1096–107.

Zabel-du Bois, A., Milker-Zabel, S., Huber, P., Schlegel, W., & Debus, J. (2007). Risk of hemorrhage and obliteration rates of LINAC-based radiosurgery for cerebral arteriovenous malformations treated after prior partial embolization. *International Journal of Radiation Oncology, Biology, Physics*, *68*(4), 999–1003.

Zhang, R. L., Zhang, Z. G., Chopp, M., & Zivin, J. A. (1999). Thrombolysis with tissue plasminogen activator alters adhesion molecule expression in the ischemic rat brain. *Stroke*, *30*(3), 624–9.

Zhao, D., Stafford, J. H., Zhou, H., & Thorpe, P. E. (2011). Near-infrared Optical Imaging of Exposed Phosphatidylserine in a Mouse Glioma Model. *Translational Oncology*, *4*(6), 355–364.

Zhao, Z., Johnson, M., Chen, B., Grace, M., Ukath, J., Lee, V., … Stoodley, M. (2015). Live cell imaging to detect phosphatidylserine externalization in brain endothelial cells exposed to ionising radiation: implications for the treatment of brain arteriovenous malformations. *Journal of Neurosurgery*, 1–8.

Zheng, H., Wang, F., Wang, Q., & Gao, J. (2011). Cofactor-free detection of phosphatidylserine with cyclic peptides mimicking lactadherin. *Journal of the American Chemical Society*, *133*(39), 15280–3.

Zhou, Q., Zhao, J., Stout, J. G., Luhm, R. a., Wiedmer, T., & Sims, P. J. (1997). Molecular Cloning of Human Plasma Membrane Phospholipid Scramblase: A PROTEIN MEDIATING TRANSBILAYER MOVEMENT OF PLASMA MEMBRANE PHOSPHOLIPIDS. *Journal of Biological Chemistry*, *272*(29), 18240–18244.

Zhou, X., Perez, F., Han, K., & Jurivich, D. (2006). Clonal senescence alters endothelial ICAM-1 function. *Mechanisms of Ageing and Development*, *127*(10), 779–85.

Zwaal, R. (1978). Membrane and lipid involvement in blood coagulation. *Biochimica et Biophysica Acta*, *515*(2), 163–205.

Zwaal, R., Comfurius, P., & VanDeenen, L. L. M. (1977). Membrane asymmetry and blood coagulation. *Nature*, *268*, 358–360.

Zwaal, R. F. A., Comfurius, P., & Bevers, E. M. (2005). Surface exposure of phosphatidylserine in pathological cells. *Cellular and Molecular Life Sciences*, *62*(9), 971–88.

Zwaal, R. F. A., & Schroit, A. J. (1997). Pathophysiologic Implications of Membrane Phospholipid Asymmetry in Blood Cells. *Blood Journal*, *89*(4), 1121–1132.

Appendices

Appendix 1.

- **70% (v/v) Ethanol (RNA isolation and PCR experiment):** 70 mL ethanol + 30 mL Milli-Q water

- **Blocking solution (ICC experiment):** 5% (w/v) bovine serum albumin (BSA) in PBS

- **Blocking solution (western blot experiment):** 5% (w/v) non-fat milk powder in PBST

- **Lysis buffer: (western blot experiment)**: 2X RIPA stock (300 mM NaCl, 100 mM Tris-HCl pH 7.5, 2% (w/v) sodium deoxycholate , 0.2% (w/v) SDS, 2% (v/v) Triton-X100). Prepare 2 X RIPA stock as described. Prior to extraction, prepare sufficient 1X working stock containing 1 X RIPA, 1 x protease inhibitor mix (GE Healthcare) and 10 mM EDTA, pH 8.0.

- **Phosphate buffered saline (PBS; ICC and western blot experiment and perfusion procedure):** 137 mM NaCl, 2.7 mM KCl, 10 mM Na_2HPO_4 1.8 mM KH_2PO_4. Adjust pH to 7.4.

- **Tris-buffered saline with Tween-20 (TBST, western blot experiment):** 0.5 M NaCl, 20 mM Tris HCl, 0.1% (w/vol) Tween-20, pH 7.4

Appendix 2.

Biosafety approval and Animal Research Authority (ARA)

Biosafety/Biohazard workshop- feedback

Bio Safety <biosafety@mq.edu.au>   Mon, Mar 10, 2014 at 10:41 AM
Bcc: newsha.raoufi-rad@students.mq.edu.au

Dear all,

Thank you for attending the Biosafety/Biohazard workshop on the 26th February 2014. We will not be issuing attendance certificates for this workshop as previously indicated, however, a list of all the attendees has been sent to lab managers. If you require further confirmation of your attendance please email me.

The presentations for the workshop will be available from the Institutional Biosafety Committee website (http://www.research.mq.edu.au/for/researchers/how_to_obtain_ethics_approval/biosafety_research_ethics) from next week.

If you would like to send us any constructive feedback from the workshop, please feel free to email me on this address (biosafety@mq.edu.au).

Thanks again for attending this workshop and we hope you all found it useful.

Kate

Office of the Deputy Vice Chancellor (Research)

Macquarie University Biosafety Secretariat

Research Office

Level 3, Research HUB, Building C5C

Macquarie University

NSW 2109

Ph: +61 2 9850 4194

Fax: +61 2 9850 4465

Email: biosafety@mq.edu.au

ANIMAL RESEARCH AUTHORITY (ARA)

MACQUARIE UNIVERSITY

AEC Reference No.: 2011/011-15

Date of Expiry: 03 May 2014

Full Approval Duration: 04 May 2011 to 03 May 2014 (36 months)

This ARA remains in force until the Date of Expiry (unless suspended, cancelled or surrendered) **and will only be renewed upon receipt of a satisfactory Progress Report before expiry.**

Associate Investigators:

Marcus Stoodley	0407 896 492
Andrew Davidson	0416 157 859
Vivienne Lee	0416 250 779
Jude Amalraj	0435 830 607
Saleh Kashba	0415 789 600
Newsha Raoufi-rad	0415 599 087
Zhenjun Zhao	0426 532 358
David Bervini	0452 497 513
Miikka Korja	0434 795 200
Rajesh Reddy	0412 725 577

Principal Investigator:

Dr Hong Duong
Australian School of Advanced Medicine
Macquarie University NSW 2109
0404 246 318
hong.duong@mq.edu.au

Investigator:
Biyi Chen   0412 941 115

Visitor:
Nirav Patel   0415 946 569

> **In case of emergency, please contact:**
> *the Principal Investigator / Associate Investigator named above, or*
> **Animal Welfare Officer** 9850 7758 / 0439 497 383
> **Manager, CAF** 9850 7780 / 0428 861 163

The above-named are authorised by MACQUARIE UNIVERSITY ANIMAL ETHICS COMMITTEE to conduct the following research:

Title of the project: Developing new treatments for brain arteriovenous malformations: Characterisation of Gamma Knife Radiosurgery-induced endothelial molecular changes
Purpose: 4 - Research (human or animal biology)
Aims: This project aims to develop a new treatment for brain arteriovenous malformations (AVMs) that is safer and more effective than the current methods of surgery and Radiosurgery, using biological methods to promote intravascular thrombosis after Radiosurgery.
Surgical Procedures category: 5 (Major Surgery With Recovery)
All procedures must be performed as per the AEC-approved protocol, unless stated otherwise by the AEC and/or AWO.

Maximum numbers approved (for the Full Approval Duration):

Species	Strain	Sex	Weight	Age	Total	Supplier/Source
Rat	SD	male	250-500g	6-12 weeks	414	ARC Perth

Location of research:

Location	Full street address
Australian School of Advanced Medicine	Level 1, Clinic Building, 2 Technology Place, Macquarie University NSW 2109
Central Animal Facility	Building F9A, Research Park Drive, Macquarie University NSW 2109
Macquarie University Hospital	3 Technology Place, Macquarie University NSW 2109

Amendments approved by the AEC since initial approval:
1. *Addition of Dr Nirav J Patel as visitor assisting in the anastomosis (Approved 11 August 2011)*
2. *Addition of Dr Saleh Kashba as Associate Investigator (Approved 11 August 2011)*
3. *Amendment of technique – Addition of Doppler ultrasound to check vessel patency (Approved 11 August 2011)*
4. *Amendment of technique – Addition of angiography (Approved 8 September 2011)*
5. *Amendment of technique - Addition of Doppler ultrasound directly on vessel intraoperatively (Approved 20 October 2011)*
6. *Addition of Newsha Raoufi-rad as other personnel (Approved 8 December 2011)*
7. *Addition of Dr Zhenjun Zhao as Associate Investigator (Approved 16 February 2012)*
8. *Addition of David Bervini to the protocol (Approved 17 May 2012)*
9. *Addition of Miikka Korja to the protocol as Associate Investigator (Approved 4 Oct 2012)*
10. *Addition of Biyi Chen to the protocol as Investigator (Exec Approved 2 Apr 2013, ratified AEC 18 April 2013)*
11. *Addition of Rajesh Reddy as Associate Investigator (Approved & AEC ratified May 2013)*
12. *Addition of 10 male SD rats as negative control (Approved AEC 13 June 2013)*
13. *Modify experimental design – additional time point for imaging (Approved AEC 18 July 2013)*

Conditions of Approval:
1. *AEC Meeting 21 April 2011 - Animals must be acclimatised for seven days prior to treatment to reduce stress.*
2. *AEC Meeting 8 September 2011 - Please document the appropriate dosage of contrast in both mg/ml and mg/kg.*
3. *New rodent researchers must successfully complete the MQ rodent basic training courses*
   a. *Rodent Handling and Care*
   b. *Rodent anaesthesia with injectable and inhalant anaesthetics*
   c. *Clean and Aseptic surgical techniques*
   d. *Post-operative monitoring and pain relief*

Being animal research carried out in accordance with the Code of Practice for a recognised research purpose and in connection with animals (other than exempt animals) that have been obtained from the holder of an animal suppliers licence.

Prof Mark Connor (Chair, Animal Ethics Committee)

Approval Date: 18 July 2013

Adapted from Form C (issued under part IV of the Animal Research Act, 1985)